

***SEDIMENTOLOGICAL ANALYSIS OF DEEP WATER, UPSLOPE-  
MIGRATING CROSS-BEDDED DEPOSITS IN A DISTALLY STEEPENED  
CARBONATE RAMP (MENORCA, BALEARIC ISLANDS, SPAIN).***

**Rachele Andreetta**



*University of Ferrara  
Department of Earth Science*

*Thesis for the Doctor of Philosophy degree  
in Earth Science*

## ABSTRACT

*The upper Miocene units cropping out along the southern coast of the Island of Menorca (Balearic Islands, Spain), are mainly represented by two carbonate depositional systems: an early Tortonian distally steepened ramp (Lower Bar Unit) and an upper Tortonian – lower Messinian reef-rimmed platform prograding complex (Reef Complex). Within the distally steepened ramp, Pomar et al. (2002) distinguished four facies belts: fan-delta conglomerates passing upwards to bioturbated packstones (inner ramp), cross-bedded grainstones (middle- ramp), clinostratified rhodolithic rudstone (ramp slope) and fine-grained wackestone-packstone with planktonic foraminifera (outer ramp).*

*The backset-bedded units analysed in this work are placed at the transition between toe-of-slope and outer ramp sediments, below the wave-base-level. They infill the axial depression of large slide/slump scars. These scars truncate the gently, 10°- 12° basinward dipping, slope-to-outer ramp clinofolds.*

*Backset beds are cross-bedded forms that dip against the direction of flow of the depositing currents, therefore they present foresets migrating upcurrent (Gary et al., 1972).*

*These sedimentary structures are well known and largely described on the foreset and toeset of Gilbert-type fan delta (Postma, 1984; Massari, 1984, 1996; Nemeč, 1990). In carbonate depositional systems these type of bedforms are rarely found and only little described.*

*The backset-bedded units, here analysed, are channel-like, wedge-shaped, 10-12 m thick, pinching out landward and extend laterally for tens of meters. Each unit is formed by several amalgamated set of backset beds, 40 cm to 2 m thick. These units are mainly conglomerates composed by bioclastic coarse-grained grainstone to rudstone. Large components are rhodoliths, bivalves, skeletal and ooid-rich pebbles to boulders, gastropods and corals. Matrix is of a bioclastic coarse-grained sand to fine gravel, made of fragments of bivalves, gastropods, rhodoliths, bryozoans, algae, echinoids, loose ooids and planktonic and benthic foraminifera. Ooids are locally very abundant both in matrix and as main components of pebbles. Pebbles are mainly flattened, elongated, of average size 6-8 cm (a-axis) and sometimes have mollusc borings on their surface: large (20-30 cm) rounded and spherical boulders are locally present. Intergranular and intergranular porosity is very high, cementation low and dolomitization patchy.*

*Foreset laminae dip upslope with varying angles ranging from almost horizontal to 30°; higher angles are mostly found in the basinward part of the unit. Lamination is underline by the orientation along laminae of coarser components especially of bivalves, pebbles and rhodoliths. Grain-size distribution has a particular trend that*

*shows a progressive decrease in size landwards and upwards. Sorting may noticeably vary being high or absent in different bodies.*

*The lower boundary of the backset-bedded units is represented by scour surfaces which, on a parallel-to-flow section are almost concordant with the stratification below, while on a perpendicular-to-flow section are concave-up shaped, presenting the very steep walls.*

*The study of different outcrops along the coast evidenced some important variation in components: moving northward composition changed from almost completely rhodolith-dominated to rhodolith-bivalve-oid-pebble-dominated to bivalve-oid-pebble-dominated with first findings of corals.*

*Upslope bedform migration has been explained as forming when a supercritical flow encounters a local obstruction or a local break on the slope, and a hydraulic jump may occur within the flow, upcurrent from the obstruction. Sediment will be therefore deposited at the obstruction forming an up-flow-dipping slipface that will tend to accrete and migrate in the upflow direction (Nemec, 1990 and reference therein).*

*The backset deposits of Menorca are found in deep-water settings but they are composed of shallow-water sediment. The formation of these backset beds is interpreted to be related to high energy storm-events able to remove sediment from shallow water and to transport it into deeper position. The sediment-rich outgoing flows channalized and accelerated along slide-scar axis, eroding and rapidly infilling up-slope the scours. In this portion of the ramp preservation potential is higher thanks to sediment deposition which buries and preserves these structures.*

*The repetitive occurrence of backset bedded units within the outer-ramp sediments and the progressive variation in composition suggest that those processes were probably active at the transition between the ramp and the reef systems. Therefore the formation of these sedimentary structures is interpreted to be strictly link to concurrence of peculiar morphological features, hydrodynamic energy and grain-size availability.*

*Computational fluid dynamic (CFD) numerical simulation have been performed as an integrated part of this work to improve the understanding of the development of hydraulic jumps within concentrated density flows. The simulated parameters do not refer to the example of Menorca but to turbidity currents for which finer-grain size (sand-size) have been used in a smaller-scale topography compared to the one studied in outcrop. The work presented proposes some new stating points for further simulations to constrain more precisely the main parameters controlling and determining the occurrence of a hydraulic jump and the consequent deposition of sediment with backset bedding.*

## RIASSUNTO

*Le unità mioceniche affioranti lungo le coste della regione meridionale del Migjorn dell'Isola di Minorca (Isole Baleari, Spagna) sono caratterizzate da due sistemi deposizionali carbonatici: una rampa carbonatica di tipo distally steepened di età Tortoniano Inferiore (Lower Bar Unit) e una piattaforma carbonatica a margine biocostruito di età Tortoniano superiore-Messiniano inferiore che vi prograda sopra (Reef Complex). Nella rampa di tipo distally steepened, Pomar et al. (2002) ha distinto tre cinture di facies: dei conglomerati di fan-delta passanti verso l'alto a packstone bioturbati (rampa interna), grainstone a laminazione incrociata (rampa-media), rudstone clinostratificati a rodoliti (scarpata della rampa) e wackestone/grainstone a granulometria fine e foraminiferi planctonici (rampa esterna).*

*Le unità a laminazione a backset analizzati in questo lavoro si trovano alla transizione tra sedimenti di piede scarpata e quelli di rampa esterna, al di sotto della base d'onda. Queste strutture sedimentarie si trovano lungo gli assi di ampie superfici di collasso che troncano la successione di scarpata-rampa esterna, la quale immerge verso bacino con angoli di circa 10-12°.*

*I corpi a laminazione a backset presentano una laminazione incrociata che immerge nella direzione contraria a quella della corrente che li ha depositati, e quindi presentano una laminazione che migra contro corrente (Gary et al., 1972).*

*Queste strutture sedimentarie sono conosciute e ampiamente descritte lungo i foreset e i toeset di delta di tipo Gilbert (Postma, 1984; Massari, 1984, 1996; Nemec, 1990). Nei sistemi deposizionali carbonatici queste forme di fondo sono state raramente riconosciute e solo brevemente descritte.*

*Le unità a backset, qui descritte, sono canalizzate, a forma di cuneo, spesse circa 10-12 m, tendono ad assottigliarsi verso terra e si possono estendere lateralmente per decine di metri. Ogni unità è formata da una serie di set a laminazione a backset amalgamati, spessi da 40 cm a 2 m. Queste unità sono prevalentemente dei conglomerati composti da grainstone e rudstone bioclastici a granulometria grossolana. I componenti più grandi sono rodoliti, bivalvi, ciottoli a frammenti scheletrici e ricchi in ooidi, gasteropodi e saltuariamente coralli. La matrice è composta da un sabbia bioclastica grossolana a ghiaia fine, composta da frammenti di bivalvi, gasteropodi, rodoliti, briozoi, alghe calcaree, echinoidi, ooidi e foraminiferi bentonici e planctonici. Gli ooidi sono localmente abbondanti sia nella matrice che nei ciottoli. I ciottoli sono prevalentemente appiattiti ed allungati, mediamente di dimensione 6-8 cm (asse a) e talvolta presentano tracce di bioerosione da molluschi sulla superficie: grandi blocchi (20-30 cm) arrotondati e tondeggianti sono localmente presenti. La porosità inter- e*

*intra-granulare è molto alta, la cementazione tendenzialmente bassa e la dolomitizzazione casuale.*

*I foreset delle lamine immergono contro corrente con angoli che variano da quasi orizzontali a 30°; gli angoli maggiori si trovano prevalentemente nella parte più verso bacino dell'unità. La laminazione è evidenziata dall'orientazione lungo le lamine dei componenti più grandi in modo particolare dai bivalvi, ciottoli e rodoliti. La distribuzione granulometrica mostra degli andamenti particolari con una progressiva diminuzione della granulometria sia verso l'alto che verso terra. La cernita può variare molto da un corpo all'altro o essere da bassa ad assente.*

*Il limite inferiore delle unità a backset è rappresentato da superfici erosive che sono sub-parallele alla direzione di stratificazione dominante lungo la sezione parallela alla direzione del flusso, mentre nella sezione perpendicolare hanno una forma a concavità verso l'alto, con pareti anche molto ripide.*

*Lo studio di diversi affioramenti lungo la costa ha evidenziato alcune importanti variazioni dei componenti: spostandosi verso nord, la composizione varia dall'essere quasi totalmente dominata dalle rodoliti ad essere ricca di rodoliti, bivalvi, ooidi e ciottoli ad dominata da bivalvi, ooidi e ciottoli con primi ritrovamenti di coralli.*

*Quando un flusso supercritico incontra localmente un ostacolo e una rottura del pendio, nel flusso si genera un risalto idraulico, in posizione sopracorrente rispetto all'ostacolo: questo meccanismo spiega la migrazione verso l'alto rispetto alla scarpata di queste forme di fondo. Il sedimento si deposita quindi all'ostacolo, formando una superficie immergente contro corrente che tende ad accrescersi e a migrare in direzione contraria alla direzione del flusso (Nemec et al., 1990 e riferimenti).*

*I depositi a backset di Minorca si trovano in ambienti di acque profonde, ma sono composti da sedimento prodotto in acque poco profonde. La formazione di queste unità è stata interpretata come conseguenza di eventi di tempesta ad alta energia capaci di rimobilizzare sedimento dalla porzioni meno profonde della rampa e di trasportarlo in posizioni più profonde. I flussi ricchi di sedimento diretti verso bacino si incanalavano ed acceleravano lungo gli assi delle superfici di collasso, erodendo e rapidamente colmando le incisioni generate. In questa porzione della rampa il potenziale di preservazione è maggiore grazie alla successiva deposizione di sedimento che copre e fossilizza queste strutture.*

*Il ripetersi di queste unità nei sedimenti di rampa esterna e la progressiva variazione nella composizione suggerisce che questi processi erano probabilmente attivi alla transizione da sistema di tipo rampa a quello di tipo orlato (scogliera). Di conseguenza la formazione di queste strutture sedimentarie risulta essere strettamente legata alla concorrenza di fattori quali particolari caratteristiche morfologiche del fondo, energia idrodinamica e disponibilità granulometrica.*

*Simulazioni numeriche computazionali di fluido dinamica (CFD) sono state svolte come parte integrante di questo lavoro per migliorare la comprensione dello sviluppo di risalti idraulici in flussi a densità concentrata. I parametri simulati non si riferiscono all'esempio di Minorca ma a correnti di torbida a granulometria più fine (sabbie) ed anche la base topografica usata è più piccola rispetto a quella dell'affioramento. Queste simulazioni propongono alcuni nuovi punti di partenza per simulazioni future, ponendo costrizioni più precise ai principali fattori che controllano e determinano il verificarsi di un risalto idraulico e la conseguente deposizione di sedimento a laminazione a backset.*

*To my mother, Carla*

## CONTENTS

<b>1. Introduction</b> .....	<b>1</b>
1.1. The aim.....	1
1.2. Methodologies.....	2
1.3. Introduction to backset beds.....	3
1.4. Studied area.....	4
1.5. Definition of carbonate ramps.....	5
<b>2. Geological setting</b> .....	<b>10</b>
2.1. The Migjorn ramp.....	14
2.2. The Reef Complex.....	19
<b>3. Sedimentary Facies</b> .....	<b>22</b>
3.1. Basic concepts and definitions.....	22
3.2. The studied outcrops.....	26
3.3. Barranc des Pou.....	30
3.3.1. Facies description.....	33
3.4. Forma.....	48
3.4.1. Facies description.....	51
3.5. Nalinot.....	73
3.5.1. Facies description.....	75
<b>4. Facies Association</b> .....	<b>103</b>
4.1. Facies association A1: base-of-slope deposits.....	103
4.2. Facies association A2: turbiditic wackestone/packstone to grainstone...104	
4.3. Facies association A3: coarse calcarenite with planar parallel lamination.....	105
4.4. Facies association A4:backset bedded deposits.....	106
<b>5. Summary of data</b> .....	<b>109</b>
<b>6. Supercritical flows and backset bedding</b> .....	<b>121</b>
<b>7. Interpretation</b> .....	<b>135</b>
7.1. Previous interpretation of the backsets of Menorca.....	135
7.2. Depositional model.....	135
<b>8. Numerical simulations</b> .....	<b>152</b>
8.1. Introduction to computational fluid dynamics (CFD).....	152
8.2. Flow-3D™.....	152
8.3. Research method.....	156
8.4. Results of the present study.....	158
8.5. Conclusion.....	177
<b>9. Conclusions</b> .....	<b>179</b>
<b>10. Acknowledgment</b> .....	<b>182</b>
<b>11. References</b> .....	<b>183</b>



# 1. Introduction

## 1.1 The aim

This thesis presents a sedimentological study and analysis of some large-scale cross-stratified deposits cropping out at the base-of-slope of a distally steepened carbonate ramp of Upper Miocene in the Island of Menorca (Balearic Islands, Spain). These deposits are characterized by coarse-grained breccia and conglomerate- beds with foreset migrating upslope, and have been interpreted for the first time by Pomar *et al.* (2002) as backset beds ("*cross-stratification that dips against the direction of flow of the depositing currents*" - Gary *et al.*, 1972).

The peculiarity of these kind of bedforms is that they have never been described within a carbonate depositional system, and so far the example cropping out in Menorca is the only one describe in a carbonate environment. These bedforms are still poorly understood and mainly known from siliciclastic environments therefore found in different depositional system dominated by different processes.

The main purpose of this study is to give a detail sedimentological analysis of the backset bedded deposits in terms of composition, geometrical architecture, grain-size of sediment involved and the relationships with the embedding deposits. Then, an interpretation is given for the processes that were responsible for the entrainment of the sediment in shallow-water settings (middle ramp, upper-slope), the processes that transported it seaward to the slope-break and the ones that transported it down to the base-of-slope where it has been deposited.

A particular attention will be given to the understanding of the parameters that drove and allowed their formation in this sedimentary environment.

The backset bedded deposits studied in the Island of Menorca are then compared to the ones known from different depositional settings. In siliciclastic environments in fact, scour-filling gravel and sand showing backset bedding are largely described on the foreset and toset of Gilbert-type fan delta by many authors. These structures have been interpreted to develop at very high concentration of sediment during transport, and thus, the genesis of scour-filling backset beds on the foreset slope of a Gilbert-type systems may reflect the upstream migration of chutes and pools In carbonate environment these sedimentary structures have been reported only in few papers where they are shortly described (Lickorish and Butler, 1996; Massari and Chiocci, 2006) and they refer only to another example, the one at Monte Capodarso (Sicily, Italy).

The description of these deposits in this study will implement the still poor knowledge about the distribution of facies in carbonate ramp settings that so far still lack the numerous and extended references in literature if we compared to the studies about rimmed carbonate platforms. In detail the base-of-slope to outer-ramp facies model has been implemented with new data.

Since the knowledge about the formation of backset beds is still poorly understood, the present thesis has been implemented with a section dedicated to a parallel work where computational fluid dynamic numerical simulations have been run using the dedicated software Flow-3D™. Performing these simulations implemented the knowledge on the hydrodynamic characteristics of the flows and the conditions that allow this bedforms to develop in submarine environments. The aims of performing these simulations was to give a quantitative analysis of the flow hydraulic conditions and their relationship to surface morphology, to better understand some of the major factors that control the deposition of sediment developing backset lamination along slope foreset and toeset.

## ***1.2 Methodologies***

The sedimentological description of the backset bedded deposits have been develop through a wide collection of data during an overall three months period of fieldwork spent in Menorca. The collection of information have been organized to obtain observation both at the smallest scale of the microfacies analysis in thin section, to the very large scale of the whole outcrop. In order to do this a large number of logs have been measured in several location along the sea-cliffs of the southern coast of the island. Each log has been sampled in detail for thin section analysis. Facies analysis and microfacies analysis has been done to improve the description of sediment composition and matrix and grain types, dominating skeletal grains and skeletal associations, to define the source of the sediment composing these beds. Samples of the embedding deposits have also been taken to improve the understanding of the position of these units and to better constrain the time of their deposition.

To facilitate the understanding of the vertical and lateral relationships with the embedding deposits and of the stratigraphical relationship between different sections in different locations, the measurement of logs has been coupled with drawing over photomosaics tied together with detailed measurements of each unit. This method has been widely used to reconstruct the geometries and architectures of these units in three dimensions. Facies distribution and geometries have been therefore mapped on photomosaics directly during field work when the outcrop was not too impervious.

Hydrodynamic studies have been carried out making use of dedicated software thanks to a collaboration with Prof. Wojtek Nemeč, at the Department of Earth Science, University of Bergen (Norway).

Due to the large scale of these bedforms it would have been impossible indeed to reproduce them in a laboratory tank experiments, therefore computational fluid dynamics (CFD) numerical simulations, through the use of the dedicated commercial software Flow-3D™, have been used to attempt to reproduce a hydrodynamic flow conditions along a slope that may lead to the development of backset bed deposition at its base. This method allows to up-scale laboratory data and perform simulation at a scale of natural sedimentary structures even if

there are still numerous constraints on the grain-sizes of sediment that can be adopted. Therefore the software does not allow to reproduce parameters corresponding to the ones observed in the studied outcrops in Menorca. The simulations have been done in collaboration with Complex Flow Design AS in Trondheim, Norway.

### **1.3 Introduction to backset beds**

The formation of “backset bedding” (cross-stratification that dips against the direction of flow of the depositing currents - Gary *et al.*, 1972, Reineck and Sing, 1980 and reference therein) has been attributed to 1) to the upstream migration of antidunes (e.g., Skipper, 1971, Alexander *et al.*, 2001), 2) to flow under chute and pool conditions (Schmincke *et al.*, 1973), and 3) to the upper-current migration of rhomboid ripple-marks (Wunderlich, 1972; 1973). In some of Hand’s (1974) experiments on density currents, chutes and pools developed at Froude number  $>1$ , sedimentation being related to up-stream migrating hydraulic jumps. Flows generating bedforms typical of supercritical flows, have been observed in flume experiments by Simons *et al.* (1965) and steeply-dipping backset beds have been experimentally produced for example by Jopling and Richardson (1966) in laboratory experiments.

In outcrop, scour-filling gravel and sand showing backset bedding are largely described on the foreset and toeset of Gilbert-type fan delta by Postma (1979, 1984a), Postma *et al.* (1983), Massari (1984, 1996), Postma and Roep (1985), Colella *et al.* (1987, 1988), Nemec (1990). These structures are interpreted to develop at very high concentration of sediment during transport, and thus, the genesis of scour-filling backset beds on the foreset slope of a Gilbert-type systems may reflect the upstream migration of chutes and pools.

Komar (1971) stated “hydraulic jumps (a hydraulic jump occurs when a supercritical flow,  $Fr > 1$ , turns into a subcritical flow,  $Fr < 1$ ) are commonly expected to develop in the toeset, due to enlargement, dilution, strong reduction of the velocity and competence of the flow as it reaches the base of the slope”. The genetic link between backset beds and hydraulic jumps has been proposed by Massari (1984), Massari and Parea (1990) and Nemec (1990) who widely treated the behaviour of supercritical sediment gravity flows on steep slopes. When a supercritical flow encounters a local obstruction (or a local break on the slope: sites of abrupt flattening or even upflow inclination of the slope surface), a hydraulic jump may occur within the flow upcurrent from the obstruction. Sediment will be deposited at the obstruction forming an up-flow-dipping slipface that will tend to accrete and migrate in the upflow direction. According to Nemec (1990), hydraulic jumps can occur in granular material flows, and also in turbulent flows, in which case the effect will be roughly analogous to the formation of an antidune.

## 1.4 Studied area

Menorca is the northernmost island of the Balearic archipelago (Fig.1.4.1). This archipelago is the emergent part of the Balearic Promontory, the north-eastward extension of the Betic Range in western Mediterranean (Fig.1.4.1). This area underwent extension during the Mesozoic associated to the opening of the Tethys, and subsequent compression and thrusting during the Cenozoic. Paleo-relieves inherited from middle Miocene compressional tectonics resulted in paleo-islands during late Miocene and shallow water carbonate platforms developed around them especially on the southern coasts.



Fig.1.4.1 Geographical map (above) showing the position of the island of Menorca in the Western Mediterranean Sea and (right) respect to the other islands of the Balearic archipelago.



The Menorca Island can be subdivided in two main regions elongated in a NW-SE direction. The Tramuntana region to the north, is composed of Palaeozoic, Mesozoic and lower Tertiary rocks (Fig.1.4.2). To the south, the Migjorn region is composed by upper Miocene carbonates that unconformably overly the pre-late-Miocene basement, and have undergone only slight tilting and flexure associated with normal and strike-slip faulting during Late Neogene to Middle Pleistocene times (Obrador 1972-73).

The upper Miocene has been interpreted as being formed by two depositional sequences: the lower sequence was first defined as the Lower Bar Unit (Obrador et al., 1983, 1992) and later as the lower Tortonian distally steepened ramp by Pomar (2001a).

The study area is found in the south-eastern part of the Migjorn region, along the sea-cliffs close to Es Canutells where are excellent large outcrops. Three sites have been analyzed in detail: Barranc des Pou, Forma, Nalinot (Fig.2.1.2).

These outcrops allow studying the backset bedded deposits both along depositional dip and along strike. In Forma the section is E-W oriented while at Barranc des Pou and Na Linot the successions extend NE-SW and NW-SE. Those outcrops clearly document the relationship

between the coarse-grained bioclastic backset-bedded deposits and the units lying above and below.

## **1.5 Definition of carbonate ramps**

The definition of *ramp* is "the sloping surface connecting two levels". Previous studies done during the 1950s and 1960s, authors would have referred to such setting as a "typical shelf model". The term "shelf model" was defined in 1888 by H. R. Mill as "...*the shallow and gradually sloping ground from sea margin out to the 100-fathom line, beyond which the descent to abyssal depths is abrupt*". This definition resulted to be quite inadequate in some carbonate depositional systems.

Nowadays, the term *ramp* is widely used by siliciclastic sedimentologists for low-gradient submarine slopes, particularly on continental platforms. This term is used within carbonate depositional system with a different meaning. In order to avoid misunderstandings, a brief description of what is meant with the term *carbonate ramp* and the related classification is given below.

The ramp depositional model was defined by Ahr (1973), as a system in which the ramp is an inclined platform that extends basinward without a pronounced break in the slope. Therefore this model is characterized by the absence of a shelf-margin barrier. The allocation of facies was distributed parallel to coastline and it reflected the greater wave and current activity near the mainland shore. Therefore a *carbonate ramp model* is a sloping surface on which carbonate facies are deposited while subjected to open conditions from the surf zone to depth of hundreds of metres. Ahr (1973) underlines that the distribution of facies is different from the shelf model (the author calls "shelf model" the nowadays called "rimmed platform", citing for example the Bahama Banks) . In the ramp model, grainstone and packstone are landward facies and the sediments become muddy as one moves seaward, while in the "shelf model" the landward facies are muddy, and they pass seaward into shelf-margin grainstones and boundstones. Anyway, this model is an old obsolete one that today has been widely enlarged.

The major features of this model are the concentric facies belts which follow bathymetric contours, the rather monotonous wedge-shape deposits thickening seaward except where local topography modifies the depositional trend and the absence of a continuous reef margin even if patch reefs may be present locally.

Wilson (1975) presents a classification of carbonate platforms (fig.1.5.1) and gave a definition of carbonate ramp based on the configuration of regional features "*huge carbonate bodies built away from positive areas and down gentle regional paleoslopes. No striking break in slope exists, and facies patterns are apt to be wide and irregular belts with the highest energy zone relatively close to the shore*".

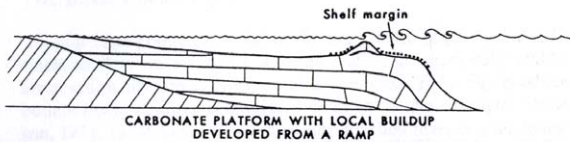
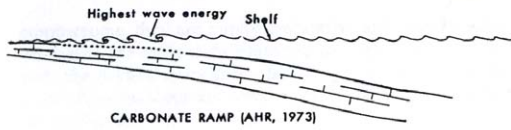


Fig. II-2. Definition of carbonate ramps and platforms

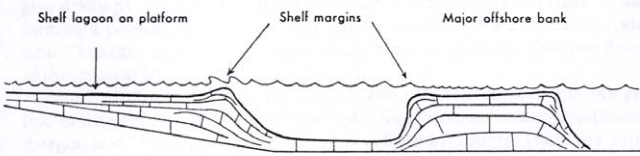


Fig. II-3. Definition of carbonate platforms, shelf margins and offshore banks

Fig. 1.5.1 Definition of (A) carbonate ramp, (B) carbonate platform and (C) definition of carbonate platforms, shelf margins and offshore banks (from Wilson, 1975).

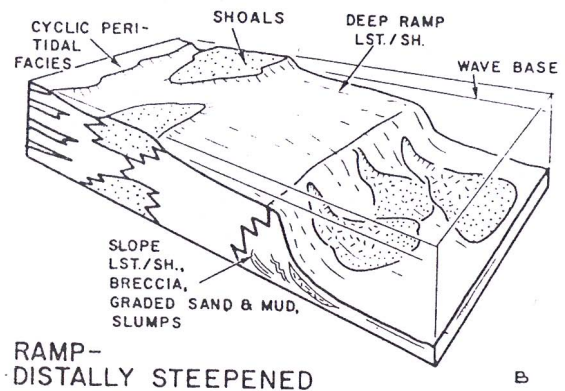
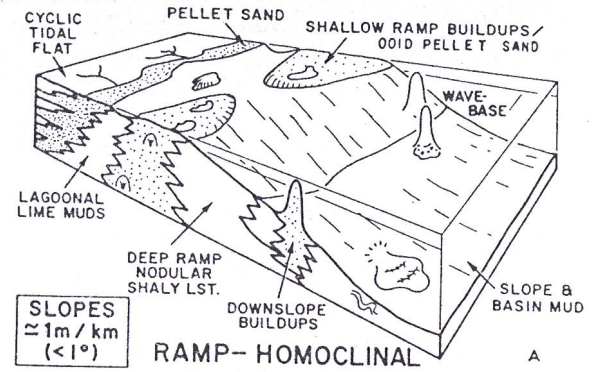


Fig. 1.5.2 (A) Block diagram of homoclinal carbonate ramp; (B) block diagram of distally steepened ramp (From Read, 1982).

Another classification of carbonate ramps came with Read (1982) where the carbonate ramp has been defined as a gently sloping (generally less than  $1^\circ$ ) platform on which shallow wave-agitated facies of the near-shore zone pass downslope (without marked break in slope) into deeper-water, low energy deposits (Ahr, 1973). The difference from rimmed platforms is marked by the absence of a continuous reef margin and by the absence of sediment gravity flow deposits containing clasts of cemented, shallow water facies in deeper water facies. Near-shore skeletal complexes or ooid-pellet shoal complexes may characterize ramps.

Carbonate ramps have been classified in two different types *homoclinal* ramp and *distally steepened* ramp (Read, 1982; see Fig. 1.5.2). *Homoclinal* ramps are characterized by having a gentle slope that dips into deep water, they may have skeletal or ooid/pellet sand shoal complexes, which pass without break in slope into deep-ramp nodular limestone, and then into pelagic/hemipelagic basin facies; deeper water facies usually lack significant slump and sediment gravity flow deposits. Homoclinal ramps are relatively rare in the Holocene and appear to be more common during the initial development of carbonate miogeoclines.

*Distally steepened* ramp is characterized by a marked increase in slope at the seaward edge of the deep ramp, and they present frequent slumps, slope breccias and turbidites. Nevertheless, clasts of shallow platform margin facies are generally absent from breccias (Read, 1982).

A review of the occurrence of reef rimmed platforms and carbonate ramps through the Phanerozoic (Wright and Burchette, 1992) show that carbonate ramps are common in all geological periods, but were dominant at times when reef-constructing organisms were absent or inhibited. The authors also proposed a subdivision of the ramp environments based on wave-base (see fig. 1.5.3). Therefore they defined the *inner ramp* as the part of the ramp that goes from the shoreline to fair-weather-wave-base, the *mid-ramp* extends from fair-weather wave-base (fwwb) to normal storm-wave-base, although the water depths which these boundaries represent vary and the *outer ramp* which occurs in distally steepened ramp, that goes from base-of-slope basinwards.

The four main environmental areas are characterized by a distribution of facies which is described and shown in fig 1.5.4 and 1.5.5.

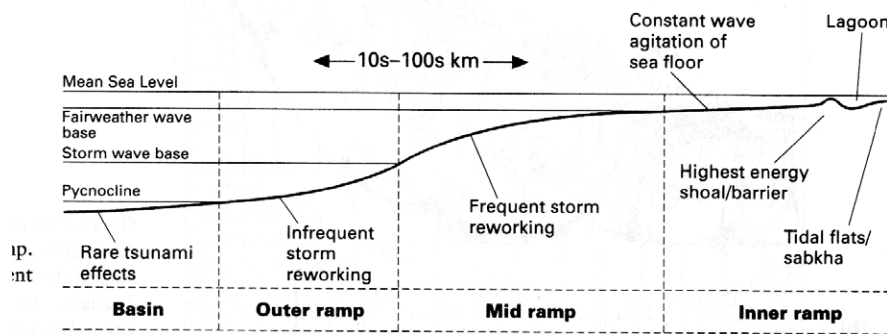


Fig.1.5.3 The main environmental subdivision of a "homoclinal" carbonate ramp. MSL= mean sea level; FWWB= fair-weather wave-base; SWB= storm wave base; PC= pycnocline (not always identifiable in the rock record). Water depths corresponding to these boundaries are variable (From Burchette & Wright, 1992).

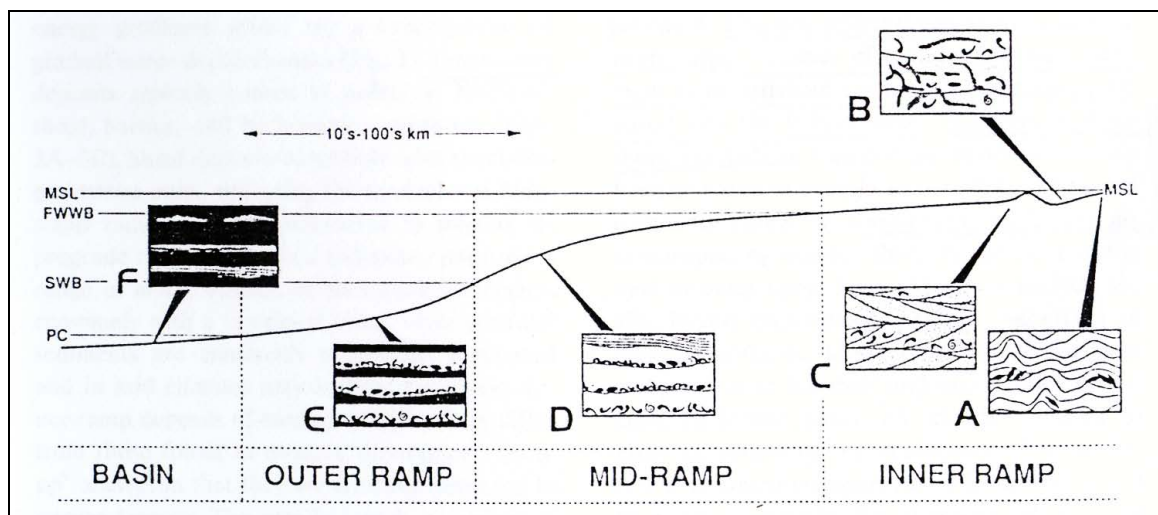


Fig.1.5.4 "Homoclinal" carbonate ramp showing main sedimentary facies. Inner ramp: (A) peritidal and sabkha facies with stromatolitic algae and evaporates; (B) bioturbated and variably bedded lagoonal lime mudstone, packstone and wackestone; (C) shoreface or shoal cross-laminated oolitic or bioclastic grainstone and packstone. Mid ramp: (D) amalgamated coarse, graded tempestites, commonly with hummocky cross-stratification. Outer ramp: (E) fine grained, graded tempestites interbedded with bioturbated or laminated lime or terrigenous mudstone; (F) laminated or sparsely rippled silt-grade carbonate sediment or quartz silt in a predominantly terrigenous mudstone succession. All these boundaries are gradational (Burchette & Wright, 1992).

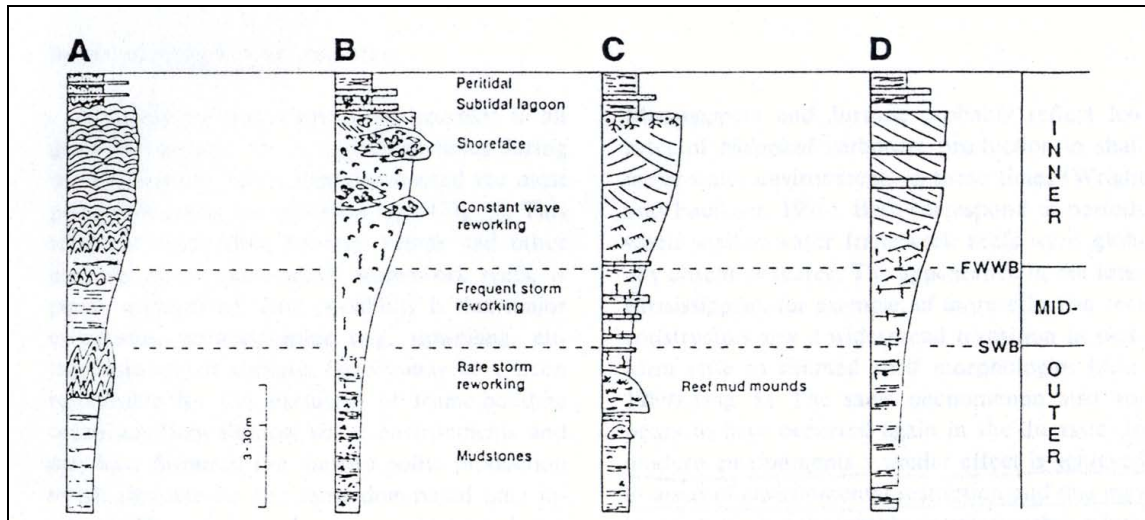
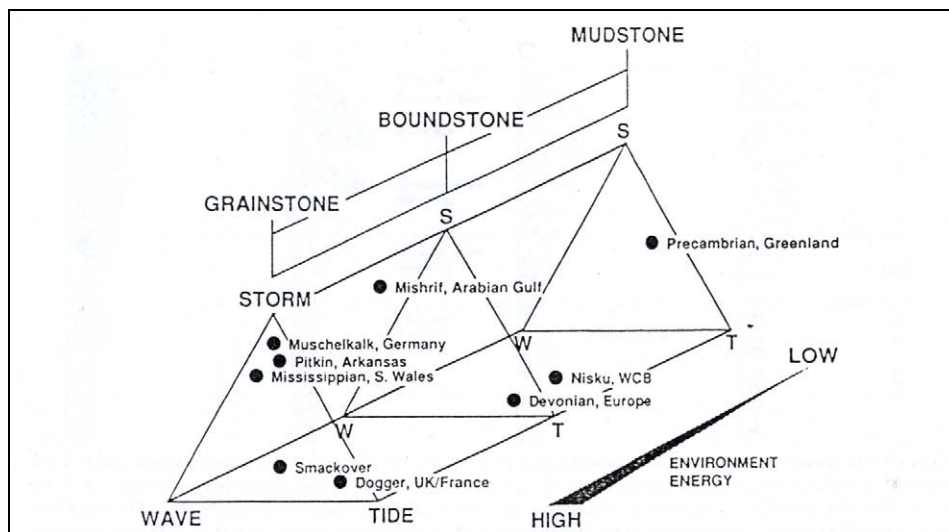


Fig. 1.5.5 Highly schematic vertical section through several end-member ramp depositional systems, showing variation of facies within inner-, mid-, and outer- ramp depositional environments and how these are related to fair-weather wave-base (FWWB) and storm wave-base (SWB). (A) Proterozoic stromatolite-dominated ramp, showing variations in stromatolite morphology with depth. Based on Grotzinger (1989). (B) Skeletal boundstone-dominated ramp, typical of early Palaeozoic and later Mesozoic succession. Based on Burchette (1981) and Burchette & Britton (1985). (C) Grainstone dominated ramp, typical of early Carboniferous and Jurassic, and some modern ramps. Based on Ahr (1973), Baria et al. (1982) and Burchette et al. (1989). (D) Large-foraminiferan shoal-dominated ramp, characteristic of those in the Paleogene and early Neogene. Based on Aigner (1983). Profiles are valid for several scales of sequence (Burchette & Wright, 1992).

In the models proposed by these authors, carbonate ramp system the carbonate productivity of carbonate ramp system in the inner ramp shows lower production rates than comparable shallow-water facies on rimmed shelves. Anyway this is again an old concept since several authors believe that the rate of dissolution is very high and production may be comparable to rimmed shelf (e.g. Chems et al., 2008; James et al., 2005).

As for the type of sedimentary basin, the authors observed that these systems best develop where subsidence is flexural and gradients are slight over large areas, as in foreland and cratonic-interior basins along passive margins. Moreover it is noticed that ramps compared to rimmed shelves, respond differently during relative sea-level changes because of their low-angle slopes, even though it seem to be strongly dependent on the rate of sea-level change.





*Fig. 1.5.6 Ternary diagram showing suggested classification for carbonate ramps based on the degree of storm, wave or tidal influence which they exhibit in the mid- and inner-ramp zones. An additional axis accommodates the various lithologies which dominate ramp sediments and seem to reflect the level of environmental energy (see arrow). Several representative ramps have been entered. See text in Burchette & Wright (1992) for source references on the characteristics of individual ramps (Burchette & Wright, 1992).*

In the work here presented the “distally steepened carbonate ramp” is intended *sensu* Read (1982), a ramp which is similar to an homoclinal ramp, but with a distinct increase in gradient in the outer, deep ramp region. The width of this kind of ramps is between 10 and 100 km. A modern analogue can be the platform of the Northeastern Yucatan, western Florida.

## 2. GEOLOGICAL SETTING

Menorca is the northernmost island of the Balearic archipelago. This archipelago is the emergent part of the “Balearic Promontory”, the north-eastward extension of the Betic Range in western Mediterranean (Fig.2.1).



Fig.2.1 Location map of Menorca showing its position on the Balearic Promontory and the surrounding basins.

The opening of the Atlantic ocean caused the collision of the African plate with the Euroasiatic plate, with subduction of ocean crust below the European margin. This convergence, that has been estimated to be of 400-500 km in the western part and of 1500 km in the eastern part (Krijnsman, 2002), occurred from the mid-Cretaceous to the Palaeogene times and gave rise to the Alpine orogeny and to the progressive closing of the Tethys ocean that during the Mesozoic was separating the African plate from the Euroasiatic plate.

The opening of the Western Mediterranean occurred during two main quick phases of subduction migration to the east consuming the westernmost part of the Tethys, creating smaller basins. During the first phase the Balearic–Algerian Basin was formed due to the radial extension originated by the rotation of the subducted plate which caused the drift of the Sardinia-Corsica block with an anti-clockwise rotation. From the Tortonian to the Quaternary, the second phase was dominated by an extensional deformation, more pronounced to the east where the Tirrenian Basin opened.

The architectural structure of the Western Mediterranean is therefore dominated by extensive faults trending NE but with significant differences at the margins. The north-western margin, corresponds to a passive margin where series of horst and graben are aligned along a

NE direction; those formed during the Oligocene and lower Miocene and were buried by more recent sediments that fossilized this extensive structure. On the other hand, the south-east margin was more complex; the Sardinia-Corsica block and the Balearic Promontory are separated by a directional fracture with right-movement and NW direction.

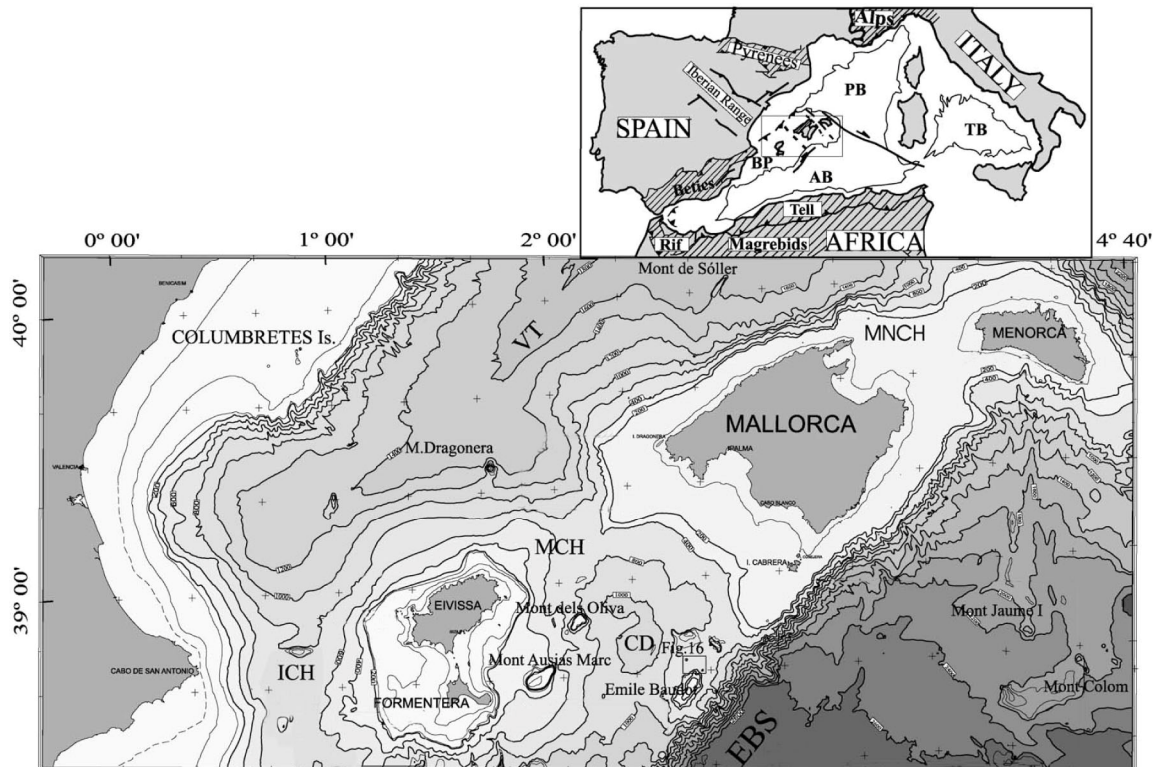


Fig. 2.2 Location and bathymetry of the Balearic Promontory. Bathymetric contour interval is 200 m. ICH, Eivissa Channel. MCH, Mallorca Channel. MNCH, Menorca Channel. VT: Valencia Trough. CD: Central Depression. EBS: Emile Baudot Scarpment. Insert: Geographic and structural scheme or bathymetry shows only 2000 m isobath. BP: Balearic Promontory. AB: Algerian Basin. PB: Provençal Basin. TB: Tyrrhenian Basin (modified from Acosta *et al.*, 2003).

While the eastward movement of the Sardinia-Corsica block was creating the Liguro-Provençal Basin, the Balearic margin was formed by the NE extension of the Betic Range, developed following the rifting phase that opened the Valencia Trough, a northeast trending aborted rift. This V-shaped Trough has a maximum width of 400 km and to the northwest it limits the Balearic Promontory (Menorca is found in the northernmost part), while to the southeast it is limited by a NE-SW steep scarp, the Emile Baudot Scarp, which has been interpreted as a possible transform fault of tectonic origin (Acosta *et al.*, 2001).

The Balearic Promontory is therefore a structural high, 1000 to 2000 m high with respect to the surrounding basins. It is bounded to the north by the Balearic-Provençal Basin and to the south by the Balearic-Algerian Basin. To the southeast it is limited by the Emile Baudot Scarp (Fig.2.2). The present configuration of the Balearic Promontory is due to the westward migration of the Alboran microplate which caused the clockwise rotation of the Mallorca and Ibiza blocks (Andrieux *et al.*, 1971; Auzende *et al.*, 1973a,b; Balanyá and García-Dueñas, 1987, 1988; Lavecchia, 1988; Mantovani *et al.*, 1990; Vegas, 1992; in Acosta *et al.*, 2003).

The Promontory is morphologically subdivided into two tectonic blocks: the Menorca and Mallorca block and the Ibiza and Formentera block. Menorca and Mallorca share the same narrow continental platform which is steeper to the north and wider and more gentle inclined to the south.

With regard to Menorca, the platform to the north-east is structurally controlled and it is very narrow ( about 10 km) and steep (6°). On the margin there are numerous gorges and valleys incised during the Messinian crisis (Hsü et al., 1973) due to the lowering of base-level. To the south-west the platform is wider with a constant depth and continuous without interruption to Mallorca (maximum depth -60 m). To be noted, offshore of Son Bou, the presence of an incised submarine canyon oriented N-S, whose head is at about 5 km from the shoreline and at about -80 m, which extends down to the toe-of-slope at -1400 m. Associated to this canyon there is a turbiditic fan that expands down to the abyssal plain at -2400 m. This canyon works collecting biogenic sediment produced by the platform and transporting it downslope (Maldonado & Stanley, 1979).

The geology of the Balearic Islands is characterized by Mesozoic, Palaeogene, and Middle Miocene folded and thrust rocks which are flanked by areas covered with slightly deformed Late Miocene to Pleistocene sedimentary rocks (Fig.2.3).

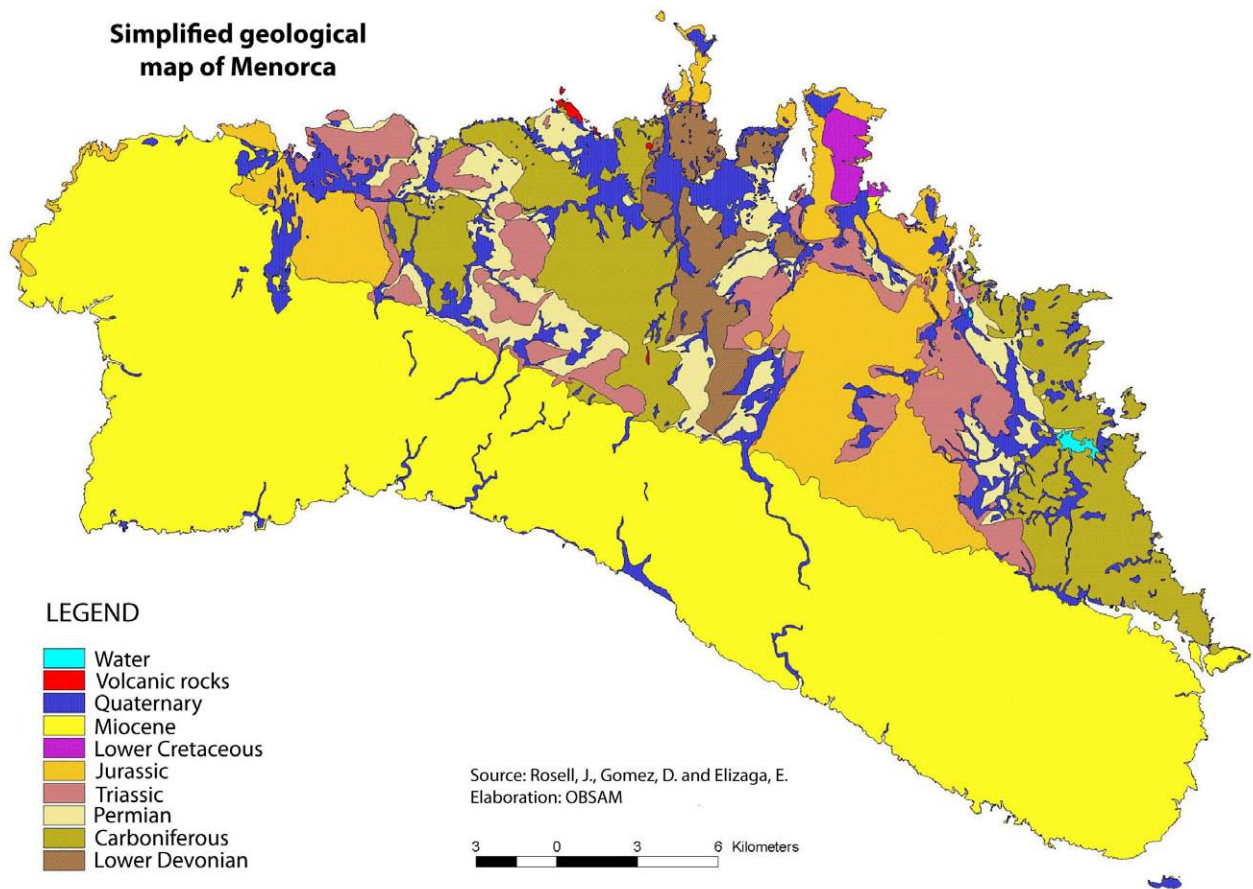


Fig.2.3 Simplified geological map of the Island of Menorca: the northern part of the island is mainly composed of Palaeozoic and Mesozoic rocks, while Tertiary rocks are found in the southern region (Rosell et al.).

This area underwent extension and thinning during the Mesozoic associated to the opening of the Tethys related to the break up of Pangea. During the Palaeogene, this continental-crust segment suffered a lithospheric flexure produced by the onset of the Alpine orogeny. The major compressional events occurred during mid Miocene, as well as in south-eastern Spain (Betic Range) and northern Africa (Maghrebides Ranges). These ranges have a northeast trends and the dominant structural style is that of stacked thrusts sheets which during the Middle Miocene, were placed toward the northwest. Paleo-relieves inherited from middle Miocene compressional tectonics resulted in paleo-islands during late Miocene and shallow water carbonate platforms developed around them especially on the southern coasts. The Upper Miocene deposits suffered only slight tilting and flexure related to normal and strike-slip faulting during the late Neogene to middle Pleistocene time.

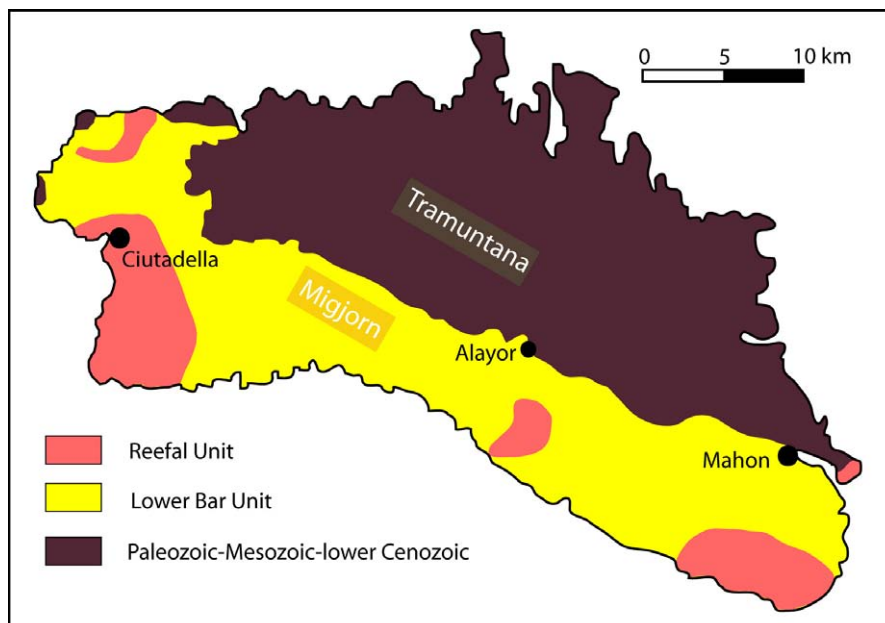


Fig.2.4 Simplified geological map of the Island of Menorca (modified from Pomar et al, 2002).

The Menorca Island can be subdivided in two main regions elongated in a NW-SE direction (Fig.2.4). The Tramuntana region to the north, is composed by the Silurian shales, Devonian limestones and Carboniferous siliciclastic turbidites (Palaeozoic), by the Triassic red sandstones, dolostones and red marls, Jurassic dolostones and some Cretaceous limestone (Mesozoic) and Oligocene limestone conglomerates (lower Tertiary rocks) . To the south, the Migjorn region is composed by upper Miocene carbonates that unconformably overly the pre-late-Miocene basement (Obrador 1972-73), and have undergone only slight tilting and flexure associated with normal and strike-slip faulting during Late Neogene to Middle Pleistocene times.

## 2.1 The Migjorn ramp

The Migjorn ramp is, volumetrically, the most significant deposit in the Island and it represents deposition on a progradational distally steepened carbonate ramp (*sensu* Read, 1985). The Migjorn ramp reaches a thickness of up to 500 m in the subsurface. The carbonate ramp is dated early Tortonian in age (N16 zone of Blow) according to Bizon *et al.* (1973). Lithofacies, bedding patterns and internal architecture have been described in Pomar (2001), Pomar *et al.* (2002), Brandano *et al.* (2005) and more recently, a depositional model and paleoecological interpretation (Fig.2.6) based mainly on large benthic foraminifera as carbonate-producing biota, in Mateu-Vicens *et al.* (2008).

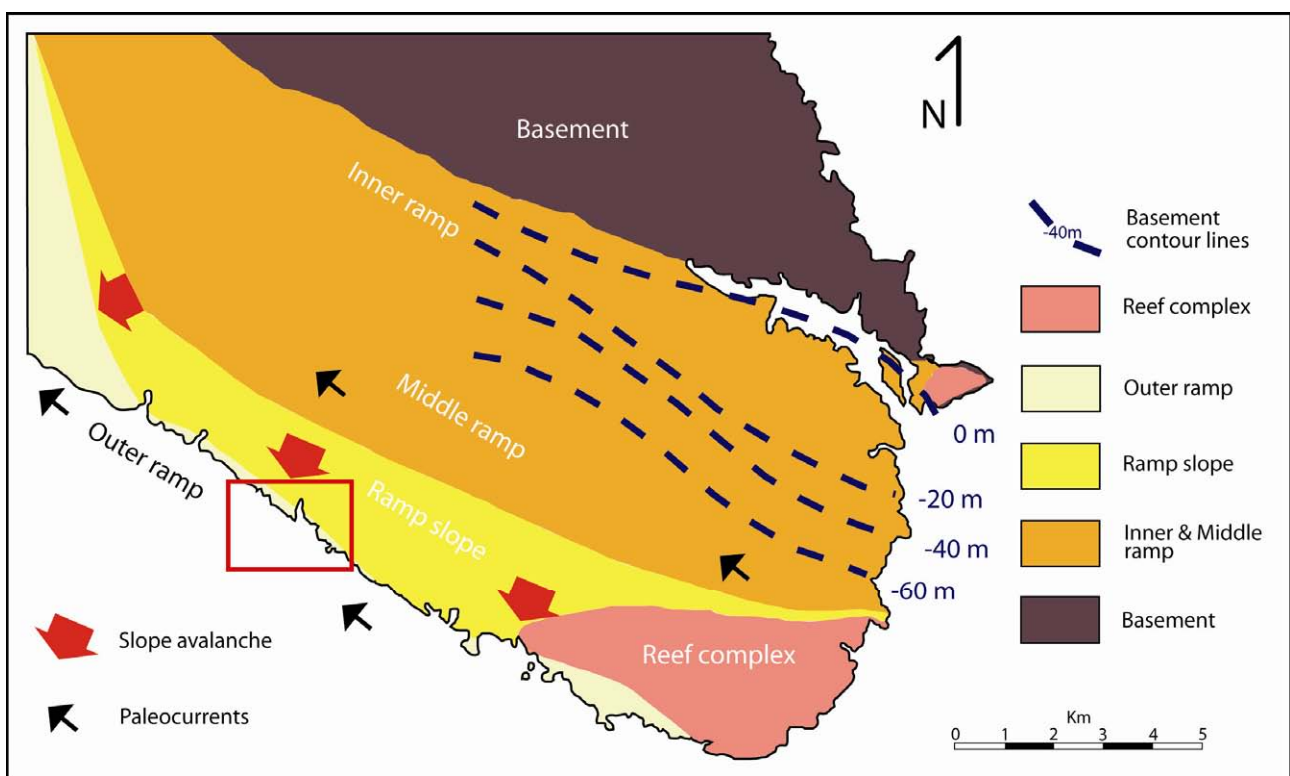


Fig.2.5 Lithofacies of the Lower Tortonian Lower Bar Unit and the overlying Reef Complex on the eastern side of Menorca (modified from Pomar *et al.*, 2002).

This carbonate platform corresponds to a highstand system tract prograding and aggrading over a Palaeozoic, Mesozoic and locally lower Tertiary basement.

### *Inner ramp*

The inner-ramp extends seawards from the palaeoshoreline to about -15m depth as estimated by Vicens-Mateu *et al.* (2008), which corresponds to the fair-weather wave-base (Fig.2.5). Deposits next to shoreline are composed of siliciclastic sandstones and conglomerates; Pomar *et al.* (2002) distinguished two main lithofacies: *conglomerates and sandstones* which are subdivided in three more subunits, and *bioturbated packstones*.

*Conglomerates and red sandstones to siltstones*: this facies is composed of clasts derived from Palaeozoic siliciclastic rocks and Mesozoic carbonate and siliciclastics. Crudely to well stratified pebble and cobble conglomerate are interbedded with conglomeratic red sandstones and red siltstones sometimes with landward-dipping imbrication. Matrix is of reddish sand or sandy silt and red siltstone present root structures sometimes with scattered pebbles. Carbonate clasts are not bioeroded and marine fossils are absent. This lithofacies has been interpreted to represent continental deposition in an alluvial-dominated environment.

*Cross-bedded pebbly sandstone*: this facies has well stratified beds of matrix-supported, pebbly sandstones. Beds gently dip (up to 10°) in a seaward direction and the presence of echinoids and marine gastropods point to a marine depositional environment. Components are quartz sand with some pebbles and cobbles, with pebbles showing seaward imbrication. Some clasts are subangular and mica is sometimes present, suggesting a short transport distance.

This lithofacies has been interpreted to represent foreshore deposits of a low-wave energy environment.

*Structureless conglomerates and pebbly sandstones*: beds are stratified from horizontal to gently dipping basinwards. With a lower conglomeratic interval that passes upwards into a structureless pebbly sandstone. Bounding surfaces are diffuse and undulate to sharp and erosive. Conglomerate are mainly clast-supported. Most clasts composing this facies are derived from Palaeozoic sandstones and shales or from Mesozoic carbonate rocks. Pebbles may be bored by sponges and when disc-shaped they are imbricate both landward and seaward. Sandstones are composed of poorly sorted quartz sand with few granules and pebbles, commonly structureless and bioturbated. Moulds of bivalve and whole skeletons and fragments of echinoids also characterize this unit. This lithofacies has been interpreted to represent small point-sourced fan-delta deposits reworked in a shoreface environment.

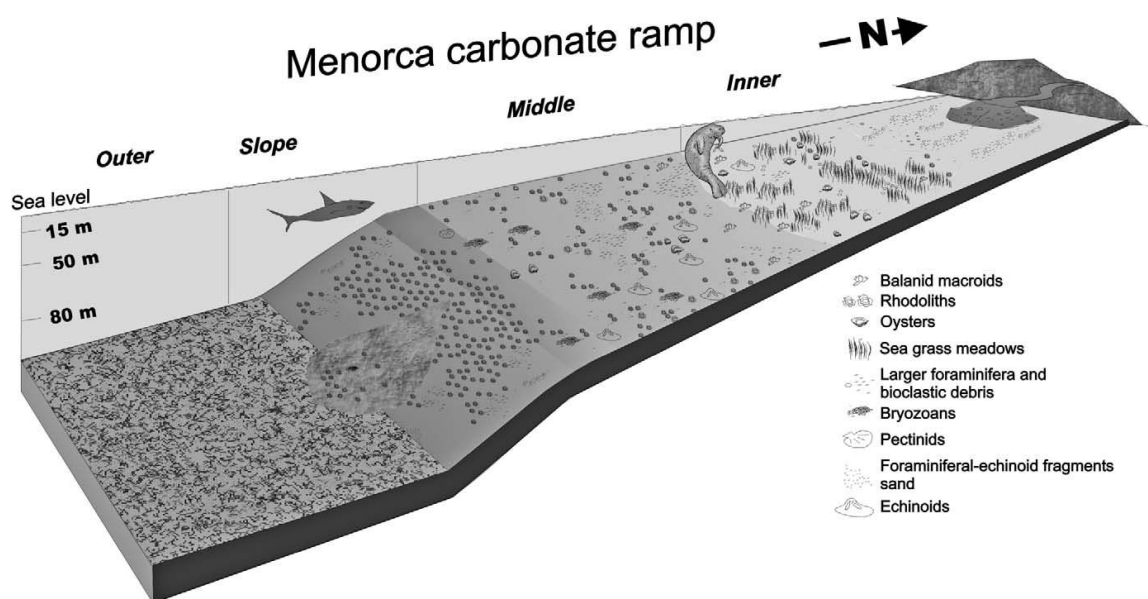


Fig. 2.6 Paleoenvironmental interpretation of the lower Tortonian carbonate platform of Menorca (from Mateu-Vicens et al., 2008).

The siliciclastic sandstones and conglomerates pass basinwards into *bioturbated carbonate packstones*. Sediments of this facies are structureless, wave-related structure are absent and pervaded by bioturbation. Beds may be subhorizontal to gently seaward-dipping, crude to well stratified. Components are mollusc fragments and foraminifera with scattered whole-shell bivalves, the basal beds are rich in echinoid fragments, bivalve and gastropod moulds. Sediment is mainly structureless with slightly visible large-scale cross lamination dipping both landward and seaward. Ichnofossils are locally frequently found (*Ophiomorpha*).

This facies has been interpreted as a shallow-water, euphotic environment subjected to wave agitation but where transport and sorting of sediment was prevented by trapping, baffling and sheltering in seagrass beds (Pomar et al., 2002; Mateu-Vicens *et al.*, 2008).

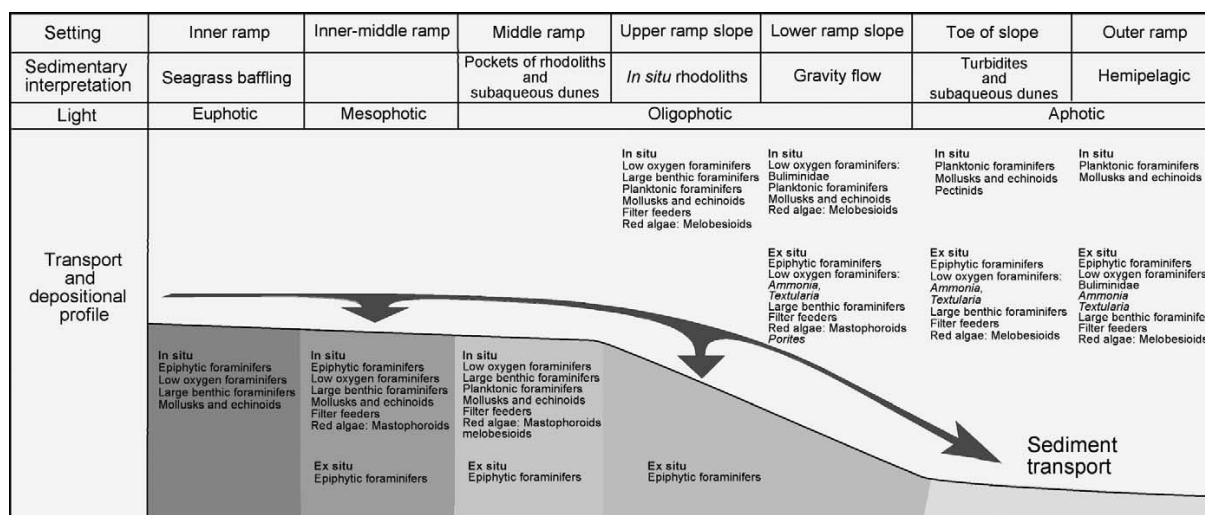


Fig.2.7 Carbonate production and sediment accumulation in the lower Tortonian carbonate platform of Menorca (from Mateu-Vicens *et al.*, 2008).

### Middle-ramp

Seaward, the middle-ramp is composed of medium- to coarse-grained cross-bedded largely dolomitized dolopackstone-grainstone with matrix of dolomite cement, with red algae (*Mastophoroids* and *Melobesioids*), molluscs and echinoids, bryozoans, low oxygen foraminifers, large benthic foraminifera (*Heterostegina* and *Amphistegina*), scarce planktonic foraminifera, ex situ epiphytic foraminifers (rotaliids and textularids). Subangular, quartz sand-sized grains and lithoclasts are also present. This facies is characterized by planar to trough cross-bedding dipping angles of 4°-5° and internal lamination mainly dipping W-NW of about 10°-20°. Cross-stratification may be locally destroyed by bioturbation. These bedforms have been interpreted as subaqueous 2D-dunes with compound cross-bedding produced by the migration of superposed small bedforms (*sensu* Ashley, 1990, in Pomar *et al.*, 2002).

Based on foraminifera and red algae associations and on wave related structures, depth range of -15 to -50 m has been suggested for the middle ramp (Fig.2.5 and 2.6-7) (Mateu-



Vicens *et al.*, 2008), which means the part of the ramp between fair-weather wave-base and storm-wave-base. Large benthic foraminifera such as *Amphistegina* and *Heterostegina*, in fact, occur preferentially in the middle and deeper part of the photic zone in tropical to subtropical environments (Hottinger, 1997). Red algae are often found in pockets of rhodoliths embedded in cross-bedded grainstones, in the lower part of the middle-ramp.

The presence of cross-bedded grainstones represent subaqueous dunes produced by episodic, unidirectional sub-wave-base currents; the middle ramp is thought to be dominated by unidirectional currents, paralleling the bathymetric contour lines that were able to rework bioclastic sediment produced below fair-weather wave-base.

#### *Ramp slope: Upper ramp slope and Lower ramp slope*

Ramp slope facies are present as large-scale clinobeds dipping 15°-20° basinwards, those have a minimum visible length that ranges from 100 to 200 m and prograde mainly on a SW direction, for 2,5 km. Clinobeds are composed of rhodolithic rudstones to floatstones, that alternate with grainstone intervals containing rhodolithic rich-layers. The *Upper ramp slope* is mainly composed of red-algae rudstone to grainstone clinobeds: *in situ* rhodoliths and red algal debris interbedded with coarse- to medium-grained grainstones, rich in red algal fragments, echinoids, bryozoans and foraminifera (low oxygen foraminifers, *Heterostegina*, *Amphostegina* but not very abundant), planktonic foraminifers, molluscs and echinoids, filter feeders). Red algae genera found in the ramp slope include Melobesioids (*Lithothamnion*, *Mesophyllum*), mastophoroids (*Spongites* and *Lithoporella*), lithophylloids (*Titanoderma* and *Lithophyllum*) and *Sporolithon* (Pomar *et al.*, 2002; Brandano *et al.*, 2005) and their fragments range from rounded to angular. Quartz grains and lithoclasts can be abundant. The occurrence of complete rhodoliths together with red-algal fragments indicate a deposition close to the production locus. The more rounded fragments may represent the sediment fraction transported seaward from the middle ramp by currents. Dolomite replacement is pervasive.

The progradational character of the clinobeds and the steepened slope indicate a zone of increased sedimentation rate due to sediments produced in situ and to sediment swept by waves and currents from inner and middle ramp (Pomar, 2001a). The association of LBF and red algae found along the slope correspond to diminishing light intensity as a consequence of increasing depth or nutrient flux and water depth has been estimated being -50m in the upper slope and -80m at the toe-of-slope (Mateu-Vicens *et al.*, 2008).

These progradational clinofolds represent a progressive seaward shifting of the locus of main deposition, forming a depositional slope below wave-base. Rhodoliths and coralline algae (branching and foliose), growing in the deepest part of the photic zone (oligophotic), were episodically moved by storm-induced currents but mostly represent 'in situ' accumulation.

The rhodolithic clinobeds in the *Lower ramp slope facies*, pinch out and interfinger with graded, cross bedded or massive rudstones to grainstones/packstones. These coarser-texture layers can be found both in tabular and channalized beds and they have been interpreted to

represent turbiditic and debris flow deposits. These intervals are composed by LBF (including *Borealis*), epiphytic foraminifers and red algae. Massive or with convex-up to horizontal lamination floatstones are composed of fragments of echinoids, molluscs, large bivalves, bryozoans and very rare fragments of coral (*Porites*) and they can be found in a sandy matrix. Pectinids, serpulids and entire brachiopods are found in more massive grainstone/packstone intervals. The very low P/B ratios has been interpreted by Mateu-Vicens et al. (2008) as reflecting active downslope sediment-transport processes along slope.

Small-scale bedforms of cross-bedded grainstones migrating westward, parallel to the slope, represent reworking of carbonate sands by bottom current flowing parallel to depositional strike, on a slope dipping up to 10° (Pomar et al., 2002). They are composed of recrystallized skeletal grains with accessory quartz. The absence of photo dependent organisms place the lower slope in the lower end of the photic zone. The deposits found in this environment represent sediment that has been transported downslope by gravity flows and successively reworked by bottom currents.

#### *Toe-of-slope and Outer ramp*

Passing towards the outer ramp the slope interfingers basinward with thinly bedded, gently undulated fine-grained dolopackstone/wackestone graded beds that have been interpreted as turbiditic deposits. Common skeletal components of the outer ramp lithofacies are planktonic and small benthonic foraminifera with subordinated echinoid tests and spines, pectinids and bryozoans colonies are frequent in some beds. Channel-fill deposits and graded packstones/grainstones are present in more proximal settings and they contain fragments of red algae, echinoids, molluscs and bryozoans, planktonic and benthic foraminifera (mainly rotaliids and textulariids). The laminated fine-grained wackestone/packstone in proximal settings may interfinger with graded packstone/wackestone that are interpreted as distal turbiditic deposits, and channel-fill deposits that have been interpreted as tongue of debris-flow at the toe-of-slope. Those are composed of fragments of red algae, echinoids, molluscs and bryozoans, planktonic and benthic foraminifera.

The absence of in situ light-dependent skeletal components places the outer ramp below the photic zone (Pomar, 2001a; Mateu-Vicens *et al.*, 2008). These sediments dip gently SW (basinward) (<10°). On a larger scale, bedding is slightly undulated in a strike direction with some 100 m in wavelength and up to 1-2 m in height. Wavy features are partly attributed to depositional processes, but others are associated with shear bands and to syndimentary gliding deformation (Pomar *et al.*, 2002).

The gently basinward-dipping beds are truncated by large scale troughs, up to 1km wide and 60 m deep with axis oriented along depositional dip. These troughs are in-filled with the same fine-grained wackestone/packstones. The coarse-grained backset-beds are commonly found along the axis of these troughs.

At the base-of-slope in a distal position, large-scale coarse-grained cross-bedded grainstone units interbedded with the fine-grained wackestone/packstone. These units are composed of well-sorted, coarse-grained, red algae debris and benthic foraminifera (mainly miliolids and textulariids). Laminae dip 10-20° NW. These grainstone have been interpreted by Pomar et al., (2002), to correspond to large 3D subaqueous dunes (*sensu* Ashley, 1990). They represent extensive along-slope transport and accumulation of carbonate sands by bottom currents flowing towards the NW, paralleling the depositional strike.

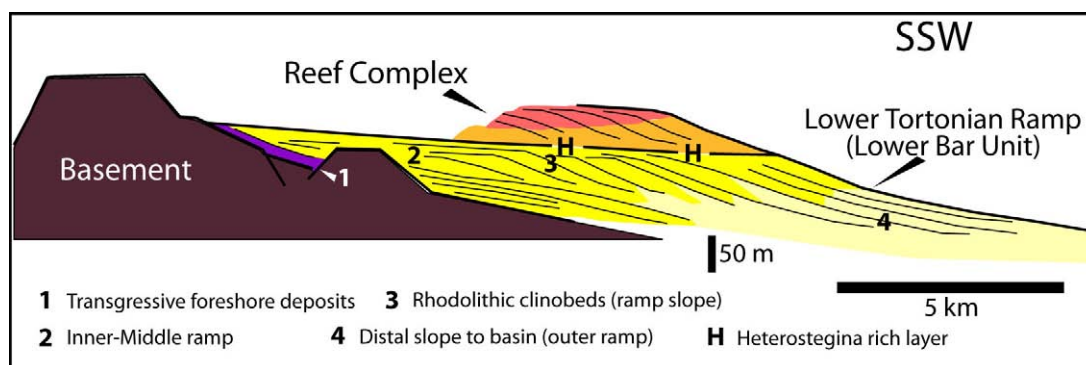


Fig. 2.8 Synthetic cross-section of Menorca, showing the stratigraphic relationships of Upper Miocene depositional units. Based on outcrop data, mainly from the eastern and western sides of the island, and water-well data (modified from Obrador et al., 1992). (Slightly modified from Pomar et al., 2002). The architectural geometry of the carbonate platform noticeably changed from the lower Tortonian ramp to the Reef complex. The change from a distally steepened ramp into a rimmed platform completely change the profile, the morphology of the topography of the depositional system.

## 2.2 The Reef Complex

The Upper Tortonian-Lower Messinian unit is represented by the Reef Complex, a progradational reef-rimmed platform that reaches a maximum thickness of about 180 m and it is found in all the Balearic Islands. On Mallorca, it conformably overlies at the depocenter the *Heterostegina calcisiltites* and unconformably on the margins on the folded basement. The upper boundary is an erosion surface with Karstic caves and paleocliffs.

These reef complexes developed in shallow submerged areas around islands, extensively prograding on the southern margins of the three largest islands (Menorca, Mallorca and Ibiza-Formentera), suggesting that this was their leeward side (Pomar, 2005).

The most extensive accumulation of this rimmed platform is the Lluçmajor Platform, a 20 km-wide platform cropping out in Mallorca. The Reef Complex is composed of similar lithofacies defined by their lithology, constituents, stratification and relationships on both Menorca and Mallorca islands (Pomar, 1991; Pomar and Ward, 1994, 1995, 1999; Pomar et al., 1996).

The Reef Complex on the Island of Menorca, is just partly exposed where it has been mostly removed by erosion but it is very well and largely exposed on Mallorca (Pomar and Ward, 1995; Pomar et al., 1996), (Fig.2.4). The Reef Complex in Menorca (Obrador *et al.*, 1983a, b,

1992; Jurado 1985) unconformably overlies the pre-late Miocene rocks (Fig.2.8). The lower boundary is erosive at the margin of the basin while it's conformable over the Migjorn ramp. The upper boundary is an erosive surface. The Unit presents lithofacies very similar to those described at the near Island of Mallorca. The rocks of this depositional sequence are commonly partly-to completely dolomitized and four major lithofacies have been distinguished (Pomar et al., 1996).

Lagoonal lithofacies have been subdivided in outer-, middle- and inner-lagoon lithofacies: *outer lagoon* rocks are characterized by coral patch reefs (*Porites*, *Tarbellastraea* and minor amounts of *Siderastraea*) and horizontal layers of skeletal grainstone and packstone with lenses of coral breccia. Outer-lagoon grainstone and packstone are composed of abundant red algal fragments and rhodoliths, echinoids, benthic foraminifera and molluscs; common to rare constituents are also serpulids worm tubes, *Halimeda*, bryozoans, miliolids and peloids. *Middle lagoon* lithofacies is composed mainly of unstratified packstone/grainstone with red algae, echinoids, benthic foraminifera and molluscs, bryozoan, *Halimeda* and coral fragments, peloids and ceritid gastropods can be present. *Inner lagoon* rocks are composed of thin- to medium-bedded grainstone, packstone, and mudstone layers with abundant foraminifera and molluscs. Foraminifera like alveolinidis, soritids and trochamminids can be found. Some beds are dominated by pellets and peloids, while others by ceritid gastropods. Ooids, ostracods, red algae, oncolites, and oogonia of charophyta are also present. In this lithofacies stromatolites, thrombolites, sub aerial crusts and paleosoils are also found with frequent rhizcretions preserved in mangrove-swamp lime mudstone.

*Reef-core lithofacies*: this lithofacies interfingers landward with lagoonal lithofacies and basinward with fore reef-slope lithofacies, and it is composed by massive coral-reef limestone and dolostone. The reef framework is constructed only by three genera: *Porites*, *Tarbellastraea* and minor amounts of *Siderastraea*. Secondary components of the reef-structure are encrustation of red algae, foraminifera, bryozoans, worm tubes, vermetid gastropods and microcrystalline rinds and crusts (cyanobacteria?). In the lower part of the reef, coral build-ups are inter layered with medium to coarse skeletal dolograins.

*Reef slope lithofacies* have been distinguished in distal and proximal; they consist of a succession of clinoform-beds tens to hundreds of meters long, composed of dolomitized coarse-skeletal grainstone and packstone. Distal-reef-slope deposits are gently dipping (<10°), poorly stratified, intensely burrowed, red algae-mollusc dolopackstone to dolograins. These beds are characterized by rhodoliths, large whole-shell bivalves, sclerosponges and large oysters with local bioherms of branching and encrusting red algae. Proximal-reef-slope has steeper dipping angles (10° to 30°) and interfinger landward with *in situ* coral reefs. It is composed of dolomitized skeletal and intraclastic grainstone, packstone, rudstone and floatstone with red algae fragments and rhodoliths, coral fragments, bivalves, gastropods, echinoids, bryozoans and *Halimeda*.

*Open-shelf lithofacies*: this facies is characterized by flat lying, poorly bedded because of bioturbation and mostly dolomitized fine-grained skeletal packstone/wackestone. Two different types are distinguished: a *red algal lithofacies*, coarse-grained, poorly sorted, red algae-rich grainstone/packstone to rudstone/floatstone with rhodoliths and other skeletal components such as oysters, pectinids, large foraminifer *Heterostegina* and corals like *Tarbellastreae* and *Porites*; a *packstone-wackestone with planktonic foraminifers lithofacies* that usually overlies the red-algae-rich open-shelf deposits both in cores and outcrops along the western coast of the Lluçmajor Platform. This lithofacies can be followed into distal slope strata of the reef complex and it is characterized by fine-grained packstone and wackestone rich in planktonic foraminifera, ostracodes and very fine detritus of oysters, bivalves, echinoids and red algae.

The Reef Complex has been dated to late Tortonian-early Messinian based on regional considerations (Pomar *et al.* 1983, 1996; Pomar, 2001a), planktonic foraminiferal assemblages (N17 foraminiferal biozone of Blow, Bizon *et al.*, 1973; Alvaro *et al.*, 1984). Sr isotopes estimates provide a late Tortonian age (Oswald, 1992) while K-Ar dates are  $7.0 \pm 0.2$  Ma for biotite and  $6.0 \pm 0.2$  Ma for sanidine phenocrystals (volcanic ash) indicating early Messinian age near Cap Blanc, Mallorca (Pomar *et al.*, 1996). More recent Ar-Ar dating has provided an age of 6.4 Ma for the same volcanic minerals (Pomar, personal com.; unpublished data).

## 3. SEDIMENTARY FACIES

### 3.1 Basic concepts and definitions

In a sedimentological analysis one of the first step is to recognize sedimentary facies and to interpret them to understand their origin (Reading and Levell, 1996). Sedimentary facies are the basic types of sedimentary deposits, distinguished macroscopically on a descriptive basis as the elementary "building blocks" of a sedimentary succession (Nemec, lecture compendium). The aim of define sedimentary facies is to recognize the principal processes of sediment transport and deposition which may be directly diagnostic of a particular sedimentary environment while others can be found in different environments as for example current-ripples): in the latter case, facies association become fundamental because are more informative (see chapter 4).

The term "facies" appears for the first time into geology thanks to Nicholas Steno (1669) with the meaning of the entire aspect of a part of the earth's surface in an interval of time.

The modern usage of the term "facies" was introduced by Gressly (1838) who used it to refer to the sum total of the lithological and palaeontological aspects of a stratigraphic unit.

This term has long been the subject of debate, in fact it has been used with a wide variation of meanings. The discussion have been centred on: 1) does the term implies an intangible set of characteristics, as opposed to the rock body itself?; 2) does the term have to be use only to refer to "areally restricted parts of a designated stratigraphic unit" (Moore, 1949), or as used by Gressly also to stratigraphically unconfined rock bodies?; 3) does the term to be merely descriptive or also interpretative? (Walker, 1992).

Walker (1992) suggest that the most useful modern working definition of the term "facies" was given by Middleton (1978): *"the more common (modern) usage is exemplified by de Raaf et al., (1965) who subdivided a group of three formations into a cyclical repetition of a number of facies distinguished by lithological, structural and organic aspects detectable in the field. The facies may be given informal designations ("Facies A" etc.) or brief descriptive designations (e.g. " laminated siltstone facies") and it is understood that hey are units that will ultimately be given an environmental interpretation; but the facies definition is itself quite objective and based on the total field aspect of the rocks themselves... The key to the interpretation of facies is to combine observations made on their spatial relations and internal characteristics (lithology and sedimentary structures) with comparative information from other well-studied stratigraphic units, and particularly from studies of modern sedimentary environments"*.

The subdivision in facies is therefore a classification procedure, whose degree of subdivision is determined mainly by the aims of the study whereas the scale at which the subdivision has to be done depends on the detail that we want to achieve but mostly by the quality of the rocks available and at last, but not least, the time available.

Different ideas on sedimentary facies come from different groups since each group's concept is based on traditions, particular regional geology and nature of the data (outcrop, wireline log core etc.). In Reading and Levell (1996, p.18-19) three main schools are summarized: the group of the *British/Dutch/Shell School*, represented in the 1960s by Allen, Bouma, Collinson, de Raaf, Kruit, Kuenen, Middleton, Oomkens, Reading, van Straaten and Walker in Britain, Holland and Canada, by Bernard, Ginsburg, Hsü, Le Blanc, Visher, Wilson of Shell Oil in the USA, by Fischer, Klein and Van Houten from the eastern USA, Mutti and Ricci Lucchi in Italy and many others; the group of the *Gulf Coast School*, from Texas and Louisiana of south-central USA, represented by Brown, Fisher, Fisk, Frazier, Galloway and McGowen; the group of the *Cratonic/North Western/Exxon School* firstly developed by Sloss (1950, 1963) and later reviewed by the Exxon School of seismic interpreters and geologists such as Haq, Mitchum, Posamentier, Sangree, Sarg, Vail and Van Wagoner. The three schools basically came from the fact that they were working on different geological regions where different methodologies at different scales, were possible to be utilized or not, to investigate the subsurface. The first school based its attention on small-scale features of rocks, sedimentary structures and processes, and developed models based around Walter's Law; the approach comes from inland outcrops where tectonic activity made difficult to trace facies distribution both vertically and laterally, but thanks to good streams and/or coastal sections measuring of logs was possible and emphasis was laid on sedimentological, intrinsic and autocyclic causes, and external, allocyclic controls were used only when explanation of facies relationships was exhausted with intrinsic controls. The second school, is based on large areas with insignificant tectonic deformation, with poor outcrops but with data coming from cores, few good quality seismic lines and abundant electric logs; this kind of collection of data leads to regional isopach, sand thickness and sand percentage mapping which takes to interpretation of regional-scale, three-dimensional facies relationships. Therefore a detail facies analysis as in the *British/Dutch/Shell School* is neither possible nor necessary to interpret sedimentary environments, but it allows a wide, lateral correlation with large-scale facies patterns where thick "facies sequences" could be easily laterally linked together as "genetic stratigraphic units" (Frazier, 1974; Galloway, 1989). This model, that focuses on breaks in sedimentation of very slow or no sedimentation, over large-scale system, is suitable where high influx of clastic sediment supply dominate the control on facies patterns in large regions with substantial but even subsidence. The third school focus its attention on unconformities that could be traced for hundreds (or thousands) of kilometres with little apparent facies change (Sloss, 1963). Again emphasis is put on major hiatal bounding surfaces that can be traced for hundreds of kilometres to separate thin but laterally extensive packages of sedimentary facies. This can be applied to regions characterized by tectonic stability and limited sedimentary supply. Only later, the Exxon Production Research Group (Vail, Mitchum & Thompson, 1977) included changing subsidence rates and sediment influx and ideas were applied to onshore outcrop geology (Posamentier & Vail, 1988; Van Wagoner, Posamentier et al., 1988). These facies

patterns were used in models of sequence stratigraphy mainly based on theoretical concepts, largely used in understanding large-scale geology.

Thus, the categories of facies adopted by different research-groups depend upon the scope of a particular study and on the availability of data.

In the present study, the first school approach has been used, because the study area is not so wide and good coastal outcrops are available; the term "facies" has been used in the meaning stated above and suggested by Middleton (1978).

Facies classification is based on merely objective observations but each facies may be individually interpreted in different ways, and facies defined in the field may have ambiguous interpretations. This is because some characteristics that determine a facies may only define for example, a flow regime which can develop in different environment (as for example current ripples). It is therefore important to recognize the interpretative limitations of individual facies and to have the knowledge of the relationships of one facies to another, that means that the sequence in which they occur contributes as much information as the facies themselves. Middleton (1978) pointed out that *"it is understood that (facies) will ultimately be given an environmental interpretation"*. Interpretation of facies has thus to be tightly correlated to their neighbours and have to be grouped into "facies associations" that are thought to be genetically or environmentally related (Reading and Levell, 1996). A particular facies association is thus considered to be a genetically correlated assemblage of spatially related sedimentary facies (Boggs, 1995), which are interpreted to ideally represent a particular sedimentary environment or a peculiar set of physical, chemical and biological settings (Collinson, 1969 in Reading and Levell, 1996, p.20).

The concept of facies distribution and its relationship with distribution of depositional environments in space, was firstly developed and emphasized by Johannes Walther in his Law of the Correlation of Facies (Walther, 1894, p.979 – see Middleton, 1973) who stated *"it is a basic statement of far-reaching significance that only those facies and facies areas can be superimposed primarily which can be observed beside each other at the present time"* (in Walker, 1992?).

Walker (1992) proposes the following definitions:

- **Facies:** *a body of rock characterized by a particular combination of lithology, physical and biological structures that bestow an aspect ("facies") different from the bodies of rock above, below and laterally adjacent.*
- **Facies Association:** *"groups of facies genetically related to one another and which have some environmental significance" (Collinson, 1969, p.207).*
- **Facies succession:** *a vertical succession of facies characterized by a progressive change in one or more parameters, e.g., abundance of sand, grain-size, or sediment structures.*



In this thesis, the classification of facies is based on objective description of rocks that have been divided into different units on the basis of lithology and sedimentary structures. The description of the facies has then be improved with more details regarding components, colour, biogenic features (when present), geometry (thickness, lateral extent, shape, boundary types). In the study of carbonate rocks microfacies analysis in thin section are essential not only to describe and palaeontologically recognize components, but also for example to determined matrix/cement content, orientation of grains (which sometimes is obliterated by superficial dissolution of uneven distribution of dolomitization). Microfacies analysis is today regarded as "the total of all sedimentological and palaeontological data which can be described and classified from thin sections, peels, polished slabs or rock samples" (Flügel, 2004).

The grouping of facies into facies associations has been based on the interpretation of the position of the depositional environment and on the correlated process that drove facies deposition. In chapter 4, four main facies associations have been distinguished in the stratigraphic succession. The spatial organization of their geometrical architecture and relationship are shown in various figures since they don't always follow a particular pattern of distribution. The characteristics of each facies association are summarized in tables in Figures 3.3.1.7, 3.4.1.13 and 3.5.1.11. Facies association are described and interpreted to provide a sedimentological study of the processes dominating in this palaeoenvironments and an interpretation of the peculiarities of the conditions that drove the deposition of bedforms such as backset bedded deposits. Since all the described deposits are related to sediment gravity flows along the ramp slope, the subdivision has been based on two main observations: the proximity to the slope, therefore base-of-slope deposits and proximal outer-ramp deposits, and the sedimentary structures that characterize them and which provide more information to interpret the sedimentary gravity flow that deposited them.

The interpretation of facies associations is also based on previous studies (Obrador et al., 1992; Pomar et al., 2002; Mateu-Vicens et al., 2008).

The description of facies that follows, thus comprises the observations done both at a macroscopic scale and at a microscopic scale in thin section. Table showing pictures showing the major features characterizing the studied deposits are found at the end of this chapter.

In the following sections, a description of facies has been done for each studied locality and then in chapter 4 follows the relative interpretation with the grouping of facies into facies associations.

The terms used to describe carbonate porosity in thin sections are the one used by Flügel (2004) which follows the porosity classification of Choquette and Pray (1970) (see Fig.7.5 in Flügel, 2004 p.280).

### 3.2 The studied outcrops

The studied area is found along the sea cliffs of the southern coast (Fig.3.2.1) in the surroundings of Es Canutells. In this locality crop out the ramp slope deposits and the outer-ramp deposits; it is here possible to study the transition from the slope into the basin through the interfingering of the more distal base-of-slope deposits with the more proximal part of the outer ramp deposits (Fig.3.2.2). The change from one type of the deposits to the other is transitional and not sharp, the separating line in Fig.3.2.3 is meant to be a schematic drawing of this interfingering.



Fig.3.2.1 Satellite picture of the Island of Menorca and position of the study area (yellow square); in blue the three studied outcrops along the sea-cliffs.

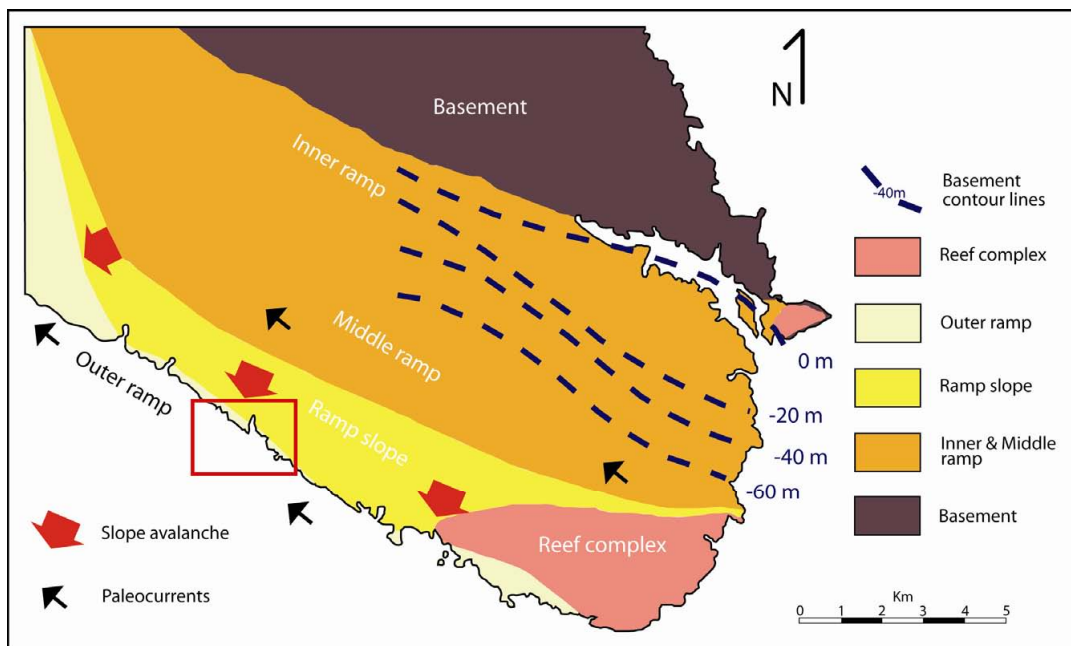


Fig.3.2.2 Geological schematic map of the southern part of the island of Menorca; the boundaries between one ramp facies to the other are transitional contact and not sharp. The red square indicates the study area (slightly modified from Pomar et al., 2002).

The sedimentary structures, backset beds, studied in this thesis are found at the base of the slope of the lower Tortonian distally steepened ramp of Menorca (Fig.3.2.3). They are embedded within toe-of-slope sediment and outer ramp sediment.

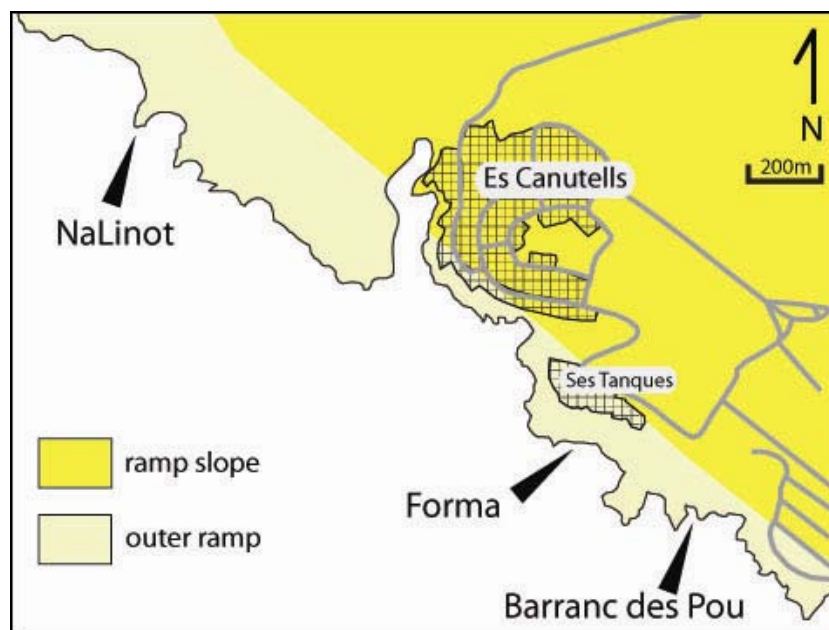
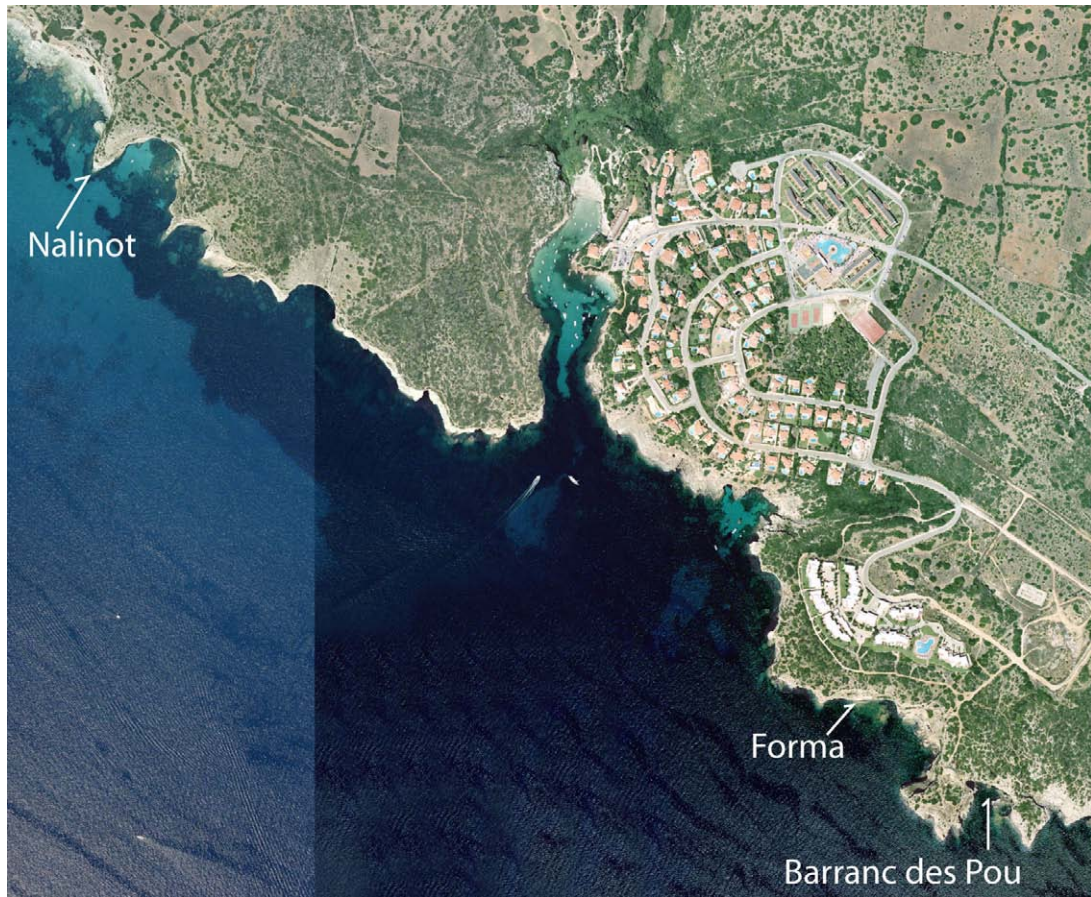


Fig.3.2.3 (Above) Satellite photo of the studied area. (Below) Simplified map of the studied area close to the locality of Es Canutells. The studied outcrops are found at the transition between toe-of-slope and outer ramp sediment.

Three localities have been study in detail representing the base-of-slope outer ramp transition: these are from south to north Barranc des Pou, Forma and Na Linot.

The studied deposits are found along the axis of large-scale slide scars that truncate the outer ramp sediments (Fig.3.2.4).

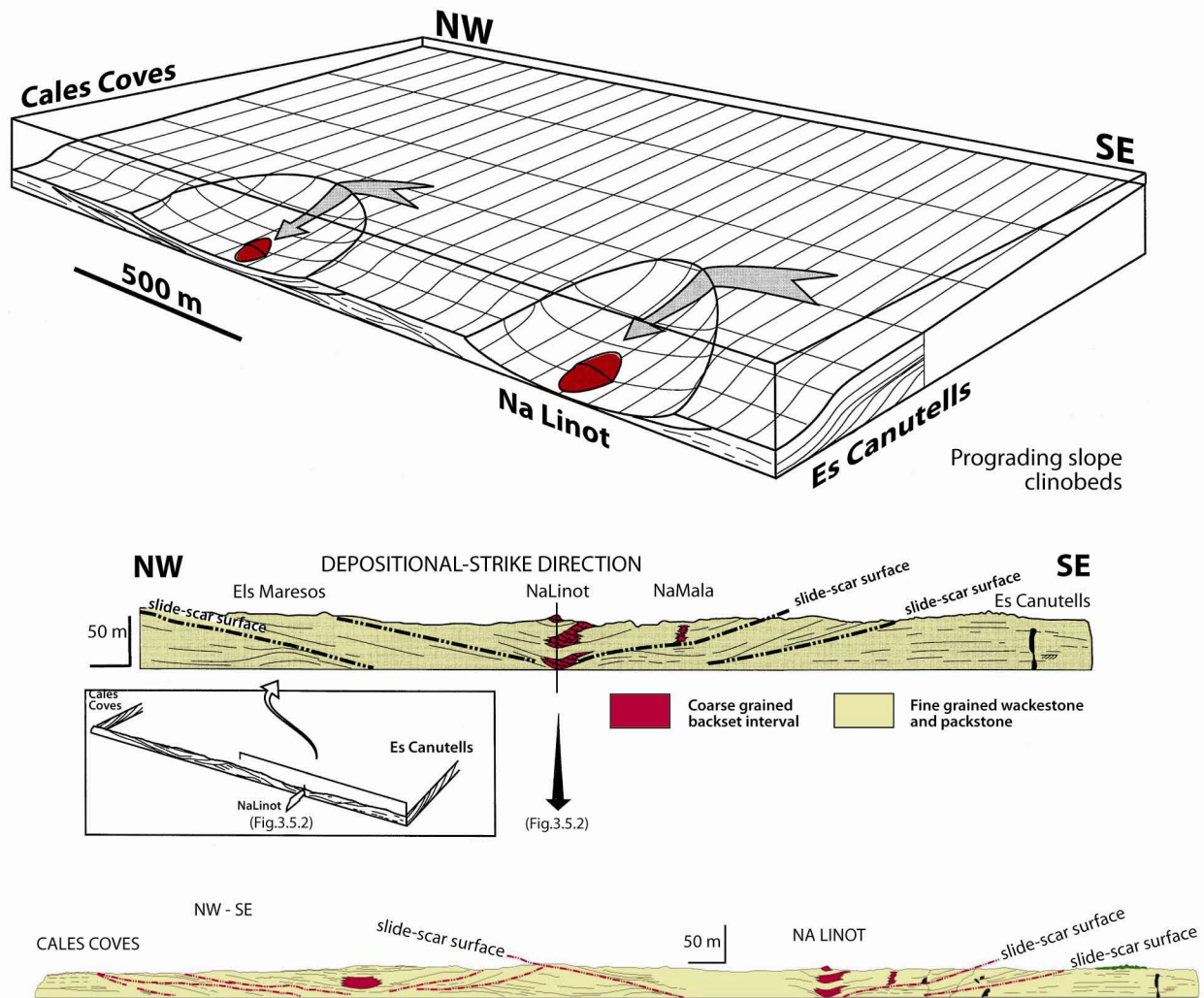


Fig. 3.2.4 (Upper picture) Position of backset beds units at the toe-of-slope of the distally steepened ramp; large-scale slide-scars produced by collapses along the slope of the Lower Tortonian ramp create large depressions that acted as channels funnelling platform debris downslope to form coarse-grained backsets. (Middle and lower picture) Section along the sea cliffs, in the direction of depositional strike; drawn from photomosaics. Coarse-grained backsets are placed along the axis of large-scale slide-scars. (modified from Pomar et al., 2002).

In all three localities deposits characterized by backset bedding have been observed and studied. These deposits described are present in different intervals, and are not related to only one depositional event, but they are found in several successive intervals.

The studied deposits and the associated slide-scars are known along the sea-cliffs only in this part of the island coastline.

### 3.3 Barranc des Pou

The outcrop of Barranc des Pou is found along the cliffs south of the locality of Es Canutells (Fig.3.3.1), and it is the first known place along the coast where coarse-grained backset bedded deposits crop out.

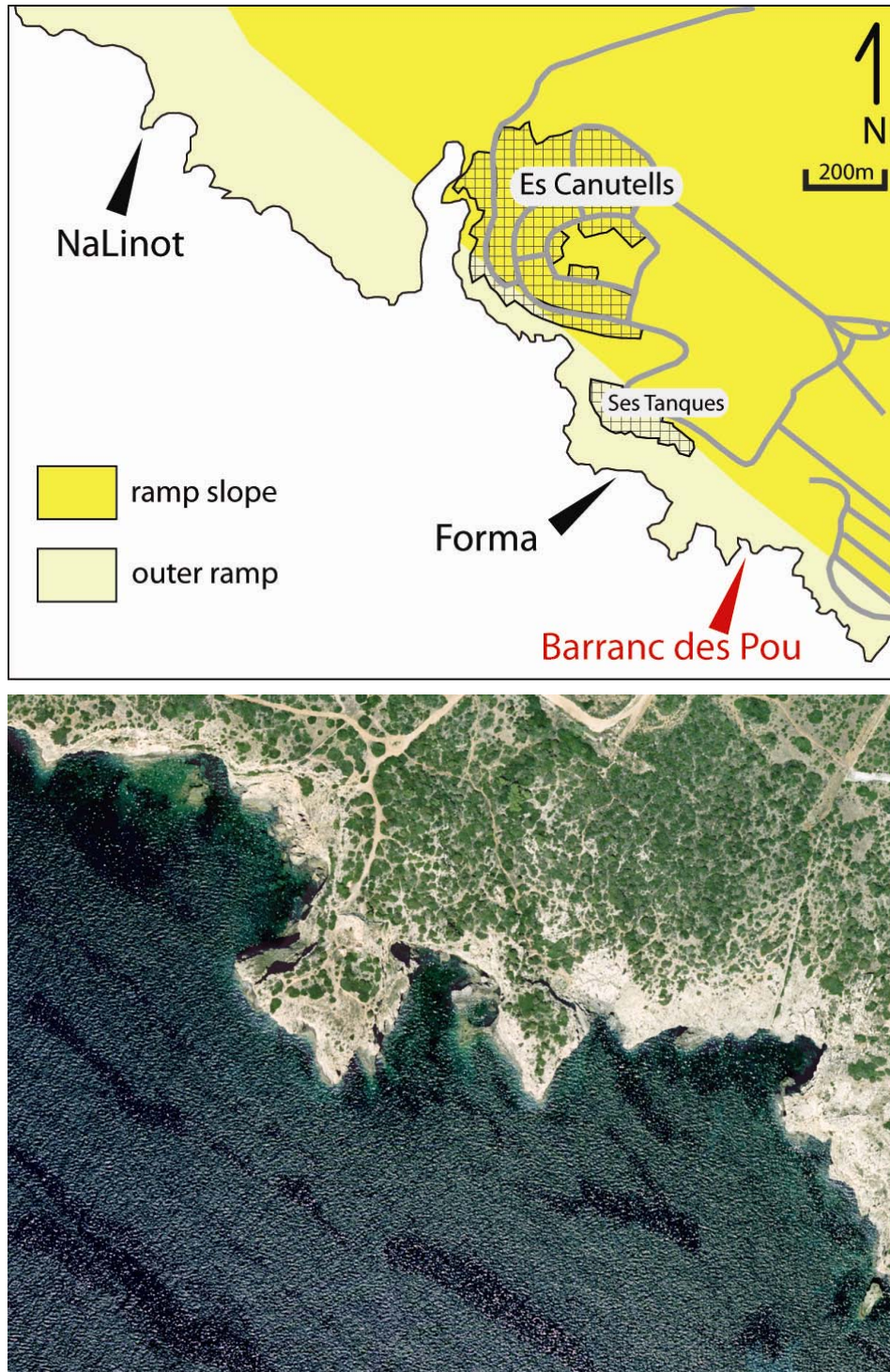


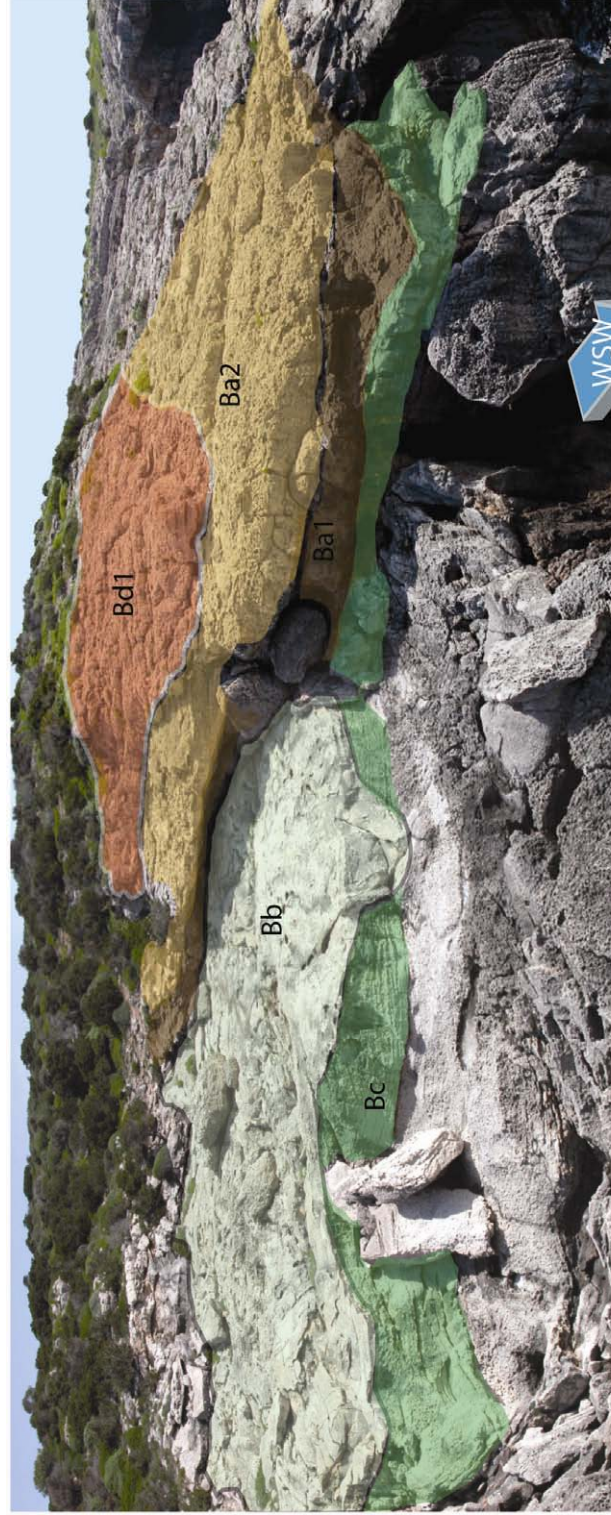
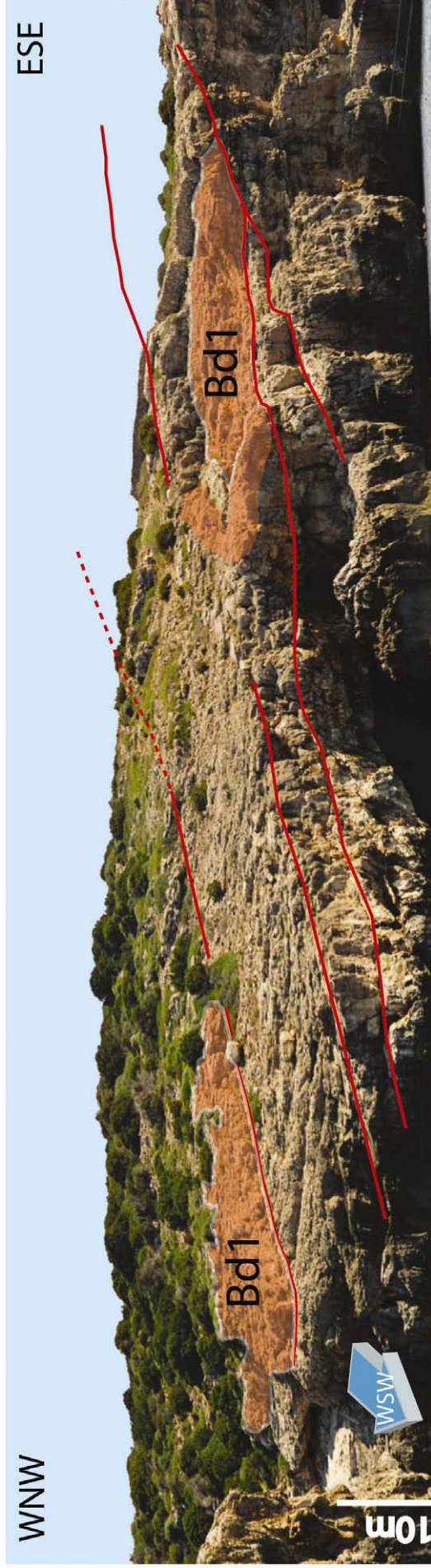
Fig.3.3.1 (Above) Location map of the locality of Barranc des Pou; (below) satellite photo of the studied area.

In this locality it is possible to study sediments belonging to the lower Tortonian distally steepened ramp; in particular here it is possible to analyze the proximal transition between base-of-slope deposits and outer ramp sediments.

This outcrop is characterized by the superimposition of different units of coarse to very coarse bioclastic sediments (Fig.3.3.2), mainly dipping southwest with angles ranging from 8° to 15°, according to the main direction of progradation of the carbonate ramp.

In this locality several logs have been measured and sampled and photo-mosaic drawing has been widely used to better understand the lateral relationships among different units since those are mainly laterally discontinuous, there are superimposed over each other with irregular erosive surfaces and truncated by large-scale slump/slide scars. The stratigraphical order of the units outcropping in this area has been reconstructed mainly on the base of geometrical and architectural relationship, since biostratigraphical resolution is too low and this tool resulted in this case to be useless.

Four main facies have been recognized based on lithological features (texture and grain-size) and sedimentary structures.



- Bd1 Rhodolitic-rich backset bedded conglomerate
- Ba2 Bioturbated packstone
- Ba1 Rippled dolomitized packstone
- Bb Channelled bioclastic grainstone
- Bc Bioclastic floatstone
- Direction of ramp progradation

FFig. 3.3.2 View of Barranc de Pou outcrop: top picture shows the position of backset beds lying on erosive surfaces; lower picture shows the distribution of underlying units and ramp prograding direction.

### 3.3.1 Facies description

#### Facies Ba

##### Subfacies Ba1

This facies is characterized by fine to very fine grained bioclastic wackestone/packstone often presenting current-ripple cross-lamination. The cross-lamination is visible at a scale from millimeters to 1 centimeter thick (Fig.3.3.1.1, A and B). Beds are sheet-like, often amalgamated, with thickness that varies from 2m to 8m. The lower and upper boundaries are sharp.

Bioclasts are mainly are mainly dissolved with cavities elongated along lamination. Where present they are fragments of coralline red algae with abundant fragments of *Mesophyllum*, echinoids plates and mollusc fragments. Benthic foraminifera, macroforaminifers and few planktonics are also present (Fig.3.3.1.1). Bioclasts are oriented along lamination (Fig.3.3.1.2, E).

Large echinoids test are frequently found. Along lamination bivalves like *Pectens*, 4-5 cm large, are very abundant in some layers. Shells are with concave-up, concave-down valves oriented along lamination. Rhodoliths are very rare but have been found. Few extra-clasts < 1 mm are also found.

Porosity is high (about 30%), both intra- and inter-granular, mainly due to dissolution and it is often reduced by the precipitation of calcitic cements. Calcitic rims are present both around the grains and partly in-filling the dissolved inner parts. Beds are sometimes pervaded by dolomitization and sometimes dolomitization is patchy.

Beds dip 8°-15° SW.

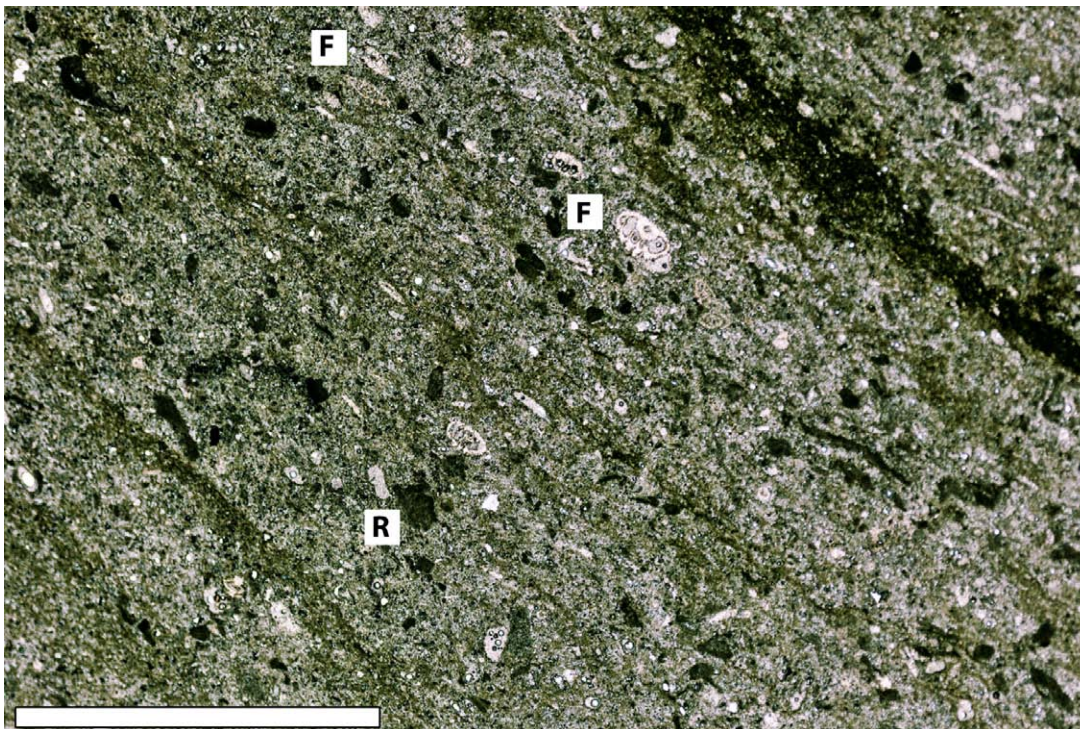


Fig.3.3.1.1  
Thin section of  
facies Ba1.  
Packstone,  
bioclastic rich.  
(F) Benthic  
foraminifers,  
(R) coralline  
red algae  
fragments. Bar  
for scale = 1cm.  
Sample BP18.



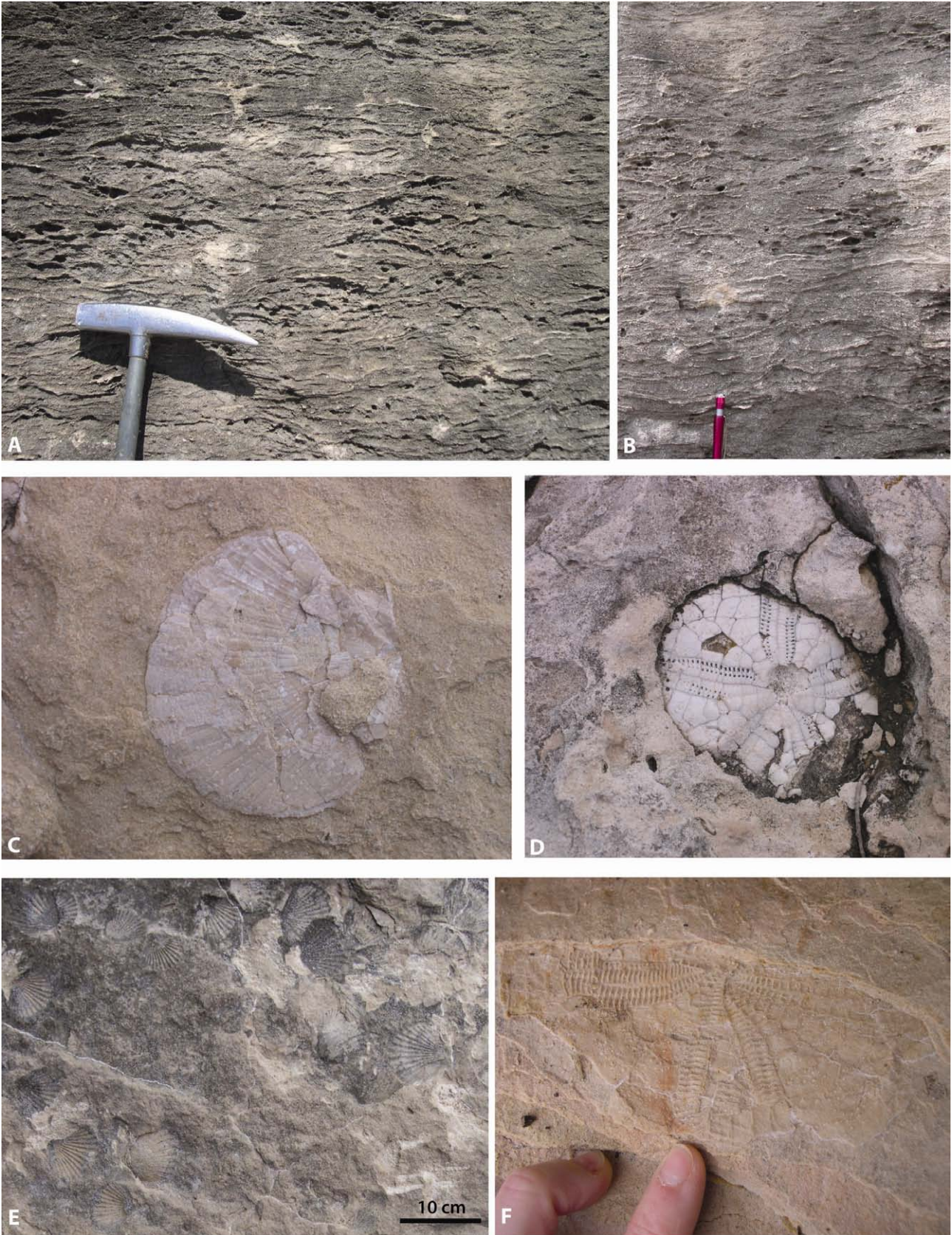


Fig. 3.3.1.2 Facies Ba1, (A,B) current ripple cross lamination; (C,D) left Pectens, right echinoid; (E) large number of pectens aligned along strata surface, (F) large echinoids.

## Subfacies Ba2

Highly bioturbated (*Glossifungites?* - *Thalassinoides??*) wackestone/packstone (Fig.3.3.1.3). This facies is composed of a fine to very fine sand-size calcarenite and destroyed by bioturbation. Any possible pre-existing sedimentary structures have been completely destroyed by bioturbation. This facies is present in sheet-like beds of thickness ranging from 1 m to 4 m. Porosity is high (30%) and due to dissolution.

Beds dip 8° -15° SW.



Fig.3.3.1.3 Pervasive bioturbation in facies Ba2.

## **Facies Bb**

This facies is a bioclastic-rich grainstone, sometimes packstone. Grains size is of a medium to coarse-grained calcarenite, sometimes normally graded at the base and sometimes with a slightly visible planar parallel stratification towards the upper part.

Matrix is of microsparitic cement, sometimes of equant mosaic type. Bioclasts composing the grainstone are foraminifers (benthic foraminifers, biserials, miliolids, macroforams), echinoid

plates and spines, small bivalves, fragments of coralline red algae (*Mesophyllum*, *Lithophyllum*, *Sporolithon*) and molluscs, bryozoans (Fig.3.3.1.4 and 3.3.1.5). Extra-clasts are also found but they are not frequent. Rhodoliths of 3-4 cm are also found (Fig.3.3.1.5), but

they are more frequent in very small fragments. Grains are well rounded, mainly smaller than 1 mm, quite well sorted. Elongated bioclasts are oriented sub-parallel to lamination.

Bioclasts are sometimes replaced by calcitic cement. Some grains present a rim of radial-fibrous cement sometimes with different growth-zones. Little bioturbation by serpulids traces have also been found.

Porosity by dissolution is strongly reduce by the precipitation of cements (<10%); it is present around grains that have a rim of granular cement. This facies is the most cemented one found at this locality and it consequently has the lowest porosity which is strongly reduced by cementation.

This facies is found in channel-shaped deposits that elongated on a NE-SW direction for at least 30-40 m, and pinch-out laterally (see two examples in Fig.3.3.2 and Fig.3.3.1.6). Along strike they have trough-shape 150 to 3 m wide and maximum thickness in the trough of 100 to 150 cm. Erosive sharp lower surface and sharp upper boundary.

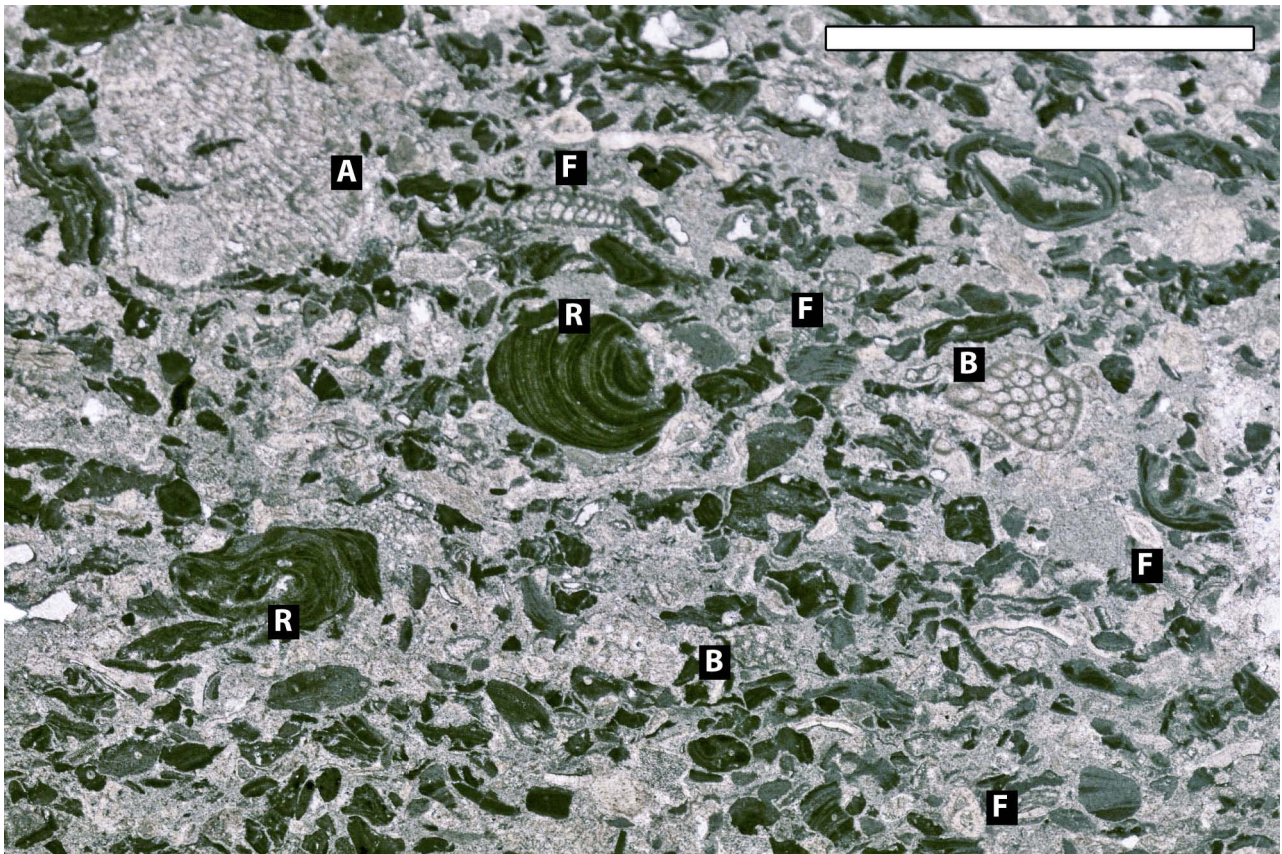


Fig.3.3.1.4 Thin section of Facies Bb. (Above) Grainstone with abundant fragments of (R) coralline red algae, (F) foraminifers, (B) bryozoans, (A) calcareous algae (Solenoporacea?). Scale 1 cm. Sample BP6.

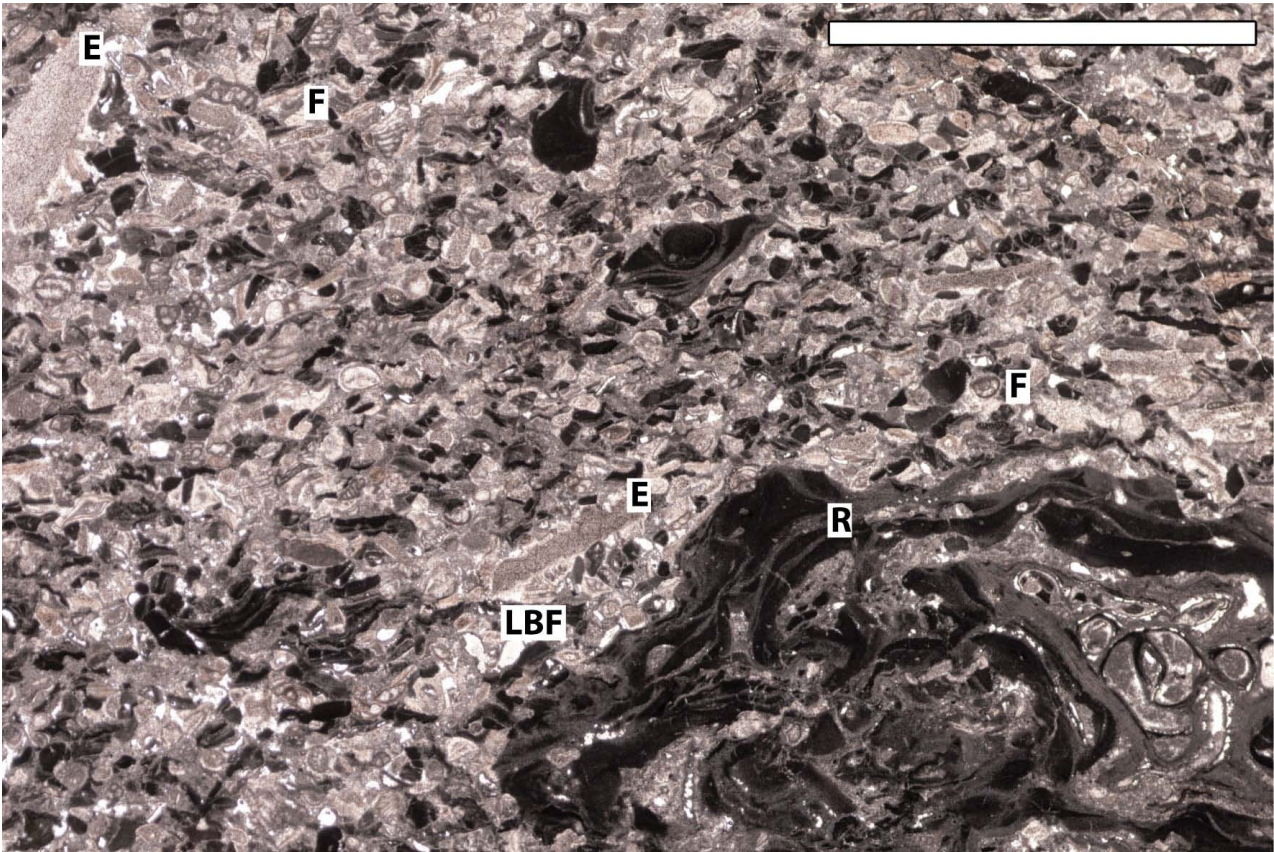


Fig.3.3.1.5 Thin section of Facies Bb. Grainstone dominated by (F) foraminifera, (LBF) large benthic foraminifera, (R) rhodolith. Scale bar 1 cm. Sample F715.

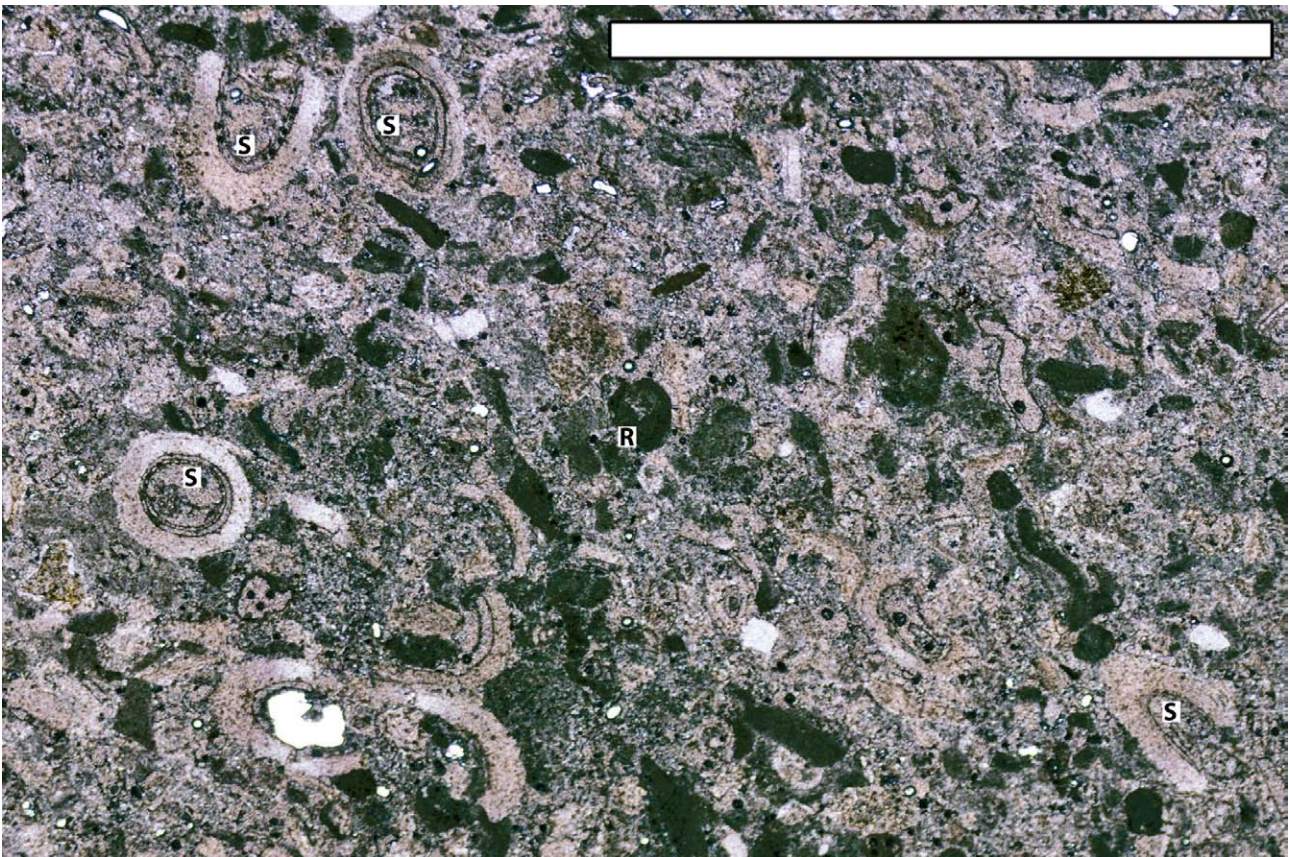
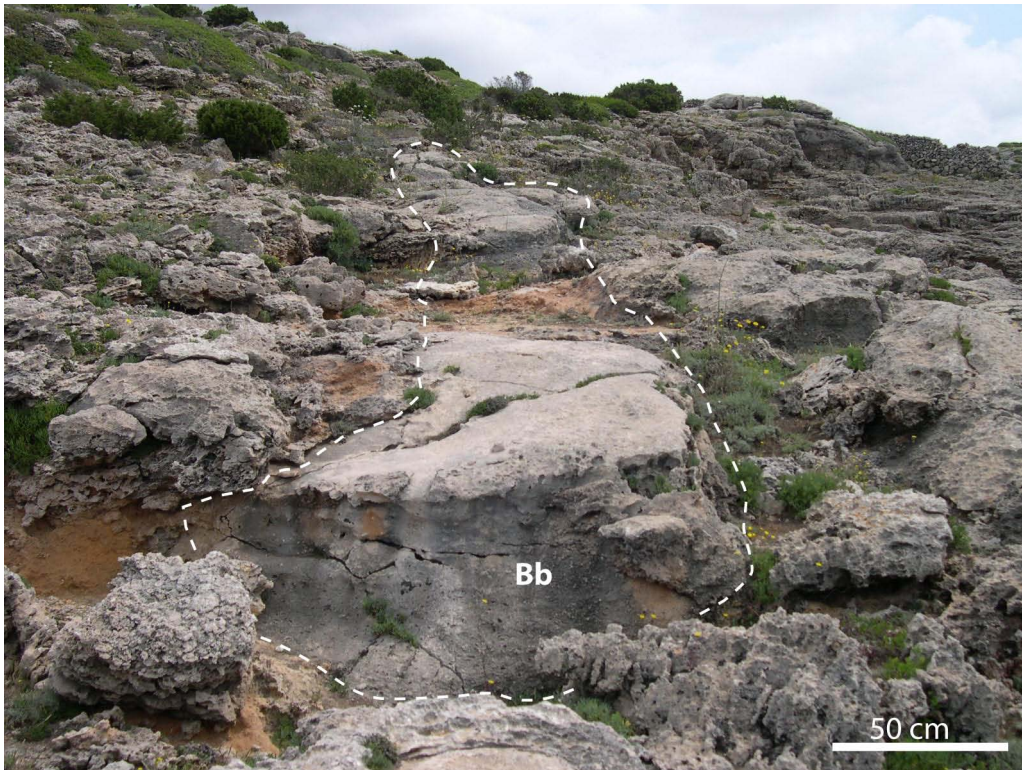


Fig.3.3.1.6 Thin section of Facies Bb. Grainstone with (R) sub-rounded fragments of coralline red algae and abundant (S) serpulids. Scale bar 1 cm. Sample F759.



*Fig. 3.3.1.7 Channelized grainstone of facies Bb. View on a perpendicular to depositional-dip section: in this photo it is visible the channel-shape of this deposit, which has trough 1 m thick.*

## **Facies Bc**

This facies is a bioclastic-rich floatstone to rudstone. The grain sizes present in this matrix-supported conglomerate vary from coarse-sand to pebble size. Beds sometimes are normally graded in the lower part, they may have planar parallel lamination and at times current-ripple cross-lamination. Planar parallel lamination is frequently present when this facies lies below subfacies Bd1 (described below).

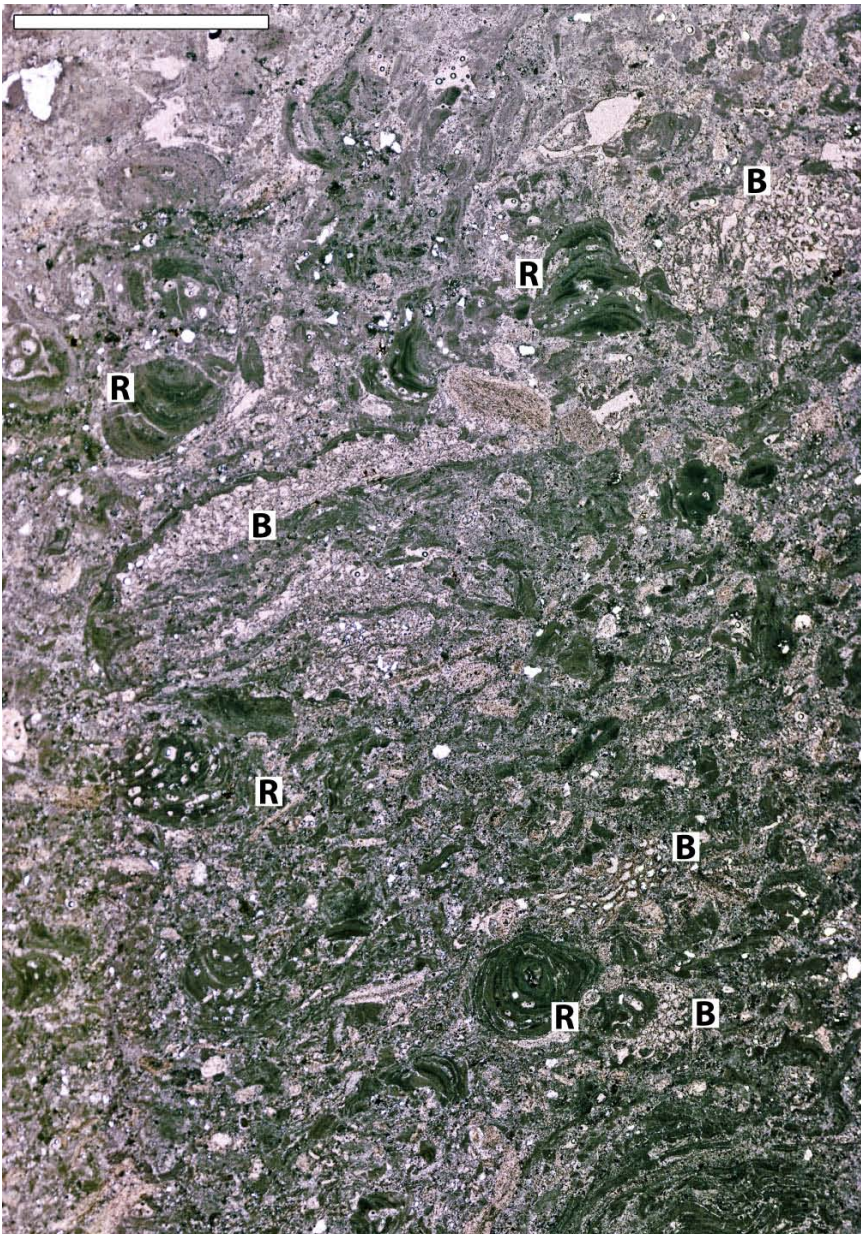


Fig.3.3.1.8 Thin section of facies Bc. Floatstone to rudstone bioclastic rich. Large pieces of (R) coralline red algae, (B) bryozoans, bivalve fragment. Scale bar 1 cm. Sample BP8.

The matrix of this conglomerate, is composed of a coarse to very coarse-grained calcarenite, of bioclastic packstone/grainstone rich in molluscs fragments, bivalves, small gastropods, echinoids and crinoids fragments and plates, bryozoans, benthic foraminifers and fragments of coralline red-algae (*Sporolithon*, *Mesophyllum*, *Lithophyllum*) which dominate this facies Fig.3.3.1.8). Few extra-clasts are also present. Some dissolved bioclasts are completely replaced by cement. Grains in average are < 0,5 mm but several fragments of few millimetres in size are also frequent. Micritic matrix content is reduced while the calcitic cement is abundant, sometimes in large crystals of blocky calcite. Porosity can be low because of precipitation of cement or where present is mainly intra-bioclasts, very probably it is primary porosity (20%).

Large clasts are represented by very large bivalves (*Ostreidae* up to 10 cm) and frequently by rhodoliths of average size 5 cm but can reach 8 cm (Fig.3.3.1.9). Dolomitization can be either patchy or pervasive.

This facies is bounded at the base and at the top, by erosive surfaces and at the base they may present a trough shape about 3 to 4 m wide and 1 m deep.

Beds dip 8°-15° SW (Fig.3.3.2).

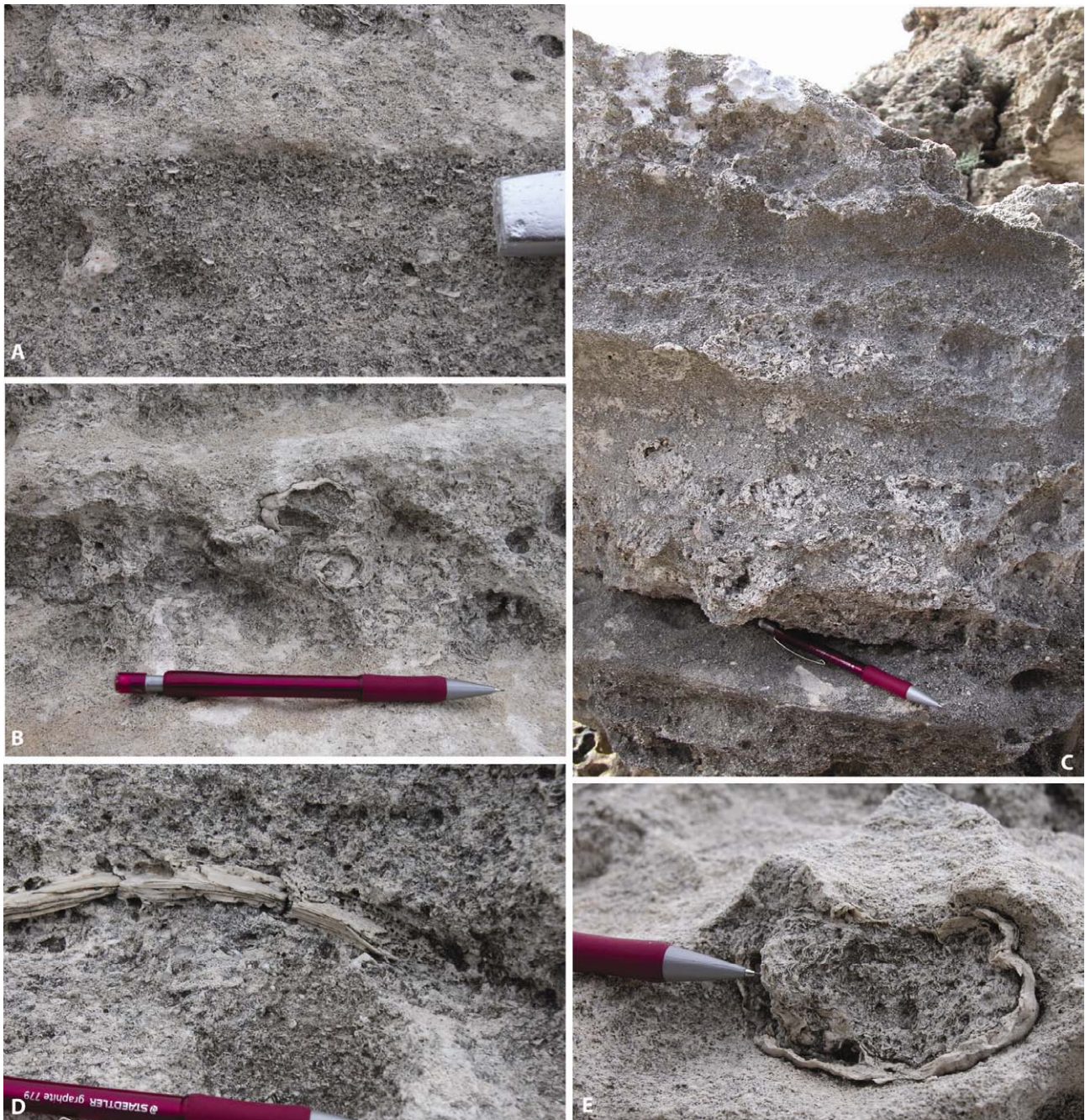


Fig.3.3.1.9 Facies Bc, (A) detail of the coarse-grained highly bioclastic calcarenite, (B) floating rhodolith within the calcarenite, (C) intervals where rhodoliths are concentrated in rows, (D) large valves of ostreids, (E) close-up of a rhodolith..

## Facies Bd

### Subfacies Bd1

This facies is composed of a rhodolith-dominated rudstone and it is characterized by a backset bedding lamination. It is a clast-supported conglomerate where the clasts are represented only by rhodoliths (*Melobesoids*) and the matrix is very poor. Most rhodoliths are 6-7 cm in diameter, but some up to 12-15 cm, they are well sorted, rounded and slightly flattened. Matrix consists of coarse-grained sand-grain-size fragments of red algae, bivalves, echinoids, bryozoans and planktonic and benthic foraminifera (Fig.3.3.1.10).

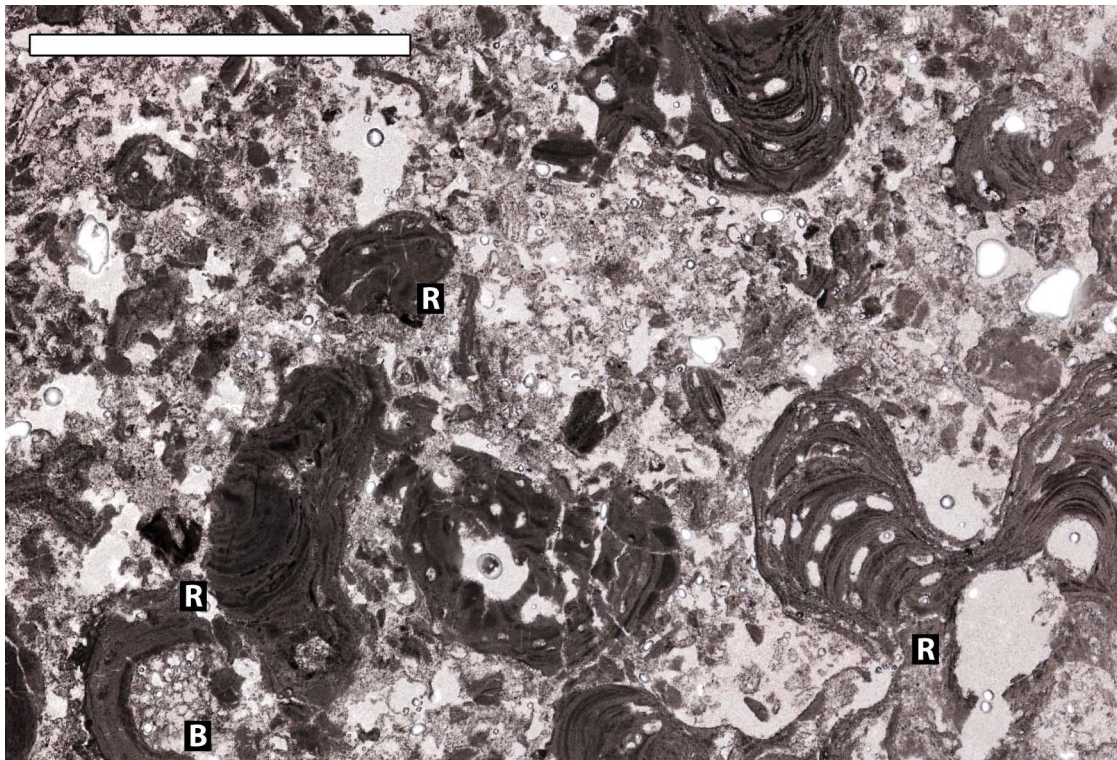


Fig. 3.3.1.10 Thin section of facies Bd1. (R) coralline red algae and rhodoliths; B) bryozoan enveloped with a red algae. Scale bar 1 cm. Sample BP21.

Large 20-30 cm up to 1 m, pieces of laminated packstone (of facies Ba) are also found within these beds (Fig.3.3.1.11). Bioturbation is rarely present. This facies is poorly cemented and porosity is very high (>50%).

Sediments are piled in discrete channel-shape, wedge-shaped bodies, pinching out landward (about 130 cm thick and 15-20 m wide) with internal backset bedded lamination (Fig.3.3.1.12). Lamination dip 75°N and laminae are 5-6 cm thick which is determined by rhodoliths average size. Laminae' s dipping angles tend to increase in the down-dip direction varying from 25° to zero. On an oblique-to-depositional dip section, a large scale trough-cross stratification is visible.

Beds are bounded by erosive surfaces that dip 10° to 15° SW (range 205°N -260°N).



These bodies are stacked in larger bodies that extend up to 30-40 m along depositional dip and 20-40 m along strike with a maximum thickness of 8m. These larger bodies are wedge-shaped pinching out landward and are laterally confined within scours (Fig.3.3.1.11).



Fig.3.3.1.11 (A) View of backset bedded facies Bd1 with channel-shape erosive base (yellow dashed line); detail in the white square shown in the left picture; (B) extra-block found within facies Bd1. It is a piece of the underlying facies Ba.

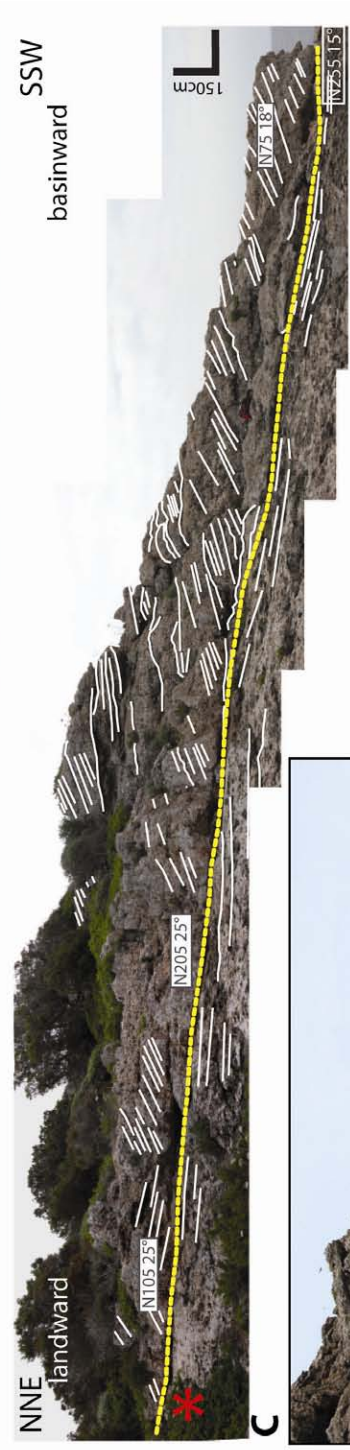
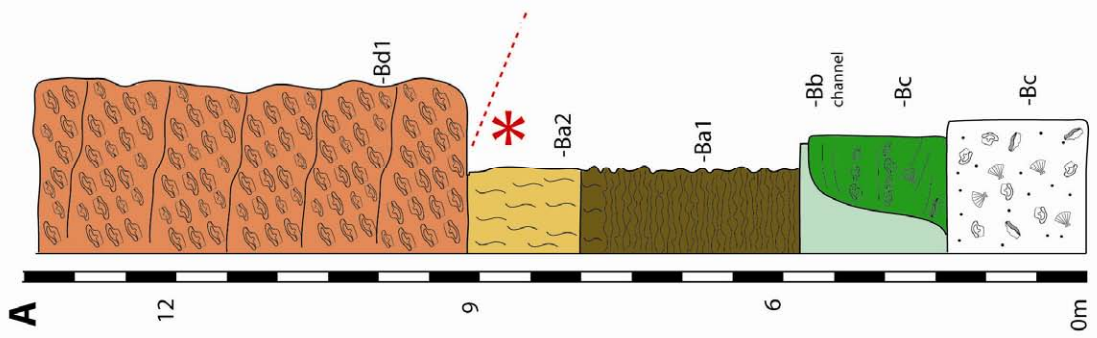


Fig.3.3.1.12 Next page. (A) Log measured of toe-of-slope outer ramp sediments at the base of backset bedded unit. (B) Barranc des Pou outcrop seen on a parallel-to-flow section. (C) Sketch on photograph of backsets foreset laminae with major dipping direction and angles. (D) Rhodolitic conglomerate composing backsets viewed on a perpendicular-to-flow section. (E) Example of a rhodolith which are the major components of these units.



Fig.3.3.1.13 View of facies Bd1 on a perpendicular to depositional dip section.

### Subfacies Bd2

This facies is composed of rhodolith-dominated rudstone which has same grain-size and components of subfacies Bd1 but it is massive and it does not present any sedimentary structures. Porosity is very high (>50%) as in Bd1.

The matrix of this “rhodolitic-supported” conglomerate is very reduced and of a very coarse bioclastic calcarenite with an high intra-clastic porosity. Rhodoliths (*Melobesoids*) are sometimes a little flattened in shape and in average 5-6 cm in size. Imprints of *Pectens* are also found.

This facies can be found in small channel-shaped lenses (with thickness of beds in the troughs ranging from few decimetres up to 1 m, Fig.3.3.1.14) or in very thick beds (5-6 m) with channel-like shaped troughs that extend laterally for 15-20 m (Fig.3.3.1.15).

The lower boundary is often an erosive channalized surface with axis dipping SW.



*Fig. 3.3.1.14 Facies Bd2, massive rhodolith-rich breccias that is frequently found in small-scale (decimeter-scale) channalized deposits. In this picture it is evidenced the presence of rhodolithic-breccias within the floatstones and the grainstones. These beds are laterally discontinuous, with an erosive base and they can be traced for several meters on a parallel to depositional-dip section.*

Tab. 3.3.1 Summary of the sedimentary facies distinguished in the locality of Barranc des Pou.

<b>FACIES</b>		<b>Subfacies</b>	
<b>Ba</b>	Bioclastic wackestone/packstone Fine to very fine sand-size	<b>Ba1</b>	Current-ripple and PPS
		<b>Ba2</b>	Highly bioturbated
<b>Bb</b>	Channalized grainstone Medium to coarse sand-size		
<b>Bc</b>	Bioclastic floatstone		
<b>Bd</b>	Rhodolith-rich clast-supported breccia	<b>Bd1</b>	Backset lamination
		<b>Bd2</b>	massive



Fig.3.3.1.15 View of the succession of facies embedding facies Bd.

<b>FACIES</b>	<b>Description</b>	<b>Grain size</b>		<b>Sedimentary structures</b>	<b>Components</b>	<b>Bed geometry</b>
		<b>matrix</b>	<b>clasts</b>			
<b>Ba</b>	Wackestone/packstone.	Fine to very fine sand-size.		Current ripple cross lamination.	Red algae, echinoids, molluscs, forams.	Sheet-like, thickness of amalgamated beds 2-8m.
				Highly bioturbated.		
<b>Bb</b>	Grainstone.	Medium to coarse sand-size.	Rhodolith 3-4cm	PPS, normal grading.	Forams, echinoid, molluscs, coralline red algae, bryozoans, rhodoliths.	Channalized beds, trough thick 100-150cm and width 150-300cm.
<b>Bc</b>	Floatstone.	Coarse to very coarse sand-size.	Ostroid up to 10cm, Rhodolith 5cm	Current ripple cross-lamination, PPS, normal grading.	Molluscs, bivalves, gastropods, benthic forams, echinoid, coralline red algae, bryozoans, rhodoliths.	Channalized beds, trough thick 1m and width 3-4m.
<b>Bd</b>	Rudstone. Clast-supported pebble-cobble breccia.	Coarse-grained sand-size.	Rhodolith 6-7cm (max 12-15cm); Blocks of facies Ba1 up to 1m.	Backset lamination.	Rhodoliths, molluscs, bivalves, gastropods, benthic forams, echinoid, coralline red algae, bryozoans.	Channalized beds, trough 100-150cm width 15-20m.
				Massive.		

Fig. 3.3.1.16 Table summarizing major features of the facies recognized at Barranc des Pou.

### 3.4 Forma

The locality of Forma is found along the sea-cliffs of Es Canutells, few tens of meters north of the locality of Barranc des Pou (Fig.3.4.1). Backset bedded deposits crop out here for almost 200 m laterally on an east-west direction and the overall thickness is of about 30 m. The outcrop exposure-direction is oblique to the depositional dip of the carbonate ramp, which is prograding SW as shown by the dipping direction of the embedding sediment (Fig.3.4.1.1).

Compared to the facies previously described in the Barranc des Pou, here again the outcrop is placed at the transition between base-of-slope and outer ramp deposits, but it is placed on a more distal position.

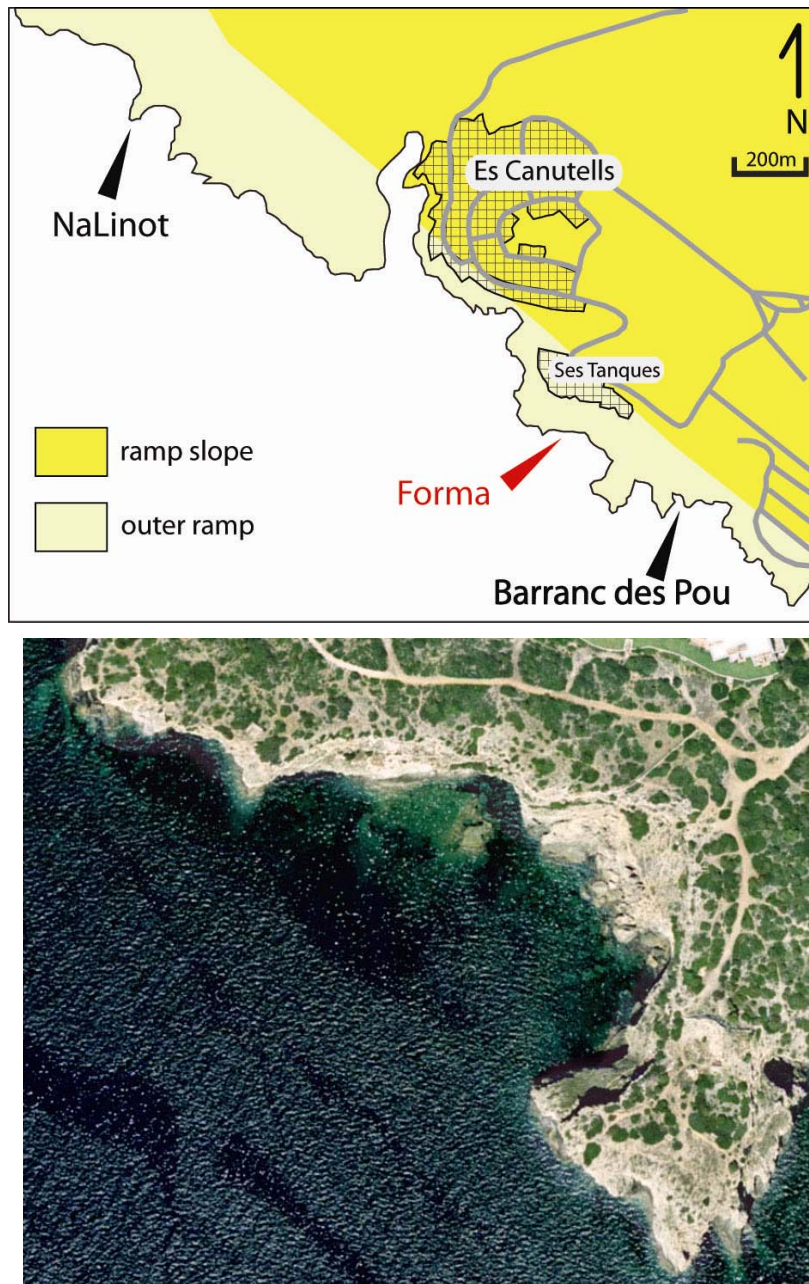


Fig.3.4.1 (Above) Location map of the locality of Forma; (below) satellite photo of the studied area.

At this locality eight different facies have been distinguished based on lithological (texture and grain size) characteristics and composition. They have been successively group into two main facies associations: facies association F1 in the lower part, that correspond to base-of-slope outer-ramp sediments (Obrador *et al.*, 1992; Pomar *et al.*, 2002), and facies association F2 that correspond to a thick, coarse-grained backset bedded interval (facies A in Obrador *et al.*, 1992).



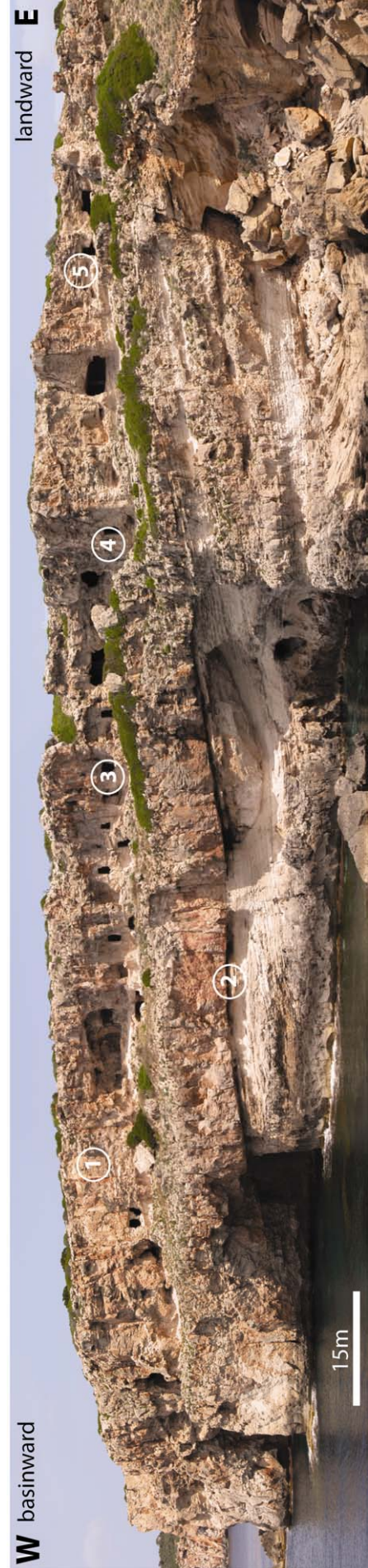
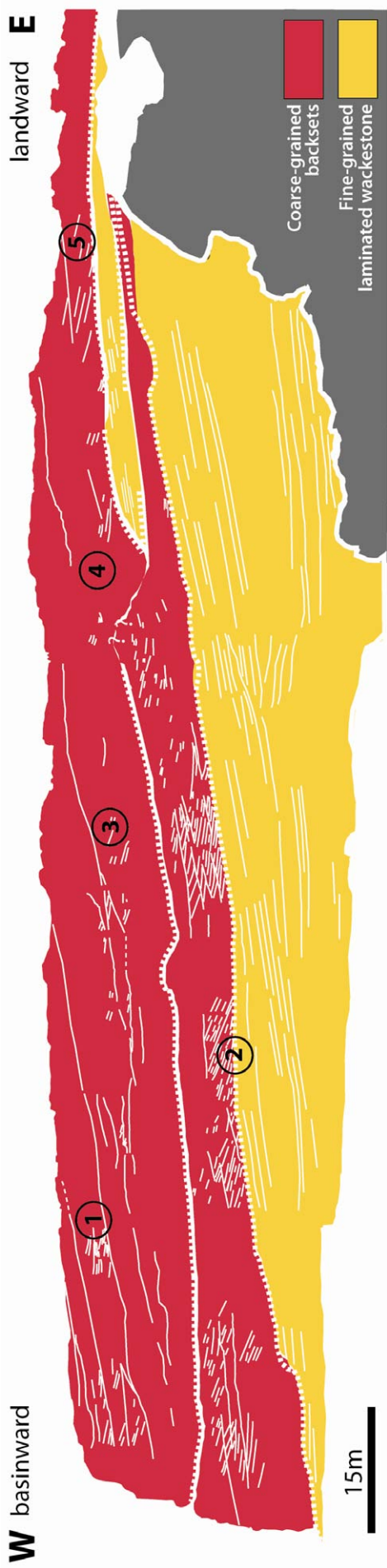


Fig. 3.4.1.1 Panoramic view of Forma outcrop. two major units have been recognized, in red are evidenced the coarse-grained backset bedded units and in yellow the underlying fine-grained wackestone and packstone representing outer ramp sediment. (1) Fig.5.3 B; (2) Fig.3.4.1.26; (3) Fig.3.4.1.8; (4) Fig.3.4.1.8; (5) Fig.4.3.1.

### 3.4.1 Facies description

#### Facies Fa

This facies is of finely laminated, thinly bedded fine-grained wackestone and packstone (Fig.3.4.1.3). It is composed of fine to very fine sand-size grains. Beds are sheet-like with thickness ranging from few millimetres to few centimetres, but beds up to 1 m thick are also present. Planar parallel stratification is frequently visible (Fig.3.4.1.3). Beds can be normally graded to massive to inversely graded. Lamination is sub-parallel to stratification which is often cross-cut by small erosional surfaces (small-scale slide/slump scars). Surface dissolution and pervasive dolomitization may obliterate any structures within beds (Fig.3.4.1.3).

Each bed is bounded at the base and at the top by an erosive surface sub-parallel to bedding (Fig.3.4.1.2).

Packstones are mainly dominated by coralline red algae fragments (*Mesophyllum*), micritized grains, and dissolved grains partly in-filled by spatic calcite cement. Grains are mainly rounded with elongated and flattened shape subparallel to stratification. Micritic matrix is present and cement is present as rims around grains and partly in-filling the mouldic grains. Porosity may vary noticeably (from <10% to 40%): where high depends on bioclasts dissolution but it can be reduced by the precipitation of calcite cement within them. Large diagenetic features are also present (Fig.3.4.1.4).

The succession of these beds is truncated at the top by an erosive surface that has a wide trough-shape whose axis dips SW. Stratification dips SW, concordant to the carbonate platform direction of progradation.

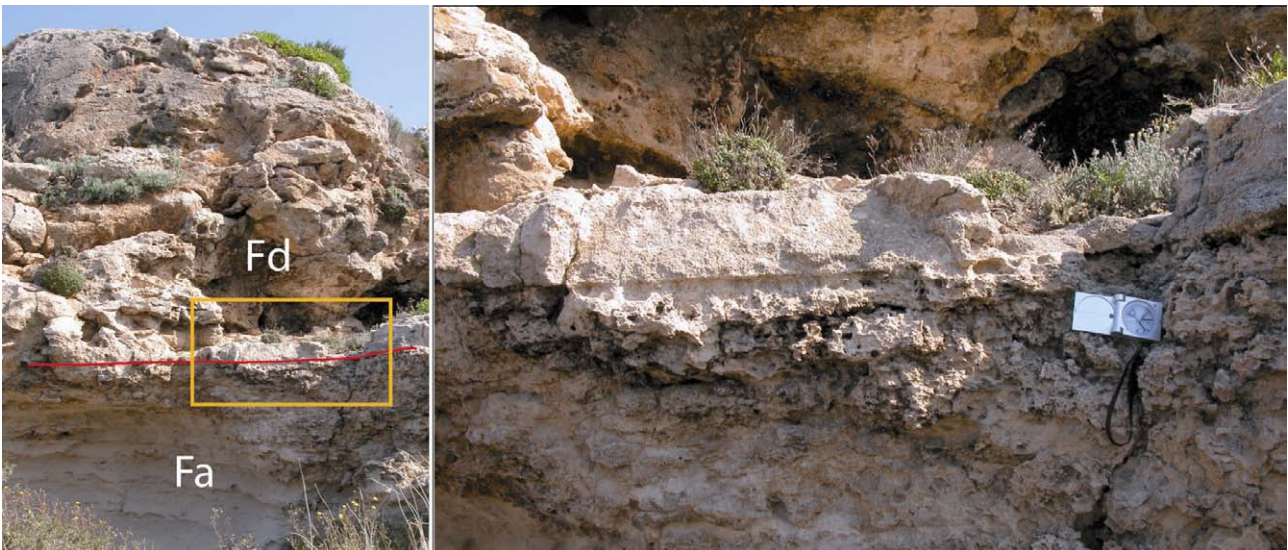


Fig.3.4.1.2 Sharp erosive surface truncating facies Fa and the overlying coarser-grained facies Fd.

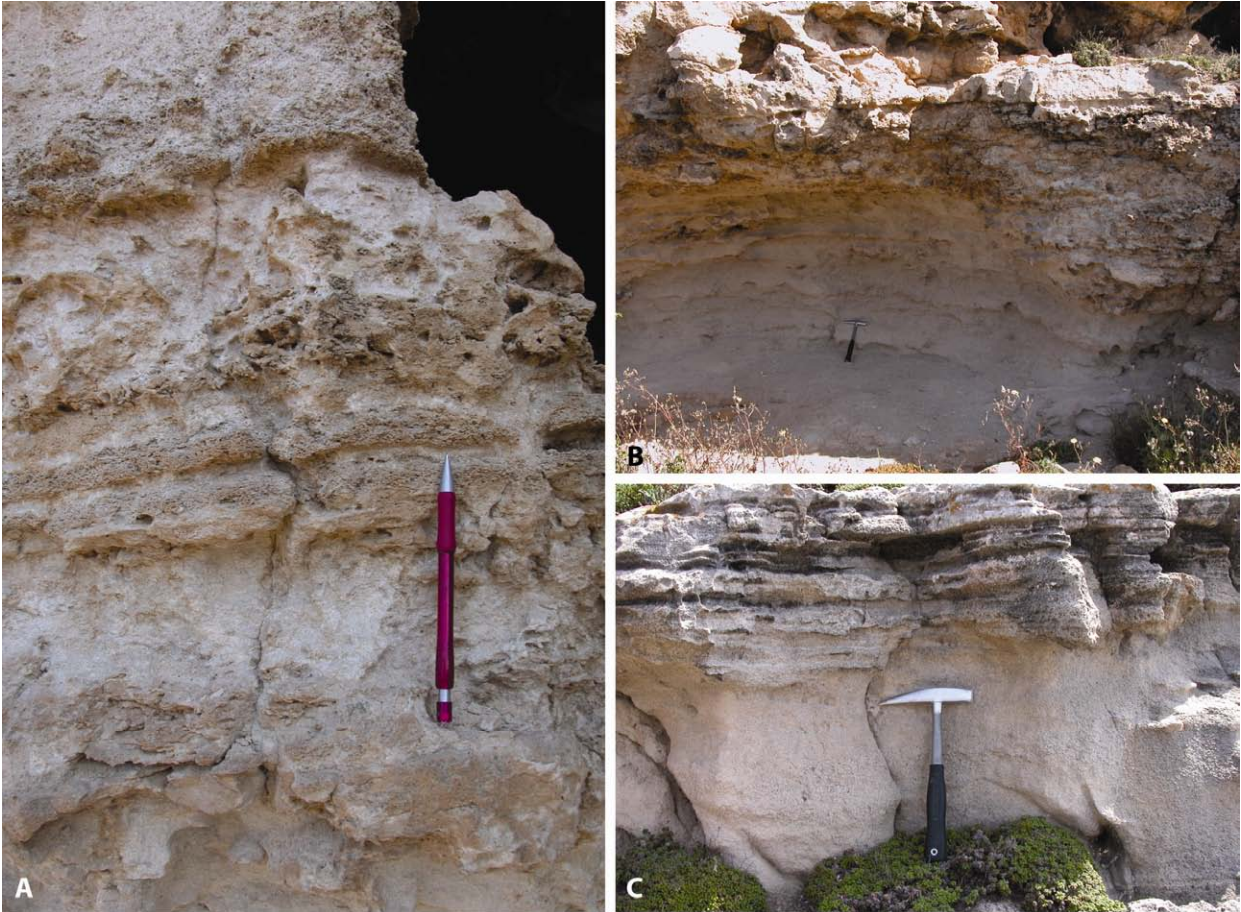


Fig. 3.4.1.3 Facies Fa, planar parallel lamination characterizing the facies with alternation of more erodible to strata with ones more compact: this effect to the uneven distribution of dolomitization.



Fig.3.4.1.4 The red line marks the slide-scar surface that truncates facies Fa; this surface correspond to (2) in picture of Fig.3.4.1.1. In this picture it also possible to see a large diagenetic feature. This features is about 20 m wide and 6 m thick.

## Facies Fb

This facies is characterized by a coarser-grained grainstone to floatstone with planar parallel lamination (Fig.3.4.1.6). Beds are normally graded and thickness of single beds is of average 50 cm with overall thickness can reach 250 cm.

Matrix is composed of coarse-sand to fine gravel size bioclastic calcarenite with larger clasts aligned along lamination. Clasts are of mollusc fragments mainly represented by bivalves which are often dissolved and cavities record an often concave-up disposition of valves. Pebbles composed of a bioclastic grainstone are also frequent floating in the matrix. Pebbles are discoidal in shape ( $c < c$ ) 2-3 cm in size and they are also aligned along lamination.

Matrix is mainly composed of rounded fragments of coralline red algae (*Lithophyllum*, *Sporolithon*) with few echinoid plates and spines.

This facies is found in few beds 50 to 80 cm thick lying one over each other either amalgamated or separated by sharp boundaries with a maximum thickness of 250 cm. Beds of this facies are often wedge-shaped, pinching out landward, bounded at the base and at the top by irregular erosive surfaces. Porosity is high and related to high dissolution of bioclasts (Fig.3.4.1.6).

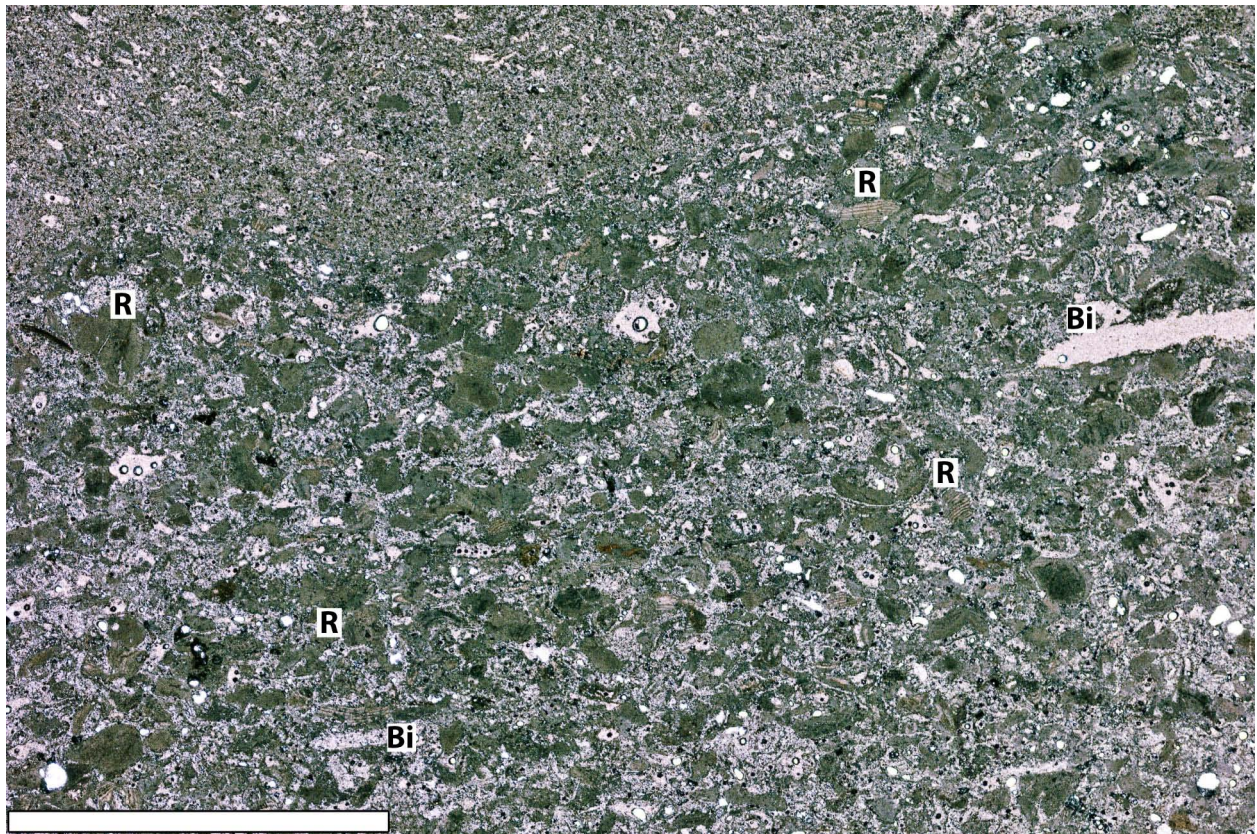
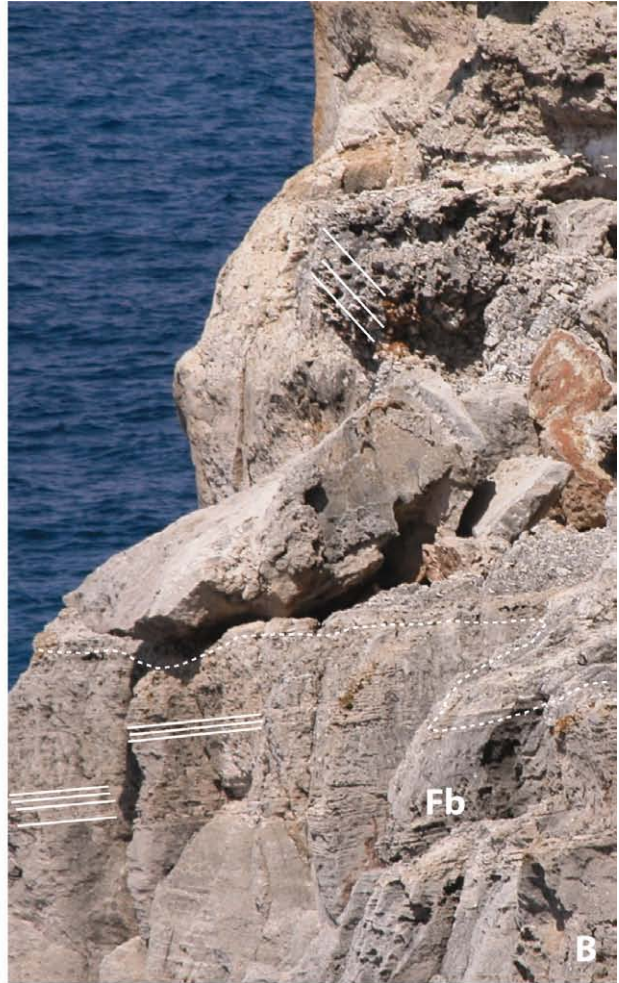
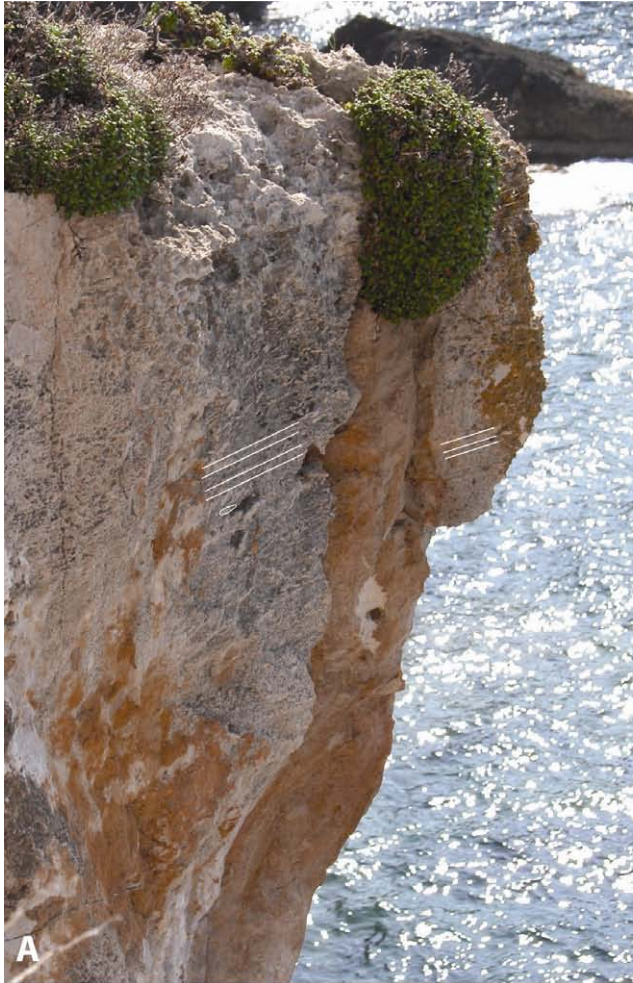


Fig.3.4.1.5 Thin section of facies Fb with abundant rounded fragments of coralline red algae, bivalves are also present. Lamination is visible also in thin section thanks to orientation of grains. Scale bar 1 cm. Sample ST10.



*Fig.3.4.1.6 Facies Fb. (A) This facies is characterized by planar parallel lamination; (D) the top boundary of this facies is represented by an erosive surface with coarse-grained backset bedded deposits lying on top; (C) lamination is often evidenced by the alignment of small flat pebbles (c<<).*

## **Facies Fc**

This facies is composed of massive medium to coarse grained calcarenite. Grains are quite well sorted, in average 1 mm in size. Large bioclasts are absent only few imprints of bivalve shell have been found. Facies Fc is not very common compared to the others described but it has been separated from the other because of its lack of bioclasts and the persistence of the same diagenetic features confined within each body.

Sedimentary structures have been completely obliterated by the presence of diagenetic features that pervade this facies. These diagenetic features are of unknown origin (Fig.3.4.1.7); they are columnar shape of few cm in diameter and they are limited to the beds of this facies Some 2-3 cm thick layers are sub-horizontal and are dolomitized.

This facies is present in beds that have a lens shape and that are about 120 cm thick and 6-7 m wide (Fig.3.4.1.8).



*Fig.3.4.1.7 Facies Fc characterized by pervasive diagenesis, with typical vertical features of unknown origin.*

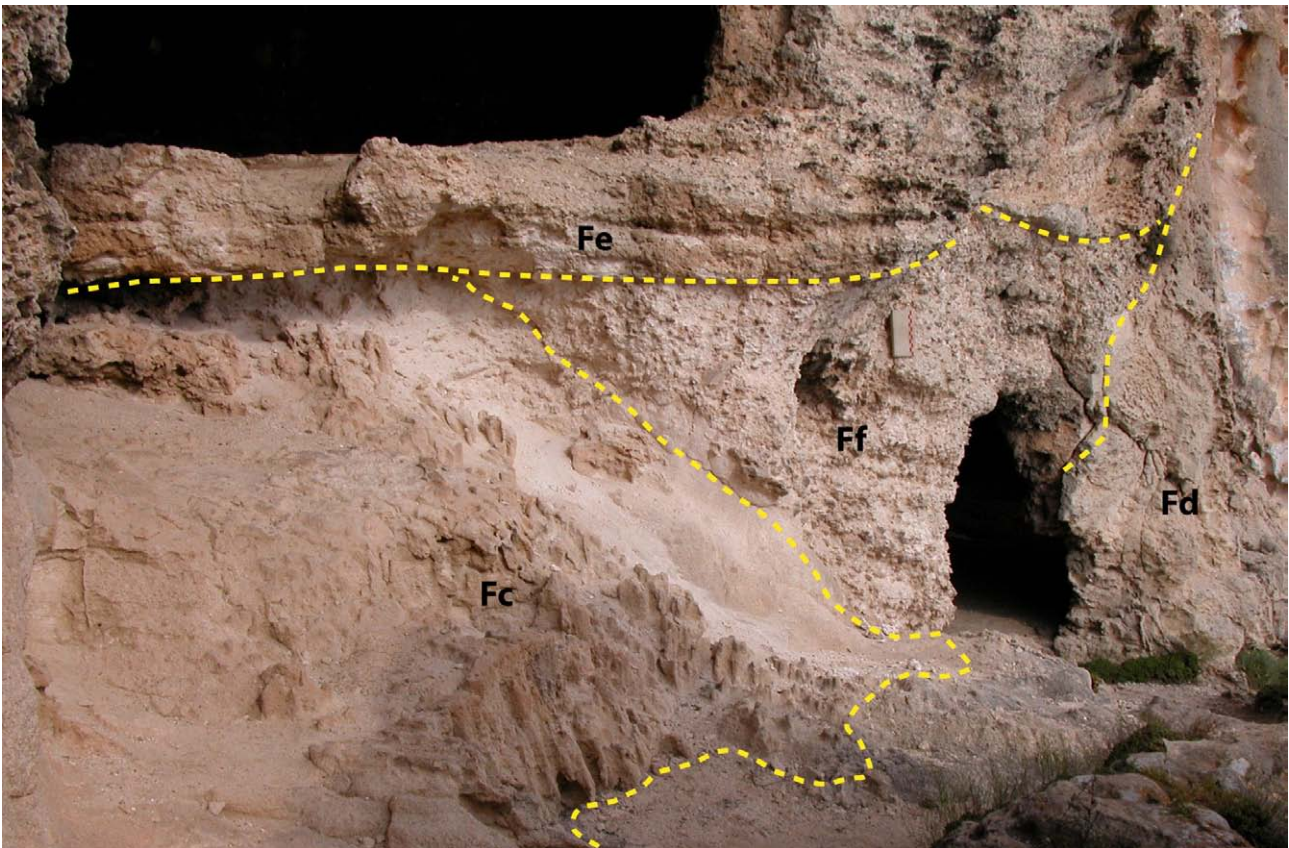


*Fig.3.4.1.8 Geometrical relationships between several facies; the view is along an oblique to depositional-dip section.*

## **Facies Fd**

This facies is a matrix-supported conglomerate (floatstone). Matrix is dominant and it is composed of a medium-coarse-grained sand to fine gravel bioclastic calcarenite (packstone/grainstone). Grains in some bodies, are sub-angular in others sub-rounded but always not well sorted. This calcarenite is mainly composed of fragments of coralline red-algae up to 5-6 mm in size (Fig. 3.4.1.9), molluscs, benthic forams, echinoid plates, bryozoans, small gastropods (Fig. 3.4.1.10). Bivalves are mainly dissolved or only partly preserved and present as imprints or inner mould large up to 3-4 cm (3.4.1.11). Mouldic grains are also present. Extraclasts are very frequent (20%), they are light-grey colour, very rounded and average < 5 mm in size. The matrix of the calcarenite is partly composed of micritic mud and partly by calcitic cement without a particular pattern. Grains often present a spatic calcite cement rim.

Rhodoliths are rare and found sparse in the sediment and are in average 3-4 cm but can be up to 10 cm in size. The abundance of rhodoliths may vary in different units but it is always very low. Porosity is inter-clasts, quite high (30-40%) and sometimes mouldic due to dissolution of small fragments of bioclasts (1-2 mm).

This facies is found in massive, 150 cm thick beds with normal gradation at the base. Backset-bedding with foreset-lamination dipping NE, is visible only where the larger bioclasts population, especially of bivalves and rhodoliths, slightly increase.

Beds are lens-shape, 3-4 m thick along strike and a tabular geometry along depositional dip that extend for 15 m. Beds are bounded by erosive surfaces which tend to be quite sub-parallel to stratification of the underlying facies Fa, therefore dipping SW.



Fig. 3.4.1.9 Facies Fd, rhodolithic floatstone.

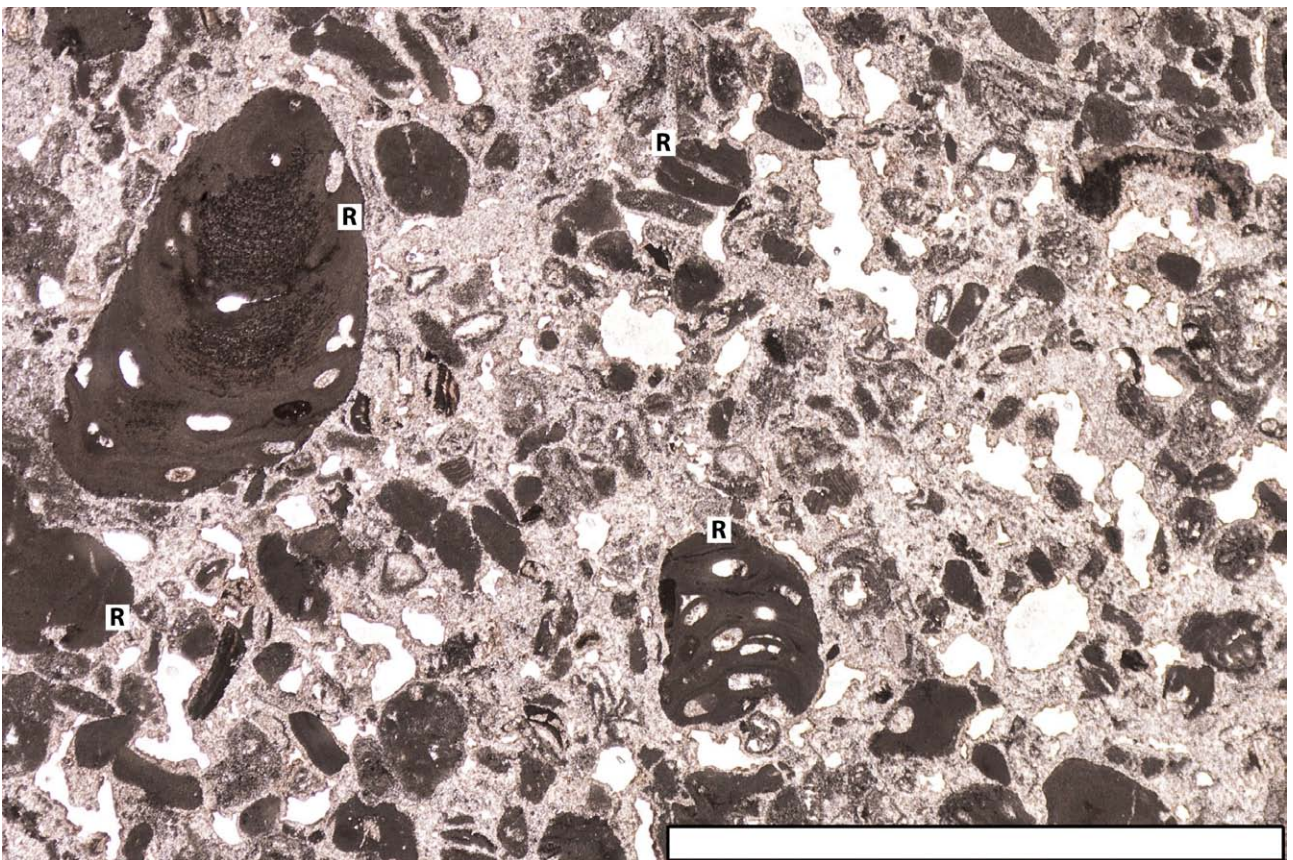


Fig. 3.4.1.10 Thin section of facies Fd, rhodolithic floatstone dominated by coralline red algae fragments and foraminifers. Scale bar 1 cm. Sample ST5.





Fig.3.4.1.11 Facies Fd with dissolved bivalves with concave-up, concave-down shells and rhodoliths sometimes concentrated in levels.

## Facies Fe

Facies Fe is a matrix-supported conglomerate with pronounced backset lamination (packstone/grainstone to floatstone). Matrix of the conglomerate is of a quite homogeneous, coarse-sand to fine-gravel size bioclastic calcarenite mainly composed of bioclastic fragments of coralline red algae (*Mesophyllum*, *Sporolithon* and less *Lithophyllum*) very abundant in few millimetre-size, oolites, small gastropods, molluscs, bivalves and foraminifera. Bioclasts are also well rounded. Among grains micritic matrix can be found as well as micro-crystalline calcitic cement. Large spatic crystals can be found in-filling mouldic grains.

Large clasts are represented by rhodoliths and by limestone pebbles. Rhodoliths are 3-4 cm in size but can reach 13-14 cm and they are found sparse in the matrix; larger ones are flattened while the smaller pieces are mainly sub-rounded in shape (Fig.3.4.1.12). Limestone pebbles consist of oolitic and bioclastic grainstone composed mainly of coated-grains with a few *Halimeda* fragments, and fragments of coralline red algae, bivalves, bryozoans, small gastropods, echinoid plates, benthic foraminifera are also common (Fig.3.4.1.13). Grains composing these pebbles are medium to very coarse sand-size (Fig.3.4.1.12).

Pebbles are discoid to bladed in shape with  $c \ll a$  and may reach 12 cm along the  $a$  axis. Many pebbles have bioerosion traces on the surface and are encrusted by serpulids. Large bivalves, up to 3-4 cm, are mainly present as moulds but sometimes with preserved convex-up valves. Light-grey small (<5 mm) and well rounded extraclasts are frequent (15-20%). Sub-

angular large boulders 50-60 cm wide and 225-30 cm thick composed of facies Fa are also found floating in the matrix (Fig.3.4.1.14, D).

Cementation of limestone pebbles is higher and porosity is high (>35%), mainly intergranular and only partly intra-granular due to dissolution.

Backset-lamination is dipping NE (N15 7°; N13 11°) with rhodoliths, bivalves and pebbles sometimes concentrated and oriented along lamination. Laminae are visible every 8-10 cm, where larger components are more abundant (Fig.3.4.1.16).

Sediment is piled up in beds of thickness ranging from 150 to 200 cm, that show a tabular geometry along depositional dip and lens-shape along strike (Fig.3.4.1.15). Beds are bounded at the base and at the top by erosive surfaces. Along depositional dip, beds are bounded by erosive surfaces that dip SW. The bounding surface at the base of this facies is erosive on facies Fa and it has a channel-shape dipping N225 10° with axis directed NE-SW.

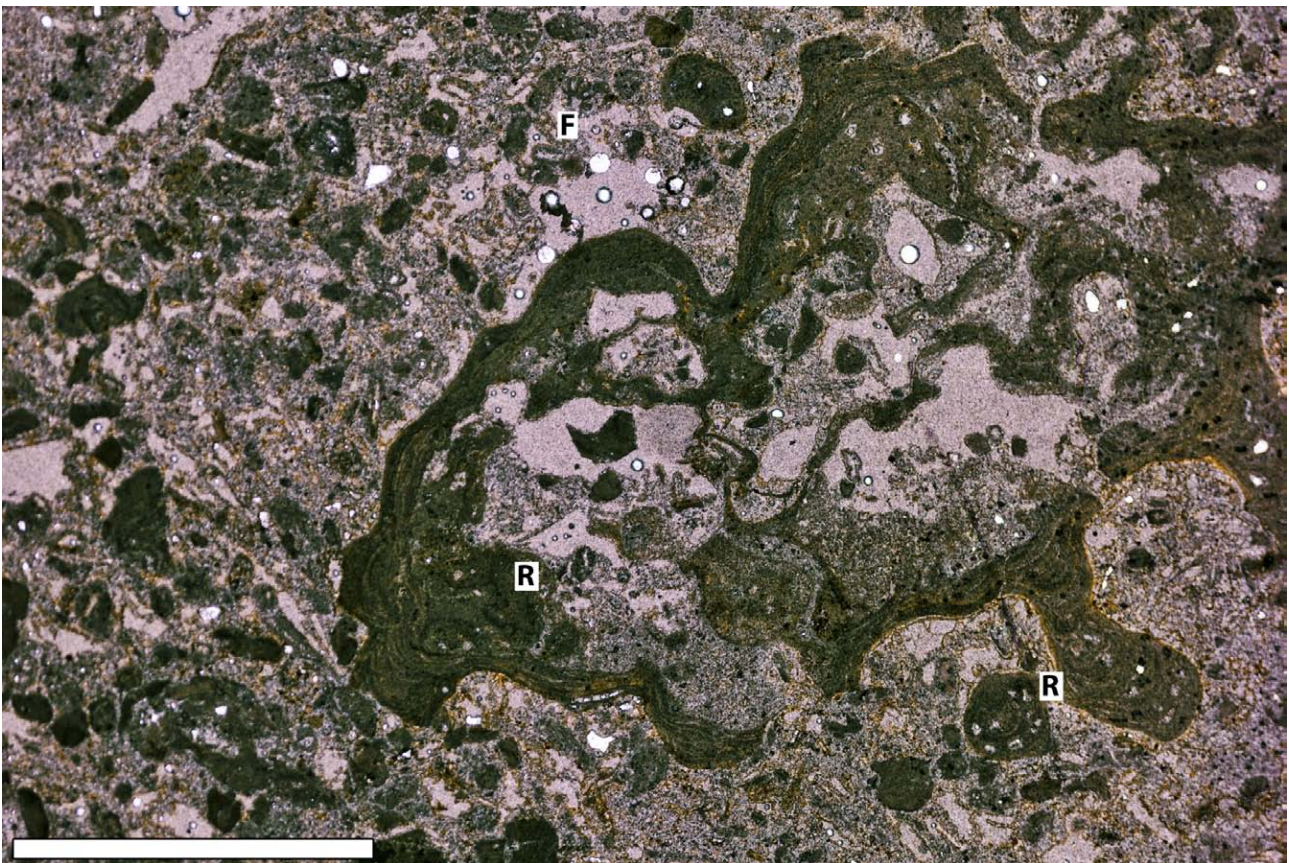


Fig. 3.4.1.12 Facies Fe, rhodolithic floatstone. Highly porous matrix of the floatstone with a rhodolith. Abundant fragments of coralline red algae and foraminifers. Scale 1 cm. Sample ST22.

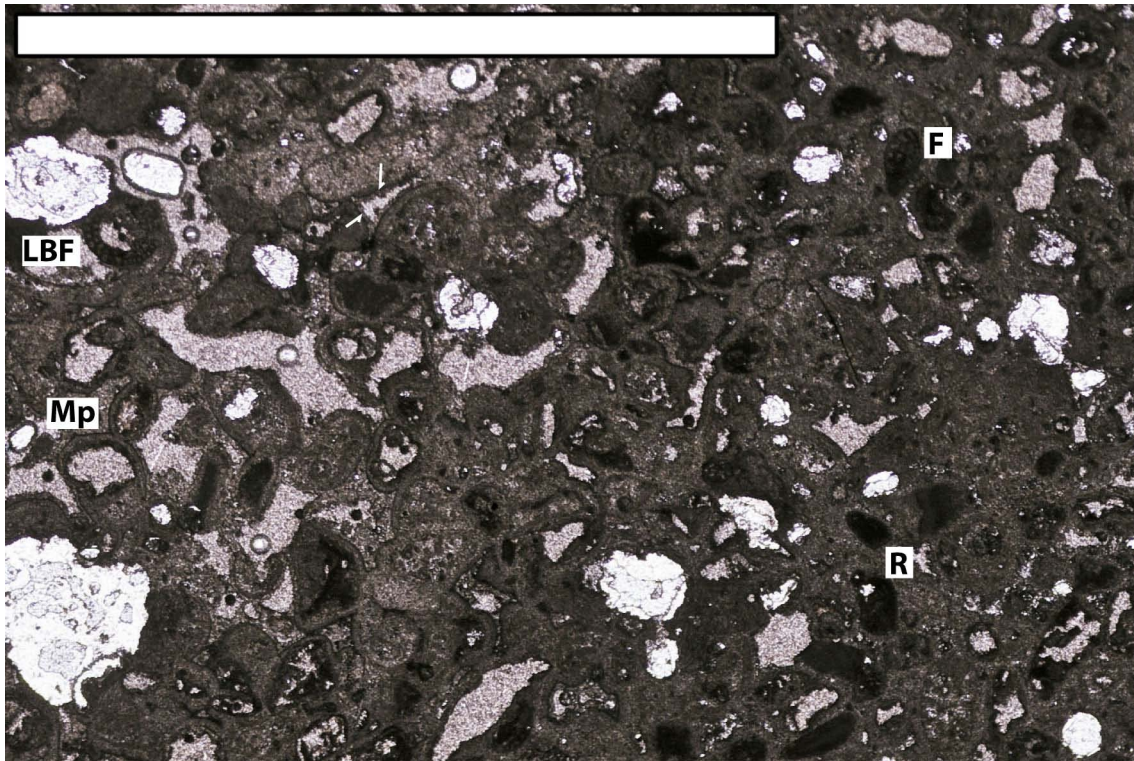


Fig. 3.4.1.13 Thin section of a limestone pebble of Facies Fe, grainstone rich in coated rounded grains. (F) Foraminifers are present (Borelis?), (R) fragments of coralline red algae, echinoid plates. Scale bar 1 cm. Sample ST2.



Fig.3.4.1.14 Facies Fe, (A,B,C) photos showing the lamination evidenced by the orientation of limestone pebbles and dissolved bivalves cavities. (D), large block of about 60cm composed of facies Fa.



Fig.3.4.1.15 View of lamination in facies Fe with flat pebbles aligned with a axis parallel to lamination.

## Facies Ff

Facies Ff is a clast-supported conglomerate with backset lamination. This conglomerate is dominated by bivalves, which are the main component. The matrix is composed of a coarse-sand to fine-gravel grained bioclastic calcarenite. Matrix is of bioclastic grainstone/packstone composed of fragments of molluscs, small gastropods, few fragments of coralline red algae (*Mesophyllum*, *Sporolithon*, rare *Lithophyllum*), bryozoans, foraminifera, ooids, echinoid plates and spines (Fig.3.4.1.19). This facies is dominated by large-size 4-6 cm bivalves mainly present as moulds composed of the same coarse calcarenite that forms the matrix. Limestone pebbles are also sparsely present; they are sub-rounded, discoid-to-blade shaped in average 5-6 cm along *a* axis, and composed of a bioclastic grainstone. Limestone pebbles are characterized by the same features as in facies Fe. Rhodoliths are rare and fragments of coralline red algae are present only in small fragments (<1 cm) but noticeably reduced in number.

Backset-lamination dip NE and it is evidenced by the alignment of bivalves and pebbles (Fig.3.4.1.17). On strike-section, this facies is found in bodies that have a large-scale trough-cross stratification, pinching out laterally with maximum thickness in the trough ranging from 120 to 180 cm and 3 to 6 m wide (Fig.3.4.1.18). The vertical strike section visible in outcrop is oriented oblique to the trough axis revealing cross-stratification planes that apparently fill the trough asymmetrically and downlap onto its base. Along depositional dip they are wedge-shaped. The direction of the trough-axis is about NE-SW.



*Fig.3.4.1.16 Facies Ff, bivalve-rich conglomerate. Large bivalves are mainly dissolved with concave-up shell; limestone pebbles are also present and as well as bivalves are aligned along lamination.*



*Fig.3.4.1.17 Geometrical relationships between different facies, note the vertical diagenetic features always characterizing facies Fc.*

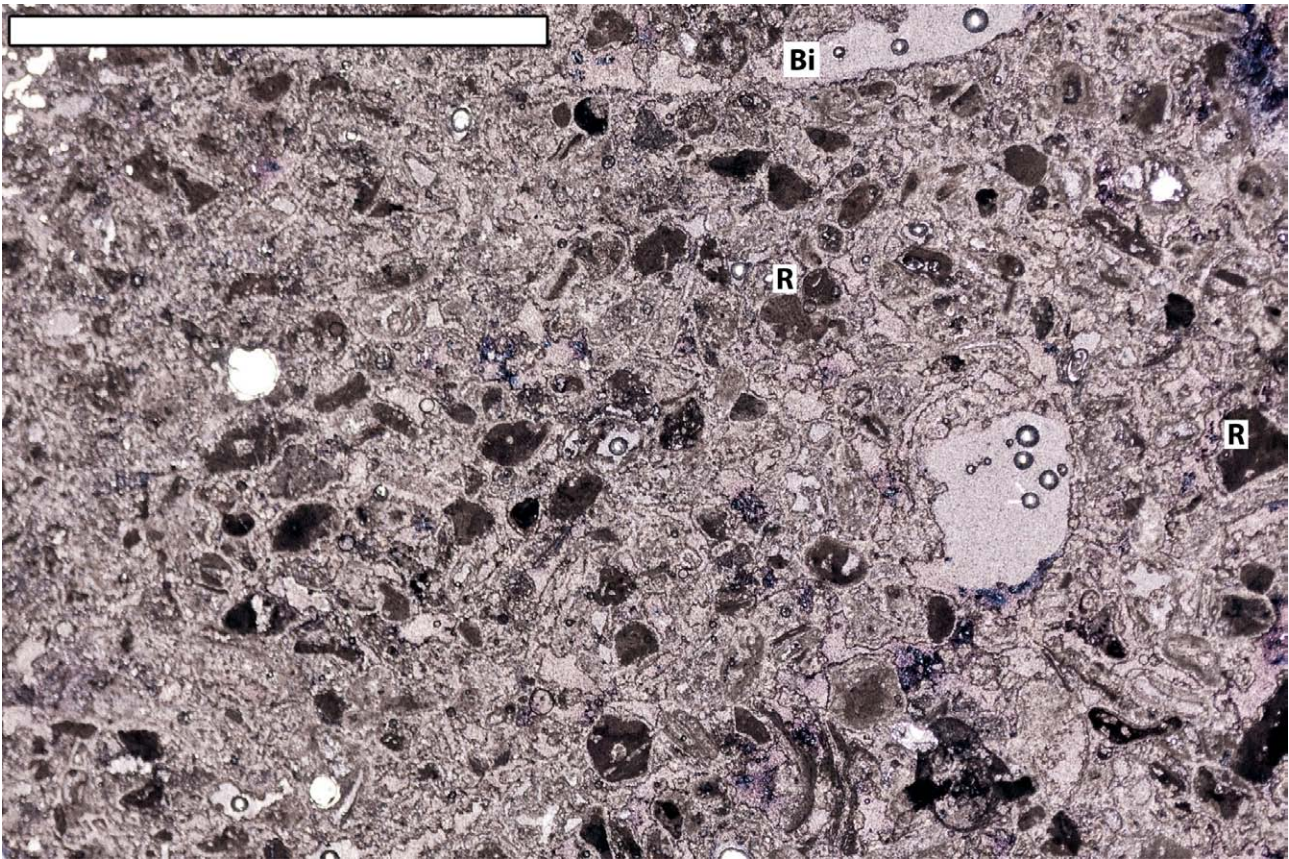


*Fig.3.4.1.18 Thin section of the matrix of Facies Ff, bivalve-rich conglomerate. Fragments of coralline red algae, thin bivalves shells mainly dissolved. Scale bar 1 cm. Sample ST34.*

## **Facies Fg**

This facies is a clast-supported conglomerate with large scale backset-lamination. Texture of this facies shows an alternation of amalgamated matrix-supported and clast-supported intervals.

Matrix of the conglomerate is of a coarse-grained to fine-gravel size bioclastic calcarenite (packstone/grainstone) (Fig.3.4.1.19) mainly composed of oolites and well rounded mollusc fragments and foraminifera; within grains micritic mud is often subordinate to calcitic cement. Clasts are represented by poorly sorted limestone pebbles, rhodoliths, bivalves and gastropods. Pebbles are made of oolitic and bioclastic grainstone ranging in size from 2-3 cm up to 7-8 cm; they are sub-rounded discoid-to-bladed in shape. Pebbles concentrate in layers with 'a' axis parallel to lamination and where very abundant are imbricate. Limestone pebbles present features as in facies Fe and Ff. Fragments of coralline red algae are also very abundant and range in size from 1-2 cm up to 7-8 cm but mainly 3-4 cm; they can be flattened or spherical and they are also sometimes concentrated in layers along lamination. Bivalves up to 10 cm but average 3 cm are still frequent and oriented with convex-up shells along lamination. Porosity is very high in the matrix where it is inter- and intra-granular because of dissolution, and it is lower within the limestone pebbles which are mostly well cemented with some intra-granular porosity (Fig.3.4.1.19).

Cross lamination is strongly evidenced by the orientation of coarser components and laminae dip NE (N10-N60) with angles varying from 8° to 25°.

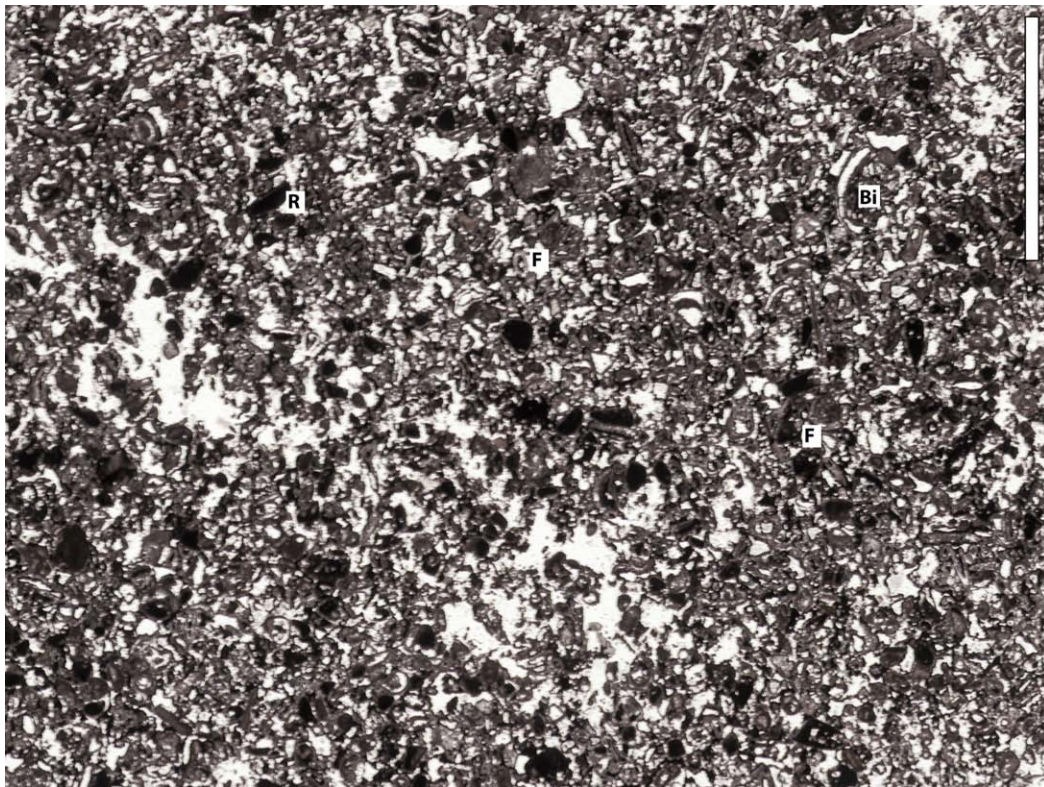


*Fig.3.4.1.19 Thin section of Facies Fg, fine grained grainstone with fragments of coralline red algae, few echinoid spines and plates. Sample ST54.*

Sediment is piled up in beds that have tabular shape along depositional dip and may be continuous for 25-30 m, while they are channel-shape along strike with thickness in the trough of 140 to 250 cm (Fig.3.4.1.20).

Beds are bounded by channel-shaped erosive surfaces with a NE-SW axis direction.

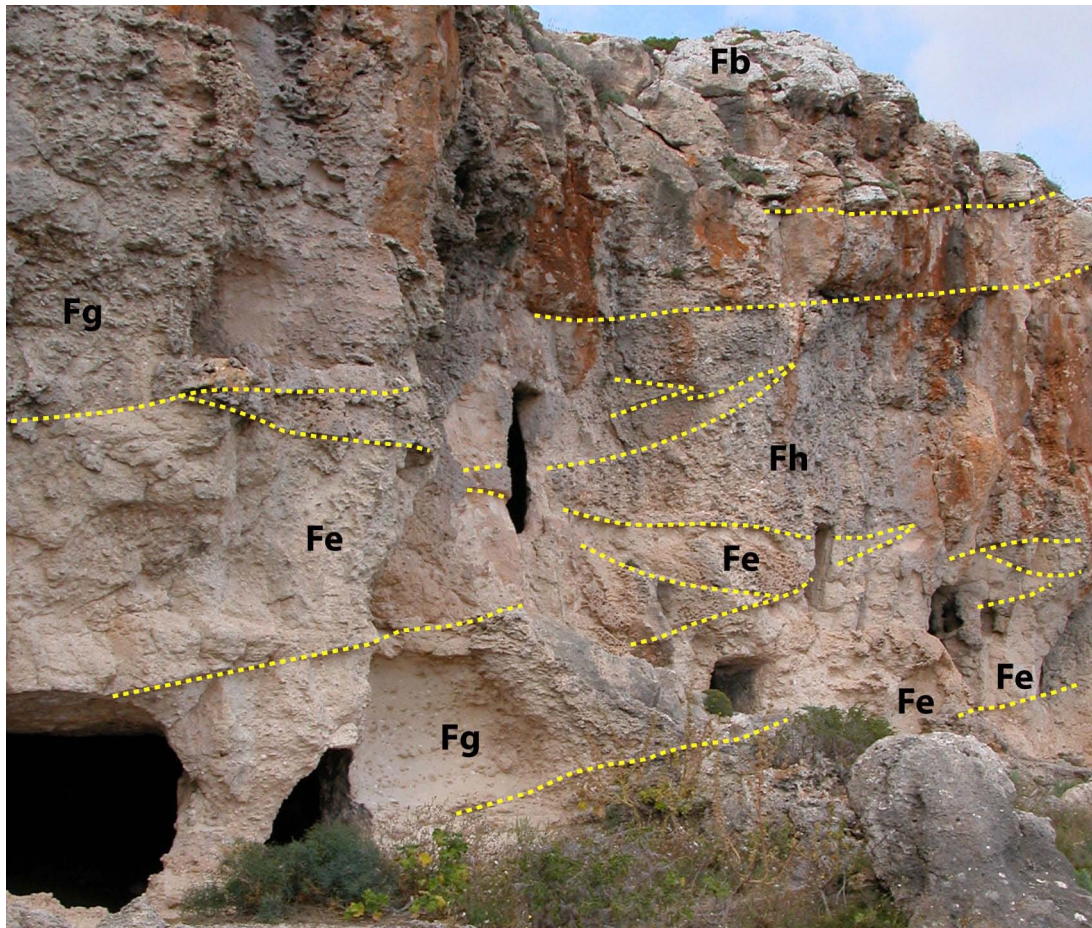


Fig.3.4.1.20 Panoramic view of the outcrop on an oblique to depositional-dip section, showing the architecture of the several units super-imposed over each other.

## Facies Fh

Facies Fh is characterized by being a very coarse grained clast-supported conglomerate with cross-lamination. The conglomerate presents a very low content of matrix which is composed of coarse sand to fine granule bioclastic calcarenite. Large clasts are mainly represented by very large rhodoliths which frequently are > 8 cm in size but often may reach up to 12-13 cm; they are white-pinkish in colour and very well rounded and most of the time spherical in shape with nice preservation of the branching structure (Fig.3.4.1.23). The limestone cobbles-to-boulders are composed of bioclastic and oolitic grainstone, some are particularly rich in oolites, while others are of foram-rich packstone/grainstone, fragments of mollusc, thin bivalves, benthic foraminifers, echinoid plates and spines, small fragments of coralline red algae are found. Bioclasts often present a micritic rim (Fig.3.4.1.21 and 3.4.1.22).

These grainstone are mostly well cemented, with porosity reduced because of precipitation of spatic cement in cavities due to dissolution; larger crystal of spatic calcite in-fill intra-granule porosity. The surface of limestone clasts is often bioeroded and encrusted by serpulids (Fig.3.4.1.27 E,F). Clasts are always subrounded while size and shape significantly vary. Size may range from few centimetres to 30 cm, in shape they are from equant to discoid to rod but mainly elongated with  $a$  axis  $\gg b, c$ . Shape of cobbles and size may sometimes be peculiar of



a single deposits, with clasts of same shape characterizing one deposit. Well rounded, spherical large cobbles, up to 12-13 cm in diameter, are also present and are mainly composed of oolitic-grainstone (Fig.3.4.23). Imbrication of pebbles and cobbles is very frequent.

Backset-lamination is evidenced by the alignment of both rhodoliths and clasts which present a axis parallel to lamination. Lamination is mainly dipping around N70 with high angles from 20° to 35° (Fig.3.4.1.24).

Beds show a tabular shape along depositional dip with channel-shape along strike with thickness in the trough of about 200–280 cm (Fig.3.4.1.26).

The deposits of facies Fh are bounded at the base and at the top by erosive surfaces.

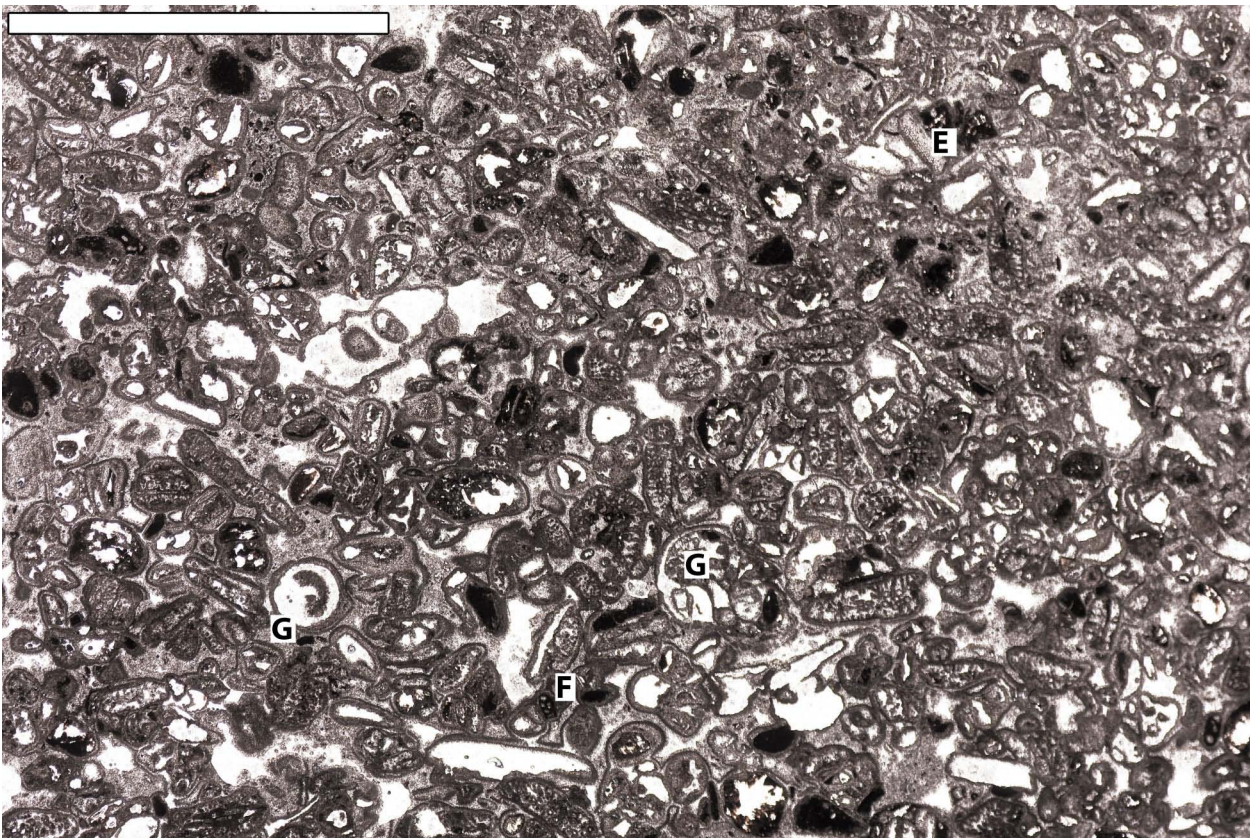


*Fig.3.4.1.21 Thin section of a limestone pebble of facies Fh. Grains are well rounded and coated by a micritic envelope with a dissolved nucleus. Fragments of red coralline algae are still present, foraminifers and dissolved molluscs fragments. Scale bar 1 cm. Sample ST11.*

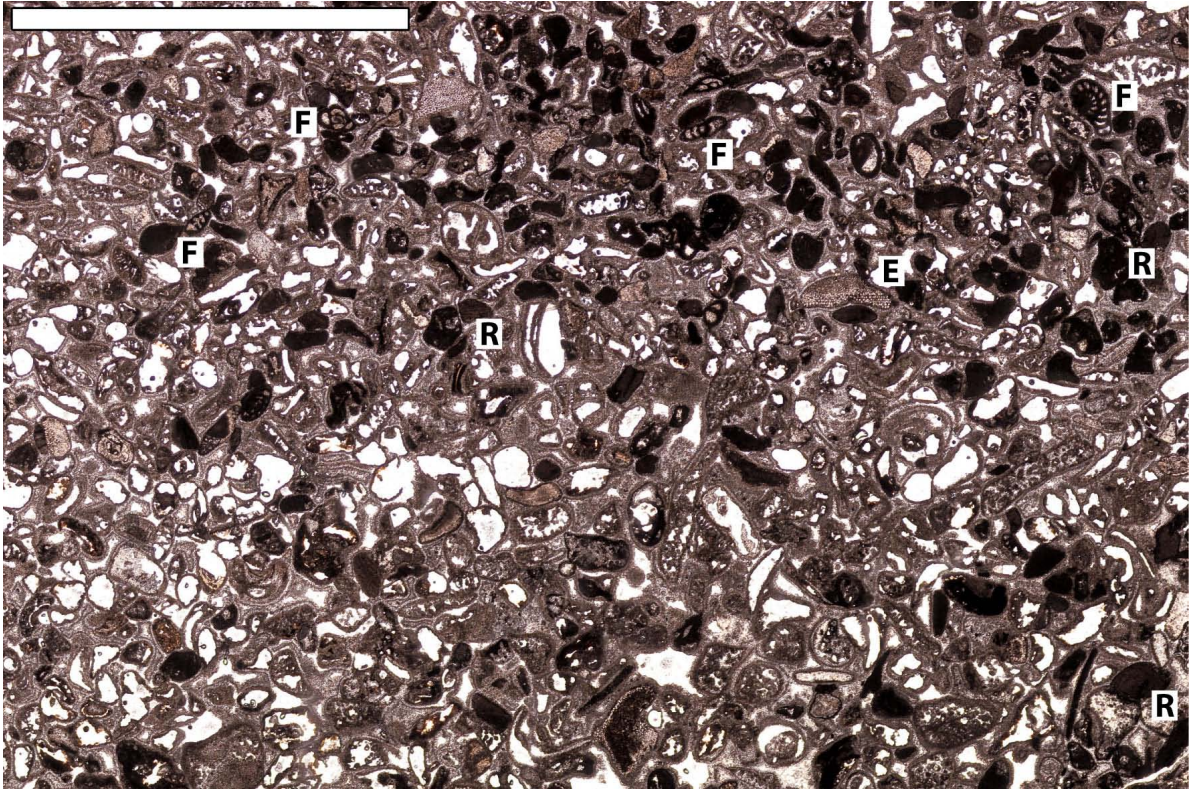


Fig.3.4.1.22 Thin section of limestone pebble of facies Fh. Grains are rounded and with a micritic envelop. The upper part is more rich in fragments of red coralline algae, foraminifers are present and echinoid plated. Scale bar 1 cm. Sample ST13.

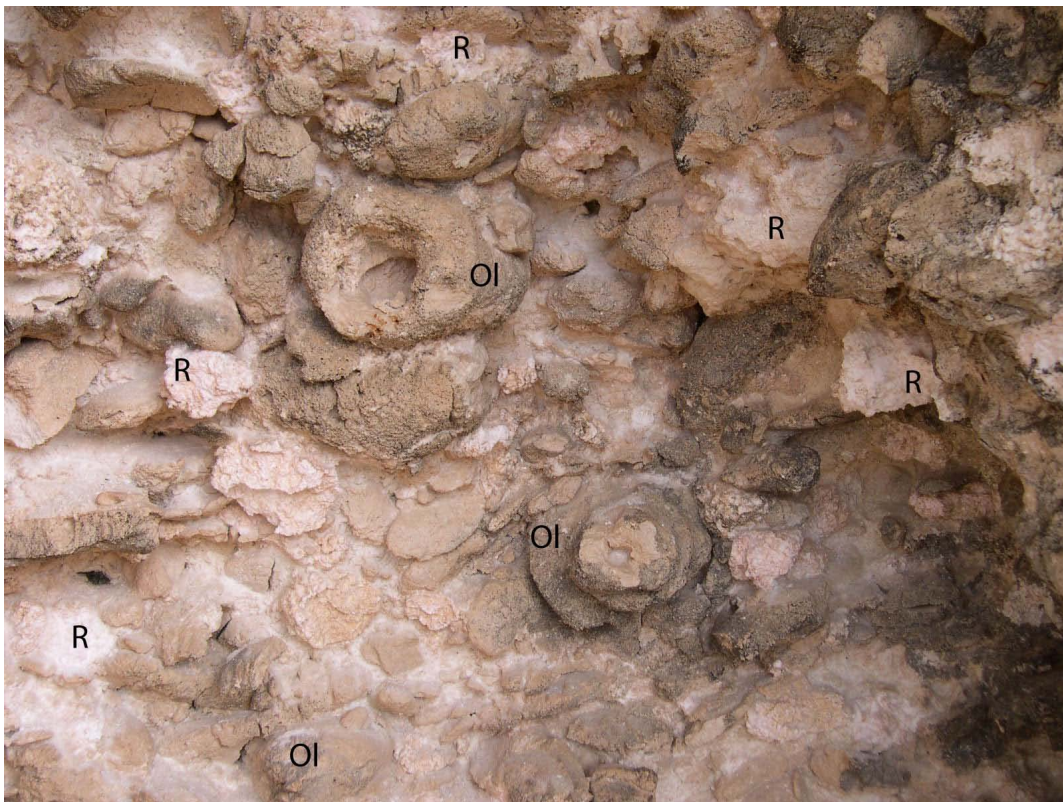


Fig.3.4.1.23 Large boulders composing facies Fh. As shown in picture pebble to boulder-size clasts are present with very variable shape from spherical to elongated to discoid. The whitish sediment among the limestone clasts are rhodoliths.



*Fig.3.4.1.24 Backset lamination in facies Fh; as shown in the picture clasts of variable size are aligned along laminations even the very large ones. Flattened clasts are arranged with a axis parallel to lamination and c axis perpendicular. The whitish sediment between clasts are rhodoliths.*



*Fig.3.4.1.25 Erosive surface of facies Fh over facies Fe.*

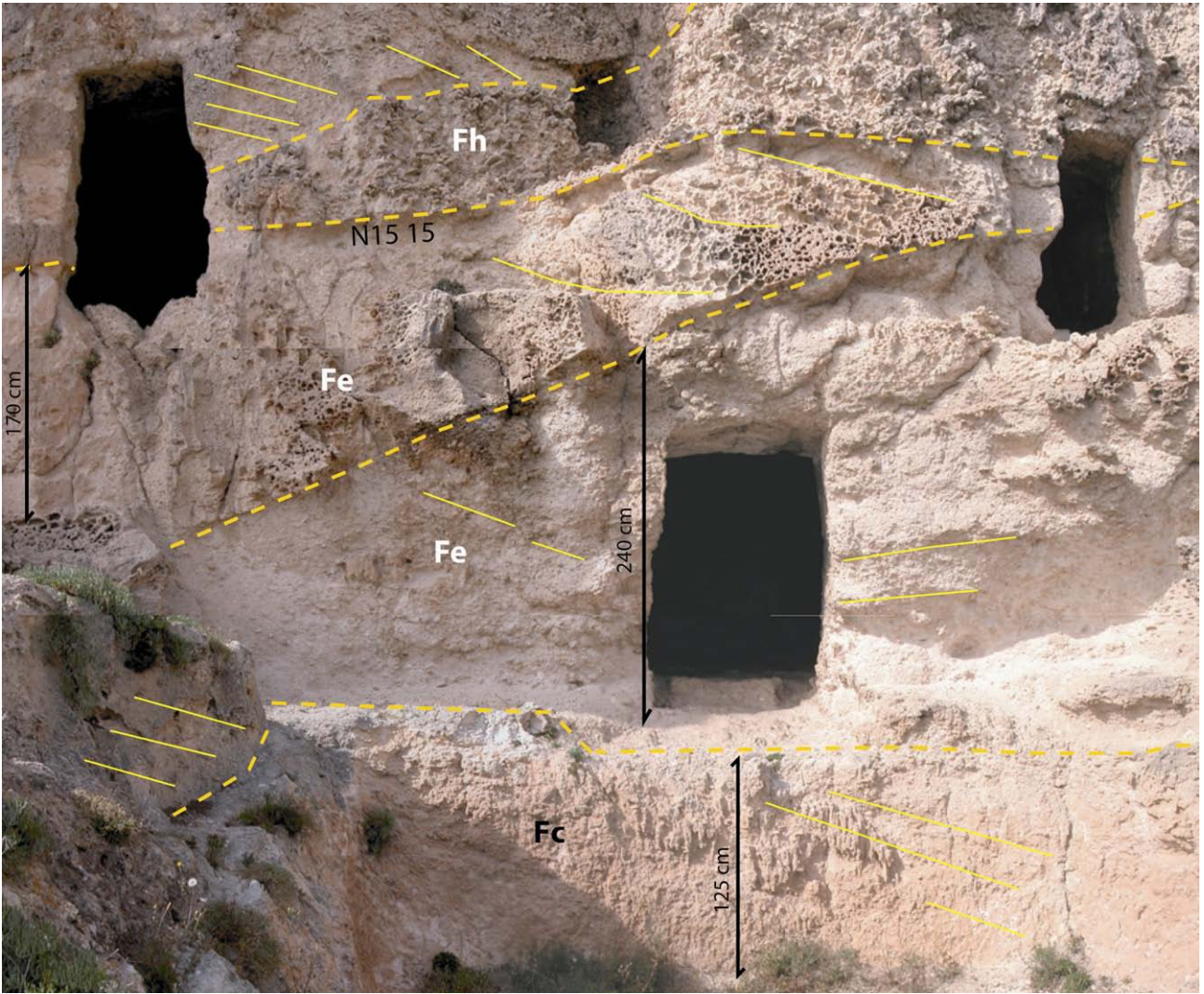


Fig.3.4.1.26 View of the geometrical architecture of the super-imposition of facies along a parallel to depositional-dip section.



*Fig. 3.4.1.27 Detail pictures of some peculiar features of the components of the coarser-grained facies: (A-B) boring on the surface of the limestone pebbles, in (A) they may be related to lithofaga, while in (B) they can be related to endolithic algae (?); (C-D) rhodoliths embedded with pebbles; (E-F) serpulids encrusting the surfaces of limestone clasts.*

Table 3.4.1 Summary of the sedimentary facies distinguished in the locality of Forma.

<b>FACIES</b>	
<b>Fa</b>	<i>Bioclastic wackestone/packstone Fine to very fine sand-size grains</i>
<b>Fb</b>	<i>Coarse-sand to fine gravel grainstone to floatstone with limestone pebbles (2-3cm) with PPS.</i>
<b>Fc</b>	<i>Massive medium to coarse grained calcarenite</i>
<b>Fd</b>	<i>Matrix supported conglomerate, floatstone, rhodoliths (3-4cm up to 10cm) and backset lamination.</i>
<b>Fe</b>	<i>Matrix-supported conglomerate, floatstone, with limestone pebbles (up to 12cm) and backset lamination.</i>
<b>Ff</b>	<i>Clast-supported conglomerate, + bivalves.</i>
<b>Fg</b>	<i>Clast supported conglomerate, + pebbles.</i>
<b>Fh</b>	<i>Clast supported conglomerate, + cobble-to-boulder.</i>

FACIES	Description	Grain size		Sedimentary structures	Components	Bed geometry
		matrix	clasts			
<b>Fa</b>	Wackestone/packstone.	Fine to very fine sand-size.		PPS, massive to normal to inverse grading.	Bioclasts, red algae fragments.	Sheet-like, thickness from cm to 1m.
<b>Fb</b>	Grainstone to floatstone.	Coarse-sand to fine gravel.	Limestone clasts 2-3cm.	PPS, normal grading.	Molluscs, red algae, echinoids, rhodoliths, limestone pebbles.	Channelized-beds, thickness 50 to 250cm.
<b>Fc</b>	Grainstone.	Medium to coarse grained sand-size.		Obliterated by diagenesis.	Not recognizable.	Lens shape, 120cm thick 6-7m wide.
<b>Fd</b>	Floatstone, matrix-supported conglomerate.	Medium to coarse-grained sand to fine gravel.	Rhodoliths 3-4cm (up to 10cm), Bivalves 3-4cm.	Backset laminated, sometimes massive.	Fragments of coralline red-algae, molluscs, benthic forams, echinoid plates, bryozoans, small gastropods, bivalves.	Channel-shape 3-4m thick, extend up dip 15m.
<b>Fe</b>	Floatstone, Matrix-supported conglomerate.	Coarse sand-size to fine-gravel.	Rhodoliths 3-4cm (up to 13cm), limestone pebbles ( up to 12cm), bivalves 3-4cm.	Backset lamination.	Fragments of coralline red-algae, molluscs, benthic forams, oolites, echinoid plates, bryozoans, small gastropods, bivalves.	Channel-shape 150-200cm trough thick, 6-10 width, extend up dip 15-20m.
<b>Ff</b>	Rudstone, Clast-supported conglomerate (bivalve dominated).	Coarse sand-size to fine-gravel.	Bivalves 4-6cm, limestone pebbles (5-6cm).	Backset lamination.	Fragments of molluscs, small gastropods, few fragments of coralline red algae (Mesophyllum, Sporolithon, rare Lithophyllum), bryozoans, foraminifera, ooids, echinoid plates and spines.	Channel-shape, trough thick 120 to 180cm, width 3-6 m.
<b>Fg</b>	Clast-supported conglomerate (+ pebbles).	Coarse sand-size to fine-gravel.	Limestone pebbles 2 to 8cm, rhodoliths 3-4cm (up to 8cm), bivalves 3cm (up to 10cm).	Backset lamination.	Fragments of molluscs, small gastropods, few fragments of coralline red algae (Mesophyllum, Sporolithon, rare Lithophyllum), bryozoans, foraminifera, ooids, echinoid plates and spines.	Channel-shape, trough 140 to 250cm, width 3-6m, extend up-dip 25-30m.
<b>Fh</b>	Clast-supported conglomerate (+ boulders).	Coarse sand-size to fine-gravel.	Rhodoliths >8cm (up to 13cm), limestone clasts from 2-3cm to 30cm.	Backset lamination.	Fragments of molluscs, small gastropods, few fragments of coralline red algae (Mesophyllum, Sporolithon, rare Lithophyllum), bryozoans, foraminifera, ooids, echinoid plates and spines.	Channel-shape, trough 200 to 280cm, width 3-6m, extend up-dip 25-30m.

Fig. 3.4.1.13 Table summarizing major features of the facies recognized at Forma.

### 3.5 Nalinot

In the Na Linot area (Fig.3.5.1) several backset bedded units can be studied both along depositional dip (NE-SW, parallel to paleo-flow) and strike directions. This outcrop is place at about two kilometers north of the outcrop of Forma. Backset bedded intervals occur intercalated with fine-grained laminated wackestone/packstone (Pomar *et al*, 2002).

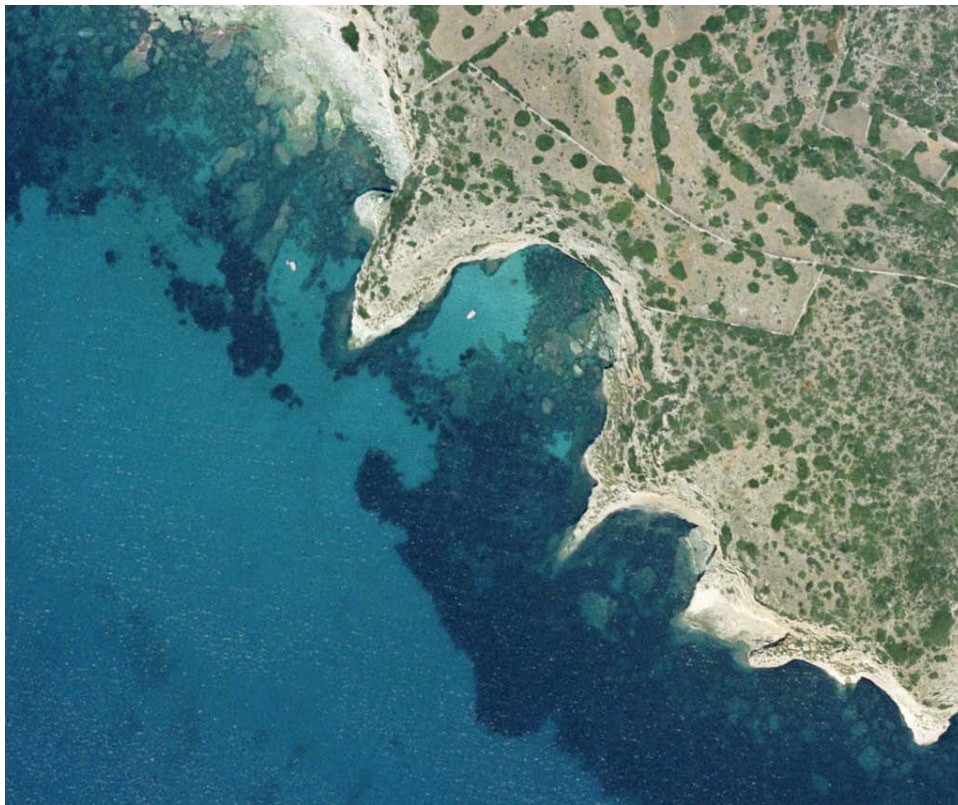
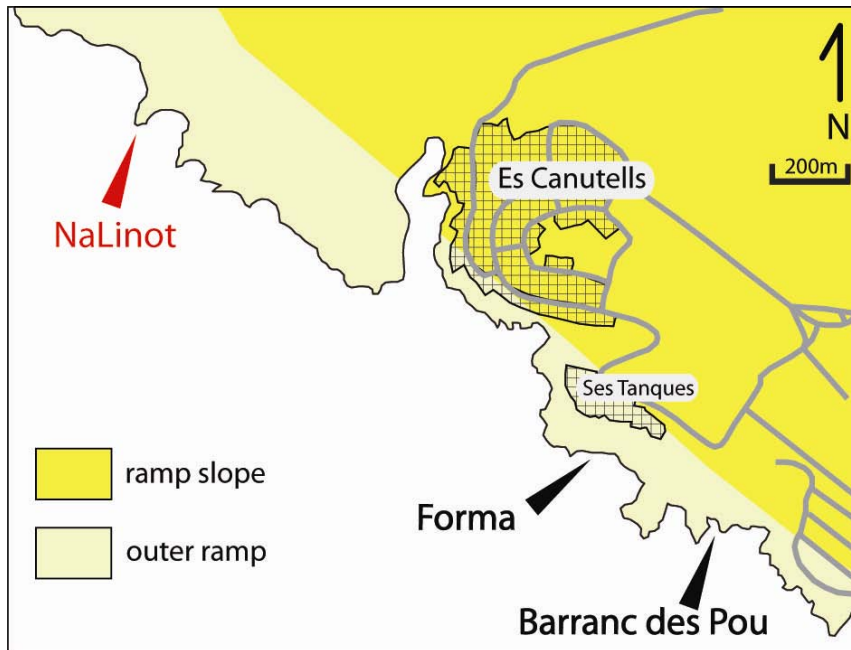


Fig.3.5.1 (Above) Location map of Nalinot outcrop; (below) satellite photo of the studied outcrop.



In this outcrop at least 4 different intervals presenting backset bedding are found deposited one over each other separated only by few meters of finer-grained sediment (Fig.3.5.2). This is the only outcrop where it is possible to observe that the studied deposits are always found in the same direction, that means along the axis of the wide slide-scars (Fig.3.5.3). This is important in the interpretation on the formation of these deposits because they are not randomly distributed along the base-of-slope of the ramp depositional system.

In this locality six main facies have been recognized, always based on observations on grain-sizes, sedimentary structures and bioclastic components.

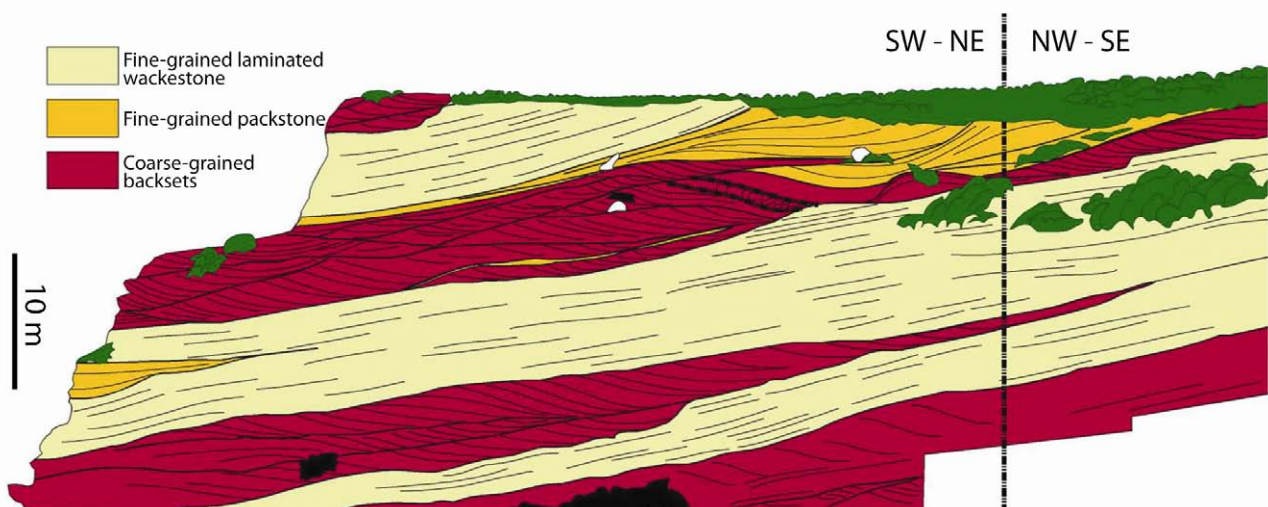


Fig.3.5.2 Panoramic view of the outcrop of the promontory of Nalinot: three different main units are recognized: the light yellowish colour are the fine-grained laminated wackestone of facies Na, the orange colour represents facies Nb, and the red colour represents the backset bedded deposits therefore facies Nd, Ne. Log 1 is in Fig 3.5.1.38; Log 2 in Fig.3.5.1.37; the detail in the squared white area is described in Fig.3.5.1.27.

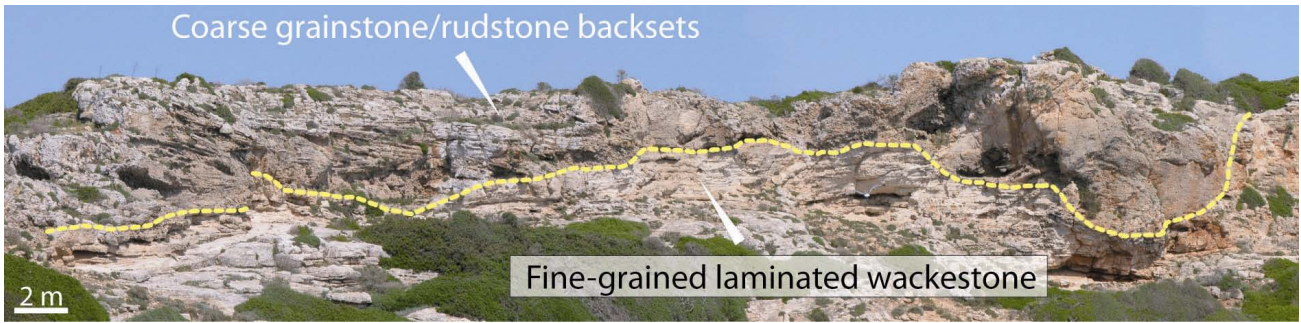


Fig.3.5.3 Erosive surface separating the fine-grained laminated wackestone below from the coarse-grained backset beds above. The surface is irregular showing a wavy trend due to erosion by several flows.

### 3.5.1 Facies description

#### Facies Na

Facies Na is composed of wackestone/packstone with grains varying from very fine to medium sand-grain-size (Fig.3.5.1.1). Grains are in average less than 0.5 mm. Beds are massive or normally graded, sometimes with planar parallel lamination and current ripples (Fig.3.5.1.5). Bioturbation is found in some layers. Mollusc fragments of size less than 1 cm and thin bivalves are found aligned along lamination (Fig.3.5.1.1 and 3.5.1.2). Foraminifers are rare especially in very fine beds while in slightly coarser one more bioclastic-rich they are more frequent. Fragments < 0.5 mm of coralline red algae are also found as well as echinoid plates.

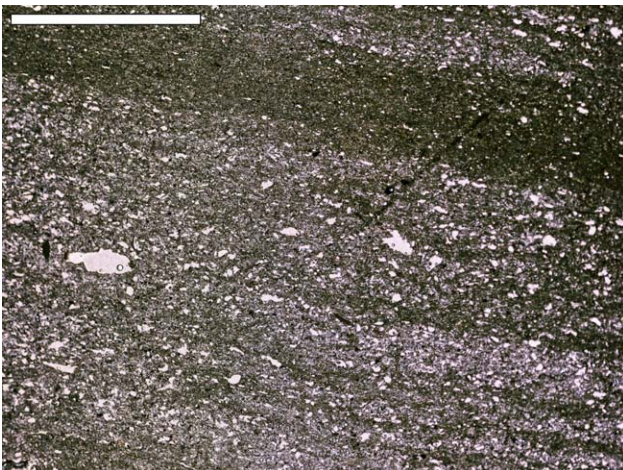
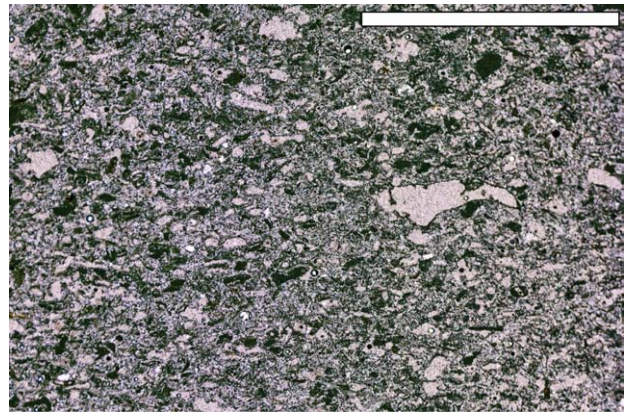
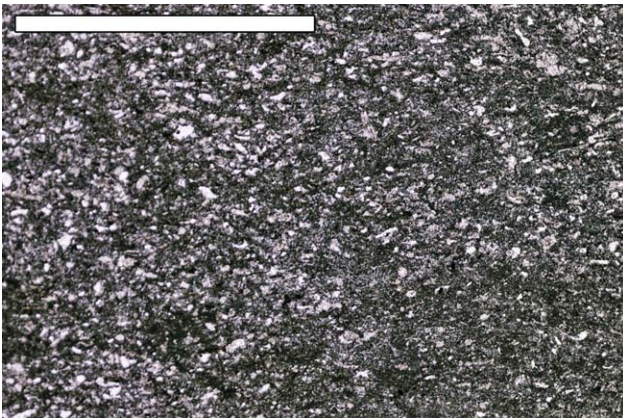


Fig.3.5.1.1 Thin sections showing facies Na, wackestone/packstone. Foraminifers and small fragments of molluscs. As shown by these pictures, grain-size may slightly change from one bed to another; (top right) coarser-grained bed with abundant fragments of coralline red algae; (bottom left) parallel lamination is evidence by grains distribution, the darker layer in the upper part has a lower porosity compared to the lower part. Scale bar 1 cm. Samples NL30, NM2, PN23.

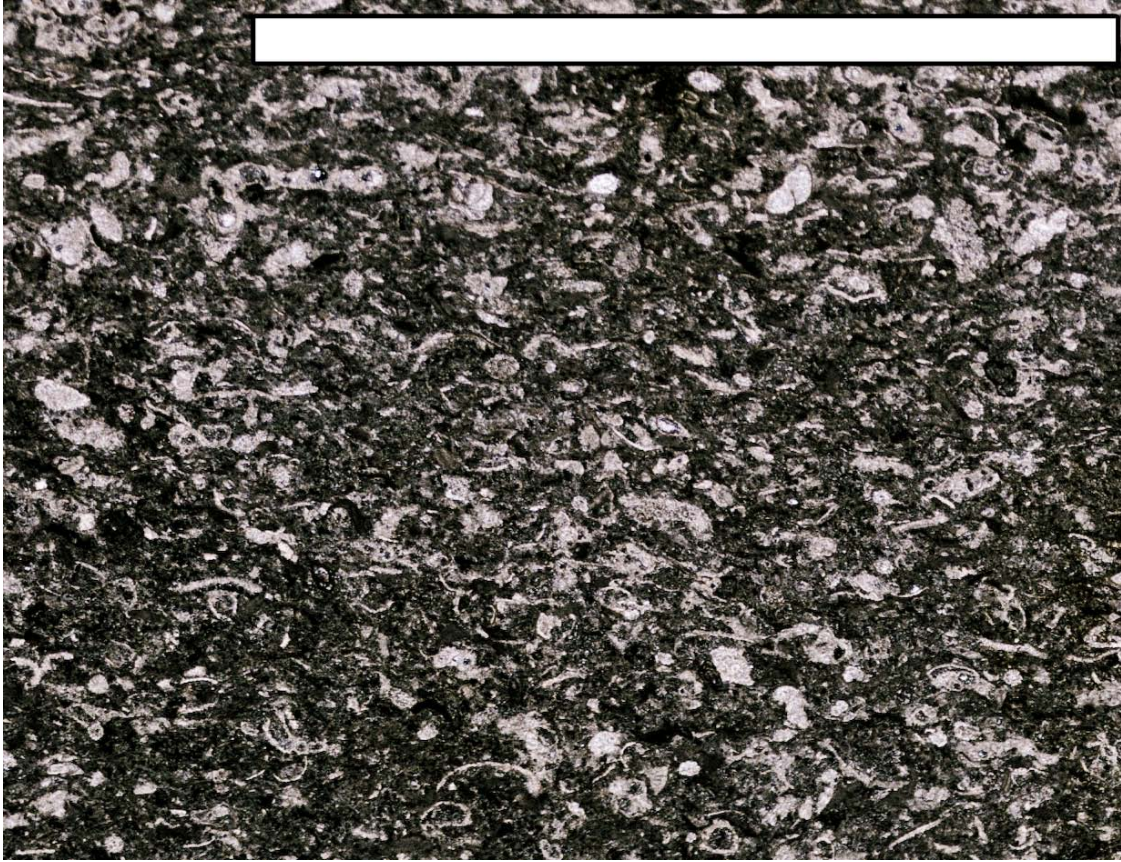


Fig.3.5.1.2 Thin section of facies Na, packstone characterized by abundance in thin bioclastic fragments and foraminifers. Scale bar 1 cm. Sample PN20.

Oblate echinoids are also found with preserved shells only slightly crushed; they are also found oriented along lamination (Fig.3.5.1.4).

Degree of porosity may vary along with grain-size (see thin sections in Fig.3.5.1.1. and 3.5.1.2): in finer grained beds, porosity is low (<20%) and it is higher in coarser beds especially due to dissolution of bioclasts (25%).

Small-scale scars (50 cm to few metres) are often truncating the succession (Fig.3.5.1.5, A). Convolute laminations probably due to rapid dewatering are also found (Fig.3.5.1.6). Brecciated intervals can be found corresponding to large-scale slide-scars (Fig.3.5.1.5, D and also Log1 in Fig.3.5.1.38). Some beds are completely dolomitized. Beds are sheet-like with thickness varying in average from 4-5 cm to 15 cm, but sometimes up to 40 cm (Fig.3.5.1.3). Thicker beds which reach 85 cm in thickness, found in the lowermost part of the NaMala Log are pervaded by bioturbation (Fig.3.5.1.38). The overall succession of facies Na outcropping at the locality of Nalinot and the adjacent NaMala is of about 45-50 m (Fig.3.5.2).

Strata dip in a SW to WSW direction (N230 to N270 7° to 12°).

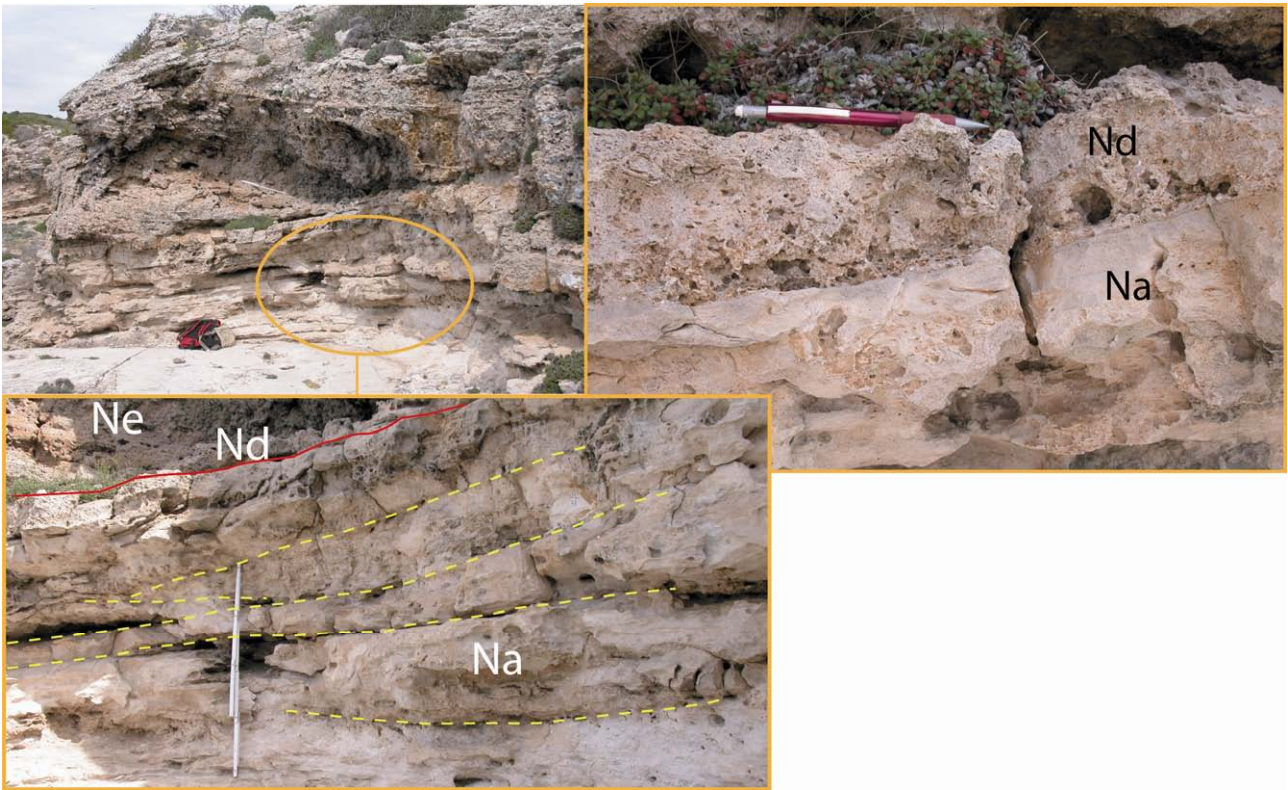
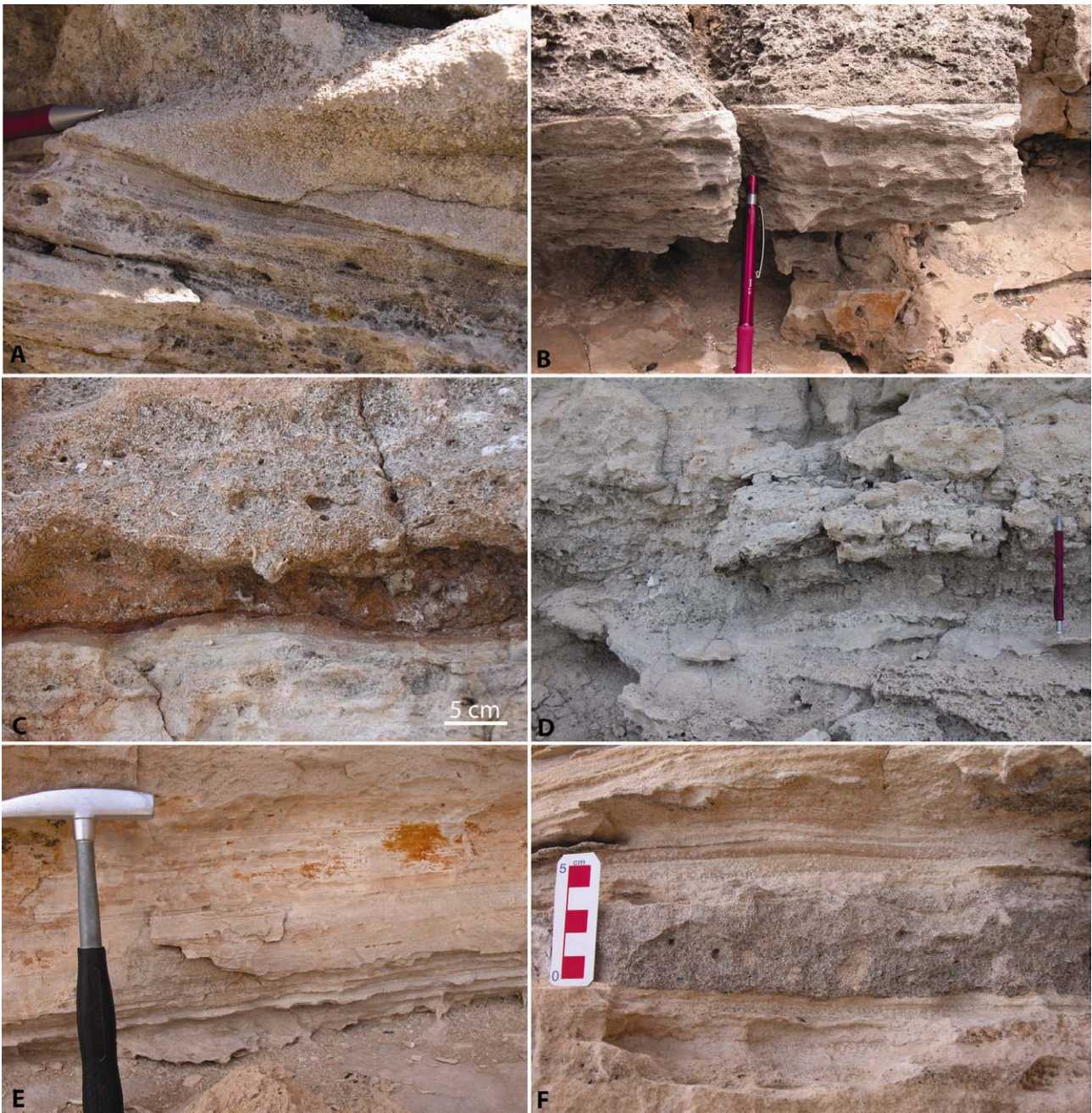


Fig.3.5.1.3 Detail of the erosive surface found at the base of the backset bedded deposit. This boundary has an irregular trend with deep scours that erode the underlying facies Na. This surface is very sharp and evidenced also by the noticeable variation in grain-sizes. In the lower picture a detail of the stratification of facies Na is reported, where it is visible that beds are here 15-20 cm thick and they are sometimes truncated by the overlying bed.



Fig.3.5.1.4 Picture of the finely laminated wackestone with echinoids aligned along lamination.



*Fig. 3.5.1.5 Details of Facies Na: (A) small-scale erosive surface within facies Na; (B) erosive surface at the top of the facies Na, note the change in grain-size that noticeably increase in the overlying erosive facies; (C) irregular, wavy erosive surface that marks the boundary between facies Na (below) and facies Nd; (D) brecciated interval corresponding to one of the large-scale slide-scar surface (E) planar parallel stratification; (F) a normally graded bed.*



*Fig.3.5.1.6 Photo of convolution of the thinly laminated wackestone; found right below one of the large-scale slide-scar.*

## Facies Nb

This facies is characterized by a packstone/grainstone composed of fine to very-coarse sand-grain-size bioclastic-rich calcarenite. Planar parallel lamination is often more visible in the upper part of the channelized deposit (Fig.3.5.1.12). Facies Nb is composed of a highly porous (>40%) calcarenite with grains smaller than 1mm and in average <0.3-0.4 mm. Components are mainly mollusc fragments, small pieces of coralline red algae (*Lithophyllum*, *Sporolithon?*) which can be very abundant in some beds, benthic foraminifers, rare bryozoans and few gastropods and oolites are also sporadically found (Fig.3.5.1.7-8-9). In some beds grains are very well rounded (Fig.3.5.1.8) while in others they present more irregular subangular forms (Fig.3.5.1.7). Grains have frequently an elongated shape and as well as bivalve fragments are aligned along lamination.

Porosity may significantly vary based on grain-size: it is always high (>40%) to very high but it increases noticeably with grain-size since it is mostly due to dissolution. Along the rims of pores a border of calcite cement is often found (Fig.3.5.1.7). Dolomitization is unevenly distributed.

Facies Nb is found in channelized deposits that deeply scour the underlying facies Na (Fig.3.5.1.11). These beds in the trough can reach a thickness of 6 m and a width of 10 m while along depositional dip they can be followed sometimes for the whole outcrop where possible (few tens of meters). Thickness tends to increase downdip (toward SW).

At the base they are bounded by a sharp, erosive surface that dips of about 12° southwest. The upper boundary is sometimes transitional (Fig.3.5.1.12), sometimes slightly erosive surface that dips in the same direction but with a lower angle.

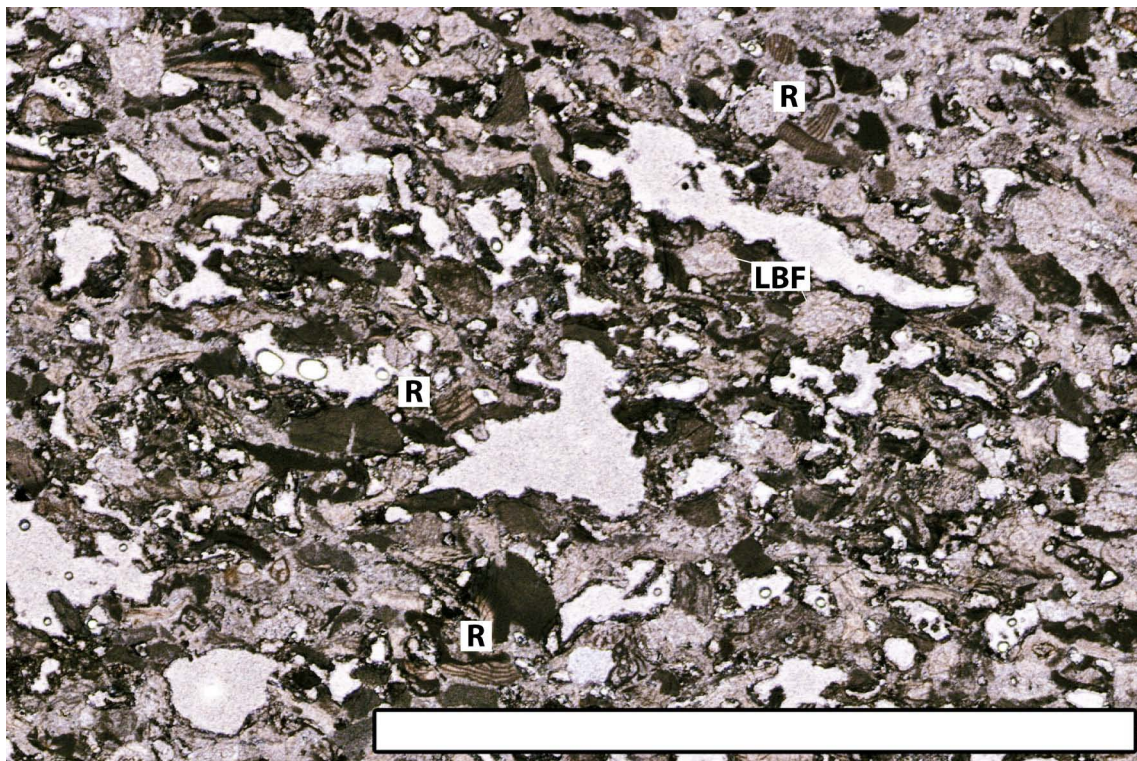


Fig. 3.5.1.7 Thin section showing highly porous facies Nb. (R) red algae fragments; (LBF) large benthic foraminifers; a lamination dipping to the right is slightly perceived. Scale bar 1 cm. Sample PN4.

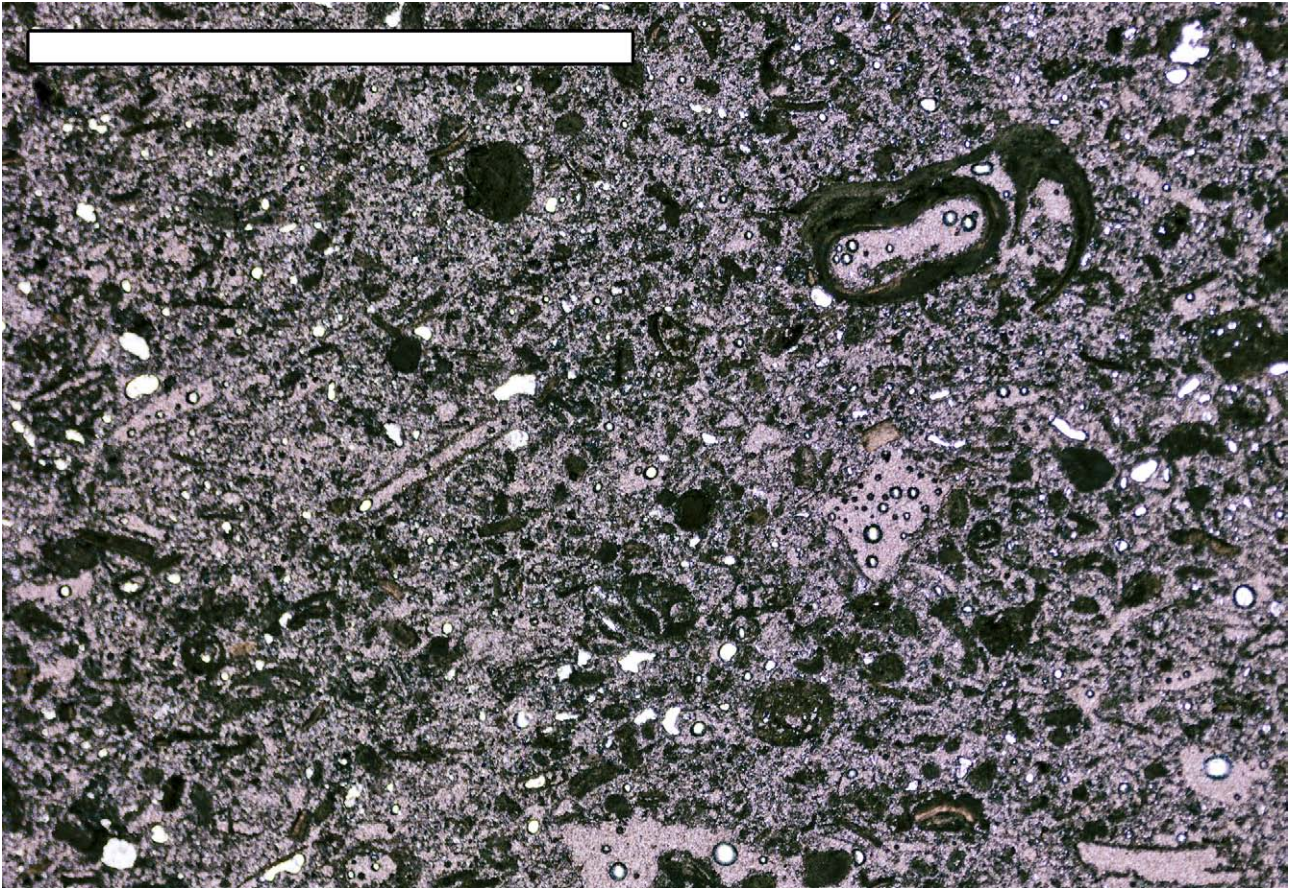


Fig.3.5.1.8 Thin section of facies Nd; bioclastic grainstone with abundant fragments of red algae and foraminifers; porosity is inter-particle and because of dissolution. Scale 1 cm. Sample GI4.

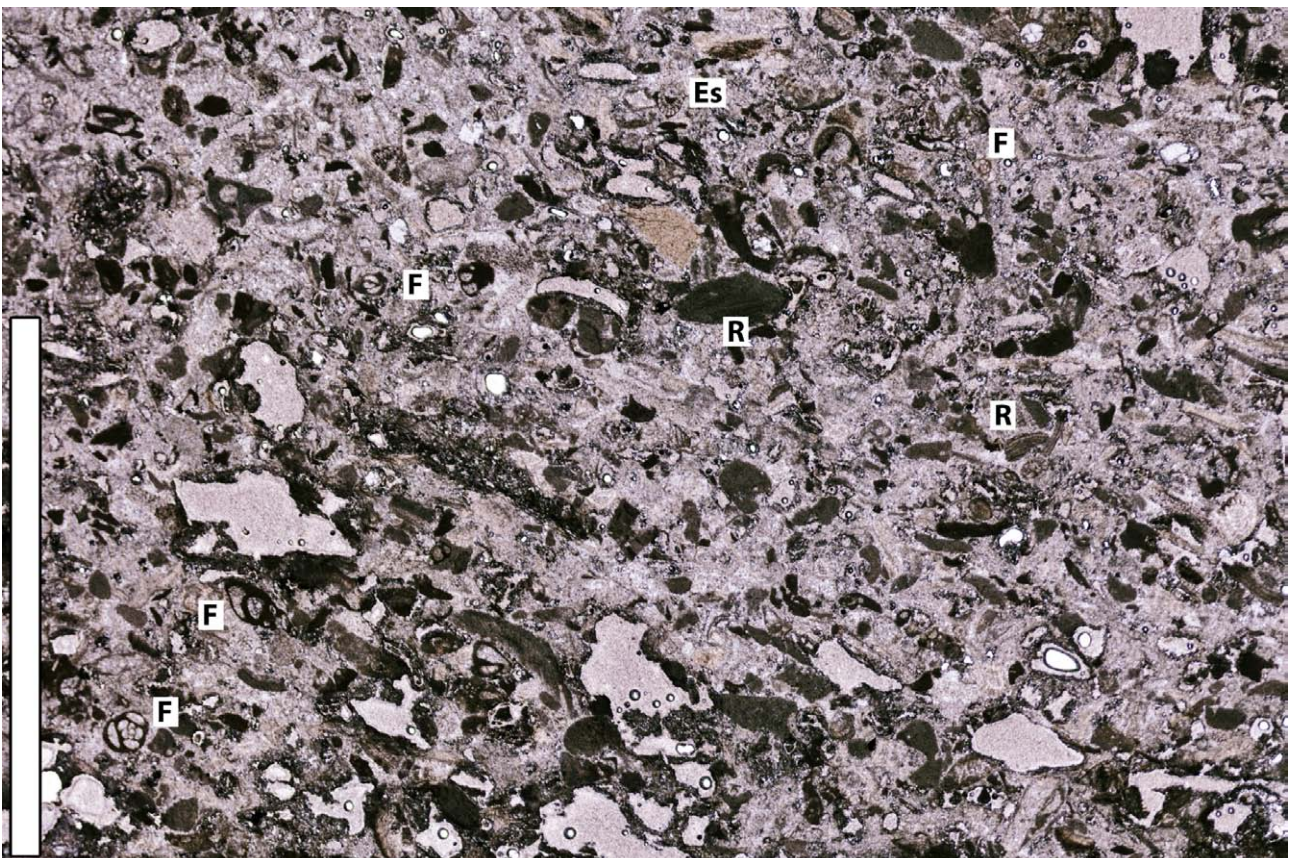


Fig.3.5.1.9 Thin section of facies Nb; abundant (R) red algae fragments, (F) foraminifers. Porosity is very high inter- and intra-particle. Scale 1 cm. Sample PN32.





*Fig. 3.5.1.10 Thin section of facies Nb. Bioclasts are average <math><0.5\text{ mm}</math> with larger fragments of red algae and frequent foraminifers. Dissolution of large bivalves noticeably increase porosity. Scale 1 cm. Sample PN24.*



*Fig.3.5.1.11 Panoramic view from the sea of the Nalinot promontory from where the channel-shaped deposits of facies Nb are more easily visible and found in different intervals.*

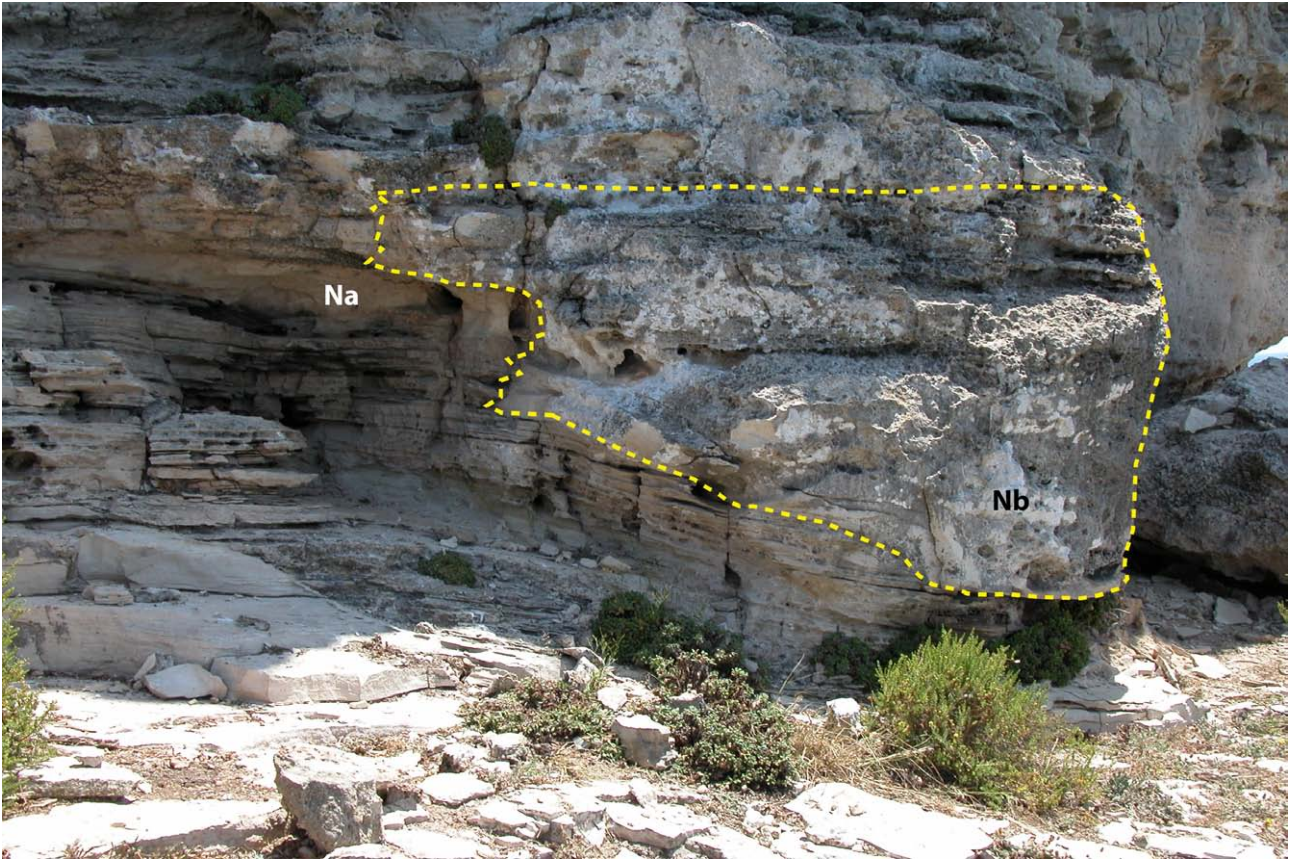


*Fig.3.5.1.12 View of a small-scale channelized unit of facies Nb; note the erosive base truncating the underlying facies Na and the pinching out laterally towards the upper part of the infilling of the channel.*

## Facies Nc

This facies consists of massive clast-supported bioclastic breccia. The matrix of this breccia is composed of a bioclastic coarse to very-coarse calcarenite. Major components are abundant dissolved bivalves present mainly only as moulds, gastropods, coralline red algae in very small fragments and bryozoans.

Clasts are composed of centimetre- to decimetre-size limestone clasts composed of a bioclastic grainstone. These clasts are sub-angular, disc shaped of size average ranging between 2 and 8 cm and composed of an oolitic-grainstone (Fig. 3.5.1.13).

The lower boundary is a sharp erosive surface that slightly scours the underlying finer-grained facies Na, while at the top it is bounded by another sharp surface which is marked by a strong variation in grain size since facies Na is also found above facies Nc (see Log.2 Fig.3.5.1.37).

Beds are found in small chute-shape units which in the trough can be thick 25-40 cm with a width of 150-200 cm. This facies has been found rarely and always in positions below the coarse-grained backset bedded units described below.

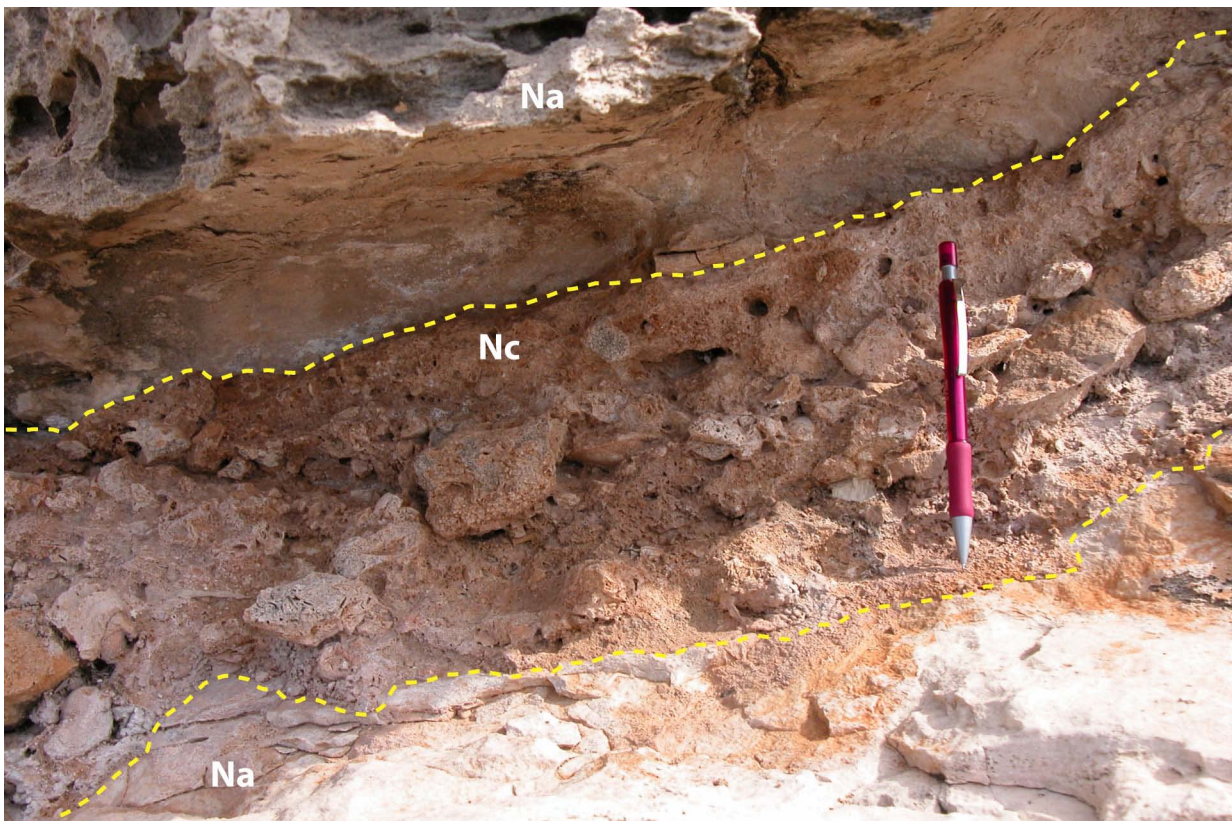


Fig.3.5.1.13 Photo of the breccia characterizing facies Nc.

## Facies Nd

Facies Nd is represented by a matrix-supported bivalve rich conglomerate characterized by cross-lamination. The matrix of the conglomerate is of a medium to very coarse sand-size calcarenite composed of oolites and bioclasts (Fig.3.5.1.14-16). Composition is of mollusc

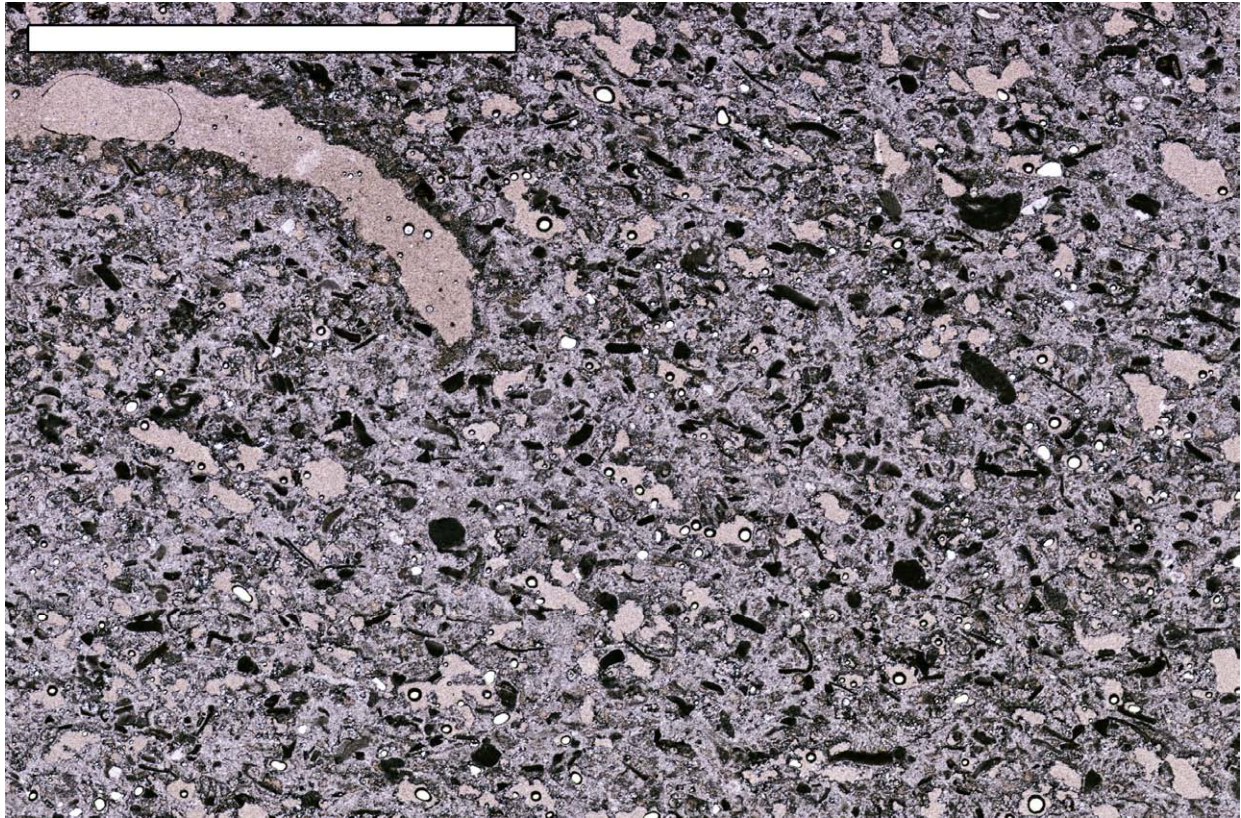


Fig.3.5.1.14 Thin section showing highly porous facies Nd. Scale 1 cm. Sample PN26.

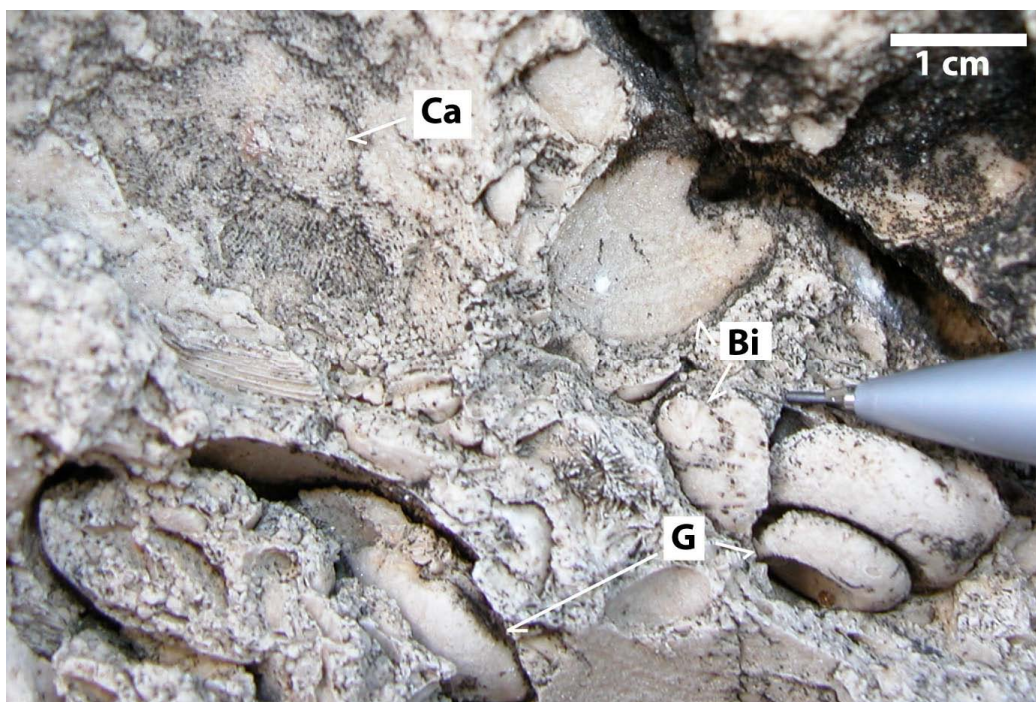


Fig. 3.5.1.15 Photo showing the major components of facies Nd, (Bi) bivalves, (Ca) calcareous algae, (G) gastropods.

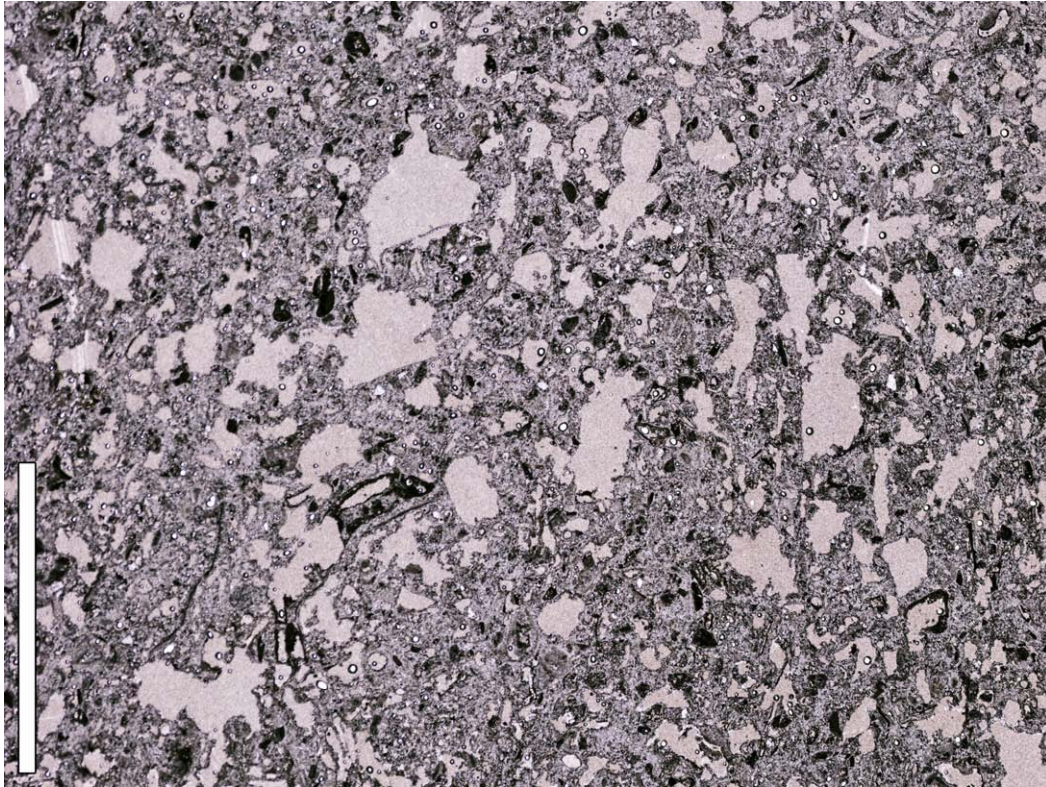


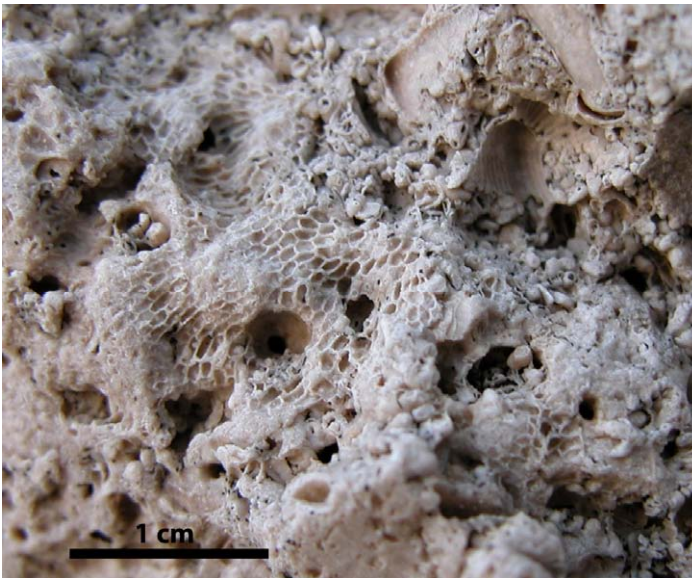
Fig. 3.5.1.16 Thin section of facies Nd. Note the high porosity of this calcarenite.



Fig.3.5.1.17 Picture showing a bivalve-rich deposit: valves are very abundant and mainly concave-up.



*Fig.3.5.1.18 Bioerosion traces on the surface of the inner model of a bivalve.*



*Fig.3.5.1.19 These three photos show a close-up of some of the bioclastic components of facies Nd; above and top right, calcareous algae; bottom right rhodolith. In this figure it is also possible to appreciate the coarse-sand-size of the matrix.*

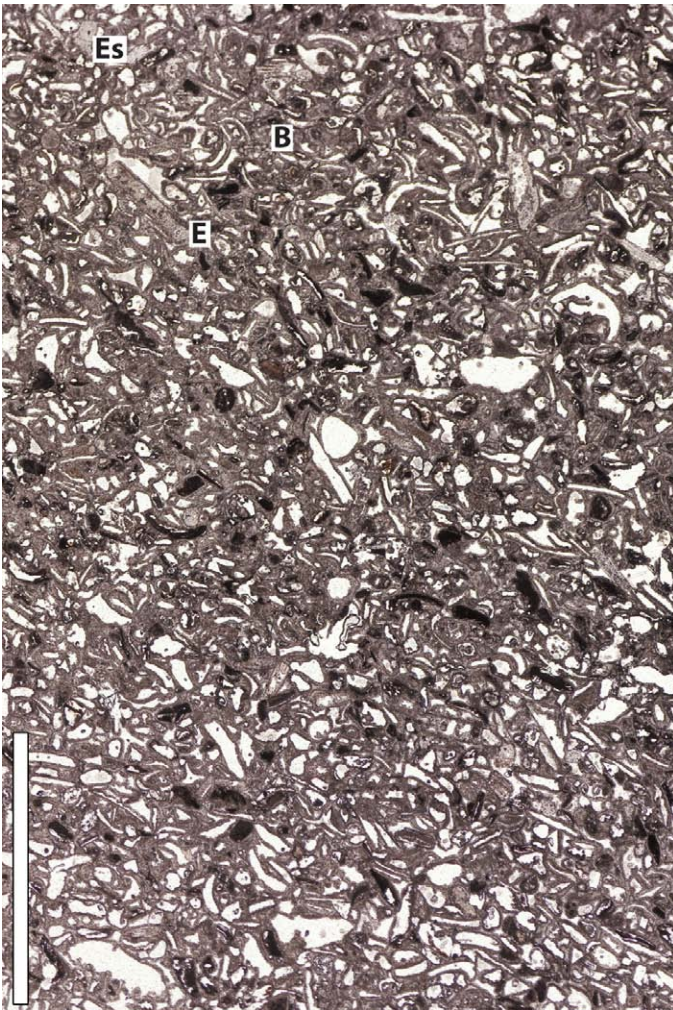


*Fig.3.5.1.20 Thin section of facies Nd. Grains are mainly represented by dissolved fragments of bivalves which show a light immersion to the right. Fragments of red coralline algae, E) echinoid plates, Es) echinoid spine, foraminifers. High mouldic porosity due to dissolution of the nuclei of grains. Scale bar 1 cm.*

fragments, mainly bivalves (5-6 mm) (Fig.3.5.1.17), very small pieces of coralline red algae (<0.5 mm), small rhodoliths (Fig.3.5.1.19) calcareous algae (Fig.3.5.1.15-19) and oolites which are mainly dissolved and present only the outer coats (Fig.3.5.1.9). Few benthic foraminifers have also been recognized. Sediment is very poorly sorted but grains are often sub-rounded. Clasts are represented by bivalves (from 1 cm up to 5 cm) mainly dissolved or present as internal moulds sometimes with bioerosion traces (Fig.3.5.1.18), with convex-up, concave-up valves oriented along lamination, so and the larger ones are concentrated in layers (Fig. 3.5.1.20 and 3.5.1.21). Gastropods, 1-2 cm and calcareous algae are also frequent (Fig.3.5.1.15). Grain-size tends to increase in the down dip part of the single deposit. Little grains of about 3 mm in size of a cemented oolitic grainstone are also present.



*Fig.3.5.1.21 Photo showing the distribution of bivalves in facies Nd, note the concentration of larger valves in layers.*

Elongated in shape, bioclastic fragments are aligned along lamination (Fig. 3.5.1.20 and 3.5.1.21).

This bioclastic rudstone has a very high porosity (>50%) and it is very weakly cemented. Porosity is related to dissolution of bioclasts which often present around the pore a rim of calcitic microsparitic cement sometimes showing different phases of growth (Fig. 3.5.1.20).

On a parallel to depositional dip direction, cross-lamination dip eastward with angles that vary from up to 10° to horizontal in the up dip direction; on the strike section lamination goes from slightly concave to horizontal to slightly convex. The cross lamination is characterized by a continuous alternation of intervals richer in matrix with more bioclasts-rich ones; the resulting effect is of an alternating normally to inversely graded transitional succession of intervals (Fig.3.5.1.21).

Beds are channel shaped with maximum thickness in the trough of 80 to 150 cm and width that varies from 1 m to 4-6 m. Along depositional dip they extend for 8-10 m with a variation in thickness which tends to increase down dip, pinching out landward.

Beds are bounded by erosive surfaces which deeply scours the underlying beds.



## Facies Ne

Facies Ne is represented by a clast-supported conglomerate with cross-lamination. Grain size of the matrix is of a medium to very coarse sand-size to fine granule size calcarenite and grains size of clasts varies from pebble to cobble to boulder size (Fig.3.5.1.22), thus the sorting of this facies is very low. Matrix is of a highly porous, weakly cemented grainstone/rudstone composed of fragments of molluscs, bivalves, gastropods, benthic foraminifera, very small pieces of coralline red algae, few echinoid plates, coated grains and of loose ooids (Fig.3.5.1.23). The nucleus of coated grains may be a bioclast, a fragment of coralline red algae or a benthic foraminifer but the majority of grains are re-crystallized (Fig.3.5.1.25).



*Fig.3.5.1.22 Photo of facies Ne; note the clear lamination dipping towards the right and the abundance of large limestone pebbles and boulders.*

Clasts are represented mainly by limestone clast, large bivalves, gastropods and fragments of corals (Fig.3.5.1.24). This conglomerate is dominated by limestone pebble, cobble to boulder-size clasts composed of oolitic- and bioclastic-rich grainstone; sorting is very low with size along the *a* axis ranging from few cm up to 22-25 cm (average/more frequent 7-8 cm), they are sub-rounded bladed to discoid in shape. In some layers where very abundant, they are imbricate.

The oolitic grainstone composing these clasts is made of partly dissolved superficial ooids ("oomolds"); the porosity results to be high due to intragranular porosity caused by dissolution

(Fig.3.5.1.26) of the cortices and/or nuclei. Ooids are in average  $< 0.5$  mm (Fig.3.5.1.26). The microfabric of the cortex is of concentric (tangential) laminae but in some clasts the ooids are partly or completely micritic with obliterated or absent laminae due to a pervasive micritization of the cortex. Sometimes the concentric laminae are preserved in the outer coats (Fig.3.5.1.26.). Aggregate grains are also present  $< 1$  mm.

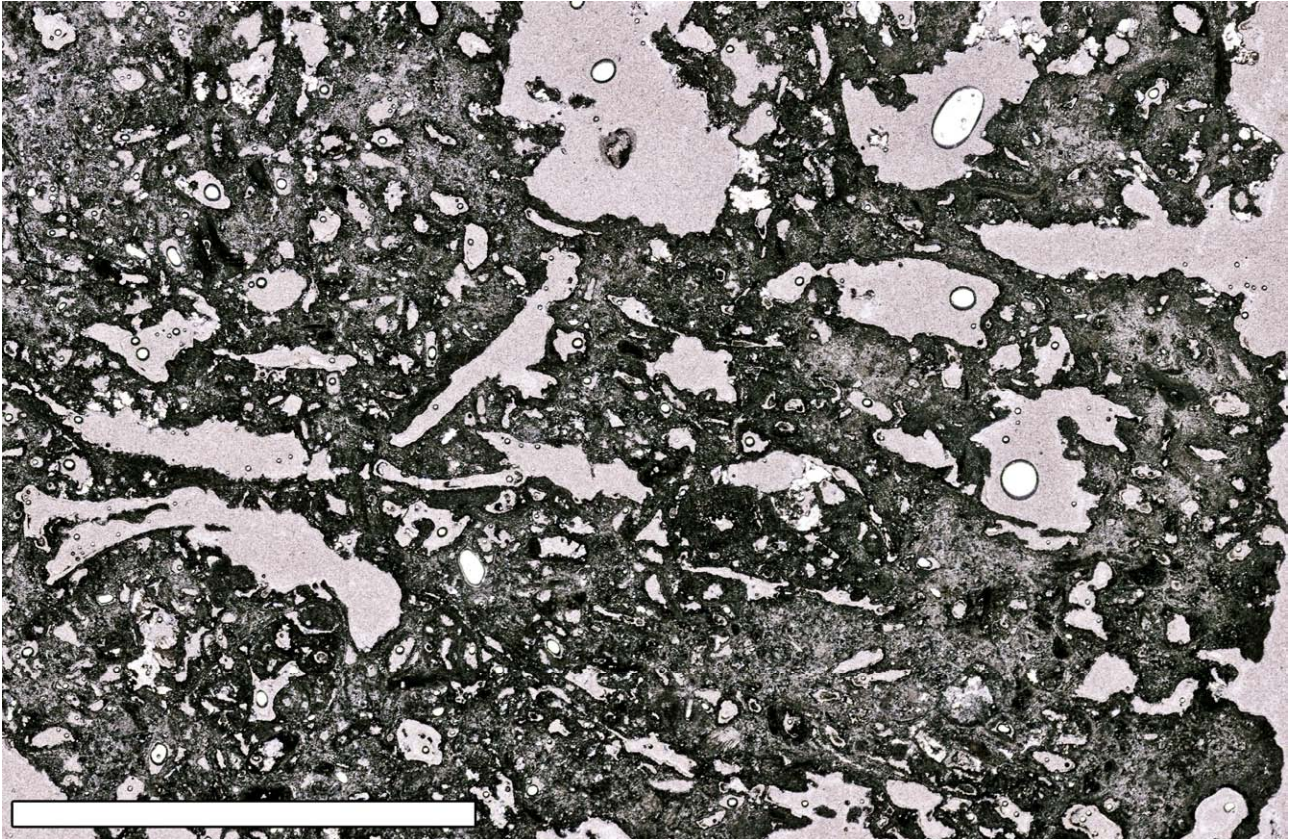


*Fig.3.5.1.23 Thin section showing facies Ne. Porosity is extremely high especially due to dissolution of mollusc fragments. Scale bar 1 cm. Sample PN35.*

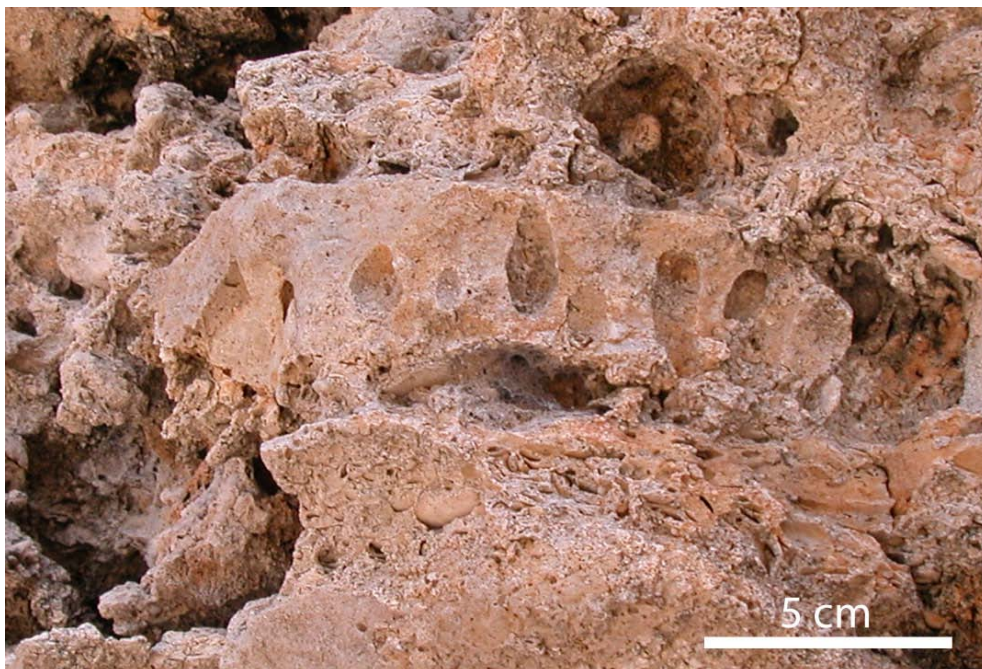


Fig. 3.5.1.24 Large limestone clast highly bored, probably by lithofaga.

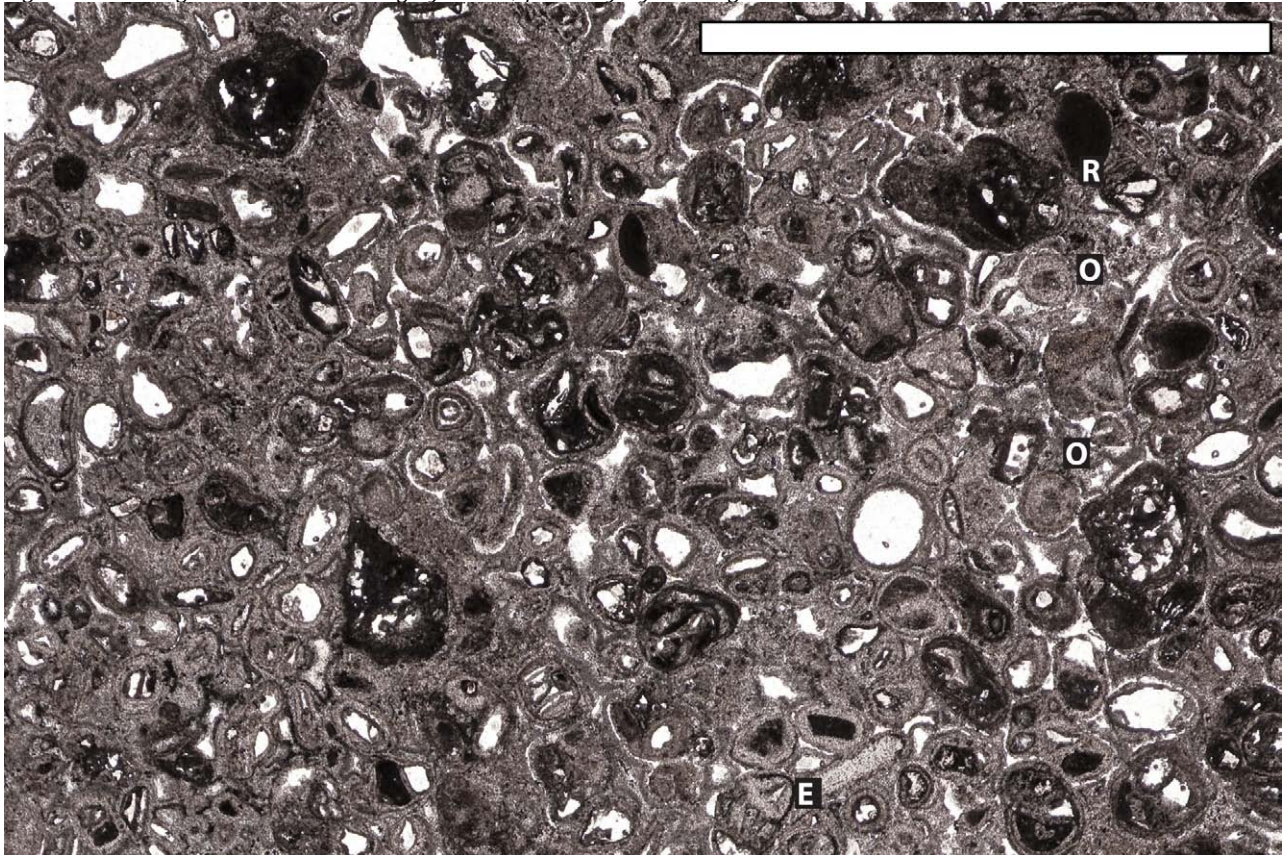


Fig. 3.5.1.25 thin section from a limestone pebble from facies Ne. Grainstone rich in rounded coated grains, with R) coralline red algae fragments; O) oolites; E) echinoid plates. Scale 1 cm. Sample NL43.

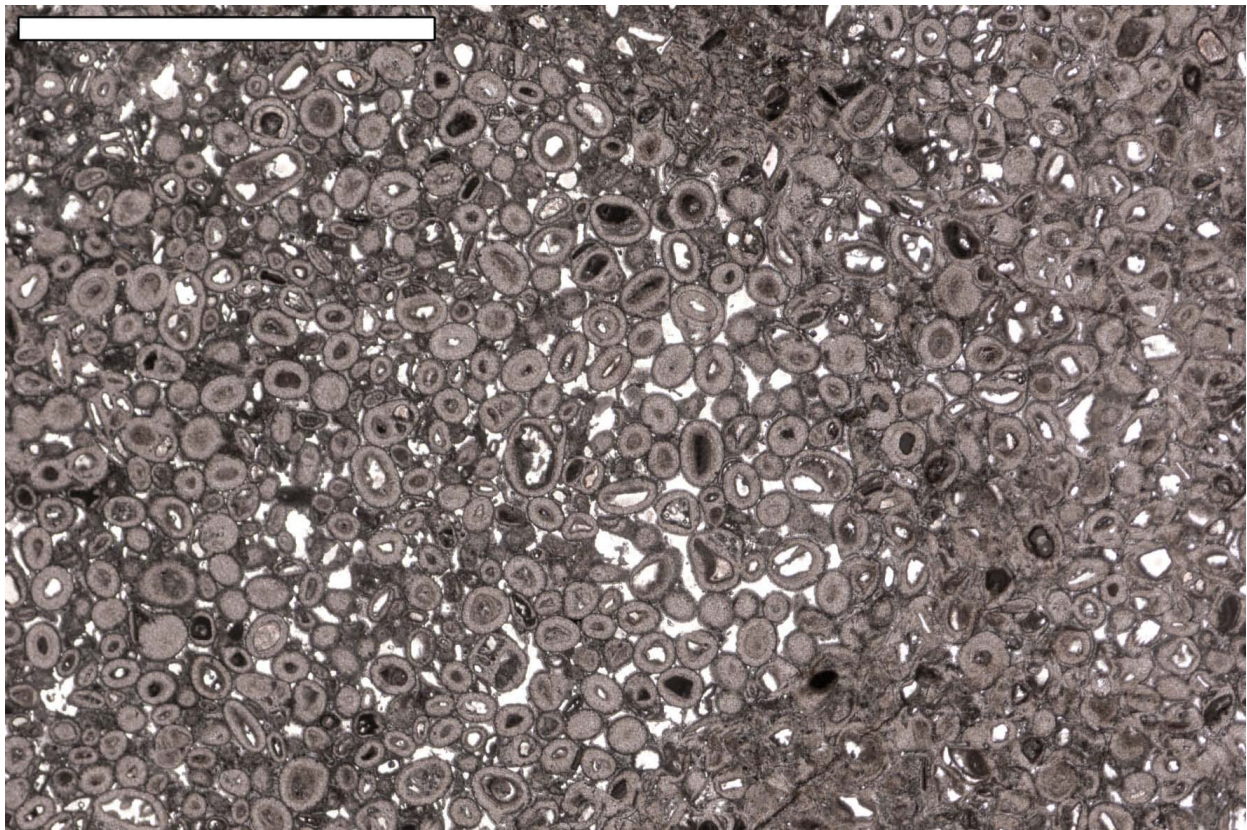


Fig. 3.5.1.26 thin section of a limestone boulder composed of an oolitic grainstone, the ooids are prevalently micritic and some are mouldic. Scale 1 cm. Sample NL33.

The surface of these clasts often presents numerous borings probably due to bioerosion by lithophaga and endolithic algae (Fig.3.5.1.24-28); clasts are also frequently encrusted by serpulids. Bivalves are mainly dissolved and only internal moulds remain, they are in average 2-3 cm in size but they reach up to 6-7 cm, valves are disarticulated, mainly concave-up and oriented along lamination. Gastropods are mainly preserved, small in size, less than 1cm mainly mm. Corals, *Porites*, appear in this facies for the first time in Nalinot, they are quite frequent in little fragments but pieces up to 10 cm have also been found (Fig.3.5.1.28, B); they are distributed along the whole body, still preserved. Rhodoliths are very rare, and when visible at a macroscopic scale they are only in fragments of maximum size 1cm.

Porosity is very high (>50%) both in the matrix and in the limestone pebbles and it is related to weak cementation and mainly to dissolution both inter- and intra-clasts; coated grains and oolites in the limestone clasts are often mouldic with an inner rim of calcitic cement that may partly or totally infill the pores but without following a particular pattern or creating geopetal structures indicating the depositional position of grains (Fig.3.5.1.25-26).

Cross-lamination mainly dips ENE (N65-N70) with dipping angles varying from 24° to horizontal in the up dip direction (Fig.3.5.1.27). Clasts and bioclasts mainly concentrate in layers along lamination so that clast-supported intervals alternate with few centimetres thick matrix-supported intervals creating a normally to inversely graded alternation.

Beds have a channel-shape with maximum thickness in the trough of about 150-200 cm and a width of 2-3 m; along depositional dip they are wedge-shaped thinning in the up dip direction and may extend for about 12-15 m. The axes of channels are directed mainly along an ENE-WSW direction.

Each bed is bounded at the base and at the top by erosive surfaces that scour the underlying bed (Fig.3.5.1.29).

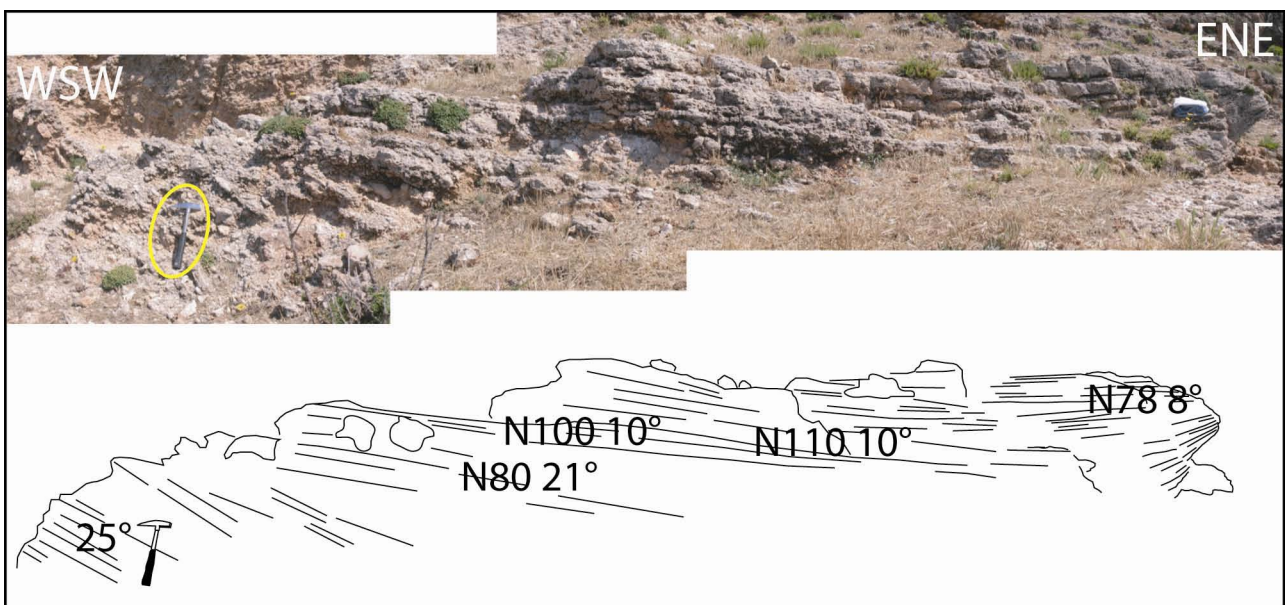


Fig.3.5.1.27 In this figure it is shown a single backset bedded deposit: in the sketch it is evidenced the dipping angles of the laminations that mainly dip on a NE direction and angles varies from 25° in the down dip part of the unit and becomes almost horizontal in the up-dip end.

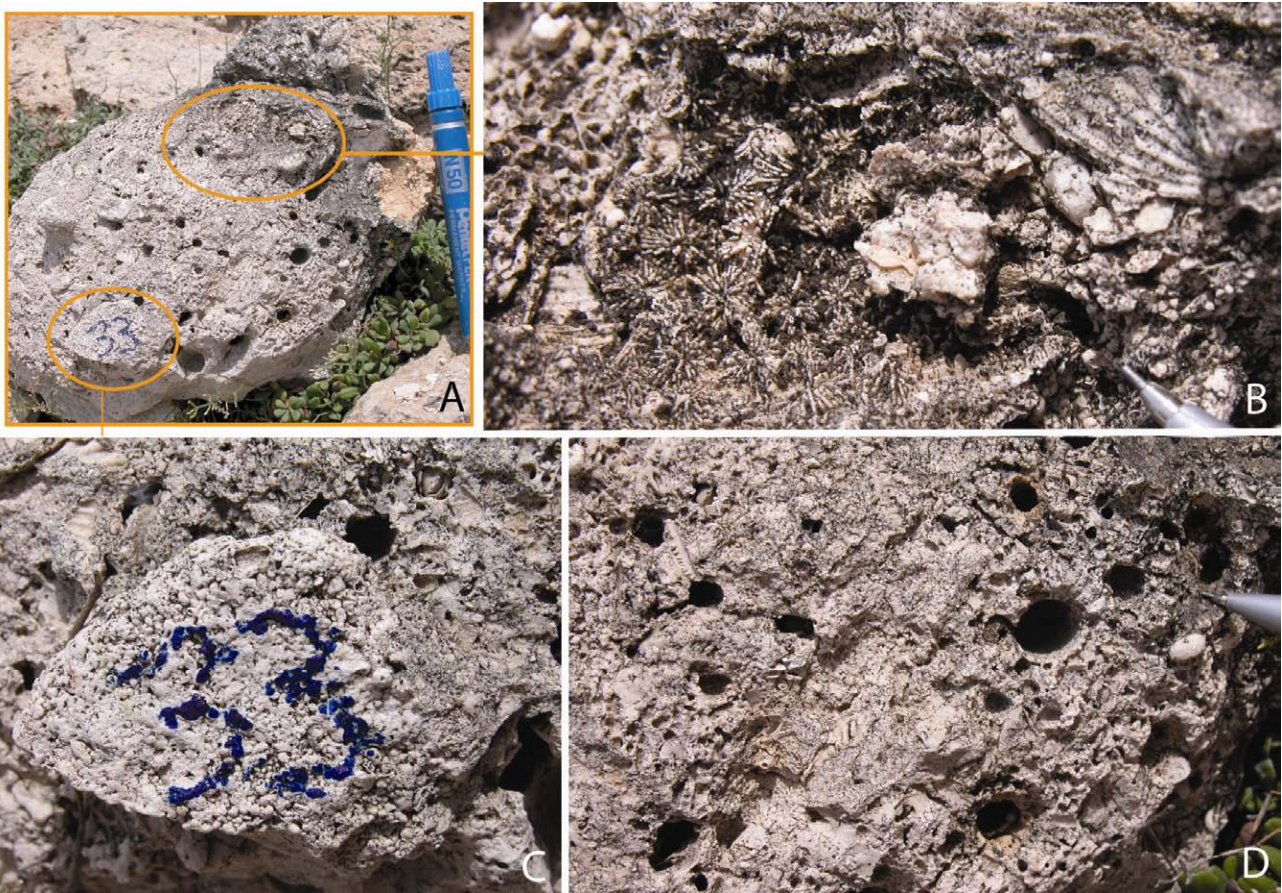
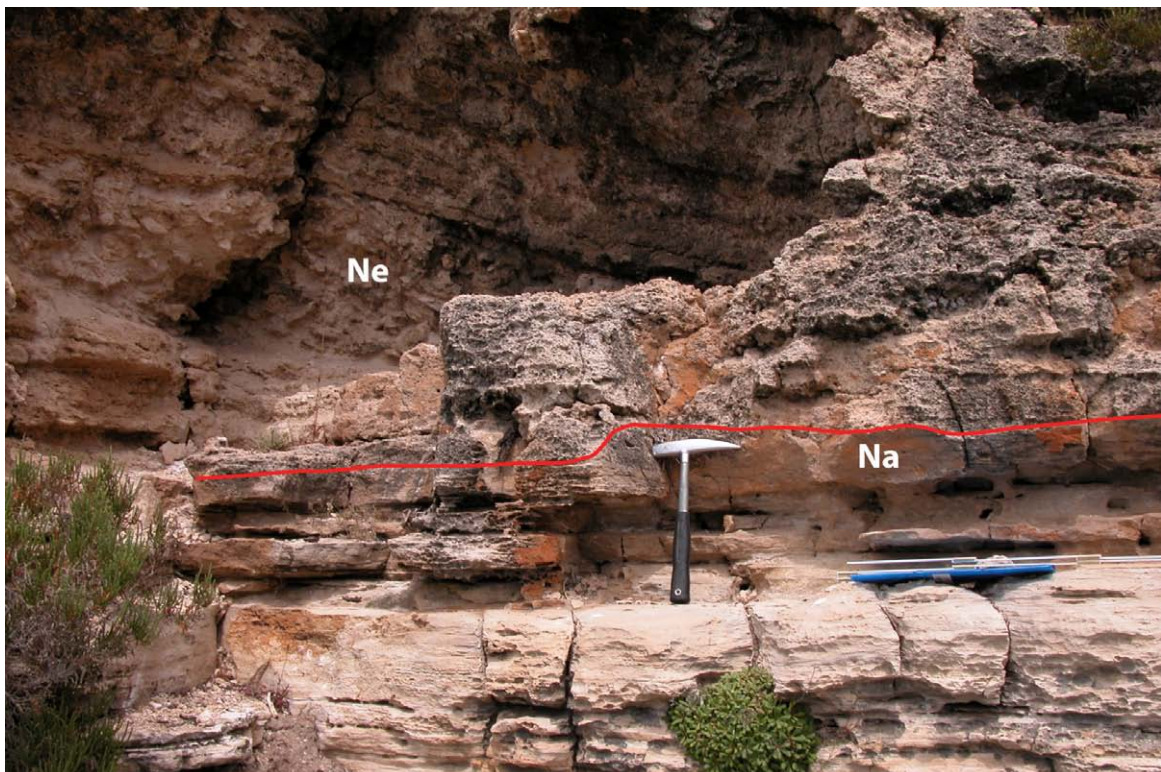


Fig.3.5.1.28 Details of one of the limestone boulders composing facies *Ne*. (A) Picture of the limestone boulder, notice the very round shape and the large size reaching 25cm along the a axis. (B) On the boulder there's also a piece of coral (*Porites?*). (C) Close up picture that shows the coarse grains that composed this limestone boulder which are visible also at a macroscopic scale. (D) Borings on the surface of the boulders, probably due to lithofaga.



*Fig.3.5.1.29 Erosive surface at the base of facies Ne.*

## **Facies Nf**

Facies Nf is characterized by a fine to very coarse-sand to fine granule grain-size calcarenite with planar parallel stratification (Fig.3.5.1.32). The bioclastic calcarenite is composed of a bioclastic-packstone/grainstone with few 1-2 cm mollusc fragments evidencing the lamination. Grains are bioclasts <0.5 mm but mainly <0.3 mm, are of molluscs, thin small bivalves, very small fragments of coralline red algae with elongated shape, benthic foraminifera and few echinoid plates (Fig.3.5.1.30-31). Larger bivalves are average 1-2 cm, mainly dissolved with convex-up, concave-up valves aligned along lamination. Gastropods are very frequent. Beds are normally graded at the base. Porosity is very high and due to dissolution (>40%).

This facies is found in more sheet-like beds, more laterally continuous tabular-sheet-like units organized in 20 to 25 cm thick beds, when found at the top of a backset bedded interval (Fig3.5.1.33). The packages of beds vary in overall thickness from 150 to 600 cm. Planar parallel lamination dip along a southwest direction with average angles ranging around 12°-15°. The features found in this facies, also characterize the up-dip tail of each backset laminated deposit.

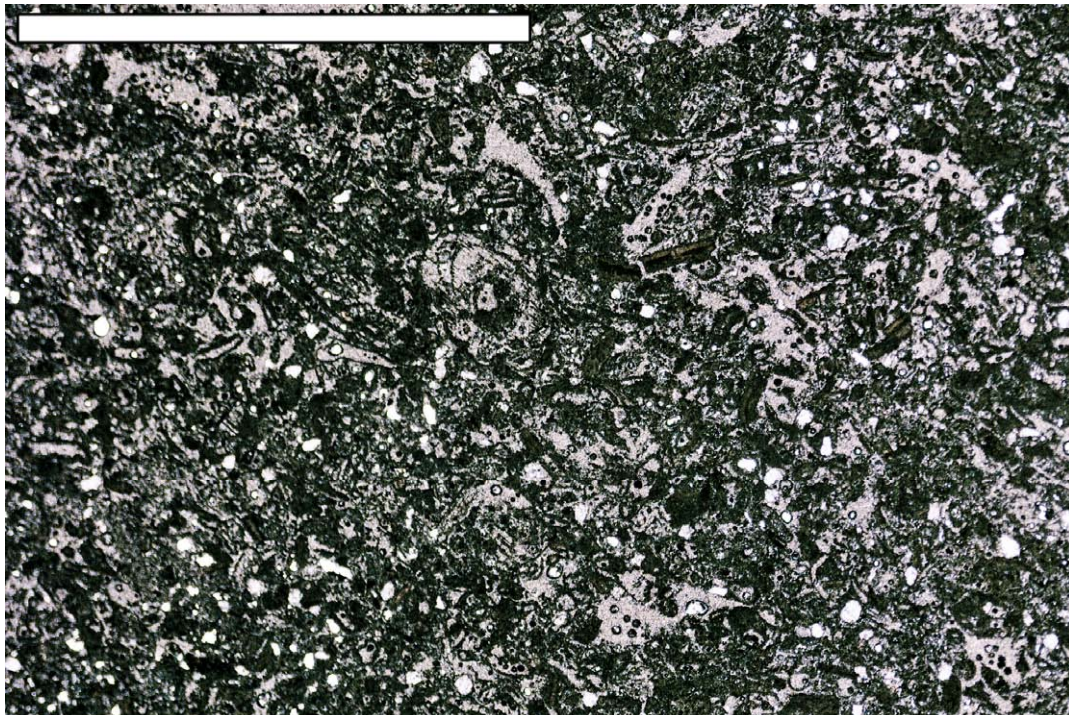


*Fig.3.5.1.30 thin section from facies Nf. Bioclastic calcarenite with fragments of bivalves mainly dissolved and few fragments of red coralline algae. Scale bar 1 cm. Sample E3.*

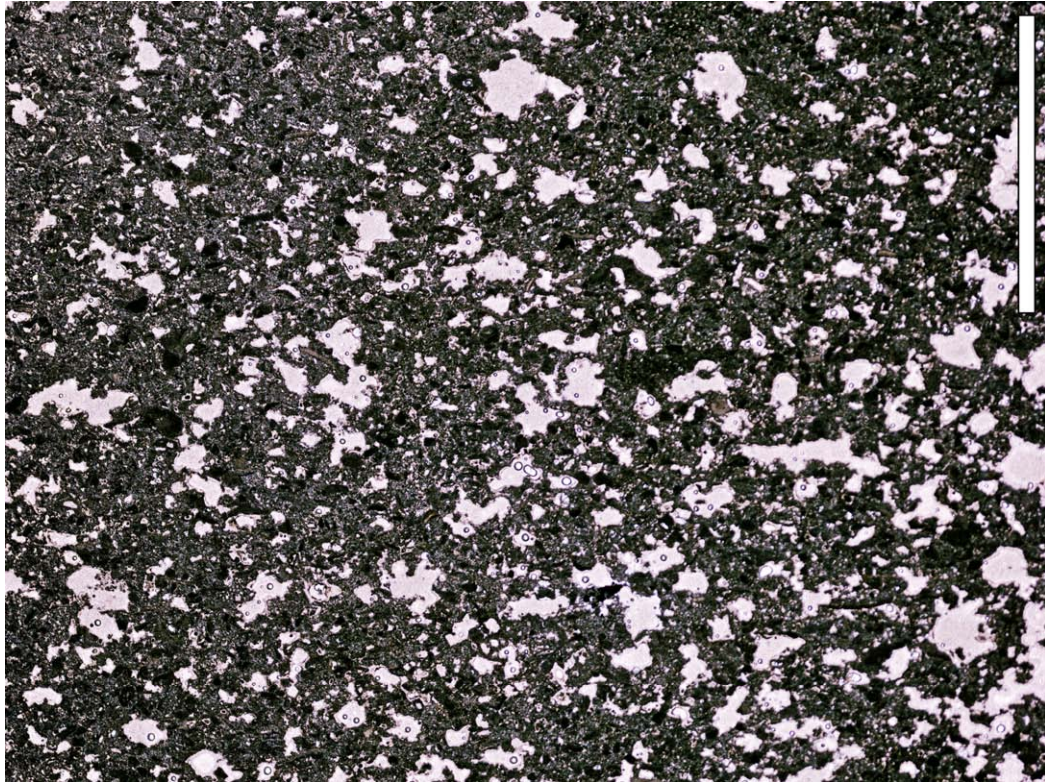


Fig.3.5.1.31 Thin section of facies Nf. Bioclastic calcarenite with porosity up to more than 50%. Scale bar 1 cm. Sample PN25.



Fig.3.5.1.32 Photo showing almost horizontal lamination of facies Nf.



Fig.3.5.33 Panoramic view of the architecture of super-imposing facies with the wide large-scale erosive surface at the base which corresponds to the surface evidenced in Fig.3.5.3. The section is oblique to depositional-dip.

The following pictures and drawings will show the geometrical relationships between different facies recognized at Nalinot. The sections shown are on oblique directions compared to depositional dip, sometimes more parallel to it some others more perpendicular to it.

Tab. 3.5.1 Brief summary of the six facies described at the locality of Nalinot.

<b><i>FACIES</i></b>	<b><i>DESCRIPTION</i></b>
<b><i>Na</i></b>	Very fine to medium sand-grain-size wackestone/packstone with PPS and current ripple cross-lamination.
<b><i>Nb</i></b>	Fine to very-coarse sand-grain-size bioclastic-rich channalized packstone/grainstone with PPS.
<b><i>Nc</i></b>	Coarse-to-very coarse-grained sand-size to pebble-size massive breccia.
<b><i>Nd</i></b>	Medium to very-coarse matrix-supported conglomerate with pebble-size clasts, rudstone, bivalve rich.
<b><i>Ne</i></b>	Medium to very-coarse to fine granule, clast-supported conglomerate with pebble to boulder-size clasts, rudstone, limestone clasts-rich.
<b><i>Nf</i></b>	Fine to very coarse sand-size to fine granule grain-size calcarenite with PPS.





Fig.3.5.1.34 View of the outcrop of Fig.3.5.3 on a close to perpendicular to depositional-dip section.

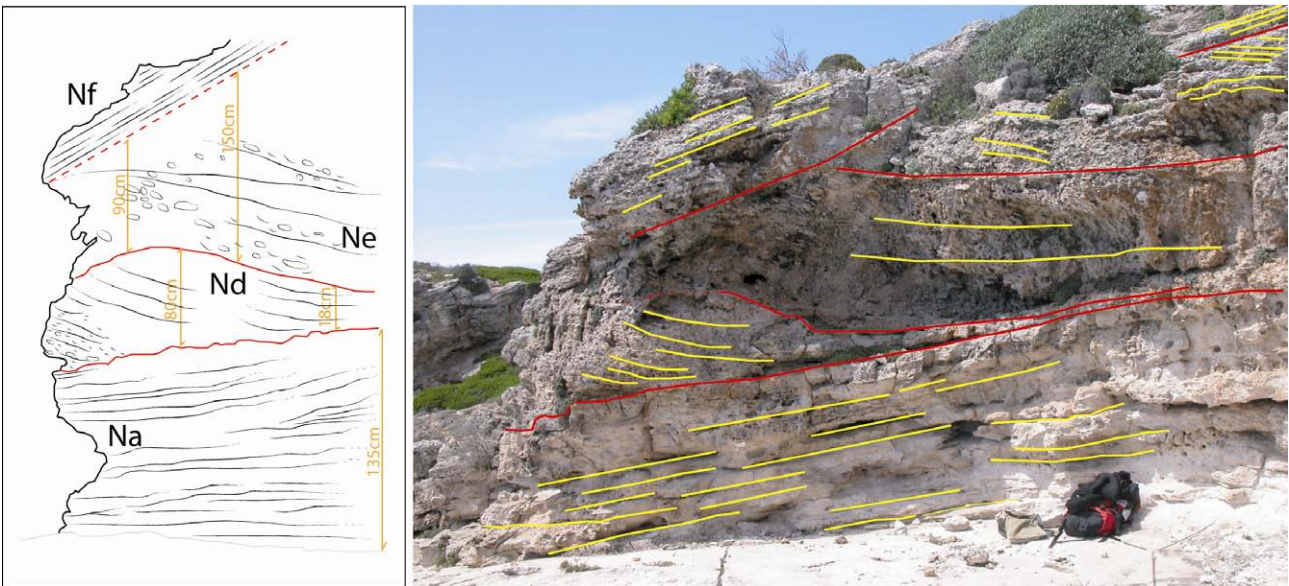
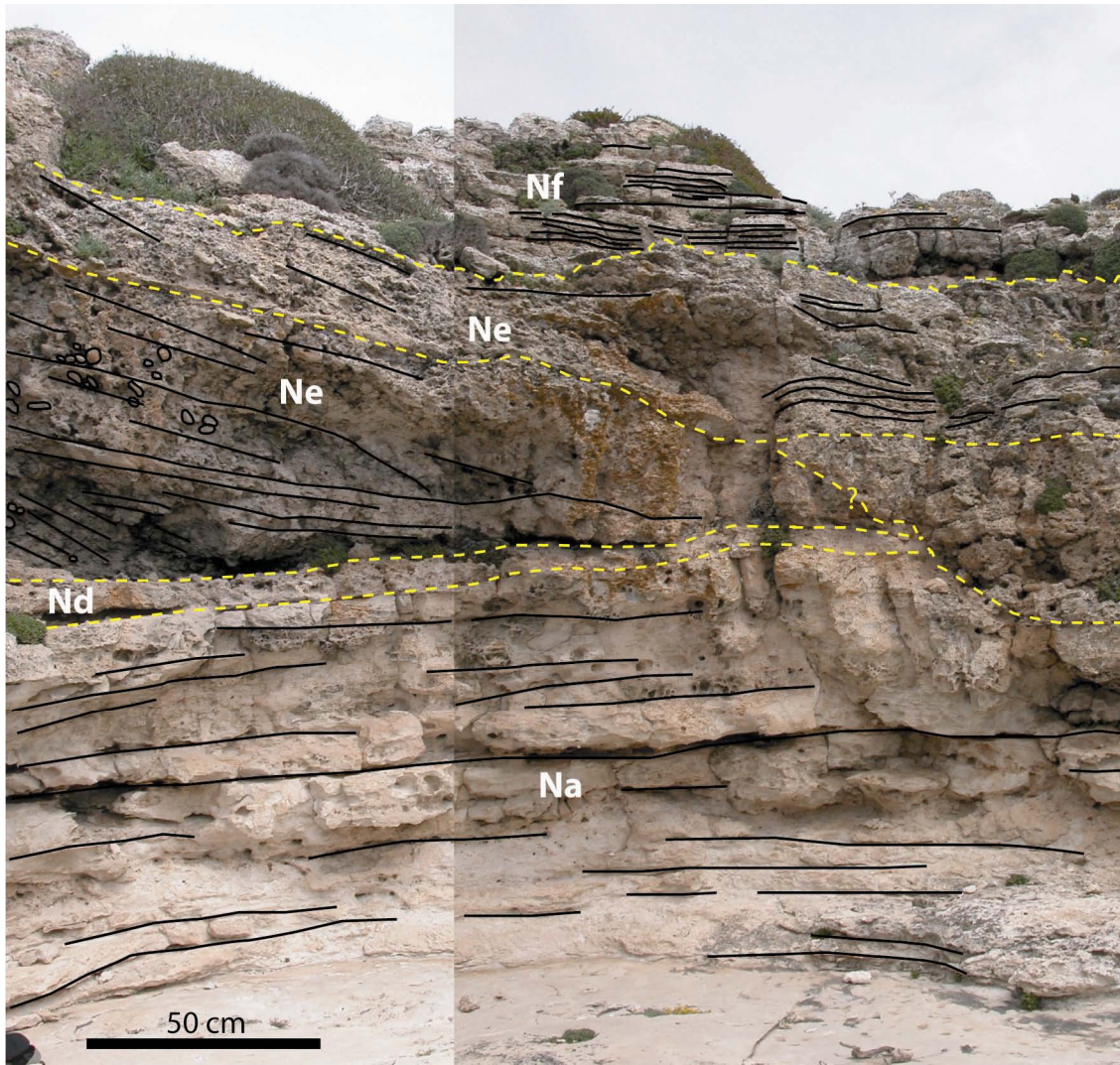


Fig.3.5.1.35 Figure and relative field-sketch showing the relationship between different facies and variation in dipping angles. Note that facies Na and Ne both dip SW.



*Fig.3.5.1.36 View of geometrical facies distribution on an almost perpendicular to depositional-dip section.*

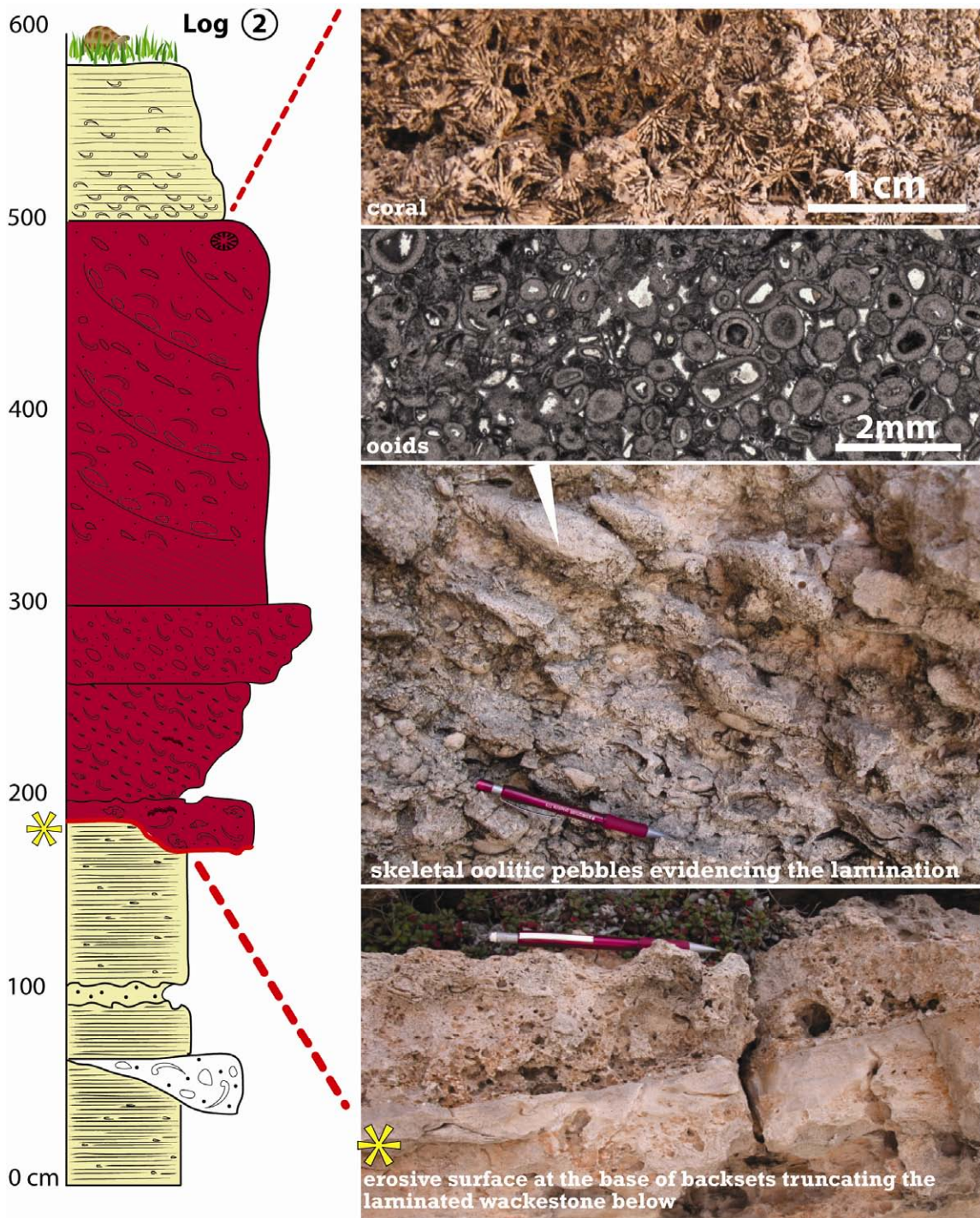


Fig.3.5.1.37 Log (2) measured in the higher backset bedded interval present at Nalinot and detail picture showing the major characteristics of the described facies (see reference for the position of this log in figure 3.5.2). From top to bottom: fragment of coral (*Porites?*), thin section of an oolitic-limestone pebble; lamination evidenced by limestone clasts alignment; erosive surface at the base of the backset bedded deposit.

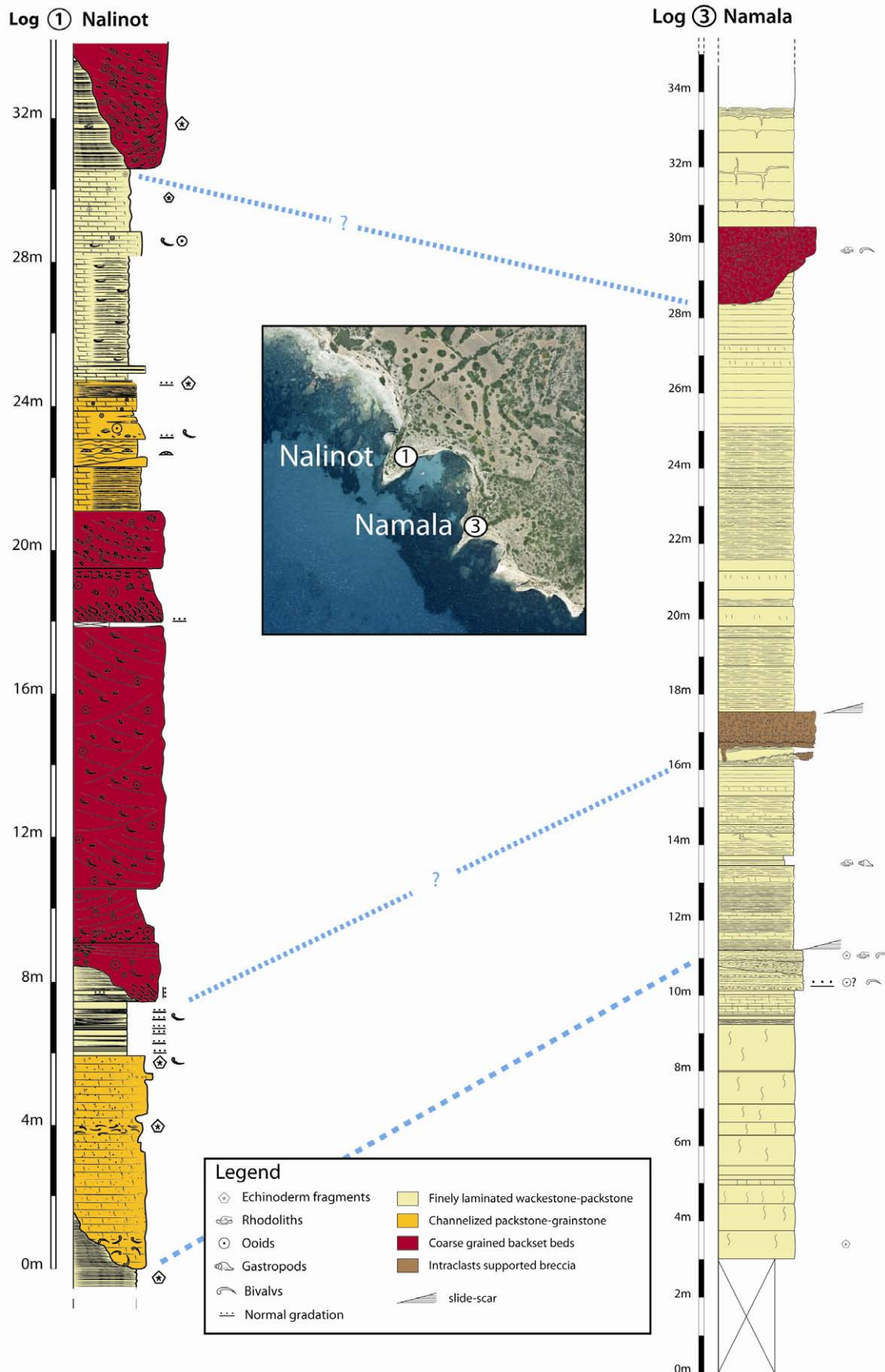


Fig.3.5.1.38 (Log 1 & Log 3) Measured logs at the promontory of Nalinot (left) and at the promontory of Namala (right); correlation lines can not be followed step by step in the outcrop but have been traced base on photos taken from the sea. One correlation line is certain while the two dashed ones are interpreted. The study of these two sections allow to defined that the backset bedded deposits of facies association N3 are not infilling the whole slide scar, draping the slide-surface, but they are found only along the axis of the slide surface and are laterally discontinuous.

FACIES	Description	Grain size		Sedimentary structures	Composition	Bed geometry
		matrix	clasts			
<b>Na</b>	wackestone/packstone	Very fine to medium sand-grain-size	Oblate echinoids 3-4cm	Massive to normal to inverse grading, sometimes with PPS and current ripple cross lamination.	Bioclasts, red algae, Mollusc fragments, bivalves, foraminifers, echinoids,	Sheet-like, thickness from 5cm to 40cm (up to 1m).
<b>Nb</b>	Packstone/grainstone	fine to very-coarse sand		PPS, normal grading, massive	Molluscs fragments, red algae (Lithophyllum, Sporolithon?), echinoids, rhodoliths, benthic foraminifers, bryozoans, gastropods, oolites, limestone pebbles.	Channelized-beds, trough thickness 50cm to 10m.
<b>Nc</b>	Clast-supported breccia.	Coarse to very-coarse sand-size.	Limestone pebbles 2-8cm.	Chaotic.	Bivalves, gastropods, coralline red algae in very small fragments, bryozoans, oolitic-limestone pebbles.	chute-shape, trough thick 25-40 cm, width 150-200cm.
<b>Nd</b>	Matrix-supported conglomerate (+ bivalves)	Medium to very coarse sand-size.	Bivalves 1-5cm, gastropods 1-2cm.	Backset laminated.	Fragments of mollusc, bivalves, coralline red algae, benthic foraminifers, oolites.	Channel-shaped with trough thickness 80 to 150 cm, width 1 to 4-6m.
<b>Ne</b>	Clast-supported conglomerate (+ limestone pebbles)	Medium to very coarse sand-size to fine granule	Limestone pebbles 7-8cm (up to 22cm), bivalves 2-3cm (up to 7cm), coral fragments 10cm.	Backset laminated.	Fragments of mollusc, bivalves, coralline red algae, benthic foraminifers, oolites, limestone clasts, coral (Porites), bryozoans.	Channel-shaped with trough thickness 150 to 200 cm, width 2-3m , up dip extend for 12-15m.
<b>Nf</b>	Packstone/grainstone	Fine to very coarse-sand to fine granule.	Bivalves 1-2cm	PPS, normal grading.	Fragments of molluscs, thin small bivalves, coralline red algae, benthic foraminifera, echinoid plates, gastropods	Sheet-like beds, beds thick 20 to 25 cm, overall thickness 1,5-6m.

Fig. 3.5. 1.39 Table summarizing major features of the facies recognized at Nalinot.

## 4. FACIES ASSOCIATION

### 4.1. Facies Association A1: base-of-slope deposits

The association of facies *A1* is represented by facies *Ba*, *Bb*, *Bc* and *Bd2* and it has been interpreted as characterizing base-of-slope deposits, where the coarser-grained, massive rudstones to packstones/grainstones of the lower slope interfinger with the finer-grained wackestone/packstone characterizing outer-ramp sediment. The angle of deposition ranges around 10° and dipping direction is mainly oriented along a NE-SW axis. These facies have been all interpreted to be the deposits of submarine gravity flows.

The finer-grained and sheet-like facies *Ba* are attributed to non-channelized turbidity currents depositing at the base-of-slope. The occurrence of planktonic foraminifers, molluscs, echinoids and pectinids place facies *Ba* in the aphotic zone (Pomar *et al.*, 2002; Mateu-Vicens *et al.*, 2008).

The channel-fill, coarse-grained facies, normally graded and with planar parallel stratification have been attributed to channelized turbiditic deposits. These units scour, pass laterally and are overlain by facies *Ba*. The channelized facies are probably related to concentrated density flows (*sensu* Mulder & Alexander, 2001) which are able to scour more deeply the substrate over which they are flowing.

The unstratified massive to normal grading beds may be interpreted as  $T_a$  intervals of the classic Bouma sequence, beds with planar parallel stratification may be interpreted as  $T_b$  intervals and current ripple cross-lamination as  $T_c$  intervals.

Facies *Bb*, *Bc* and *Bd2* are mainly composed by shallower water reworked shells, fragments of molluscs, echinoids, bryozoans, benthic foraminifers, and rhodoliths (Melobesoids) proceeding from the upper slope and middle ramp where they grew *in situ*, and planktonic foraminifers.

The dipping direction of these beds is dominantly SW, and the axis of the channels are also directed on a NE-SW direction, indicating SW as the major direction of progradation of the slope.

The presence of highly bioturbated facies (subfacies *Ba2*) within less or none-bioturbated units, is interpreted as caused by rapid deposition followed by non-deposition or lower sedimentation rates that allowed colonization of the substrate; subsequent rapid burial enabled the preservation of the first bioturbated bed. Subfacies *Ba2*, in the studied outcrop, is frequently found just below the cross-laminated rhodolithic rudstones (*Bd1*).

The succession of facies is interrupted by large-scale slide/slump scars that sharply truncate the underlying sediments and which are in-filled along the axis by sediments of facies association *B2*. Sediment instability at Barranc des Pou is evident in the frequent gliding surfaces affecting the turbiditic deposits.

This facies association is found both below and above the coarse-grained backset bedded intervals of facies Bd1.

#### **4.2. Facies Association A2: *turbiditic wackestone/packstone to grainstone***

Facies association A2 comprises facies *Fa*, *Na*, *Nb* and *Nc* and they have been interpreted as turbiditic beds representing sedimentation in the most distal part of the toe-of-slope in the outer-ramp (Obrador *et al.*, 1992; Pomar *et al.*, 2002). This association is thus an aggrading succession of turbiditic deposits.

The deposition of facies *Fa* is attributed to non-channelized but sheet-like turbidity currents of variable density but mainly of possible low density. Flows with concentrations < 9% by volume are considered true turbidity flows (*sensu* Bagnold, 1962), in which fluid turbulence is the main particle-support mechanism (Mulder & Alexander, 2001).

The succession of sheet-like, not amalgamated thin turbidites, the absence of photo-dependent biota, the repetitive occurrence of small slides and slumps and the presence of large-scale slide/slump scars hundreds metres wide and 20-30 m deep, the absence of wave-related structures, place this facies below the storm wave base in the aphotic zone at the transition between base-of-slope and outer ramp deposits where there's a little slope gradient with on going gravity processes, where the more distal-turbiditic deposit settle.

The distribution of bioturbation throughout the layer suggests a time scale of a few weeks to many months for deposition of a thick layer termed hemiturbidite (Stow & Wetzel, 1990). Extreme flow dilution as a result of reversing buoyancy and flow lofting (Sparks *et al.* 1993) may lead to very slow deposition of thick, continuously bioturbated hemiturbidites (Stow & Werzel, 1990).

The channelized facies (*Nb*, *Nc*) represent higher density flows that can develop a higher erosive potential at the base, and may exceed the 9% of sediment concentration and therefore be deposited by concentrated density currents.

The geometries and dipping angles of beds of this facies association point towards SW, conformably with the direction of ramp progradation. Compared to facies association A1, which is mainly represented in the locality of Barranc des Pou, this association (A2) represents more distal deposits compare to slope position, and they belong to outer-ramp sedimentation.

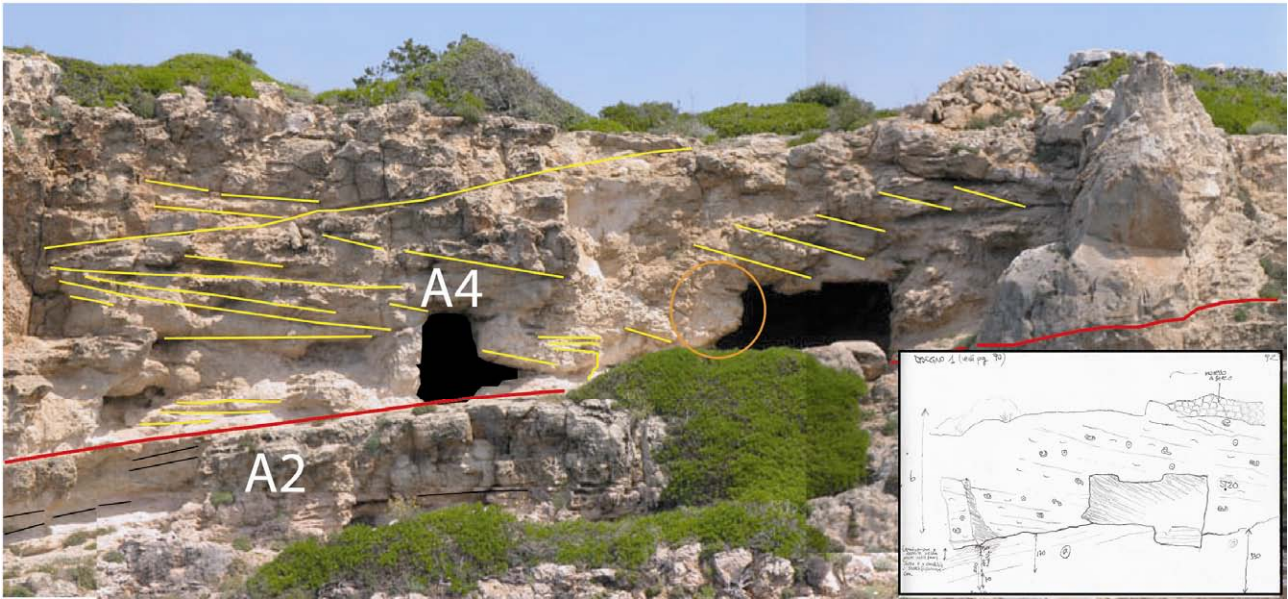


Fig. 4.3.1 Geometrical relationships between facies associations A2 and A4 at the outcrop of Forma; note the variation in dipping angle from A2 stratification and A4 laminations.

### 4.3. Facies Association A3: coarse calcarenite with planar parallel lamination.

This facies association is composed of facies *Fb* and *Nf* and they have been interpreted as the deposits of high density turbidity currents.

In the succession cropping out at Nalinot and Forma, these facies are found along the axis of the large-scale slide/slump scars, deposited above facies association A4 (described below); sometimes they are channalized and some others they are deposited in more sheet-like beds. These facies are thus associated to the sediment infilling the large slide scars, but they are found only along the central axis and they are laterally discontinuous.

This facies association is characterized by the occurrence of planar parallel lamination in very coarse sand-size to fine granule sediment. The grain-size population composing these facies is the same as the one forming the matrix of backset laminated facies, but in this case they develop another sedimentary structure. The presence of planar parallel laminated calcarenite indicates an upper flow regime for the flow that deposited it, and it represents the  $T_b$  interval of the Bouma sequence. These facies present a sheet-like to channalized base which may indicate a variation in sediment concentration that may allow a variation in scouring potential of the flow.

This facies is found at the top of backset bedded units and it also characterizes the up-dip tail of some of the backset laminated deposits where it is accompanied by a decrease in grain-size. It is thus possible to suggest that this facies association may have been deposited by a type of flow that represent the successive evolution of the flows responsible for the deposition of the coarser-grained backset bedded intervals. A higher velocity of the flow may have been enhanced by the previous dumping of the coarser components, the flow therefore loses



sediment concentration but increases its velocity to maintain itself within the upper flow regime ( $Fr > 1$ ). Another condition associated to the one just described, is that the deposition of coarser sediment within the scours partly or completely in-fill the channel: then, the surface over which the flow is running is different, it will be more flattened and the flow will not be so concentrated and confined within the channel, but will easily spill over the channel walls. The change of flow properties is thus accompanied by a variation of substrate morphology; in these new conditions the hydraulic jump does not develop and the flow does not suffer sudden variation that cause the formation of backset lamination, maintaining its supercritical behaviour. This interpretation would also explain the development of the more sheet-like shaped beds such as in facies *Nf*.

The behaviour of the sediment gravity flow changes due to a decrease of flow-energy in time and space; those currents are in fact unsteady currents which may vary in time and in distance. The flow may therefore be waning and depletive where velocity is kept high by the reducing of dumping of coarser sediment, reducing the sediment concentration in the flow.

#### **4.4. Facies Association A4: backset bedded deposits**

Facies association *A4* is composed of facies *Bd1*, *Fc*, *Fd*, *Fe*, *Ff*, *Fg*, *Fh*, *Nd* and *Ne*. All these facies have in common a backset lamination, very coarse grain-sizes, and they are all found along large-scale slide/slump scars that scoured facies association *A1* and *A2* (Fig.4.4.1).

Beds are characterized by a backset cross-lamination which dip NE with foreset laminae dipping in the up-current direction compared to the depositing flow and therefore they have been interpreted as backset beds (Pomar *et al.*, 2002).

The sediment composing this association is highly variable from medium sand-size to boulder-size (including some but rare meter-scale blocks).

Beds of this association share a similar architectural geometry. Along depositional dip, beds are tabular to wedge-shape extending laterally for 6 m to 25-30 m. Along strike, they have chute-shape with thickness in the trough of 120 to 280 cm and an overall large-scale trough-stratification due to the superposition of several channelized units. Each unit is bounded by deeply scouring erosive surfaces. The backset beds are in fact always found within channel-shaped scours, sometimes with very steep walls that indicate that deposition rapidly followed erosion.

The characteristic that differentiates the facies composing this association is the bioclastic content which varies from one outcrop to the others. In Barranc des Pou, the southernmost locality, there is a strong dominance of rhodoliths (*Melobesioids*) therefore major source of sediment for these deposits is attributed to the upper ramp slope which is characterized by *in situ* production of these coralline red algae. At Forma, this association is overall 30 m thick and 200 m wide, with an overall wedge-shape pinching out laterally. The distribution of facies along the outcrop shows a particular trend both in grain-sizes and in components. Moving from

the eastern part of the outcrop, which corresponds to the more proximal (closer to the slope) towards the western part, which mean the more basinward part, grain-size noticeably increase. The matrix is always composed of coarse bioclastic calcarenite, while the clasts are first mainly represented by rhodolith, red algae fragments and bivalves, then limestone clasts and rhodoliths dominate the deposits and oolites are found both in the matrix and in the limestone pebbles. In Nalinot, rhodoliths are very few while the deposits are dominated by bivalves, mollusc fragments and limestone clasts and oolites are found both in the matrix and in the clasts.

The presence of oolite pebbles both in Forma and Nalinot, indicate the presence of an up-dip tropical, shallow water carbonate factory that is either not preserved or not exposed (*in situ* oolites have never been found in Menorca). Oolites are found both in clasts and in the matrix and this suggests a progressive erosion of pre-existing oolitic deposits as well as their early lithification.

Each unit is erosive over the underlying ones and from the stratigraphic succession of units and architectural geometry of erosive surfaces, the coarser units mainly correspond to the younger ones.

With the increase in grain-sizes, an increase in laminae dipping angles has also been noted from horizontal to 35° (Fig.5.15). Foreset lamination are more visible where there is at least part of the population which is at least very coarse to granule in size, and it is always strongly evidence by the orientation of clast and bioclasts along lamination.

The deposition of this association of facies is attributed to the repetitive occurrence of gravity flows accelerating along the depression formed by the slope collapses. The trends are interpreted to be related to a variation of the energy (velocity and/or concentration) of the gravity flows depositing sediments down slope and a variation in the source of sediment that fed them.

The sediment composing these beds proceeds from middle ramp and slope settings and therefore it has been firstly remobilized, entrained and transported offshore by other processes different from gravity processes (detail description of entrainment and transport in chapter 7).

These beds are infilling the central portion of these large-scale slide/slump scar whose axis is directed NE-SW. The lamination within the units are on the contrary dipping NE and therefore they have been interpreted as backset beds. They are in the centre of the trough-shaped scars, and associated to the sediment infill. Each bed is bounded by erosive surfaces. The chute-troughs eroding the underlying facies associations are, along strike, often very deep and narrow with steep walls, while along depositional dip they are mainly concordant with the underlying stratification-dip of facies *Fa*. The axis of chutes are mainly directed NE-SW.

The backset laminated, coarse-grained deposits are therefore interpreted as representing a back-filling of channels that occur immediately after scouring. The gravity flows transporting this sediment down-slope has been interpreted as being a concentrated density current (*sensu* Mulder & Alexander, 2001).



Fig.4.4.1 Schematic drawing on photo showing the relationship between facies associations A2, A3 and A4 in Forma.

## 5. SUMMARY OF DATA

### *Major features of backset laminated deposits*

The backset bedded deposits studied in the different localities show some peculiar characteristics. These deposits represent facies association A4 and their geometrical-relationship with the embedding units has been already describe and shown in Fig.3.2.4. where they are found in the centre of the troughs and are associated to the sediment infill (Fig.5.1 and 5.4). The lower boundary of the backset body is a larger-scale, irregular, trough-shaped erosion surface (Fig.5.2). Because it is a composite erosion surface made by several smaller-order erosional surfaces, the base can be more irregular. The lower boundary of each backset unit is a trough-shaped erosion surface. The axis of the trough are roughly dipping SW according to the inclination of the regional slope (Fig.5.3). The boundaries separating each single unit are spoon-shaped, erosion surfaces (Fig.5.5-6).



*Fig.5.1 Large-scale slide scar truncating facies association A2, the thinly laminated wacke/packstone of the outer-ramp sediment. The surface and the wide depression caused by the slide, is draped and filled by the deposition of turbiditic beds.*

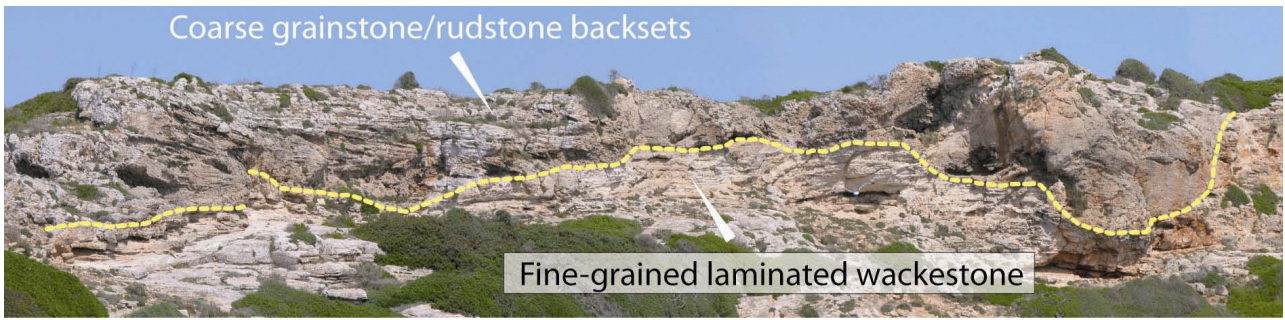


Fig.5.2 Erosive surface separating the fine-grained laminated wackestone below from the coarse-grained backset beds above. The surface is irregular showing a wavy trend due to erosion by several flows.

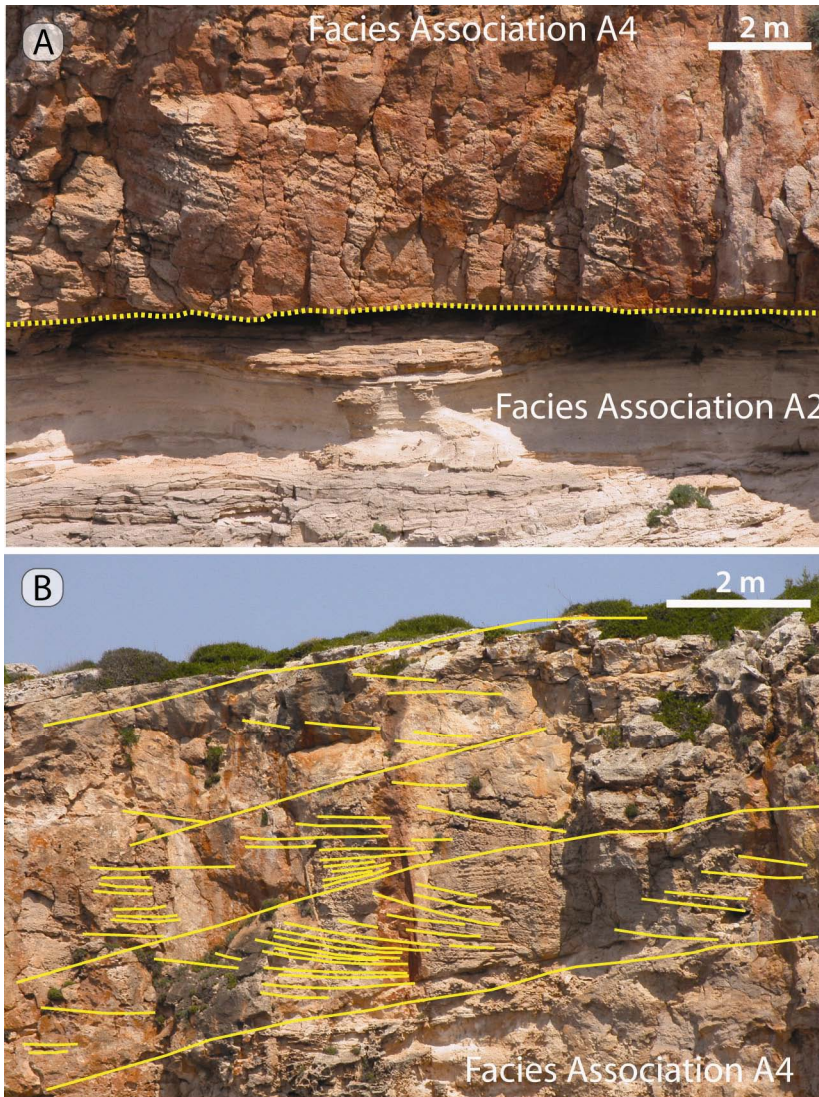
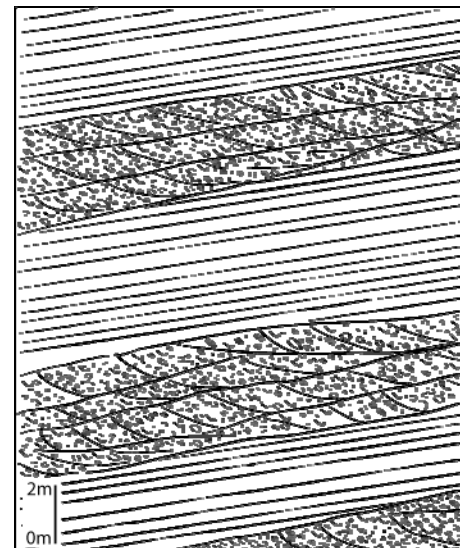


Fig.5.3 View of the backset bedded units on a parallel to depositional dip section. (A) Backset bedded deposit above the thinly laminated wackestone/packstone. Foreset downlap on the sharp erosive surface. (B) Several backset laminated units: note that on a parallel-to-flow section, erosive surfaces at the base are sub-parallel and dip on a SW direction concordant with outer ramp sediment and ramp progradation. (Bottom right) schematic sketch of erosive surfaces at the base of backset bedded intervals seen parallel to paleo flow. (Below), simplified sketch showing backset bedded deposits on a parallel to depositional-dip section.



The upper boundary is sub-parallel to stratification-dip, overlain by the finer-grained laminated packstone-wackestone (sketch Fig.5.5 see also Fig.3.5.2).

The shape of the backset bodies tends to be lenticular, with along-dip elongated spoon-shaped boundaries. In some examples is possible to see the up-dip pinching out, while the down-dip terminations have never been observed.

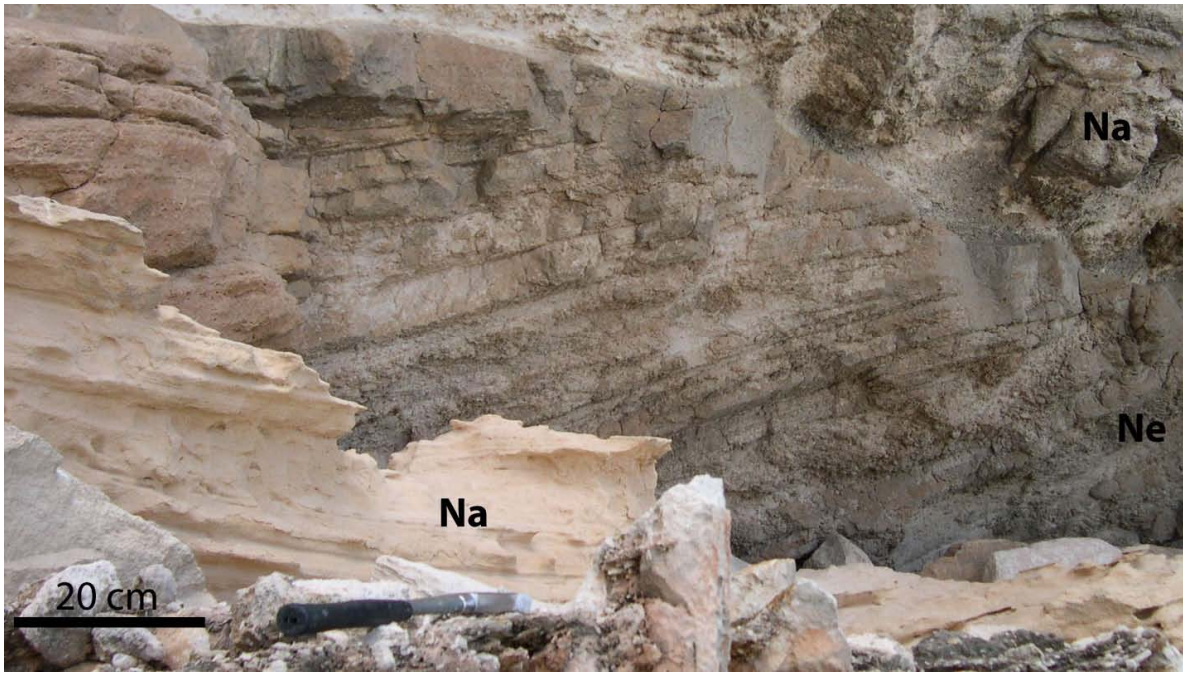


Fig.5.4 Example of backset bedded deposit of facies association A4 (Ne) embedded in outer-ramp sediment of facies association A2 (Na).

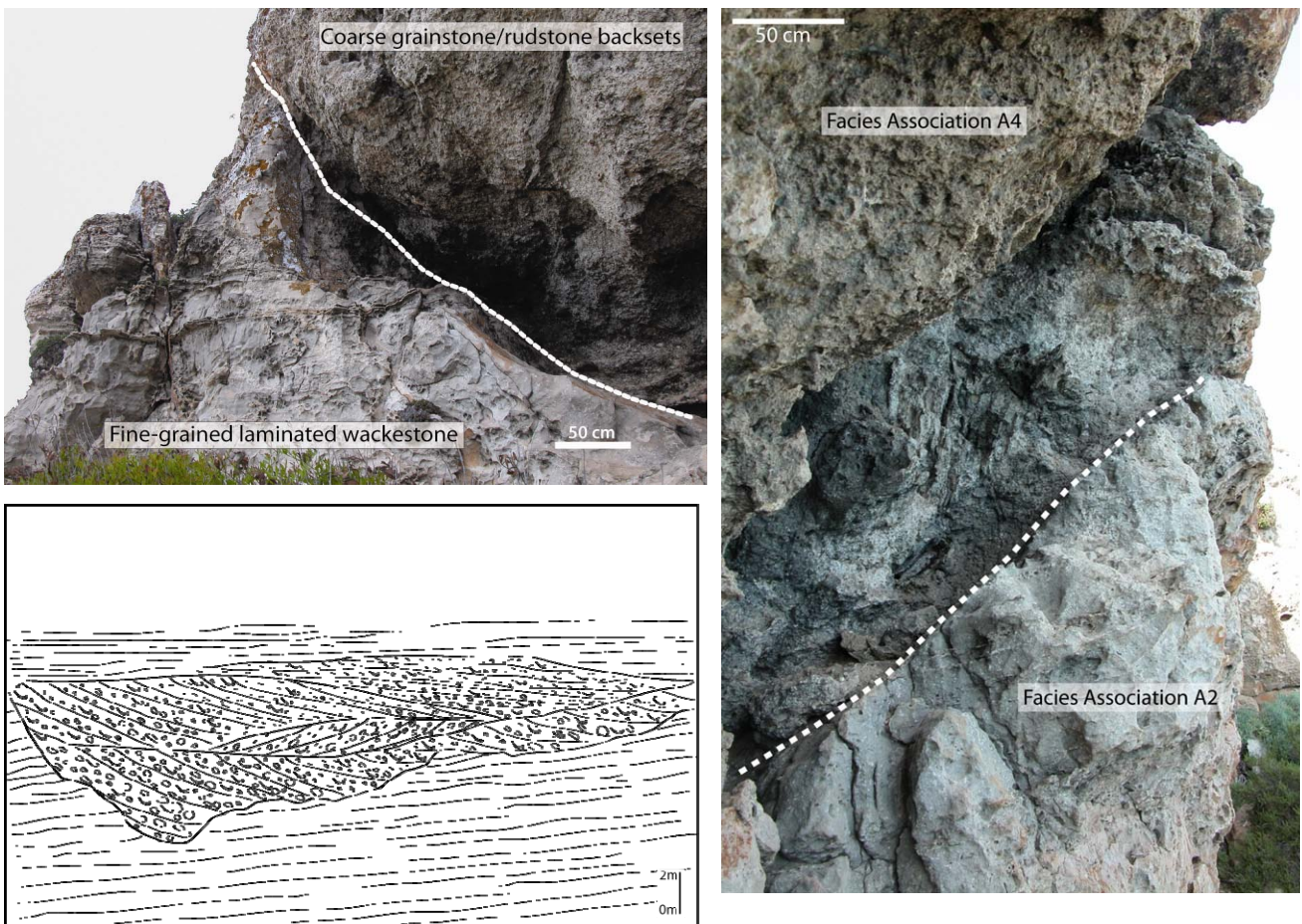


Fig.5.5 Erosive surface at the base of the backset bedded deposit that deeply scoured the underlying sediment. Top left: notice the truncation of the laminated wackestone/packstone of facies Na. Above, facies Nd erosive on facies Na: note the extremely steep walls and the meter-scale depth of the trough of the scoured channel. Bottom left, simplified sketch of the erosive surfaces along a perpendicular to depositional dip section.

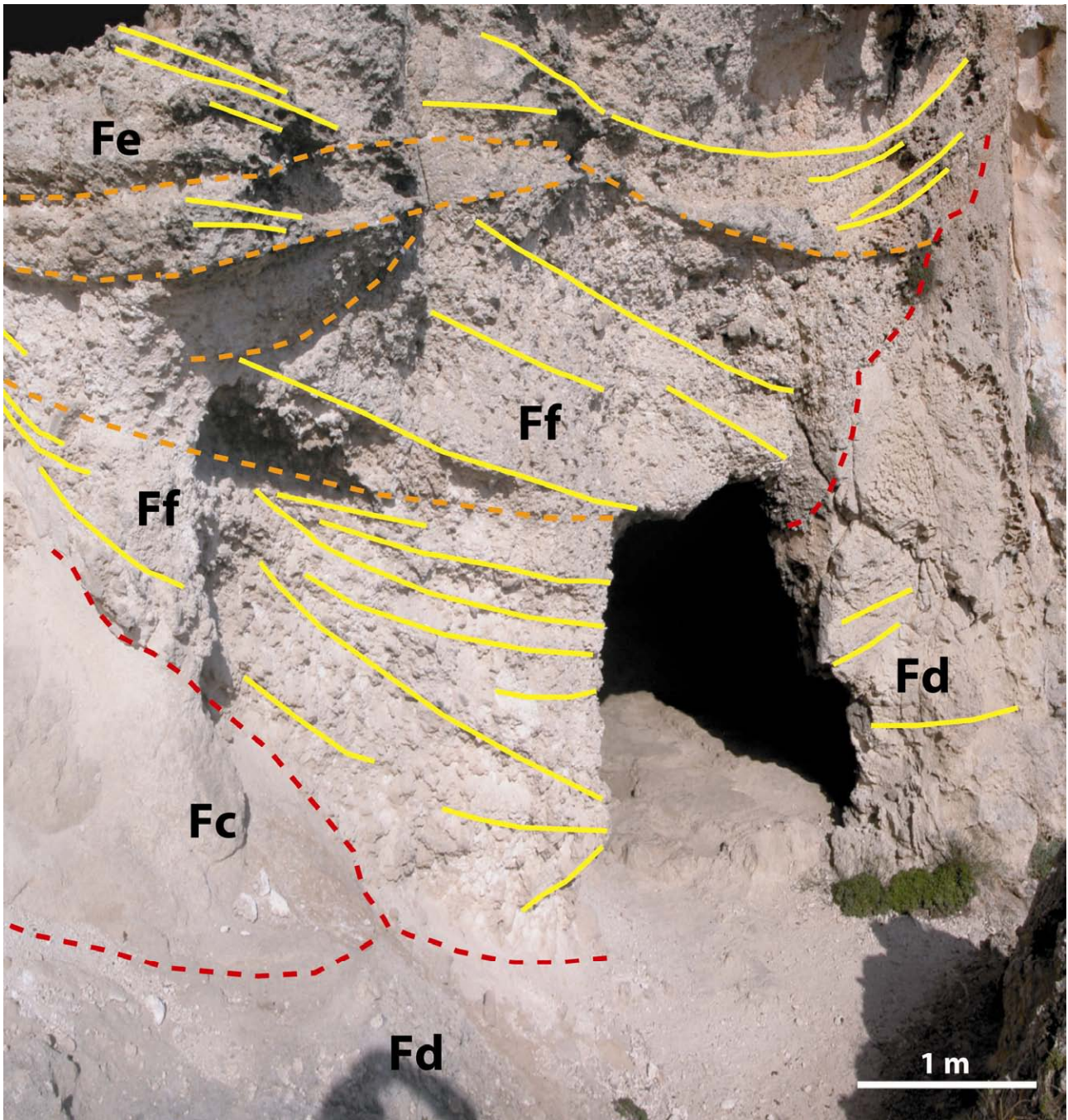


Fig.5.6 View of the channalized backset beds on a perpendicular to depositional dip section. In this section a large-scale trough-lamination is observed created by the superimposition of several deposits eroding over each other.

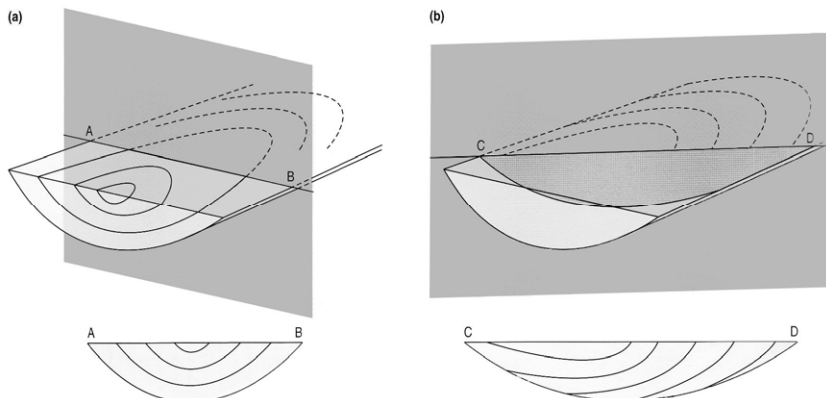


Fig.5.7 Schematic illustration of the geometric complexity of trough-cross strata: (a) a vertical section orientated transverse to the trough axis reveals symmetrical cross-stratification planes that are apparently concordant with the trough base; (b) a vertical section orientated oblique to the same trough-axis reveals cross-stratification planes that apparently fill the trough asymmetrically and downlap onto its base (from Collinson et al., 2006, p.100).

The cross-lamination characterizing each backset bedded deposit dips mainly on a roughly NE direction, and it is locally underlined by the abundance and orientation of larger clasts. As shown in the sketch in Fig.5.7, for the aim of defining palaeotransport direction from trough-shape cross-strata, the measurement of foreset dip azimuths present often many problems depending on the available section.

Large limestone clasts (pebbles and cobbles) are found with *a*-axis parallel to lamination, often imbricate when abundant (Fig.5.8).

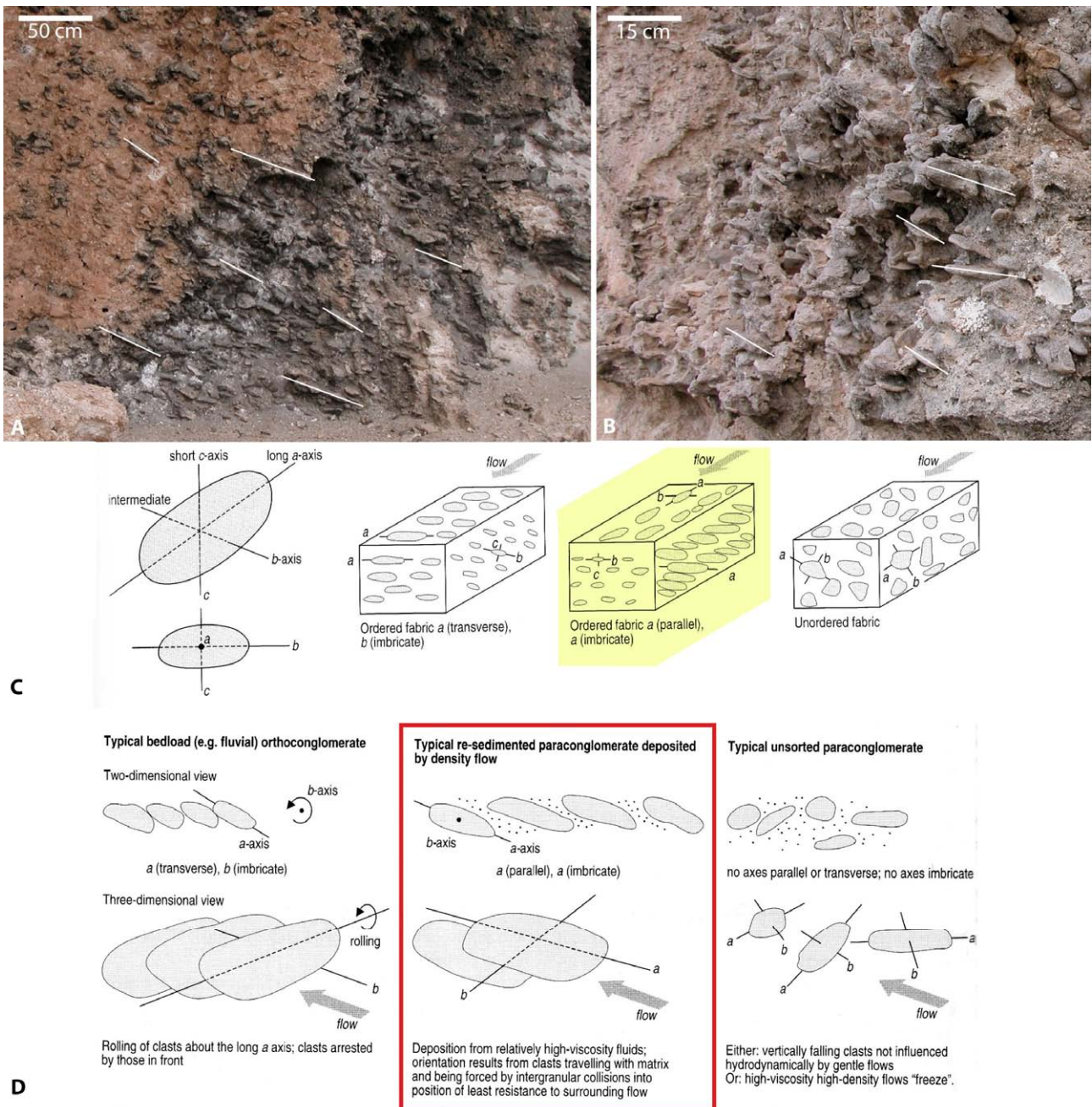


Fig.5.8 Photo and sketch of clasts orientation compared to lamination: (A, B) photos from studied outcrops that show limestone pebbles' *a*-axis elongated parallel to lamination; (C) axial nomenclature of clasts and fabrics of ordered and unordered fabrics, the one evidenced in yellow-colour is the one that better described the conglomerates studied; (D) the nature and processes of origin of imbricated disc- and blade-shape clasts, the red square evidence the disposition of clasts in the studied deposits which corresponds to re-sedimented paraconglomerate deposited by density flow (C and D, from Collinson et al., 2006, p.149-150).



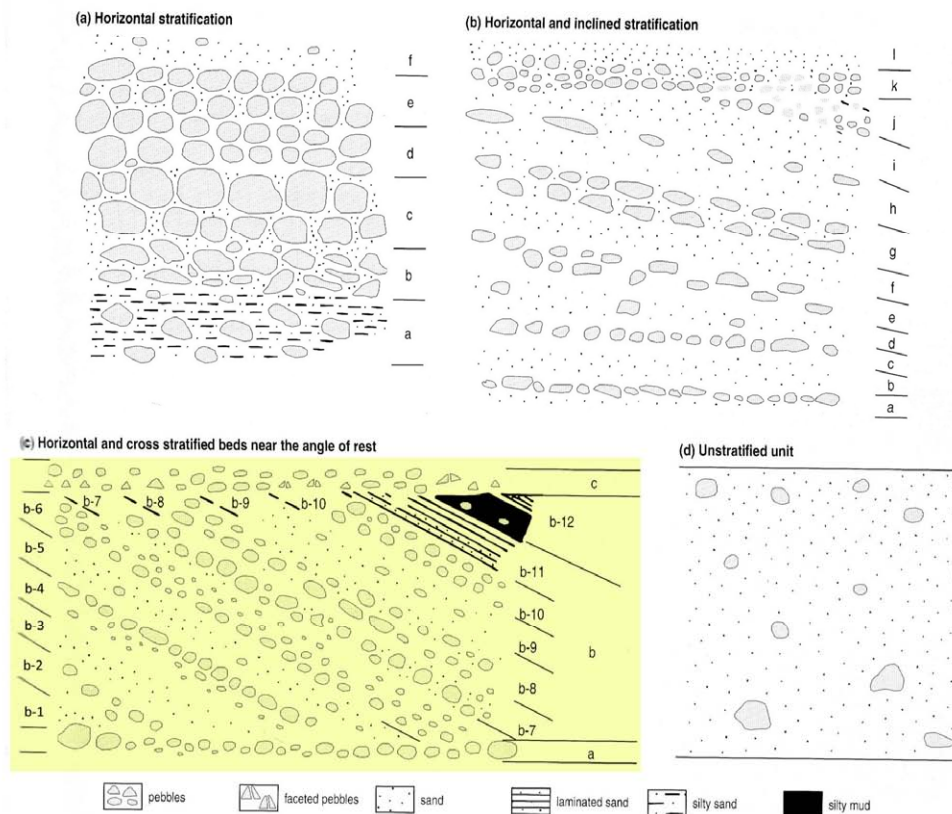


Fig.5.9 The two photos in the upper part of the figure show the concentration of larger clasts along some intervals, alternating with more fine-grained ones. Note that where pebbles are more abundant clasts are imbricated. This stratification with lamination is visible also where only bioclasts are present as evidenced in Fig.5.10. In the lower part the sketch shows possible stratification in rudites: (a) horizontal stratification units with welded contacts, (b) horizontal stratification and inclined stratification, (c) horizontal and cross-stratified units near the angle of rest, (d) unstratified unit (sketch from Collinson et al., 2006, p. 153).



*Fig.5.10 Photo that shows the alternation of larger-bioclasts intervals with more matrix-rich ones, giving an alternation of normally to inversely graded beds.*



*Fig.5.11 Photo showing lamination evidenced by more matrix-rich intervals and by orientation of limestone clasts: note the low sorting of sediment which varies from sand-size up to boulder-size grains and clasts.*

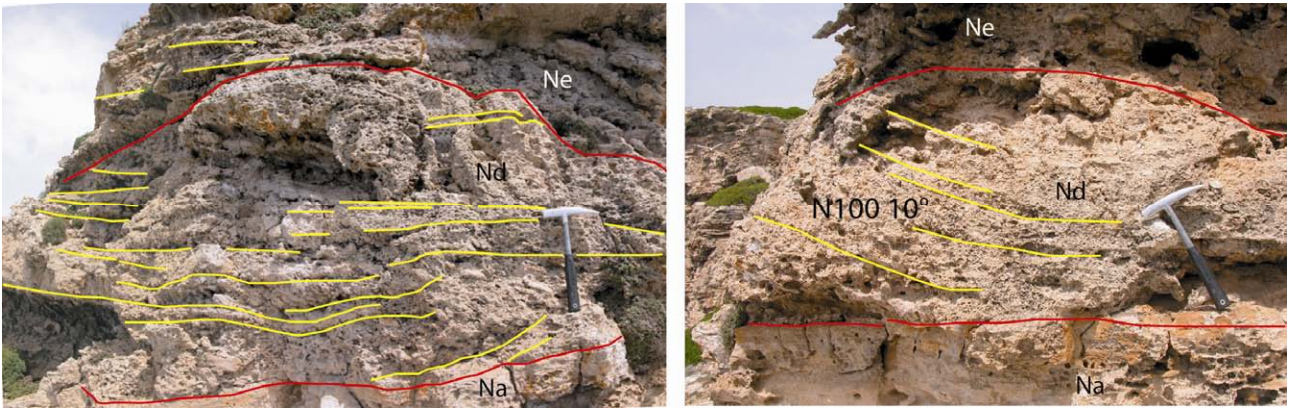


Fig.5.12 Example of facies Nd: the same deposit is shown on a section perpendicular to depositional dip (left) and on a section parallel to depositional dip (right).

Cross-lamination dipping angles vary from horizontal (parallel to depositional dip) to 30°, and it has been observed that higher angles are found in the down-dip part of units and that angles increase with increasing grain-size of deposits, that means coarser deposits present higher angles (Fig.5.13-14-15).

Sediment composing these deposits is very low sorted and it ranges from fine-sand to cobble to boulder grain-size (Fig.5.11). Beds often present an inner organization in alternating intervals with coarser-grain sizes with finer-grained intervals (Fig.5.9-10); an overall normal gradation is present within each unit and a decrease in grain-size is also observed from the down-dip to the up-dip part of each deposit (Fig.5.13-14).

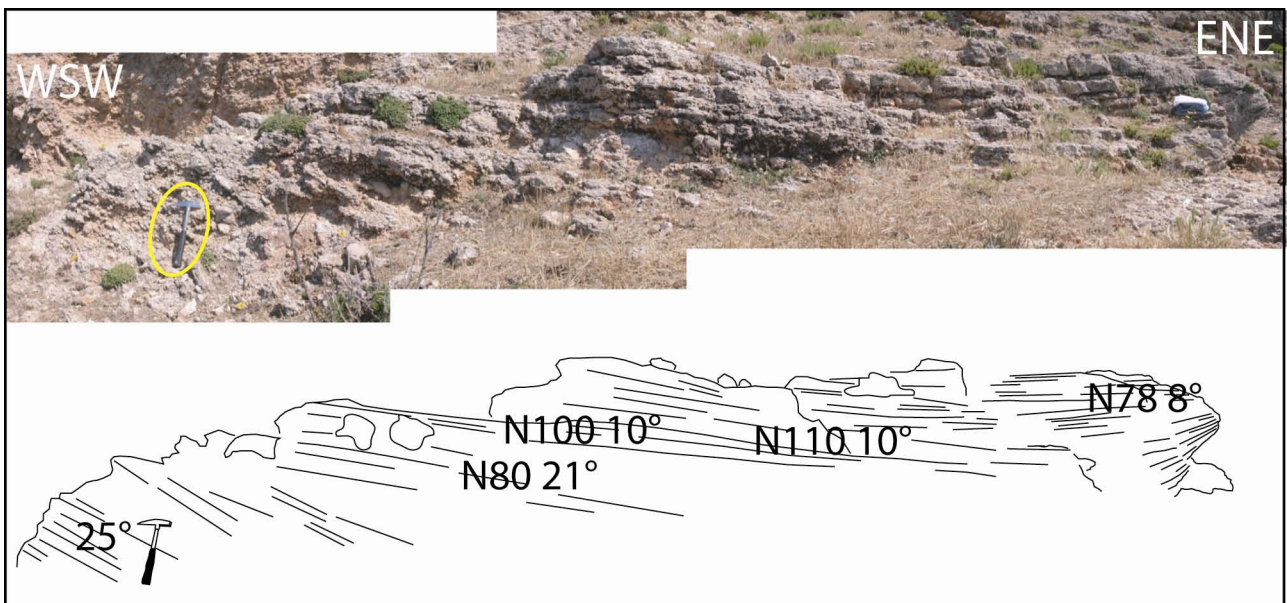


Fig.5.13 Trend of dipping angles of the backset lamination; as shown in the photo and evidenced in the drawing, the angles are higher in the down dip part of the deposit and gradually decrease to horizontal in the up-dip tail. This trend is accompanied by a decrease in grain-size that is coarser at the base and in the most down dip part, and it gradually fines upward and up-dip.

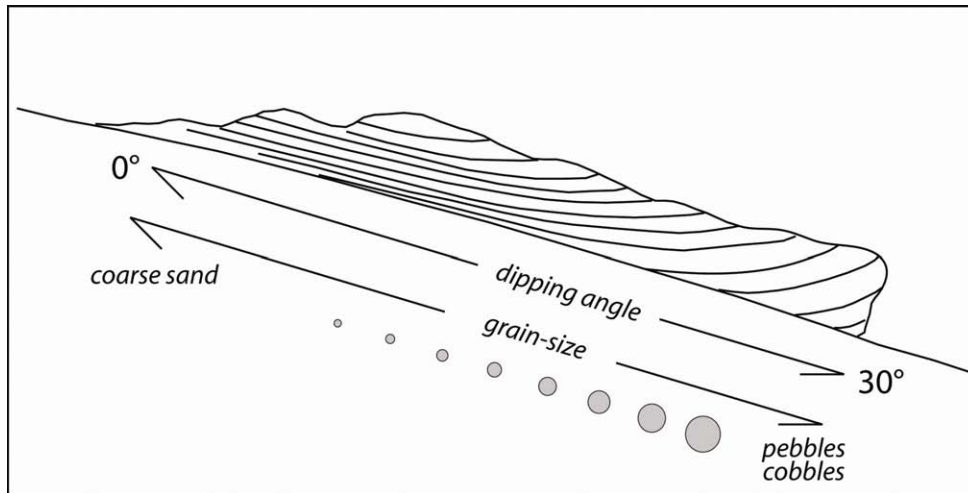


Fig. 5.14 Schematic sketch summarizing dipping angle and grain-size trend with a single backset bedded deposit.

A significant variation has been noted in the composition of the backset bedded deposits in the different localities (see Tab.5.16). At Barranc des Pou rhodoliths are the conspicuous larger components; at Forma larger components are rhodoliths, bivalves, grainstone pebbles, and ooids are present both in the matrix and pebbles; at Nalinot rhodoliths are almost absent, while bivalves, grainstone pebbles and ooids are very abundant; coral fragments are also present. Matrix always consists of coarse-grained bioclastic packstone/grainstone sand to fine-gravel, rich in red-algae, bivalve, echinoderm, gastropods and coral fragments, planktonic and benthic foraminifera. These deposits have very high porosity (mainly due to dissolution) little cementation and patchy dolomitization.

The presence and/or absence of some components has to be here underlined: rhodoliths are extremely abundant in Barranc des Pou and almost absent in Na Linot; oolites (both loose in matrix and in pebbles) are absent in Barranc des Pou, they firstly appear in Forma and are abundant in Na Linot (*in situ* oolites in the middle and/or inner ramp have never been found, they are found only as reworked sediment); coral fragments (*Porites*) have been found only at Na Linot. Expecially at Forma the variation in components has been noted also within the outcrop moving from older deposits, lower in the stratigraphic position, to younger ones, in higher stratigraphic positions.

Therefore from the southernmost outcrop (Barranc des Pou) to the northernmost (Na Linot) coralline red algae change from being dominant to rare, oolites increase from absent to very abundant as well as bioclastic and oolitic limestone clasts.

In the three localities studied a variation in the facies associations embedding the backset bedded units has also been noticed. At Barranc des Pou the slide-scar cross-cut base of slope sediments while at both Forma and Na Linot those scars truncate the fine-grained, partly dolomitized packstone outer ramp successions.

Moreover the axis of the main channels hosting the backset bedded units, show a scatter of azimuths, between NE and E. The dipping direction collected at the localities of Forma and Nalinot, show a different trend from one channel to the other one. The collection of dipping



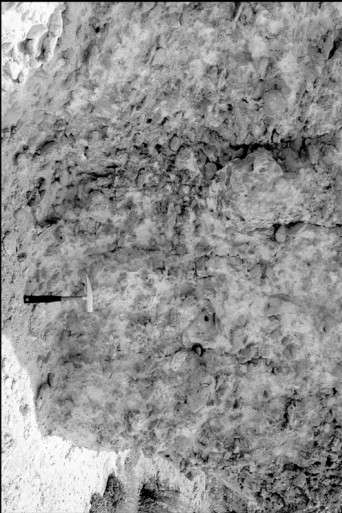
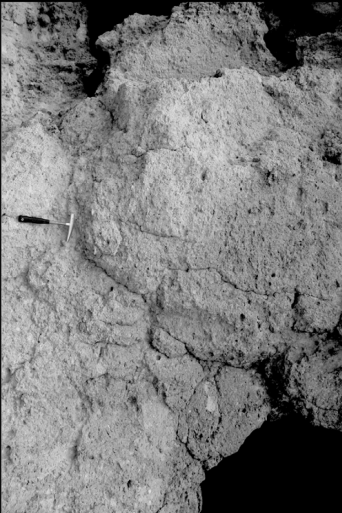
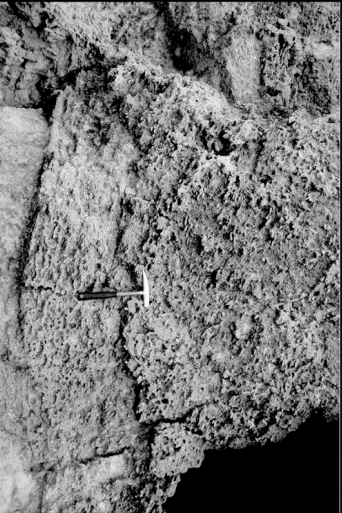

direction data indicates that at Forma, backset foreset laminations mainly dip in the NE direction (54%) while at Na Linot they mainly distribute eastward. This can be partly due to higher number of data collected at Forma and/or to a slightly different orientation of flow-direction down slope.

From the observations above, it is possible to deduce that the source of sediment feeding these deposits developed along the scars were different: at Barranc des Pou, rhodoliths probably proceeded from the ramp slope while sediment involved in Forma and Na Linot present a clear beach/shoreface derivation. Additionally, the abundance of ooids and, mostly, the presence of coral fragments suggest the backsets at Na Linot might be younger and belong to the Reef Complex upper sequence.

Therefore change in components between Barranc des Pou and Forma-Na Linot, along with the possible correlation of outcrops along strike (see figure above) suggest it may be a change in timing, being earlier at Barranc des Pou. Moreover the units at Barranc des Pou are thought to be deposited in a more updip position (more proximal, at the base of slope) compare to the ones in the other two localities.

Another possible explanation for this diversity in composition is that the paleo-shoreline was not straight elongated on a SE-NW direction as it is nowadays, but it was more irregular, this would better explain also the variation in the direction of the axis of main slide-scars. Associated to this possible variation in paleo-topography a different distribution of palaeo-environments could also be present with oolitic shoals developing only on the north-western part of the ramp. Unfortunately in place oolitic shoals have never being found so their position is still uncertain.

Fig. 5.15 Summary of the observed relationship between backset lamination dipping angles and grain-sized; as shown in this table, to coarser-grained sediment correspond higher dipping angles, while they decrease in finer-grained deposits. This relationship may also be related to the hydrodynamic energy of the flow that deposited this sediment.

Examples of the relationship between backsets' composition and dipping angles					
photo	angles	composition	photo	angles	composition
	not visible	Bioclastic conglomerate rich of large skeletal-oolitic pebbles (15-20 cm) with only few sparse rhodolites.		12°-15°	Rudstone rich in large bivalves (4-6 cm), pebbles are less abundant and rhodolites are rare.
	15°-25°	Bioclastic rudstone rich in rhodolites (<15 cm) and skeletal-oolitic pebbles (<20 cm and more).		7°-11°	Bioclastic fine gravel with few rhodolites (mm - 2 cm).
	15°	Bioclastic rudstone with less abundant oolitic elongated and flattened pebbles (7-8 cm), rhodolites are absent.		not visible	Coarse bioclastic sand to fine gravel, rich in fragments of mollusc and only few sparse rhodolites.

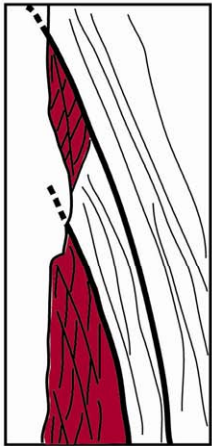
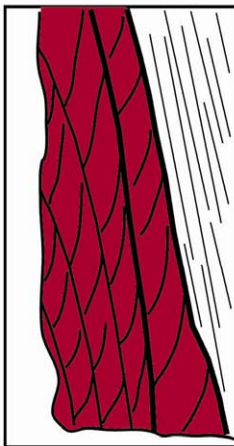
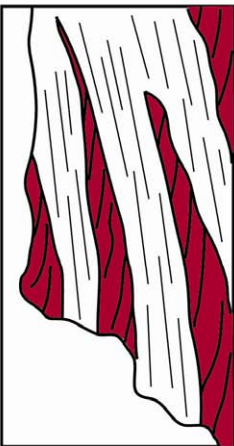
Outcrops	Location	Bedding	Despositional texture	matrix	Composition	clasts
<p><b>Barranc des Pou</b></p>  <p>Transition from toe-of-slope to outer ramp.</p> <p>Laterally extends for 30-40 m seaward; max thickness 8 m.</p>		<p>Backset bedding, foresets dip &lt;math&gt;&lt;25^\circ&lt;/math&gt; N75, tend to <math&gt;0^\circ&lt; finer="" in="" landward.<="" math&gt;="" p="" sediment=""> </math&gt;0^\circ&lt;></p>	<p>Highly porous, clast-supported, rudstone to breccia.</p>	<p>Coarse-grained bioclastic sand rich in fragments of rhodoliths, bryozoans planktonic and benthonic foraminifera.</p>	<p>Rhodoliths: average 6-7 cm (max 12-15 cm). Only few bivalves.</p>	
<p><b>Forma</b></p>  <p>Transition from toe-of-slope to outer ramp (more distal).</p> <p>Almost 200 m E-W; vertical exposure 30 m.</p>		<p>B1: Backset bedding, dip E-NE (<math&gt;4-5^\circ&lt; (thickness="" 1="" 40-50="" <math&gt;23^\circ&lt;="" cm="" extend="" for="" from="" laterally="" m,="" math&gt;="" math&gt;).="" meters).<br="" of="" several="" smaller="" sub-units="" superimposition="" to="" up=""></math&gt;4-5^\circ&lt;>B2: Backset bedding, dip NE, from horizontal to <math&gt;25^\circ&lt; an="" basinward.<="" grain-size="" in="" increase="" is="" math&gt;.="" noted="" p=""> </math&gt;25^\circ&lt;></p>	<p>Bioclastic floatstone to rudstone to clast-supported conglomerate.</p>	<p>Coarse-grained bioclastic sand-to-fine gravel, composed of fragments of rhodoliths, algae, bivalves, gastropods, bryozoans, echinoids, foraminifera, and ooids.</p>	<p>Rhodoliths, bivalves, skeletal oolitic rich-pebbles, gastropods. Rhodoliths: average 3-4 cm but reach 12 cm; bivalves: 3-4 cm; pebbles: variable in size and shape from 1-2 cm to 15 cm.</p>	
<p><b>NaLinot</b></p>  <p>Transition from toe-of-slope to outer ramp (more distal).</p> <p>Average thickness 6 m but reach 14 m basinward, laterally it extends for few tens of meters; overall wedge-shaped.</p>		<p>Backset bedding, thickness varies from 50 to 150 cm and lateral extension varies from few to several meters. Dip NE, angle varies <math&gt;10^\circ&lt; <math&gt;30^\circ&lt;="" math&gt;="" math&gt;.<="" p="" to=""> </math&gt;10^\circ&lt;></p>	<p>Floatstone to rudstone to breccia, highly porous, little cementation.</p>	<p>Coarse-grained bioclastic sand rich in ooids and fragments of algae, bivalves, gastropods, bryozoans, echinoids, foraminifera, ooids, rare fragments of rhodoliths.</p>	<p>Pebbles of skeletal-oolitic grainstone are rounded, flattened and elongated: average size 7-8 cm reach 25 cm. Bivalves range from mm to 7-8 cm. Coral are found in fragments up to 10 cm.</p>	

Fig. 5.16 Summary of the major characteristics in each studied locality.

## 6. Supercritical flows and backset bedding

### *BACKSET BEDS*

The formation of “backset bedding” (cross-stratification that dips against the direction of flow of the depositing currents - Gary *et al.*, 1972, Reineck and Sing, 1980 and reference therein) has been attributed to the occurrence of a hydraulic jump within an unidirectional flow which passes from being supercritical ( $Fr > 1$ ) to subcritical ( $Fr < 1$ ). Hydraulic jumps may develop along the slope due to dilution, enlargement, strong reduction of the competence and velocity of flow as it reaches the base of the slope or related to obstructions and/or to breaks in slope. Local slope-breaks may be produced also by slides, slumps and “frozen” debris-flow bodies. They are more abundant at the toesets but also occur in the foresets (Komar, 1971, Hand, 1974; Massari, 1984; Postma, 1984; Massari and Parea, 1990; Nemec, 1990; Massari, 1996). Hydraulic jump occurs within the flow up-current from the obstacle/slope-break, and sediment is deposited on the up-current side of it.

Example of backset bedding are also described in turbidites, for example in the Cloridorme Formation by Skipper and Bhattacharjee (1978) where backsets occur in coarse-medium sand and are interpreted to result from the upstream migration of antidunes.

In previous studies, the development of bedforms with upstream-dipping laminae, “backset” laminae, have been considered to be associated to upstream migration of antidunes in the case of a turbulent flow (Gilbert, 1914; Middleton, 1965; Middleton and Southard, 1984, p.259 Skipper, 1971; in Nemec, 1990) or to flow under chute and pool conditions (Schmincke *et al.*, 1973), to the upper-current migration of rhomboid ripple-marks (Wunderlich, 1972; 1973). In some of Hand’s (1974) experiments on density currents, chutes and pools developed at Froude number  $> 1$ , sedimentation being related to up-stream migrating hydraulic jumps. Flows generating these bedforms have been observed in flume experiments by Simons *et al.* (1965) and steeply-dipping backset beds have been experimentally produced by Jopling and Richardson (1966) and by Allen (1982).

Laminasets in which laminae dip upstream have been more recently produced by Alexander *et al.* (2001) in laboratory experiments; they studied the development of bedforms and sedimentary structures (antidunes and chute-and-pools) under supercritical water flows, over aggrading beds, obtaining deposits similar in general forms to those described by laboratory flume experiments of Middleton (1965) and Hand (1974). Their experiments anyway refers to subaerial condition comparable to river flows settings.

### *FROUDE NUMBER*

Flows are termed supercritical when their Froude number (current velocity divided by maximum wave celerity) exceed unity  $Fr > 1$ . This number represents the ratio between the inertial force and gravity force and it is a measurement of flow strength.



The Froude number is a dimensionless number that for rivers has been defined as:

$$Fr = \frac{\bar{U}}{\sqrt{gh}}$$

where  $\bar{U}$  denotes depth-averaged flow velocity,  $h$  is flow depth and  $g$  denotes the gravitational acceleration. When  $Fr > 1$ , the river flow is supercritical and it corresponds to a very swift flow. Submarine turbidity currents are intrinsically more biased toward supercritical flow than rivers.

Komar (1971), compared the forces governing supercritical flows in rivers with the ones in density currents which resulted to partly differ due to the presence of an overlaying fluid mass of non-negligible density. The Froude number has been therefore modified to take to account the density contrast:

$$Fr = \frac{\bar{u}}{\sqrt{\frac{\rho_t - \rho}{\rho_t} gh}}$$

where  $\rho_t$  is the density of the more dense fluid and  $\rho$  is the density of the overlying fluid. This new equation is the more general form of the Froude number and it is called "densimetric Froude number". This equation has been successively slightly modified and Fildani *et al.* (2006) used a densimetric Froude number for turbidity current as:

$$Fr = \frac{\bar{U}}{\sqrt{RCgh}}$$

where  $C$  is the layer-averaged volume concentration of suspended sediment carried by the turbidity current,  $h$  is an appropriate measure of turbidity current thickness and  $R$  is the submerged specific gravity of the sediment and it's given as:

$$R = \frac{\rho_s}{\rho} - 1$$

where  $\rho_s$  is sediment density and  $\rho$  is water density (sea water density 1027 kg/m<sup>3</sup>).

In turbidity currents  $C \ll 1$  because they are dilute suspensions therefore  $RC \ll 1$ . As a result for the same flow conditions, supercritical flows result to be more common in submarine condition, especially when developed along steep slopes, than in river settings.

## HYDRAULIC JUMP

When a flow pass from being supercritical to subcritical, a hydraulic jump occurs. A hydraulic jump is a short zone over which the flow makes a rapid conversion from shallow, swift supercritical flow ( $Fr > 1$ ) to deep, tranquil sub-critical flow ( $Fr < 1$ ). Through the hydraulic jump, the flow velocity is halved and its thickness increase to more than double and there's a general transformation in the nature of the energy of the flow that passes from being kinetic energy to potential energy.

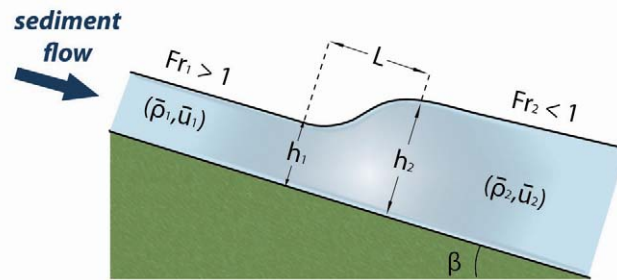


Fig. 6.1 - Definition sketch of hydraulic jump (original sketch from Savage, 1979).  $L$ =length of jump;  $h_2/h_1$ =flow thickness ratio across the jump; flow continuity requirement:  $\rho_1 u_1 \cdot h_1 = \rho_2 u_2 \cdot h_2$  where  $\rho$  and  $u$  are thickness-averaged densities and velocities, and  $Fr$  is the flow Froude number, where 1 and 2 refer respectively to regions upflow and downflow of the jump (modified from Nemeč, 1990).

Komar (1971) investigated hydraulic jumps that may occur in turbidity currents travelling through submarine canyons and channels, and those which may be generated by slumps on the continental slope. The authors compared the forces governing hydraulic jumps in rivers with the ones in density currents which resulted to be the same but some of the forces increase in magnitude while others decrease due to the presence of an overlaying fluid mass of non-negligible density. The author therefore proposed the new more general equation for the densimetric Froude number discussed above.

The results from experimental works and theoretical considerations (Yih and Guda, 1955; Ellison and Turner, 1959; Wood, 1967) suggest that the higher the pre-jump Froude number, the greater the rate of entrainment of the overlying water and hence the greater the reduction of density during the jump.

In turbidity currents, during a hydraulic jump, the current beside increasing in thickness and decreasing in velocity, entrains water through its interface and thereby reduces its density. The density is indeed a parameter that in flowing sediment-water mixture cannot be assumed to be known or constant since, along a natural slope, it will continuously fluctuate due to flow erosion and sediment deposition from the flow.

The equations used for the study of turbidity current are slightly different from the ones used for rivers because more factors have to be taken into account. In turbidity currents there's a lower density contrast with the overlying water and the drag on the upper interface as to be included as well as on the bottom.

When a flow experiences and hydraulic jump the flow suffers variation in velocity, thickness and in density: thickness of flow increases after the jump while velocity and density decrease.

In the analysis of an hydraulic jump, some parameters have not to be taken into account like mechanical energy because it is not conserved since it's lost when turbulence is created by the jump. The initial conditions are that the thickness of flow has to be such to stay in the channel while the evaluation of densities results to be more problematic. Komar (1971) describes two different types of hydraulic jump that may form in a submarine canyon-channel system, I) occur within a canyon and II) occur within a channel. The author noted that the position of the jump depends on whether the conjugate depth to the normal flow depth within the canyon  $h_g$ , is less than or greater than the normal flow depth on the low slope  $h_c$ .

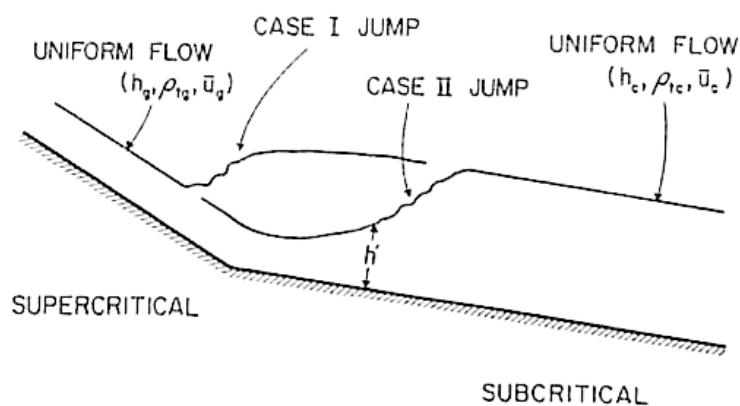


Fig. 6.2 - The two types of hydraulic jumps which may convert the supercritical uniform flow conditions  $u_g$ ,  $h_g$  and  $\rho_g$  on the higher slope within the canyon (the subscript  $g$  denotes "gorge") to the subcritical uniform conditions  $u$ ,  $h$  and  $\rho$  in the channel (denoted by the subscript  $c$ ). The case I jump occurs within the canyon, whereas the case II jump takes place in the channel. Analysis of the two cases differs. (Komar, 1971)

The author also demonstrated that the nature of the jump is essentially independent of the magnitude of the initial thickness. The height of the jump is given by the ratio of the post-jump thickness to the pre-jump thickness and it depends upon the amount of entrainment and on the pre-jump Froude number.

### BACKSET BEDDING IN LABORATORY EXPERIMENTS

In laboratory experiments, in the study of bedforms developing in turbulent flow condition backset beds were shown by Simons and Richardson(1963) and Middleton (1965) to develop on stoss-sides of antidune bedforms. Jopling and Richardson (1966) produced backset bedding in a laboratory flume under conditions of supercritical flow placing an hydraulic jump downstream. The authors observed deposition of sediment at the site of the jump and increasing the tailwater depth they cause the upstream movement of the jump. The growth of the mound was accompanied by a downstream development of cross-lamination and an upstream formation of backset bed cross-lamination. Experimental and theoretical evidence

indicate that such bedforms form when the flow either changes from one supercritical state to another with lower velocities, or from a supercritical to a critical or subcritical state.

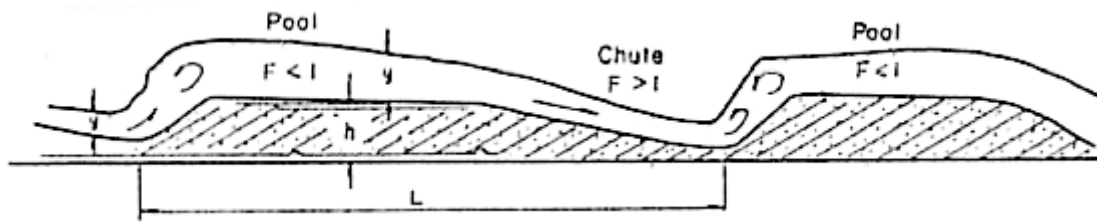


Fig. 6.3 – Schematic representation of backset bedding formed in a laboratory flume by chute and pool flow. Length,  $L$ , is about 30 feet, height,  $h$ , is about 1 foot, and depth of flow,  $y$ , varied from 0.4 to 1.00 foot. The deep of the backset bedding is  $30^\circ \pm$ , and the flow is from left to right. Jopling and Richardson, 1966).

In some of Hand's (1974) experiments on supercritical flows in density currents, the author observed that phenomena and sedimentary structures typical of supercritical flow are very common in density underflows and form spontaneously on erodible beds when  $Fr > 1$ . This is due to a variation in density contrast between fluid layers which is reduced in density current compared to open channels. In some runs the author noticed the development of antidunes from an initially plane bed, their conversion to chutes-and-pools, and finally a return to simple antidunes which evolved to the point of breaking.

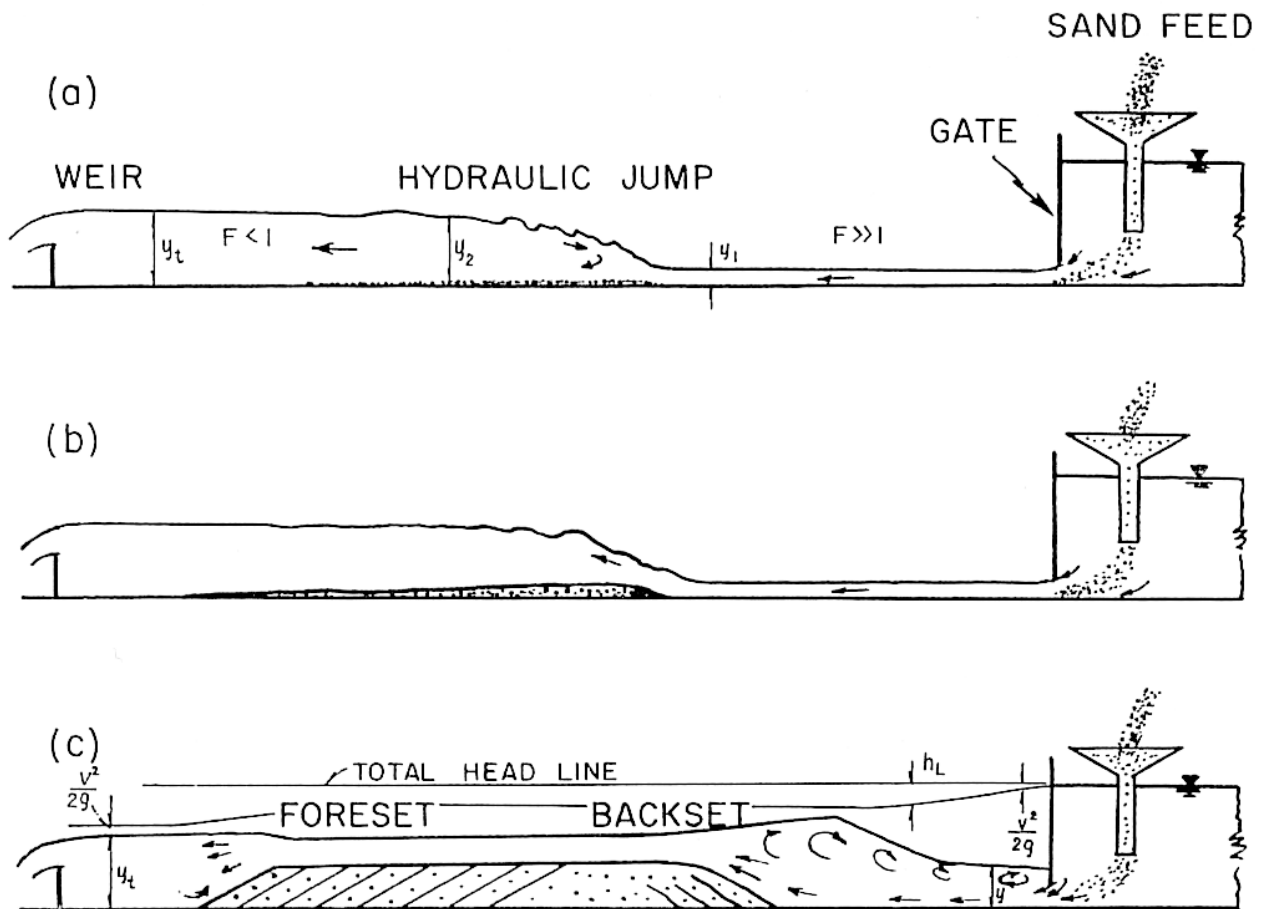


Fig.6.4 - Schematic representation of the formation of backset bedding in a laboratory flume, showing sand feed, constant head water supply, sluice gate and downstream weir. (Jopling and Richardson, 1966).

In chutes-and-pools condition, sedimentation is related to upstream-migrating hydraulic jumps; a submerged hydraulic jump is able to migrate upstream as erosion extended the low part of the bed in that direction, while sediment accretion occurred in the subcritical region behind the jump.

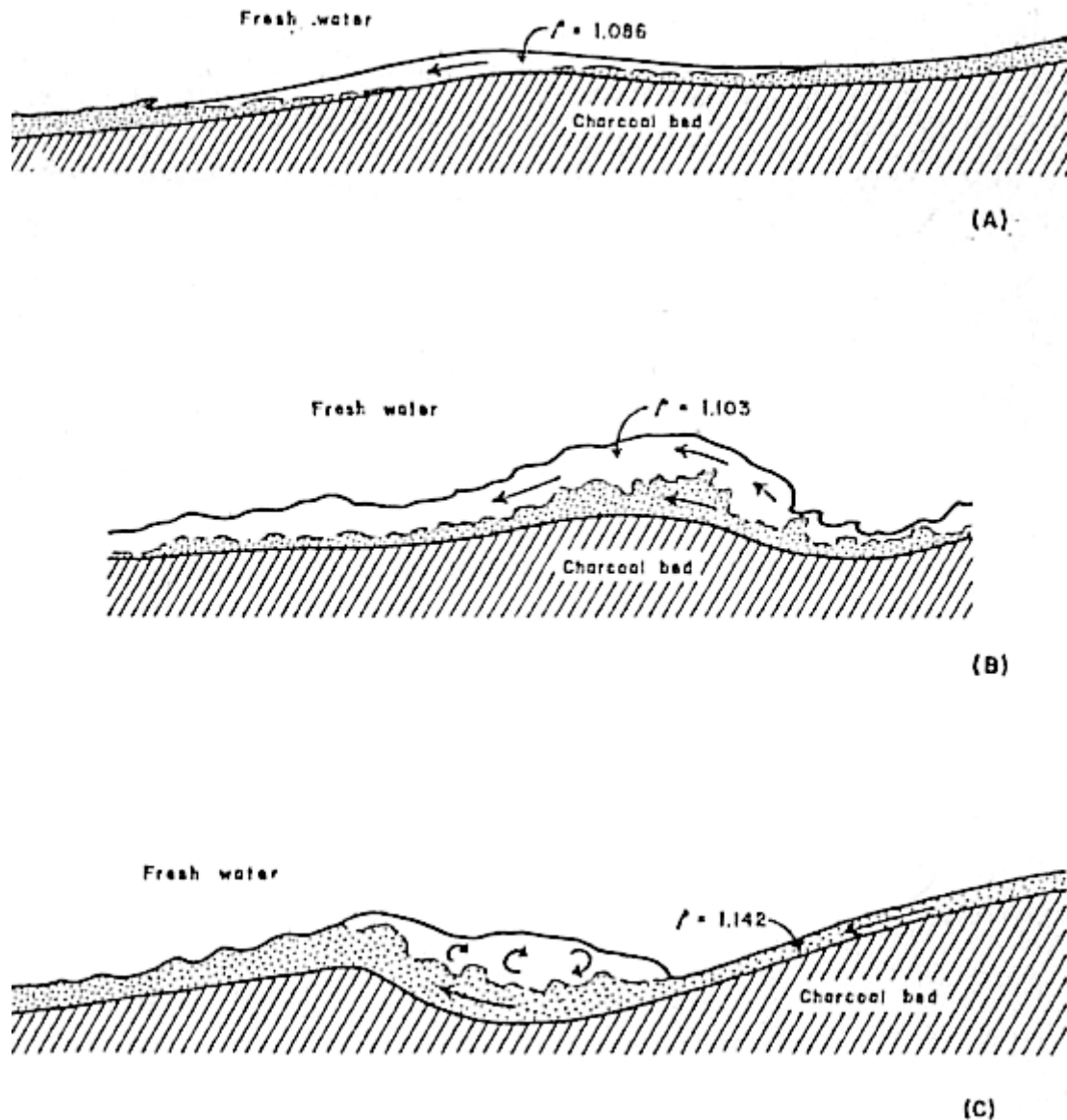


Fig.6.5 - Density currents over natural bedforms on erodible charcoal bed. Stipple indicates fluid darkened by suspended sediment. (a) Smooth flow over simple antidune. (b) Breaking antidune. (c) Chutes-and-pools. (Hand, 1974).

The development of upstream dipping cross-lamination was already described from flume experiments (Middleton, 1965) and from natural sediments (Power, 1961; Hand and others, 1969). The presence of antidunes in turbidity current flow was previously noted also by Walker (1967) in the Hatch Formation (Devonian, New York) and by Skipper (1971) who proposed that wave-like bedforms and associated backset lamination in the Cloridorme Formation (Ordovician, Quebec) represented another occurrence of antidunes in turbidites.

## BACKSET BEDDING IN NATURAL ENVIRONMENTS

In natural environments, along slopes, hydraulic jumps are thought to develop due to dilution, enlargement, strong reduction of the competence and velocity of flow as it reaches the base of the slope or related to obstructions and/or to breaks in slope produced by slides, slumps and "frozen" debris-flow bodies.

The genetic link between backset beds and hydraulic jumps was proposed by Massari (1984), and Massari and Parea (1990) and extensively treated by Nemeč (1990).

The first backset bedded deposit was probably recognized and described by Davis (1890) along the ancient steep-face deltas of a fluvio-glacial outwash deposit of New England.

Scour-filling gravel and sand showing backset bedding are largely described on the foreset and toeset of Gilbert-type fan delta by Postma (1979, 1984a), Postma *et al.* (1983), Massari (1984, 1996), Postma and Roep (1985), Colella *et al.* (1987, 1988), Nemeč (1990). These structures are interpreted to develop at very high concentration of sediment during transport, and thus, the genesis of scour-filling backset beds on the foreset slope of a Gilbert-type systems may reflect the upstream migration of chutes and pools. They are more abundant at the toesets but also occur in the foresets. (Komar, 1971, Hand, 1974; Massari, 1984; Postma, 1984; Massari and Parea, 1990; Nemeč, 1990; Massari, 1996).

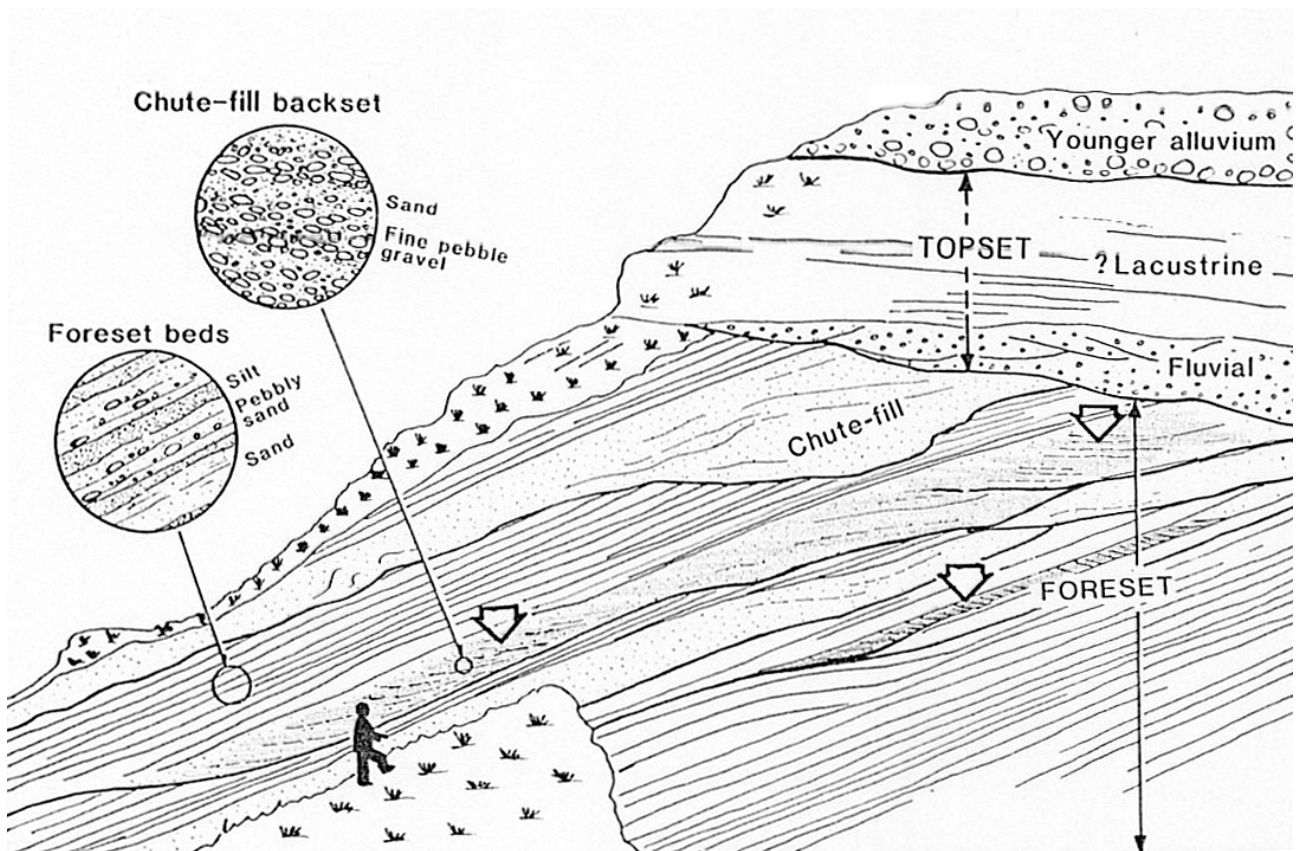


Fig. 6.7 The thicker backsets occur as relatively coarse-grained infill of chutes (from Nemeč, 1990).

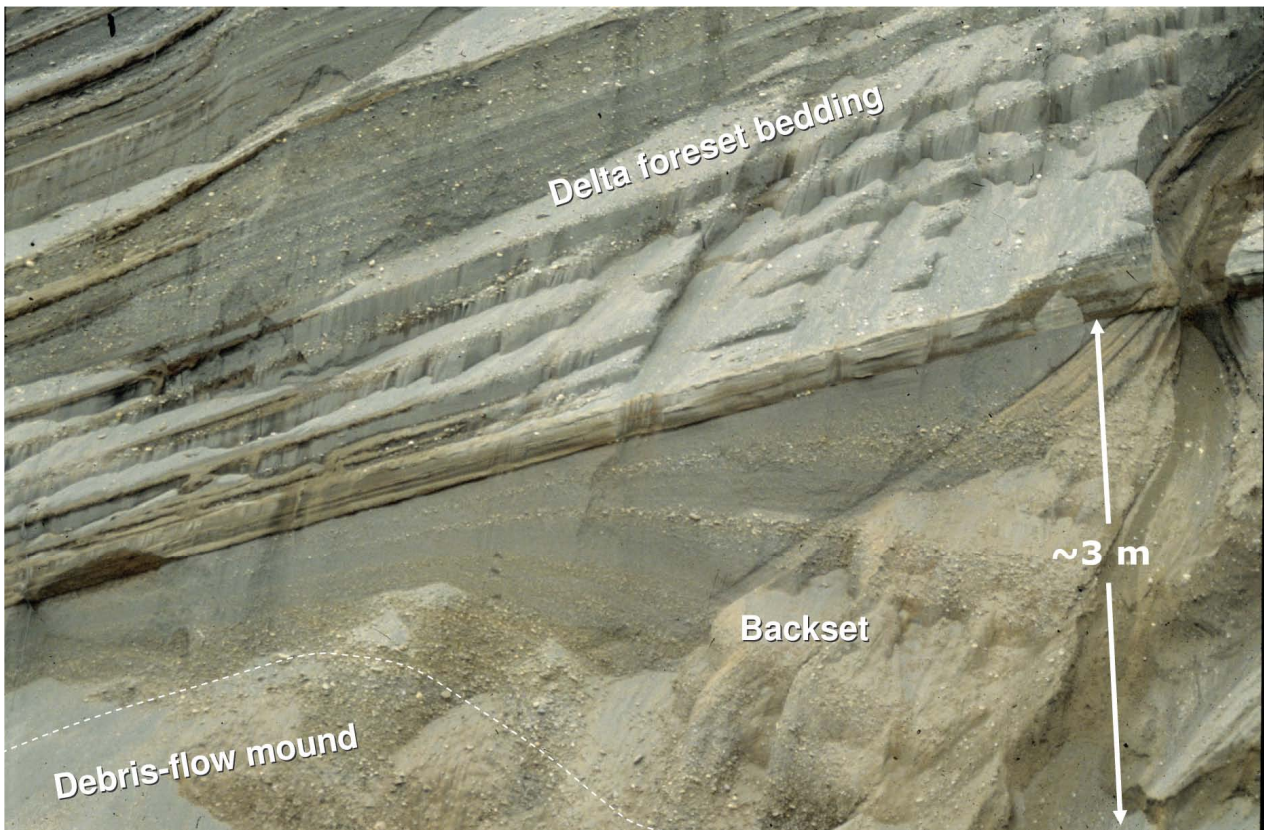


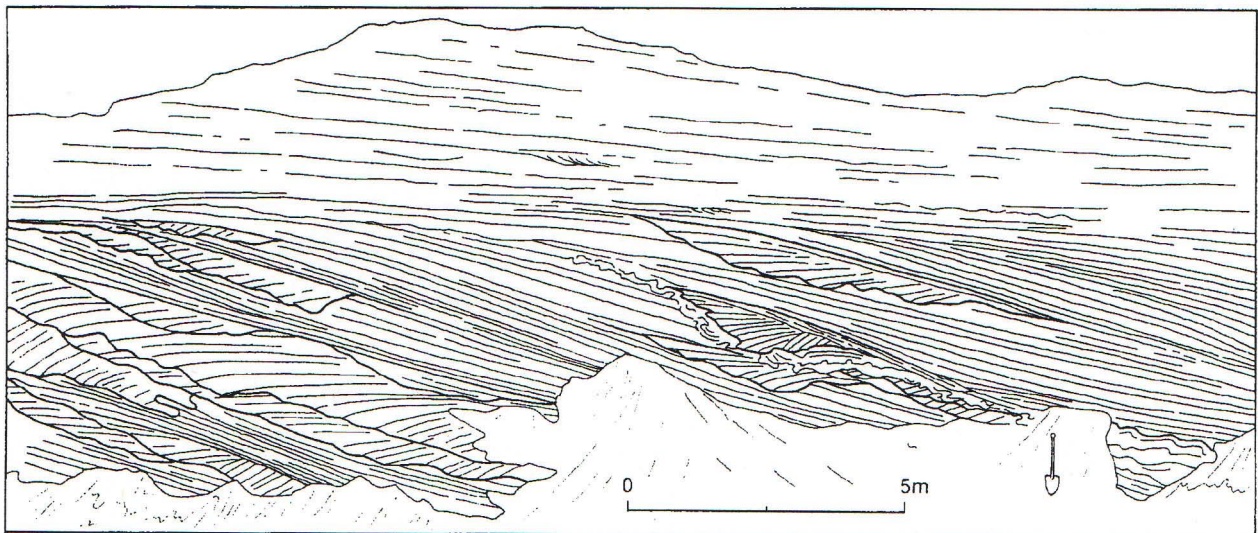
Fig. 6.8 Backsets in the glaciofluvial, Gilbert-type Kregnes delta, Pleistocene, Trondheim area, Norway (Nemec et al., 1998).



Fig.6.9 Backset beds from Gilbert-type delta, Crotona area (photo courtesy of Massimiliano Ghinassi, Gino for scale).

Massari (1996) relates backsets to occur, individually, as in-fills of "spoon-shaped" scours with downslope-oriented long axes. They are more abundant at the toesets but also occur in the foresets. In the studied Pleistocene example of a progradational Gilbert-type delta, Massari (1996) documents scours to be 2-17 m wide, 0.1-2.7 m deep and 2.2-23 m long (downslope-

oriented). The scour surface is commonly irregular and may have steep-sided walls, locally overhanging when cut into fine-grained sediments. Backsets are abundant in pebbly sand although they occur in a wide range of grain sizes. Sand is commonly very well sorted. The dip angles of backset cross-laminae tend to increase with grain size (up to 35° with respect to master foreset stratification). Pebbles show up-current dipping *a*-axis imbrication. Within some backsets, adjacent clusters of pebbles may show gradual or abrupt changes in imbrication dip. Backset cross-laminae may be, in longitudinal section, concave-up, planar, slightly convex-up or even sigmoidal but only concave-up, planar or slightly convex-up in transversal section. Large rip-up clasts of the encasing fine-grained sediments are locally present in the backsets. Deformation structures (convolute lamination, distorted bedding) may be present both in the scour infill and in the trough walls. According to this author, the scoured, spoon-shaped bases of the sets of backset cross-laminae result from erosion due to strong turbulence within hydraulic jumps, and the backsets accretion (deposition of high-angle backset cross-laminae) occurs on the downstream flank of an erosional "pool" as the hydraulic jump and related erosional pool migrate upslope (upstream).



*Fig.6.10 Photograph and sketch of the uppermost part of Cugnola Volta complex (section subparallel to direction of progradation) showing abundance of scour-filling backsets close to topset. Note fanlike pattern of backset cross-laminae in some scour infills, and locally developed broadly convex-up lamination at top of backsets. One scour infill on right side of section shows angular contact between bundles of variously inclined laminae, and folded and distorted bedding on trough walls. Note also physical continuity of transition between topsets and foresets on right. Backsets range in composition from pebbly sand to pebbly gravel; foresets are predominantly sandy (from Massari, 1996).*

Sets of upslope-dipping cross-lamination are described by Uličný (2001) from the Bohemian Cretaceous deltas (Czech Republic), where they developed in distinctly coarser sandstone than the surrounding facies. In some cases backsets rest on foresets without distinct erosion at the base of the backset while elsewhere are found as part of the chute-fill facies assemblage. In chute-fill, backsets are well pronounced and they climb up irregular erosional surface of the chute floor and upward a transition from the backset laminae into aggradational planar strata is noted. Coarse material is concentrated at the scoured base and foreset dip direction change after the filling of the chute. The author relates these coarse-grained deposits as due to



sustained, mostly unidirectional currents that were affecting the deltas and were able to transport coarse sand and gravel along the foreset slope in more than 70m water depth. The supercritical nature of the flow and upslope migration of hydraulic jump (cf. Jopling & Richardson, 1966; Nemeč, 1990) is indicated by the parallel lamination, which can be traced laterally and vertically into backsets in many cases. As observed in the experiments by Jopling & Richardson (1966), also in this example, the backset laminae show an upward decrease in grain size. The formation of spoon-shaped scour are interpreted to be caused by the formation of an hydraulic jump which can be formed by small irregularities on the delta foreset surface that are might be generated by slope failure events. The subparallel, aggradational bedding on top of backset is explained as a result of chute infilling and the establishment of a fully supercritical flow on the slope. The author therefore interpreted the mechanism of downslope transport as a liquefied sand flow *sensu* Lowe (1976), which behaved rheologically as cohesionless, pseudolaminar, debris flow (cf. Nemeč *et al.*, 1988) and may or may not have transformed into turbulent flows (Nemeč, 1990). The main depositional mechanism within the chutes (but also operating outside the chutes on the foreset slopes) was the formation of backset strata at hydraulic or granular jumps.

Another example from a Gilbert-delta-filled incised valley from the Pliocene of Ventimiglia (NW, Italy) is reported by Breda *et al.* (2007) who describe similar features characterizing these sedimentary structures. The backset beds described show different grain size ranging from pebbly to clast-supported pebbles within an individual set and they display an overall decrease in grain-size and dip angle. The backset beds downlap the basal erosion scour at high angle (from 10° to 35° relative to master bedding).

The interpretation of the formation of such structures relates erosive troughs and scours to topographic lows created by strong turbulence and erosive capacity of hydraulic jumps within gravity flows (as in Uličný, 2001). The filling of scour must be very rapid after excavation, to preserve the steep-sided walls. The backset cross-beds produced as the hydraulic jump and related erosional pool migrate upstream accompanied by sediment accretion on the downstream flank of the trough in the subcritical region behind the jump (Hand, 1974; Massari, 1984; Postma, 1984; Massari and Parea, 1990; Nemeč, 1990; Massari, 1996). The sub-parallel, aggradational beds that drape the backset strata resulted from later stage fill of the scours and the re-establishment of a fully supercritical flow (Massari, 1996; Uličný, 2001).

At Monte Capodarso (Sicily, Italy) an example of backset beds is described with a different depositional environment. Lickorish & Butler (1996) present an example from a Pliocene succession of coastal carbonates in central Sicily. Along clinoforms, the authors describe upslope-migrating cross-beds composed of reworked material from below. These beds separate packages of avalanche foresets. These structures are interpreted as formed during storm events by onshore directed currents.

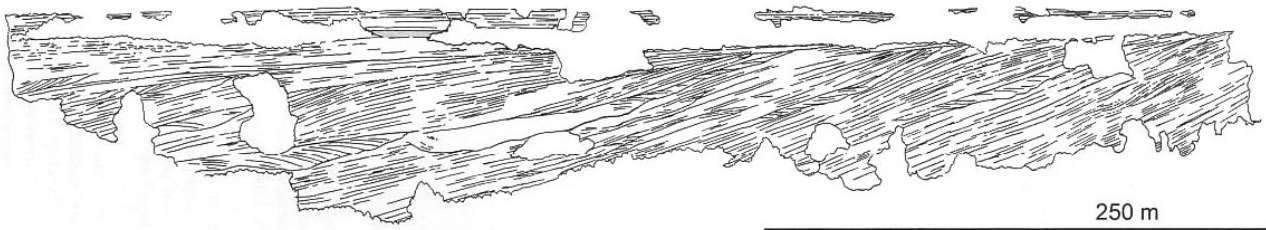


Fig.6.11 Drawing of the longitudinal section of the fifth carbonate wedge near the Capodarso bridge (eastern side of Cozzo della Guardia). Note internal unconformity surfaces, sets of backset beds on the foreset (locally with toplap truncation) and poorly cropping out sub-horizontal band at the top. Vertical exaggeration of the drawing: 1.5x (from Massari & Chiocci, 2006).

The same example studied by Lickorish & Butler (1996) was interpreted as backset beds generated in a storm-dominated environment, by Massari & Chiocci (2006). These authors attributed the backset beds to updip migration of hydraulic jumps, thought to affect downdip-accelerating gravity underflows. They are thought to reflect the incidence of major storms, probably of exceptional energy. The erosional character of the surfaces passing downdip into sets of backset beds indicates that involved flows had a certain scouring power and were able to erosively reduce the inclination of the upper part of the clinofomed ramp margin.

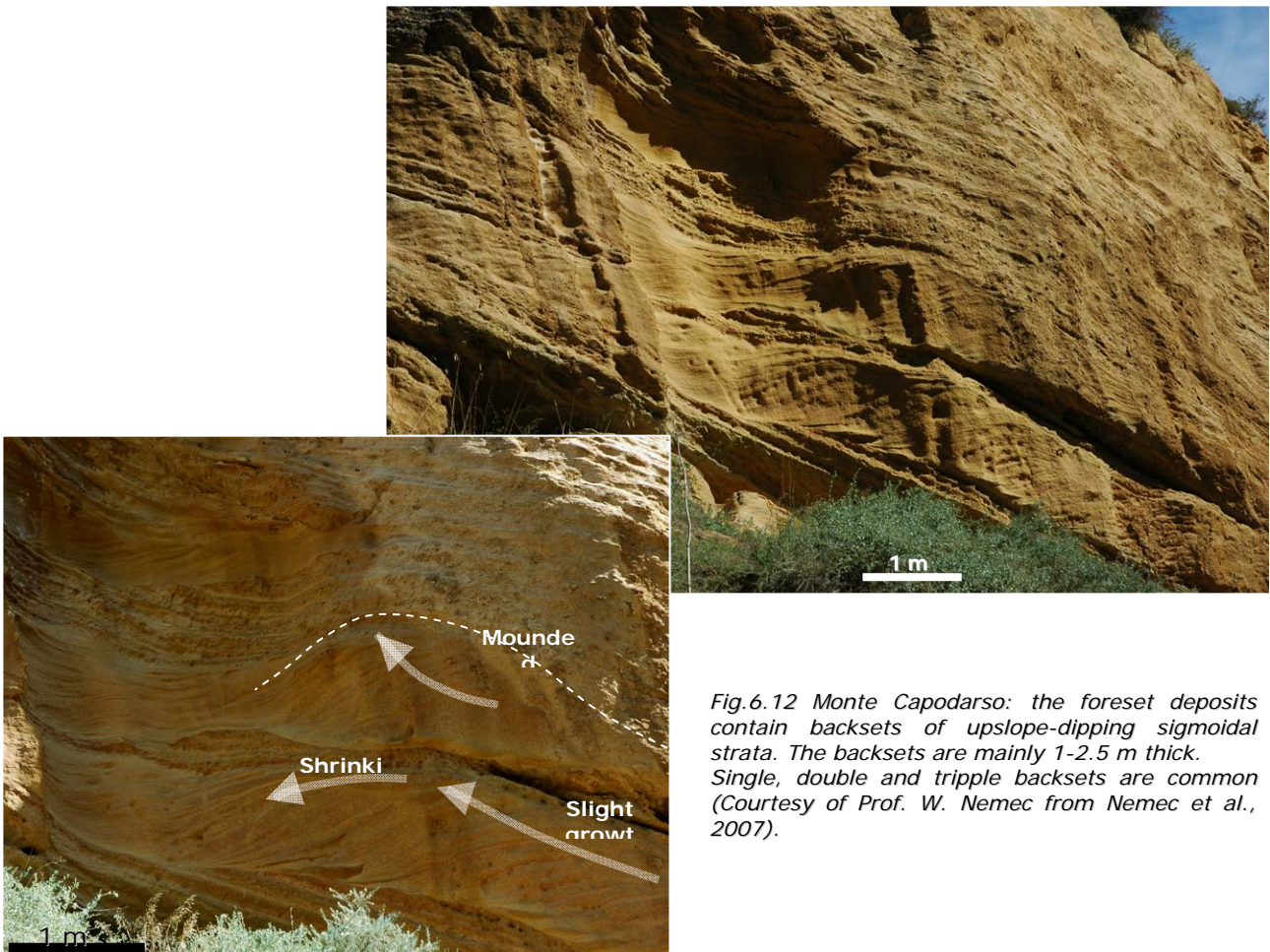


Fig.6.12 Monte Capodarso: the foreset deposits contain backsets of upslope-dipping sigmoidal strata. The backsets are mainly 1-2.5 m thick. Single, double and tripple backsets are common (Courtesy of Prof. W. Nemeč from Nemeč et al., 2007).

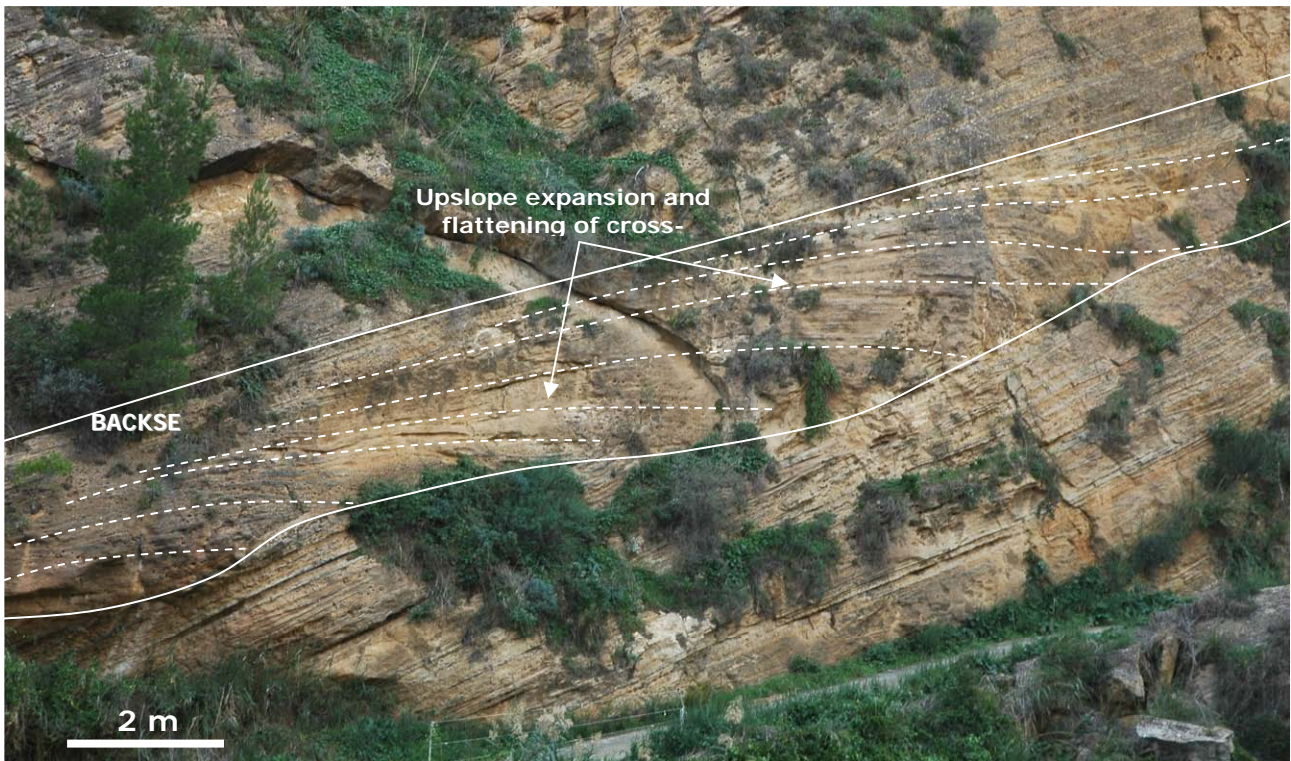


Fig.6.13 Picture and drawing of the Monte Capodarso backsets, evidencing the decrease up dip of angle of dipping laminae (Courtesy of Prof. W. Nemeč).

### **Major features of backset beds: the comparison between the same forms in different environments**

The occurrence of backset beds in siliciclastic environments, as shown by the numerous examples described in literature, is quite common and represent a common facies along the foreset and base-of-slope of Gilbert-type deltas. Unfortunately the only examples of such sedimentary structures in a carbonate depositional system is the one found in Menorca, not allowing the comparison between forms in similar carbonate environments.

If we compare the forms found in the two settings, the Gilbert-type delta ones and the ones described from Menorca, there are numerous similarities.

- found along slopes that present maximum dipping angles of 15°-20°;
- clinofolds along which they develop are in the range of few hundreds meters long;
- they are found at relatively-shallow water-depth;
- thickness of single deposit varies from few decimeters to 2 meters;
- the over whole stacking of several deposits may reach tens of meters;
- they occur in a wide variety of grain-sizes from sand to gravel and cobble;
- the finer-grained component (mud) is absent;
- the scour surface is commonly irregular and may have steep-sided walls, locally overhanging when cut into fine-grained sediments;

The major differences are fundamentally on the composition of clasts, siliciclastic *versus* carbonate, and on the type of energy that dominate these environments, unidirectional fluvial currents versus bidirectional wave energy.

The difference in composition marks a substantial difference in the definition of the hydraulic regime that drives the development of backset beds. In fact, if we consider that these bedforms are the results of supercritical flows that turn into subcritical flows, and that the Froude number in submarine condition is defined as:

$$Fr = \frac{\bar{U}}{\sqrt{RCgh}}$$

where R is defined as  $R = \frac{\rho_s}{\rho_w} - 1$ , these value depends on sediment density which

considerably change from siliciclastic to carbonate. Quartz density is 2648 kg/m<sup>3</sup> therefore the value  $R_{\text{QUARTZ}} = 1.65$  while the density in carbonate sediment may vary noticeably: from low density to high density limestone the values have been estimated to change from about 1500 to 2560 kg/m<sup>3</sup>, consequently the relative value of  $R_{\text{CARBONATE}}$  may noticeably change ranging between 0,50 to 1,56. The definition of carbonate rocks density results to be quite complicated because porosity and cementation play an important role in carbonate density therefore these numbers are to be taken with care. The carbonate sediment involved in the studied deposits is represented mainly by mollusc fragments, coralline algae, loose ooids, bryozoans and foraminifers and at the same time by lithified limestone clasts. Jorry *et al.* (2006) measured apparent density values of *Nummulites* which resulted to range from 1480 to 2610 kg/m<sup>3</sup>. This large range of density resulted to be due to the presence of cement which partly seals intra-skeletal porosity. These authors, through the used of an appropriate formula, re-calculated the porosity when the porous network is filled with seawater: the apparent density of *Nummulites* resulted then to range from 1700 to 1900 kg/m<sup>3</sup>. These observation have an important implication in the understanding of transport mechanisms in carbonate sediment.

Supposing for carbonate sediment a density of 1800 kg/m<sup>3</sup>, this would mean an  $R_{\text{CARBONATE}}$  value of about 0.75, which is more than half of the  $R_{\text{QUARTZ}} = 1.65$ . It is therefore more complicated to decide which value of density to use in bioclastic limestone also because the deposit is often composed of bioclasts or limestone clasts that have very different density varying from very low to very high. Limestone clasts are often highly cemented but at the same time intraparticle porosity may be very high due to dissolution.

The comparison of the studied backset beds of the carbonate ramp of Menorca, with the known ones from Gilbert-type deltas, evidenced therefore, a large number of similarities that allow to give more constrains on the conditions that facilitate the development of these sedimentary structures. The similarities regard grain-size populations involved, values of

backset foreset laminae dipping angles, trends of grain-size distribution and variation of lamination angles, chute- to channel-shape with erosive scouring surfaces at the base.

The major factors that resulted to be important for the formation of these bedforms can be summarized in three main points:

1) the morphology of the depositional system, intending a shallow-water, slightly inclined ramp that presents a slope-break in a distal position, the slope having an angle of 15°-20° maximum, which determined the gravitational potential energy of flows that may develop along the slope;

2) the availability of loose sediment of variable grain-size, from sand to boulder-size, that can be easily reworked and remove, partly in suspension and partly as bed-load from the shallow-water settings seaward;

3) the development of a unidirectional current directed seaward that can be related to a fluvial regime or it can be enhanced by wave-action in wave-dominated shallow-water platform (outflow such as rip-currents or tsunami backwash), able to develop velocity high enough to carry coarse and very coarse clasts off-shore while finer-grained sediment is put into suspension and transported offshore by hypopycnal flows.

The only difference regards the type of sediment even if, as previously discussed, sediment density are not easy to be compared due to high variability of bioclastic limestone density. Another difference is the hydraulic regime that origin the seaward unidirectional currents that reworked and transport the sediment across the shallow-water shelf/platform: in the Gilbert-type deltas this current is generated by the fluvial regime while in the carbonate ramp case the current is enhanced by wave action. Anyhow, the resulting current is in both cases a high energy, unidirectional current directed seaward.

## **7. INTERPRETATION**

### ***7.1 Previous interpretation of the backsets of Menorca***

The conglomerate deposits of Forma have been interpreted by Obrador *et al.* (1992) as the response of two stages in lowering sea level. During the first stage, only outer-ramp sediment have been re-sedimented, while during the second stage of sea level drop, inner ramp areas emerged causing extensive erosion of inner-ramp facies, so that the upper part of the breccias deposit present both inner-ramp and outer-ramp sediment. Those breccias deposits have been therefore interpreted by the authors as the allochthonous lowstand wedge of Sarg (1988).

Farther studies by Pomar (2001a) evidenced that skeletal components distribution at the transition between the carbonate ramp and the reef systems do not show a significant change in water depth. The back-stepping parasequences produce by the landward migration of the shoreline during the transgression are absent, and the interval is composed by oligophotic and photo-independent skeletal associations, hence important eustatic variations don't seem plausible by the author. Those breccias have been therefore re-interpreted as the backset beds found at the toe-of-slope along the axis of slide-scars affecting the lower Tortonian ramp, without direct sequence-stratigraphic meaning. The large-scale erosional scars have been interpreted as acting as channels funnelling platform debris downslope to form coarse-grained backsets (Pomar *et al.*, 2002).

### ***7.2 DEPOSITIONAL MODEL***

The observations collected in the field along with a large number of considerations regarding this depositional setting lead to the following sequence of events that drove the deposition of coarse-grained backset beds at the toe of the slope of a distally steepened ramp. In this section we identify the different processes that are thought to be involved firstly in the re-mobilization of sediment in shallow-water settings, than the ones that transported it seaward to the slope-break and finally down-slope.

As discussed at the end of the previous chapter (chapter 6), a seaward directed, unidirectional current is required to remove sediment from shallow water settings and to reach the slope-break. The triggering mechanisms for these kind of currents may be: tidal-currents such as asymmetrical ebb-flood tidal cycles where the ebb-current is dominant, wave-backwash such as undertows or rip-currents or exceptional high energy events such as tsunami-related backwash: Inflow and outflow surges produced by tsunami of tsunami train waves, can affect the platform in deeper positions (Pickering *et al.*, 1991; Puga-Bernabeu *et*

al., 2007), below the fair and storm wave base where the preservation potential is higher and normal deposition can buries and preserved the tsunami-generated deposits.

Previous studies by Pomar et al. (2002) and by Mateu-Vicens et al. (2008) do not report evidence of a strong tidal-regime, on the contrary, the carbonate ramp of Menorca is described as a wave-dominated ramp. Besides, the coarse-grained backset bedded deposits are not randomly found along the slope but they are limited to the central portion of slide-scars and to several intervals that alternate with distal turbiditic deposition of finer-sediment. This distribution in space and time let us presume that they are correlated to different episode, such as storm-events or tsunami. The hypothesis of a tsunami has been discarded because each backset bedded interval would correspond to a tsunami-wave therefore a large number of tsunami-waves would be necessary to explain each interval; moreover from the coeval depositional systems of the Western Mediterranean there are no report of tsunami-related features.

For these reasons storm-wave events are thought to be the triggering mechanism that enhanced the seaward unidirectional currents because they are able to develop strong currents capable of removing coarse-grained sediment and they justified the presence of the studied deposits only in some interval of time corresponding to storm-weather. A more detail description on how the sediment is remobilized and transported is found in the following section.

### *Entrainment of sediment in shallow water*

The carbonate ramp of Menorca has been already described as wave-dominated ramp where, to the action of waves, a strong long-shore current is also associated (Pomar *et al.*, 2002; Mateu-Vicens *et al.*, 2008). The island was facing a large basin represented by the Western Mediterranean Sea with a fetch of hundreds of kilometres allowing big sea-storms to develop and to affect the southern coastline of the island.

Waves are very efficient at stirring sediment up from the bed, but not in causing long-distance advection. Shallow-water and intermediate-waves ( $L/d > 20$  and  $2 < L/d < 20$ , where  $L$  = wavelength and  $d$  = undisturbed water depth) have the potential to exert high shear stresses on the sea bed, while deep-water waves do not feel the sea bed and are not important in sediment transport. Large storm waves with periods between 10 and 15 seconds are capable of entraining sand in water depths of 100-200m.

When the sea-bed is within reach of the waves, it experiences a periodic variation in pressure due to the passage of surface waves, what is called a cyclic wave loading. The wave action is therefore responsible of putting sediment into suspension while the transport of sediment is related to the seaward sediment-rich currents that waves can generate. (cf. in Bridge and Demicco, 2008 and Allen, 1997, Soulsby 1997).

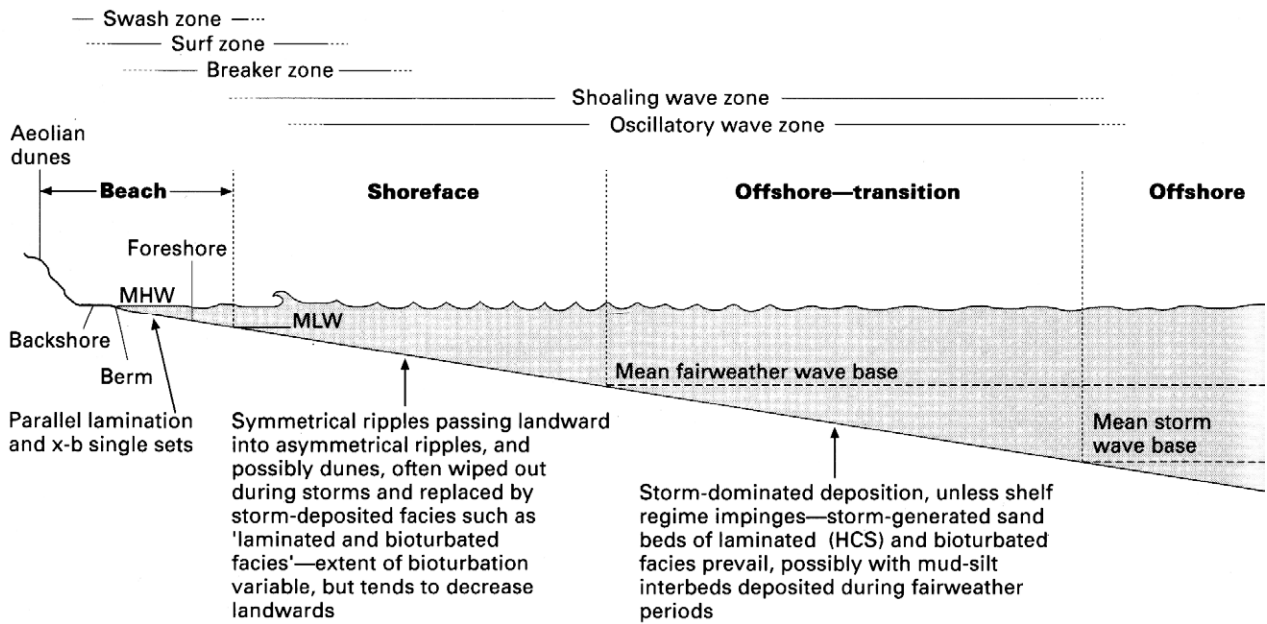


Fig.7.2.1 Generalized shoreline profile showing sub-environments, processes and facies (from Reading & Collinson, 1996 in Reading 1996).

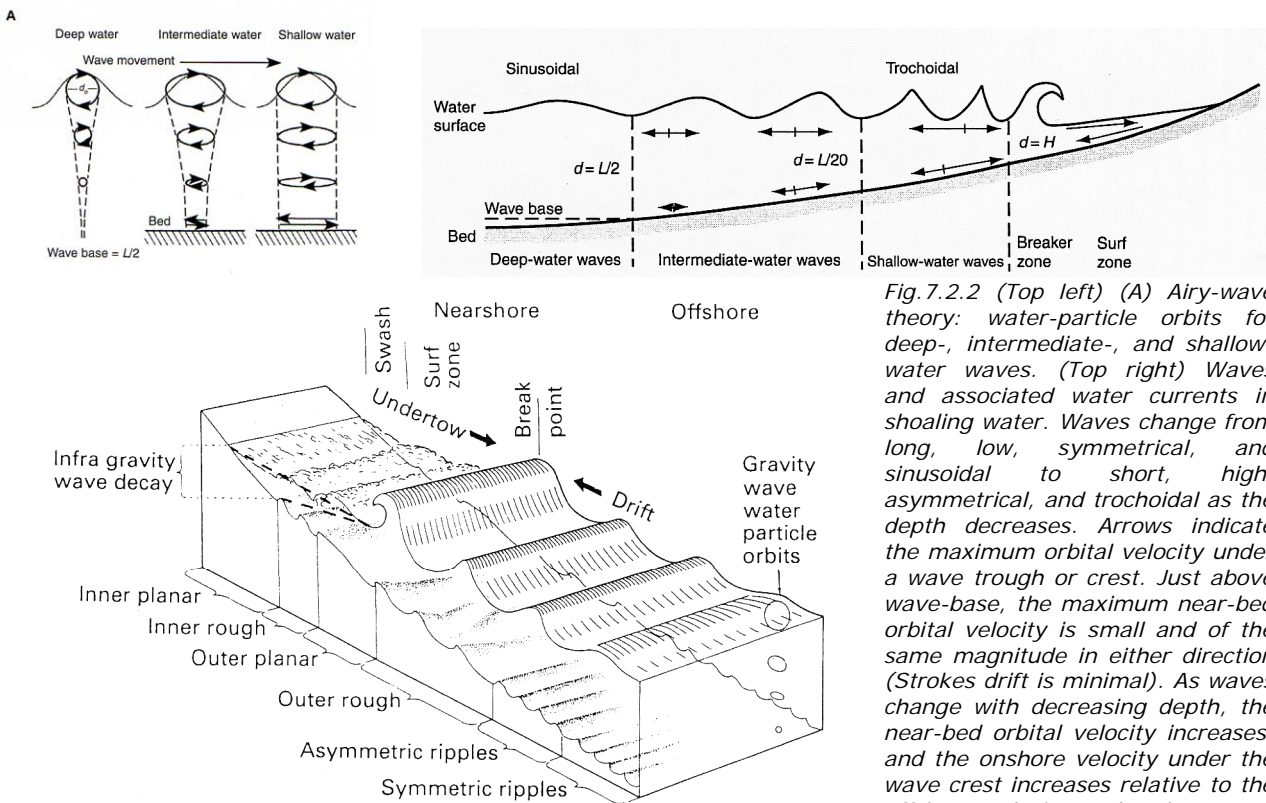


Fig.7.2.2 (Top left) (A) Airy-wave theory: water-particle orbits for deep-, intermediate-, and shallow-water waves. (Top right) Waves and associated water currents in shoaling water. Waves change from long, low, symmetrical, and sinusoidal to short, high, asymmetrical, and trochoidal as the depth decreases. Arrows indicate the maximum orbital velocity under a wave trough or crest. Just above wave-base, the maximum near-bed orbital velocity is small and of the same magnitude in either direction (Stokes drift is minimal). As waves change with decreasing depth, the near-bed orbital velocity increases, and the onshore velocity under the wave crest increases relative to the offshore velocity under the trough (due to Stokes drift). Near the water surface, the water velocity under wave crests and troughs increase in height. Differences between onshore- and offshore-directed flow velocities are due to Stokes drift. Arrows in the surf zone indicate swash and backwash from (Bridge & Demicco, 2008).

Fig.7.2.3 Beach and nearshore nomenclature and sub-environments (from Hardisty, 1994, in Pye, 1994).



In fact, the onshore movement of water caused by waves, is balanced by an offshore movement of the same mass fluid thus satisfying the continuity condition (Munk, 1949). The offshore movement is in the form of an unidirectional bottom current that flows down the pressure gradient. If the bed is sloping, then gravity provides a component of force on the grain which may increase or decrease the threshold shear-stress required from the flow (the gravity force can be added vectorially to the shear-stress force from the flow). During major storms, the seaward flow can reach velocity of m/s, decreasing offshore; such strong currents can easily cut channels in the sea bed. These seaward flows that balance the wave set-up can be represented by undertow flows or by rip currents (*sensu* Shepard, 1936). Undertows are the seaward net movement of water particles that occurs only in certain parts of water column (cf. Shadrin, 1972; Longuet-Higgins, 1983). Rip currents have been defined as "seaward moving streaks of water which return the water carried landward by wave" (Shepard *et al.*, 1941).

### *Rip currents and sediment transport*

In the example of Menorca, the submarine surface of the lower Tortonian distally steepened ramp over which wave-motion acts, it is not a simple few-degrees oblique flat-bed surface that connects the shoreline with the slope break. The slope of the distally steepened carbonate ramp suffered a number of collapses that deeply scoured the slope and the outer ramp sediments (the lack of corresponding outcrop inland do not allow us to know precisely how much those slides cross-cut the middle ramp sediments). The major role of those slides was to modify the morphology of the carbonate platform, creating large depressions about hundred of meters wide and more than 40 m deep, at least within the outer-ramp sediment (as observed in outcrop).

The effect caused by the formation of these depressions can be compared to submarine canyons which may have large effects on the refraction of storm waves. The effect of submarine canyons on wave refraction is in fact similar to the effect of sea-bottom irregularities associated with the presence of bays and headlands. The change in the morphology over which sea waves move will cause an acceleration of incoming waves above canyons.

In several modern examples it is shown that canyon heads are able to collect sediments provided by longshore and/or storm currents (Beer and Gorsline, 1971; Herzer and Lewis, 1979; Lewis and Pantin, 2002; Puig *et al.*, 2003; Normark *et al.*, 2006). Submarine canyon found close to the shoreline are mainly fed and maintained by erosion by sediment flows (examples from the California Continental Borderland are also reported by Beer & Gorsline, 1971; Shepard & Marshall, 1973; Shepard *et al.*, 1974; Puig *et al.*, 2003). If the axis-gradient of the surface generated by slope collapses is high enough, sediment proceeding from longshore and storm currents can be captured at the head of the slide (or canyon) and

transported basinward. Several authors demonstrated the ability of currents generating during storms to transport sediment down-canyon (Shepard et al., 1974; Inman et al., 1976; Fukushima et al., 1985; Puig et al., 2003). In the example of Menorca there are evidence of slope failures but evidence showing if those failures were related to canyon excavation are not visible. Anyway, nowadays, large canyons are found only few kilometers from the shoreline of the island (Fig.2.2), as remarked in chapter 2, only 5 km offshore of Son Bou at a depth of about -80 m, there is the head of submarine incised canyon that extends down to the toe-of-slope at -1400 m (Acosta et al., 2003). Thus, the possibility that in the past, those collapses at the slope were related to more distal canyons can not be discarded.

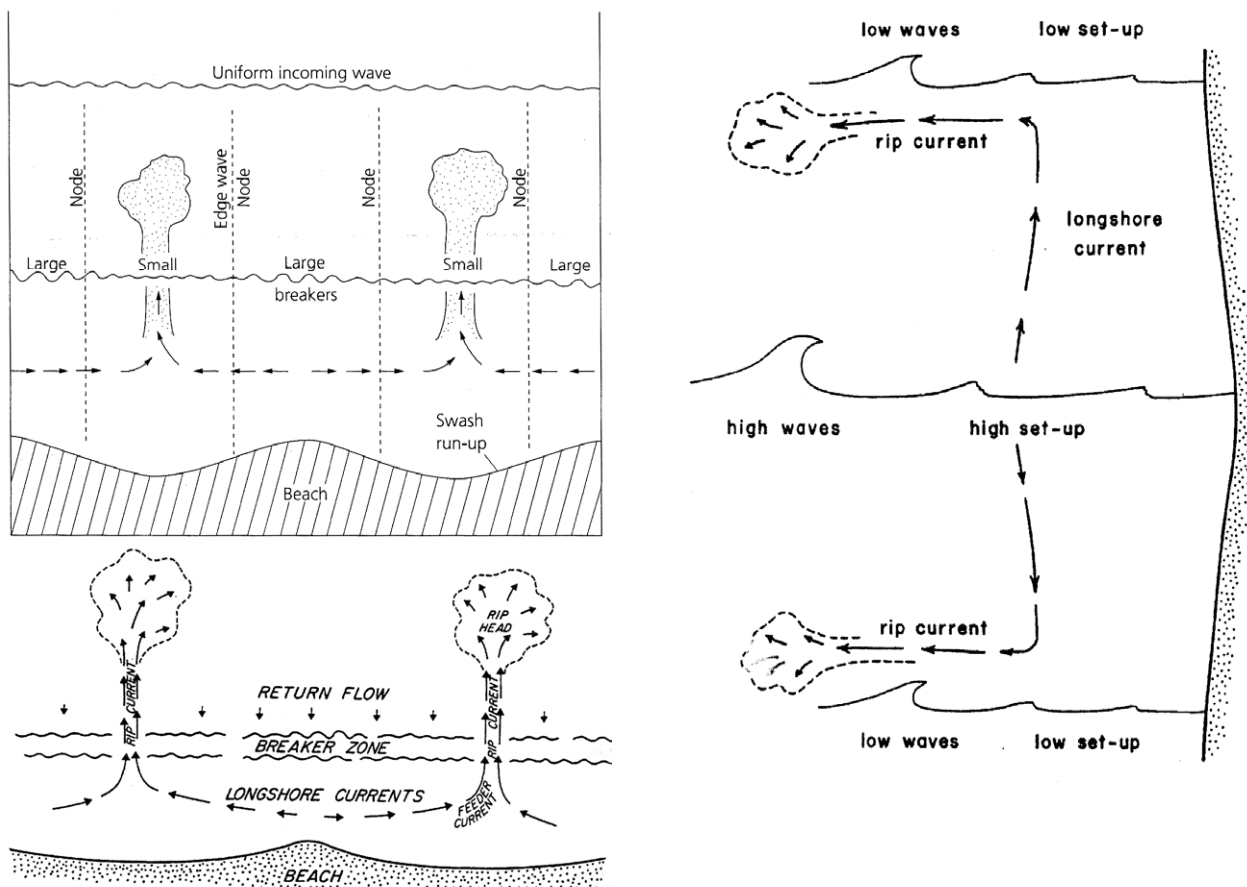


Fig.7.2.4 (Top left) Shoaling waves cause a build-up of water in the littoral zone which is compensated for by the action of seaward-flowing rip currents. These rip channels are commonly located where the breaker height is smallest (from Allen, 1997). (Bottom left) The nearshore cell circulation consists of (1) feeder longshore currents, (2) seaward-flowing rip currents, and (3) a return flow of water from the offshore into the surf zone (from Komar, 1998). (Right) Schematic illustration of the generation of the cell circulation by a longshore variation in the height of breaking waves, which produces a parallel variation in the elevation of the set-up within the surf zone. The long-shore currents flow from positions of high waves and set-up, to positions of low waves and set-up where the converging currents turn seaward as rip currents (from Komar, 1998).

The depressions formed by the collapses at the slope would therefore act like canyons: waves would accelerate above them and on the other side, they would act as preferential ways for seaward directed currents which would tend to converge and accelerate along those "canyons".

The co-presence of a strong long-shore current and the different speed of waves approaching the coast would generate a peculiar circulation pattern on the ramp. In the shore zone, where waves entering a shallowing sea bottom are sufficiently strongly deformed, rip currents may form.

Rip currents are considered to have the greater potential for the transport of coarse sediments from the beach zone to greater depths. Rip currents are strong, narrow currents that flow seaward from the surf zone and they are related to cell circulations whose speed depends primarily on longshore variations of wave-height ( $H$ ) (Shepard *et al.*, 1941; Shepard & Inman, 1950, 1951; Dolan, 1971; Kirlyys, 1971; Komar, 1971b; Davis & Fox, 1972; Sonu, 1972; Davidson-Arnott & Greenwood, 1974; Goldsmith *et al.*, 1982; Komar, 1976b; Davis, 1978). In fact, there is no reason for the generation of cell circulation if the wave height at the breakers is constant along the shore (Hardisty, 1994).

A circulation cell has been described by Bowen (1969) as “consisting of (1) a shoreward mass transport due to the wave motion carrying water through the breaker zone in the direction of wave propagation, (2) a movement of this water parallel to the coast as a longshore current, (3) a seaward flow along a concentrated lane, known as a rip current, and (4) longshore movement of the expanding rip-head”. The theory showed by Bowen (1969) showed that the rip currents occur in regions in which the wave height is low in agreement with the field observations. Rip currents are thus fed by currents which run parallel to the shoreline and which increase in velocity from zero midway between two adjacent rip reaching a maximum just before turning seawards into the rip current itself. The presence of cell circulation do not exclude the presence of steady, longshore currents but they can both be present. The current pattern is essentially the result of the sum of the two processes (Hardisty, 1994).

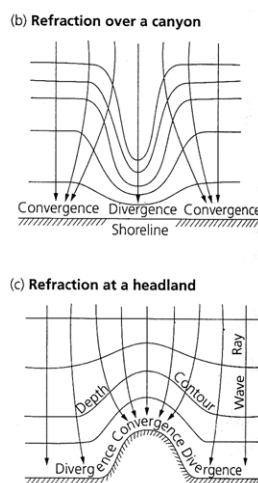
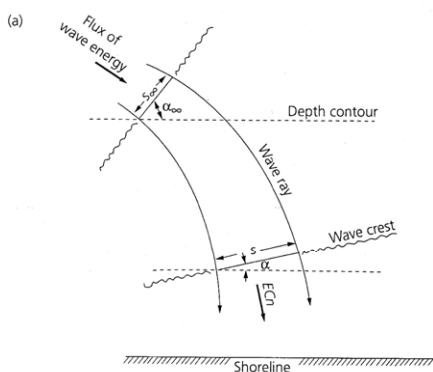


Fig.7.2.5 Wave refraction due to (a) oblique approach, where the wave energy flux  $E_{cn}$  is conserved; (b) divergence over a submarine canyon; (c) convergence on a headland (from Allen, 1997).

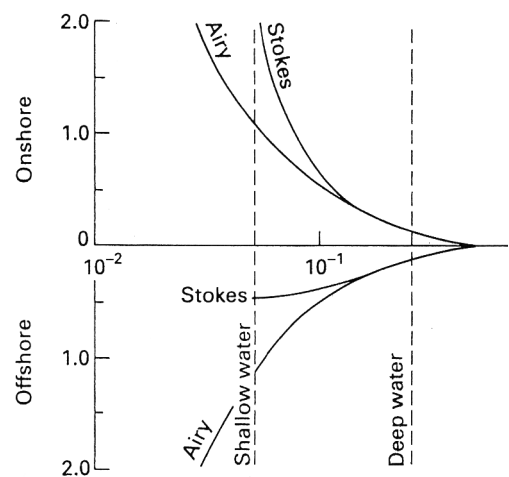


Fig.7.2.6 Changes in (a) length and celerity, (b) height and (c) peak currents of incident gravity waves as they approach the shoreline (from Hardisty, 1994).

The variation of wave height along the shore may be produced mainly in two ways: the process of wave refraction and the presence of edge wave phenomena (Allen, 1997). When

waves move into shallow water the phase speed slows down and thus for the same wave period the wavelength decreases. The deceleration and shortening of wavelength on an irregular topography, will take place earlier at one point along a wave crest than at another. The result is that wave crests close to shore will condense, steepen and orient themselves almost parallel to shore before breaking. This is known as wave refraction (cf. Allen, 1997; Bridge & Demicco, 2008 and reference therein). As shown in Fig.7.2.5 wave refraction can form also over a canyon.

Wave refraction over a canyon has been reported for example from the canyon found off the Hudson River in the north-eastern USA (Kinsman, 1965). As shown in figure 7.2.7, the storm wave rays approaching the shelf from SSE diverge over the canyon where are greater water depths. During storms, wave energy is therefore concentrated on the mouth of the Hudson River and the adjacent part of Long Island while the lowest energy would be at Long Branch on the New Jersey coast.

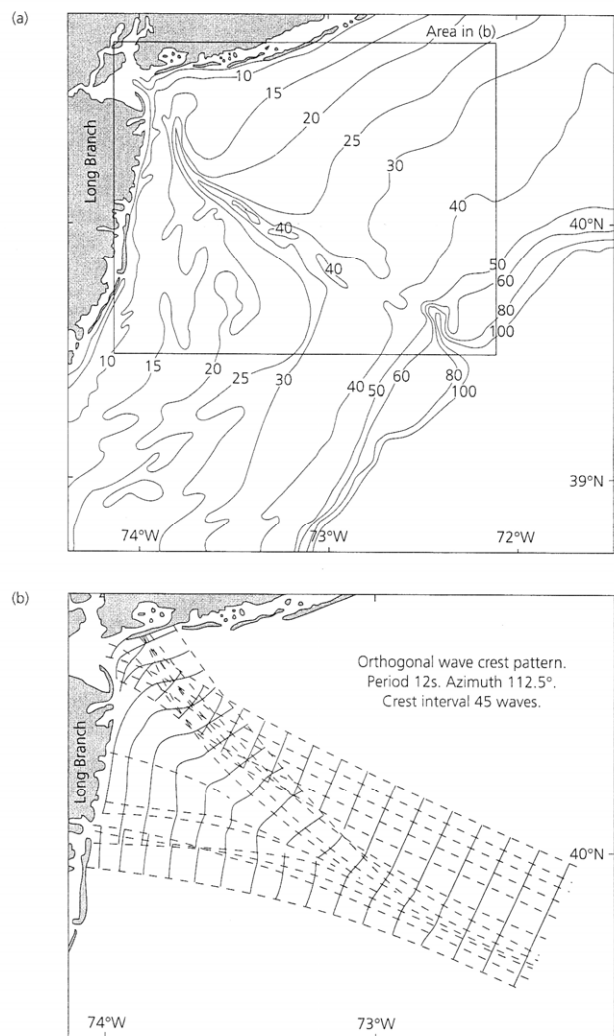
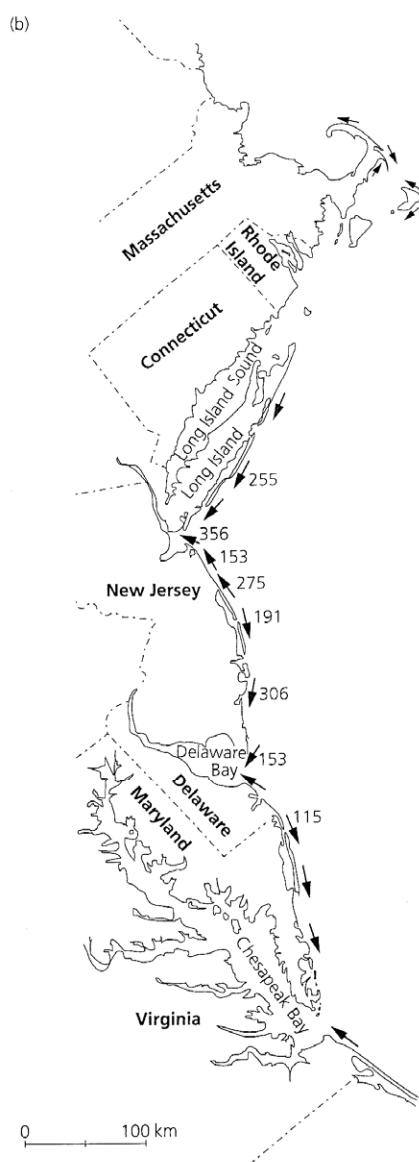


Fig.7.2.7 (left) Drift directions in the littoral zone of the north-eastern USA, with magnitudes in thousands of cubic meters per year. (After Johnson, 1956, in Allen, 1997). (right) Effects of the Hudson canyon on wave refraction. (a) Bathymetry off New York harbour at the mouth of the Hudson River. (b) Waverays (orthogonals to wave

crestlines), showing the low wave energies at Long Branch Beach. (After Kinsman, 1965 in Allen 1997).

Another example was presented by Shepard and Inman (1950b) who described rip currents and longshore currents at La Jolla, California, produced by a longshore variation in wave breaker heights caused by wave refraction over offshore submarine canyons (Fig.7.2.8).

It has been shown that rip currents are capable to carry away boulders weighing 40-50 kg, or even a 200 kg anchor (Popov, 1956), indicating that those currents may attain momentarily very high velocities.

Repeated alternation in the dominance of bedload and suspended load transport, can be caused by pulses within the current caused by changing wave energy (Gruszczynski *et al.*, 1993). The bottom flow of the current has been considered as a low velocity and low density suspension current when rip currents reach the heads of offshore canyons (Moore, 1969; Reimnitz, 1971; Pykhov, 1976). The variation in current strength is mainly correlated to variations in wave climate and it results in continuous changes in conditions of transportation and differences in the mode of deposition (Gruszczynski *et al.*, 1993).

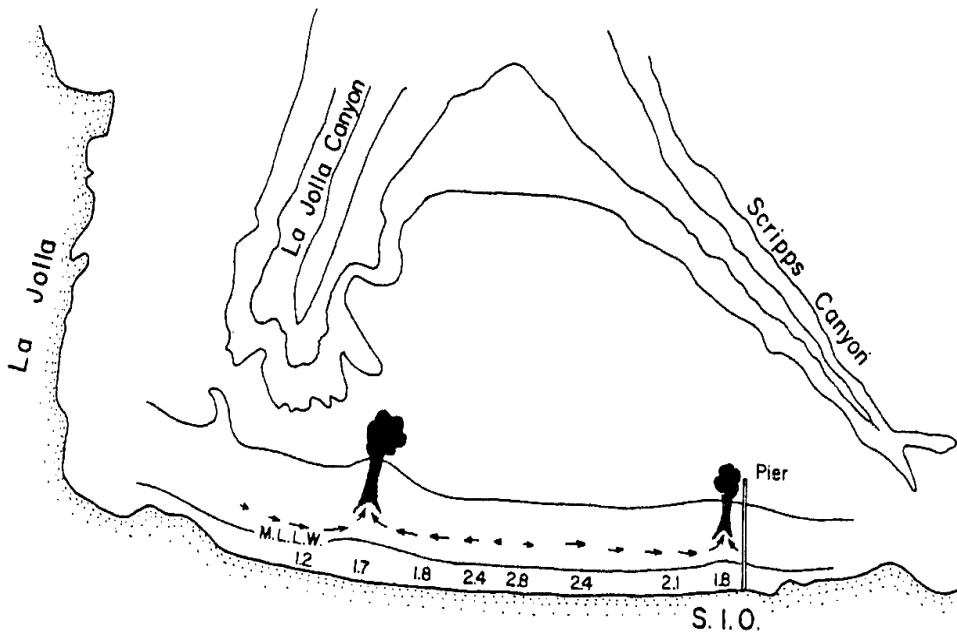


Fig. 7.2.8 Rip currents and longshore currents at LA Jolla, California, produced by a longshore variation in wave breaker heights caused by wave refraction over off-shore submarine canyons. The numbers along the shore are measured values of breaker heights in meters. (Adapted from *Nearshore Circulation*, F.P. Shepard and D.L. Inman, *Proceeding of the 1<sup>st</sup> Coastal Engineering Conference*, 1950. Reproduced with permission from the *American Society of Civil Engineers* in Komar, 1998).

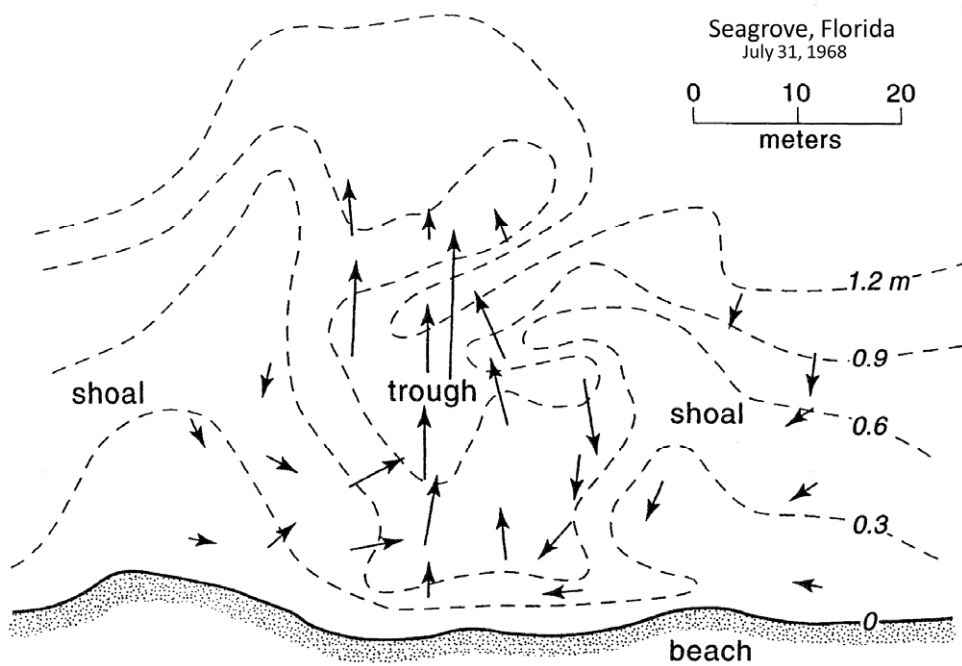


Fig.7.2.9 Observation at Seagrove, Florida, of longshore currents that flow from bar positions to the trough where the water turns seaward as a rip current. Measurements showed that the circulation was maintained by differences in set-up over the bars versus over the trough, in spite of the uniformity of breaking wave heights along the beach. (Komar, 1998 adapted with permission of American Geophysical Union, from C.J. Sonu, Field Observation of Nearshore Circulation and Meandering Currents, *Journal of Geophysical Research* 77, p.3234. Copyright © 1972 American Geophysical Union in Komar, 1998).

Rip current, thanks to their high velocity and ability to transport sediment, are therefore considered as the major agents carrying coarse sediment from the zones of wave deformation seaward. Examples of transport of coarse sediment into deeper water and at a considerable distance (tens of kilometres) from the shore zone have been presented by Mazzullo (1971), Vvdenskaya (1977), Ball *et al.* (1967), Hayes (1967), Perkins & Enos (1968) and Popov (1956).

In the study case of Menorca, rip currents may represent the connecting link between sediment movement in the wave transformation zone with sediment transport by gravity flows along submarine slopes (or in "canyons").

During sea storm climate, storm rip currents may have developed on the inner-middle ramp and they transported sediment seaward. The fact that coarse-grain deposits are found only along the axis of slide scars let us suppose that either the rip currents formed somehow aligned in correspondence to the depressions produced by slope collapses, or there was not a direct correspondence, but some of these seaward sediment-rich flows were caught at the head of the depression and then transported downslope by gravity, while some others were not able to reach the slope-break and deposited their sediment on the distal part of the middle ramp and where it was successively reworked by the action of longshore current (Fig.7.2.10). Cross-bedded deposits found along the middle ramp are described by Pomar *et al.* (2002).

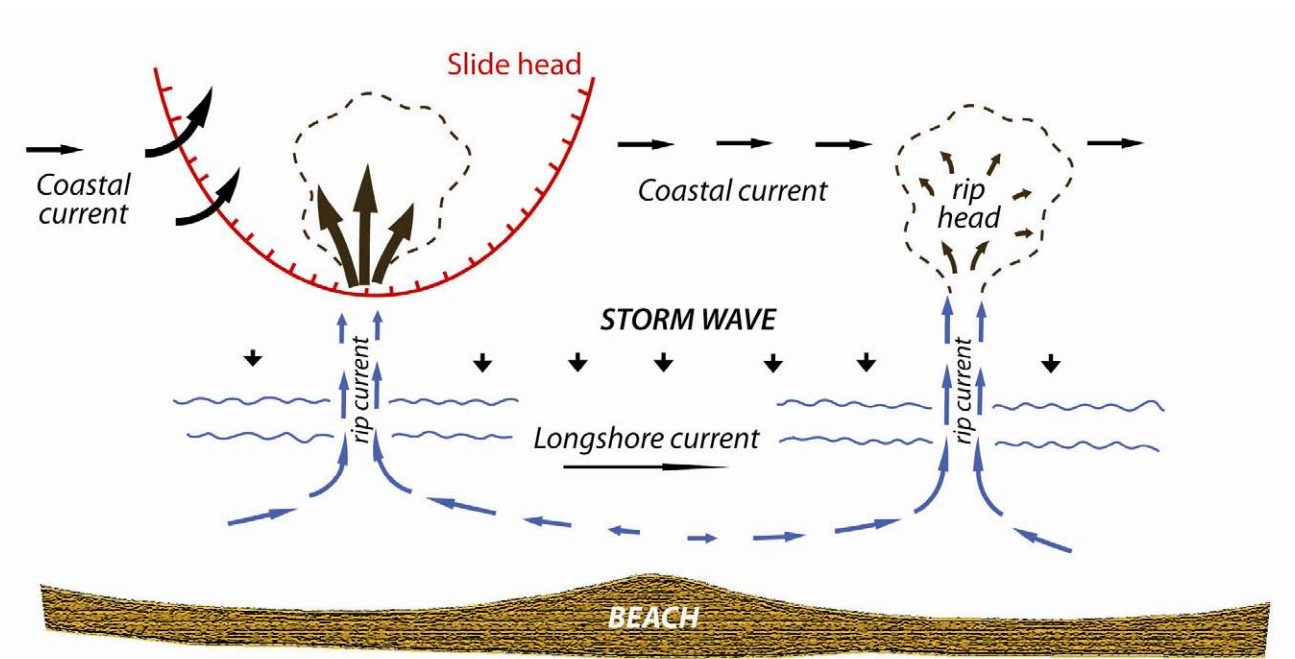


Fig.7.2.10 Sketch showing a possible explanation for sediment capture at the slide head (the "canyon" head): in the left part of the drawings it is shown that the sediment collected at the edge of the slide-scar may proceed both from sediment swept by coastal currents as well as by rip currents; the collapses at the slope moves the slope-break closer to the shoreline. To the right it is shown the case in which the slide-scar is absent and therefore the sediment is reworked and dispersed by coastal currents and it is prevented from reaching the slope-break.

### *Downslope transport – sediment gravity flow*

The aim of this section is not to discuss the nature of the wide range of sediment gravity flows that dominate along the slope of a distally steepened ramp, but to give a tentative interpretation of the characteristics of the original flow that deposited the studied forms from observations of the sedimentary record. In fact, the features characterizing a sedimentary deposit largely reflect the process by which it was deposited and may not be related to the sediment transport history.

To avoid possible misunderstandings that may arise from the large number of nomenclatures and classifications of sediment gravity flows adopted by different authors (Fig.7.2.11), here the classification proposed by Mulder and Alexander (2001) has been used.

The authors recently proposed a simple review of the classification of subaqueous sedimentary density flows based on physical flow properties and grain support mechanisms such as cohesivity of particles, flow duration, sediment concentration and particle-support mechanism. A summary of the proposed classification is summarized in Fig.7.2.12. This classification has been chosen because the subdivision of frictional flows is based on the observation that flows with different sediment concentrations behave differently (e.g. Hallworth & Huppert, 1998) and also the corresponding deposit present different features.

The boundaries between different classes of flows is very difficult to defined for both the flows and the deposits. Soft-sediment deformation structures and post-depositional features

may alter original deposits depositional characteristics making classification of flow type impossible.

The studied deposits have been interpreted to be the result of concentrated density flows (*sensu* Mulder & Alexander, 2001). This interpretation is based on several observations such as: the scoured erosive-base, the lack of mud and abundance of very coarse-grained clasts, the thickness of deposits and sedimentary structures.

Hydroplaning at the base of debris flow or in some hyperconcentrated flows, may reduce the fluid drag, thus allowing high flow velocities while preventing large-scale erosion. On the contrary, concentrated density flows may be highly erosive and subsequently deposit sediment in-filling the scour. Because of the laminar character and high density of liquefied flows, their deposits will tend to show flat, unscoured bases (Lowe, 1982). Grain-flow deposits are usually less than 5cm thick because of the inability of grains at the base of the flow to produce dispersive pressure sufficient to support against gravity a thick overlying column of dispersed sediment (Lowe, 1982).

Fine-grained sediment lacks from the studied backset bedded deposits. This absence can be related to the high energy due to wave action across the middle-ramp, in shallower water, which put into suspension the finer-grained sediment transporting it off-shore through hypopycnal flows. Otherwise, the finer-grained sediment can be transported into suspension by turbulence in the upper part of the density flow and after deposition of the coarser-grained lower part, it may develop turbidity flows that deposit farther down slope in a more distal position as thin turbiditic deposits.

The sediment involved into backset bedded deposit belong to two main particle grain-size populations that correspond essentially to population 2 and 3 of Lowe (1982). Population 2 is of coarse-grained sand to small-pebble-sized gravel which can be fully suspended in large amounts mainly in highly concentrated suspensions where grain fall velocity is substantially reduced by turbulence, hindered settling resulting from their own high concentration and buoyant lift given by the interstitial mixture of water and finer-grained sediment. Population 3 is of pebble- and cobble-sized clasts in concentrations higher than 10 to 15%, again sediment would be largely supported by the result of fluid turbulence, hindered settling, matrix buoyant lift and largely by dispersive pressure resulting from clasts collisions.



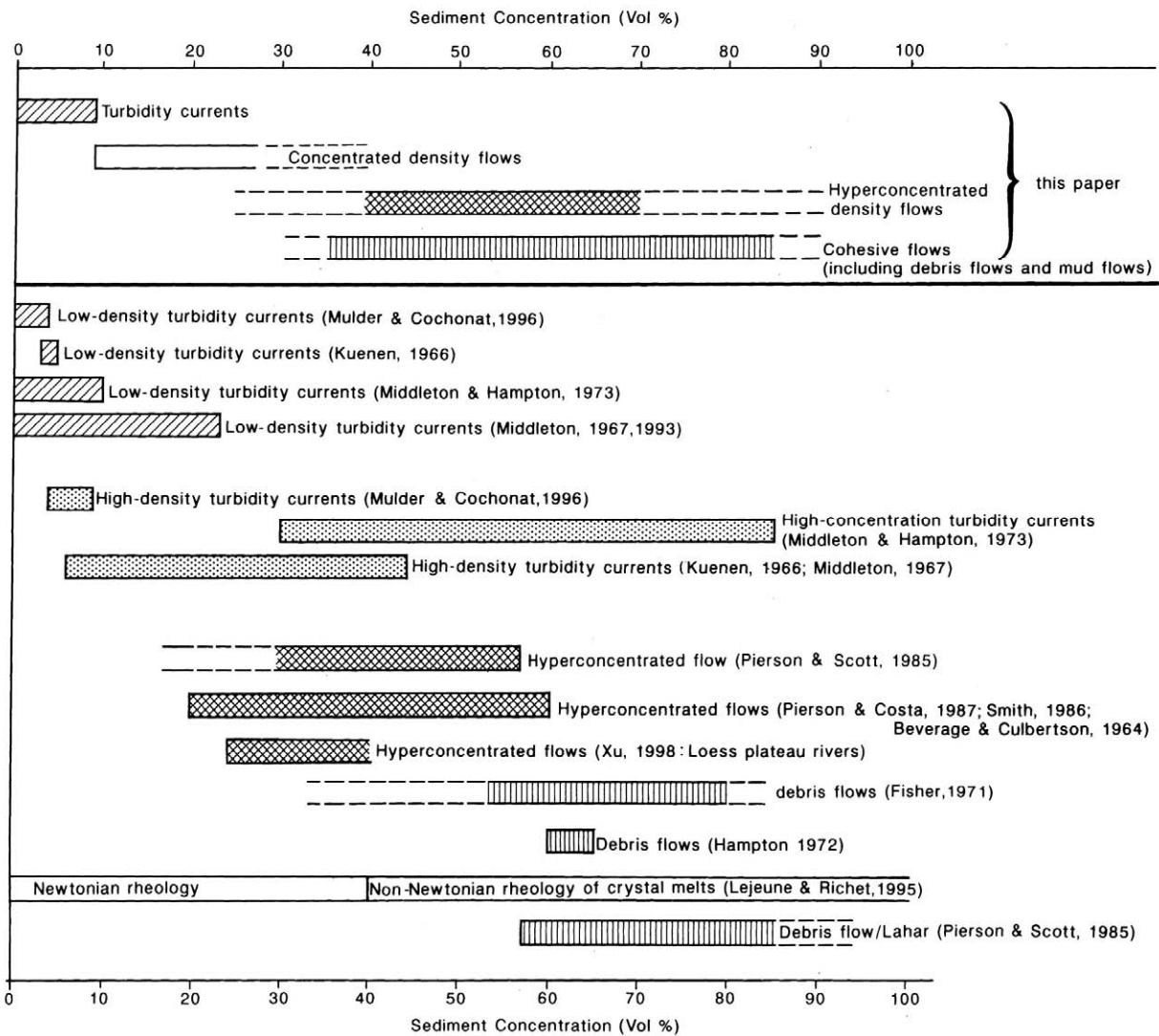


Fig. 7.2.11 Terminology and usage of flow type nomenclature according to sediment concentration as a percentage by volume. Many of the published limits are quoted as weight per cent but, as both water and sediment density varies, volume per cent is perhaps more useful. Consequently, the published weight percentages have been converted assuming a water density of 1000 kg m<sup>3</sup> and a sediment density equivalent to quartz. In many cases, a single sediment concentration cannot be defined as the boundary conditions, because the threshold volume per cent depends on other factors such as clay content. The ranges of possible conditions for boundaries are represented by dashed lines. From Mulder and Alexander, 2001).

According to Lowe (1982), grain population 2 and 3 are likely to be transported in large amount only within flows having high particle concentrations, probably in excess of 20% solids by volume and will tend to be deposited rapidly once sedimentation begins and particle concentration decreases. During the '60s experiments on density and turbidity currents by Middleton (1966, 1967), Bagnold (1954), Wallis (1969) suggested that particle support due to dispersive pressure and hindered settling may become efficient in particle support at high grain concentrations, above 20 to 30%. Below such values flows become unstable and tend to rapidly collapse and damp sediment unless exceptionally turbulent.

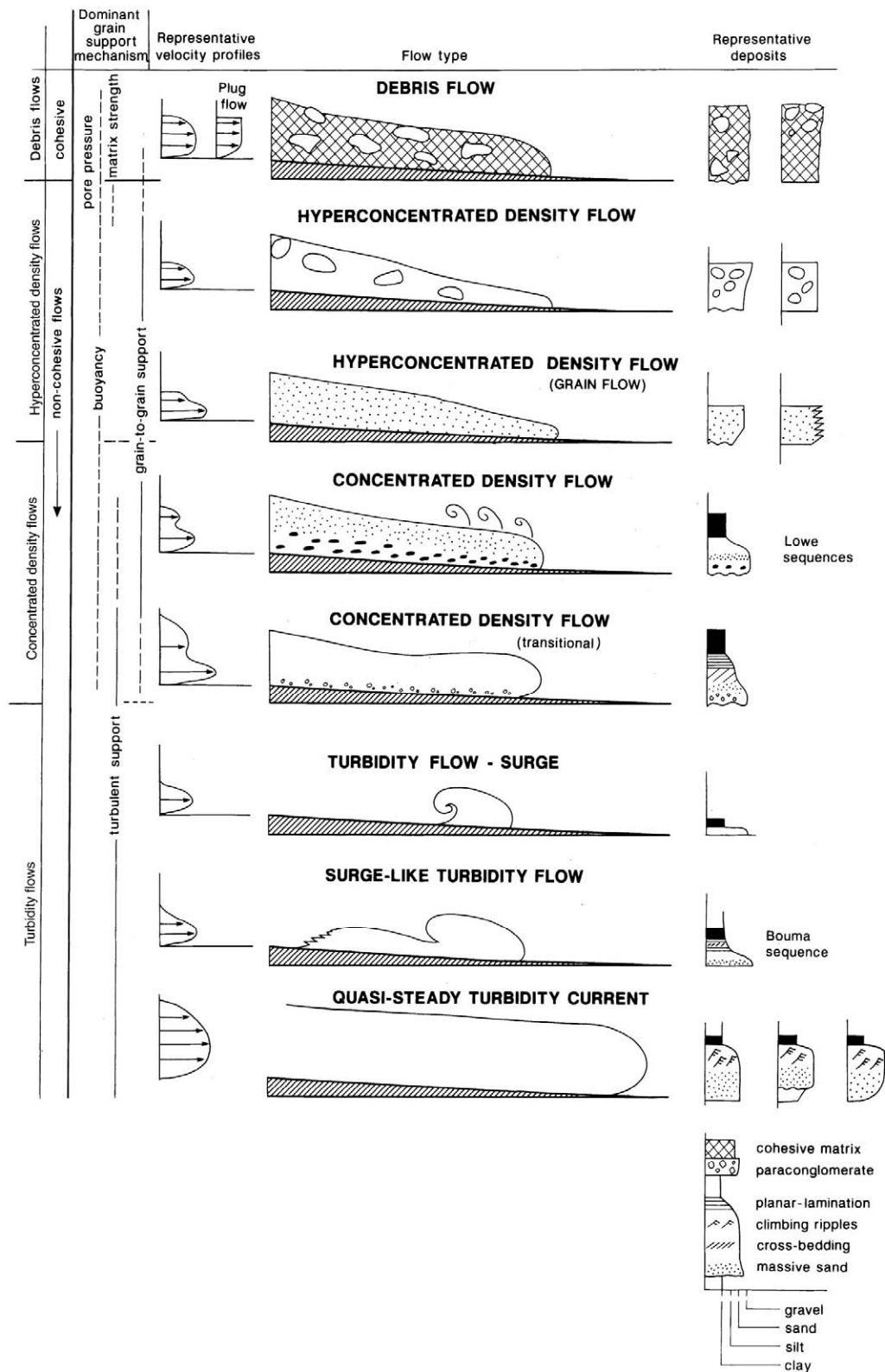


Fig. 7.2.12 The classification of subaqueous sedimentary density flows and related deposits, proposed by Mulder and Alexander, 2001.

The coarse-grained deposits analyzed in this work, are characterized by backset lamination and few of the Lowe or Bouma sequence have been recognized (not within the backset laminated sediment but in other facies) as in few coarse-grained sand-size facies with PPS found at the top of the backset bedded intervals. Within the lamination an alternation of

coarser-grained intervals with finer-grained ones has been frequently noted, with coarser components often aligned along lamination, into rows of larger bioclasts (mainly bivalves), rhodoliths or imbricate limestone pebbles. The deposits therefore appear to be normally to inversely graded, with thickness of layer often related to clasts size. The distribution of grains evidence the oscillating and unsteady nature of the flow responsible to their deposition. The flow is therefore here interpreted to be unsteady but not as a real surge. The flow has to maintain its main characteristics, velocity and concentration, within a small range of values to allow the occurrence and migration of the hydraulic jump up-slope and consequent up-flow deposition of the sediment into backset laminae for a certain interval of time.

The classical concept of turbidity currents, from Kuenen and Migliorini (1950) to Lowe (1982), pertains basically to a surge-type turbidity currents (flows of short duration and inherently unsteady, waning at locality along their route after the passage of the flow's head). However, Nemec (lecture communication) underlined that some turbidites provide a compelling evidence of sustained (long-duration) currents, often remarkably steady for considerable time intervals and hence referred to also as "quasi-steady flows" (Mulder and Alexander, 2001).

In this study case, the topographic surface over which those density flows develop is relatively small since the clinoforms extend 150-200 m with a maximum angle of inclination of 15° to 20°. Therefore the flows generated may accelerate down-slope along a short distance and then deposit at the base of the slope. The deposition is related to the sudden occurrence of a hydraulic jump, therefore the deceleration of flow is extremely rapid, almost instantaneous, and deposition may begin directly from suspension. The gradation within the bed suggests that deposition has to be related to a series of sedimentation waves with a high frequency small variations in flow velocity which continuously decelerate and accelerate during very short intervals. Many deposits show an overall normal gradation trend within the single deposit which indicates that each sedimentation wave tends to show increasing unsteadiness and progressive deceleration and/or decrease in sediment concentration, with a first coarser clasts deposition at the base.

These "sustained" currents may be generated and fed by a multi-point or multiple source of simultaneous sediment supply as for example a retrogressive slumping where a multitude of surges may merge into a large-volume and long-duration flow. On narrow shelf (Nemec, lecture communication) this mechanism can be promoted by earthquakes, retrogressive slumping and sea storms. As well can also regional climate through river floods. In the example of Menorca there are clear evidence of the occurrence of major slides along the slope which could have been followed by successive smaller-scale retrogressive slumping. Since the backset bedded intervals do not take place randomly along the slope but seems to be constrain within specific intervals, the flow that generated them were also related to particular conditions such as sea-storms.

Puga-Bernabeu *et al.* (2008), describe the development of a canyon close to the shoreline, cross-cutting a Late Tortonian shallow-water carbonate ramp; the canyon is thought to be excavated during sea-level fall with development of a river valley on the exposed carbonate ramp. During sea-level highstand, the erosion was carried on by the river flow deepening the valley. In this example, the authors explained the occurrence of shallow water bioclastic sediment infilling the canyon as being transported at the head of the canyon by longshore currents and during storms.

The most peculiar feature in the studied depositional system are the collapses along the slope, which seem to be the most important factor in driving the whole process that defines the deposition of backset bedded units. Those slides played different roles: they locally moved closer to shoreline the slope-break and at their head they capture coarse-grained, shallow-water sediment; the depression they created modified the slope morphology increasing slope steepness allowing supercritical concentrated density flows to develop.

Slope collapses may be triggered by different causes such as tectonic instability or be seismic-related; slumps and slides may also be provoked by over-pressuring related to relative-sea level changes or to over-pressuring due to sediment accumulation on the slope-break or, as discussed before, be associated to canyon excavation. The tectonic cause doesn't seem very plausible since the Upper Miocene deposits suffered only slight tilting and flexure related to normal and strike-slip faulting during the late Neogene to middle Pleistocene time. Since there are no clear evidence to establish which was the cause of the slope instability also because the stratigraphical resolution is very low and it is also very difficult to laterally correlate the various outcrops. Nevertheless, observations on the palaeontological composition, let us presume that those slides occurred at the transition between the distally steepened ramp and the reef-rimmed platform that successively prograded above it.

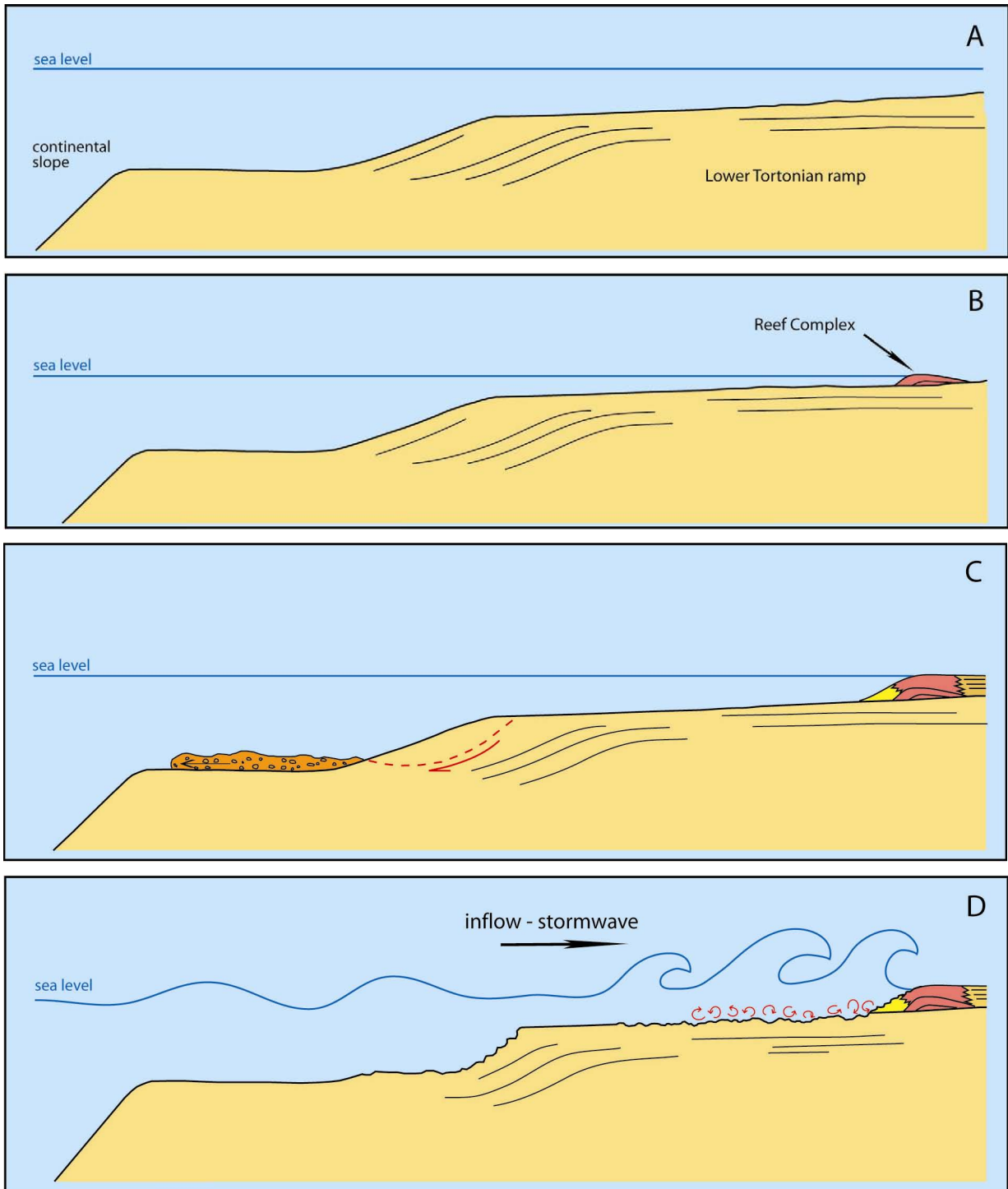
## SUMMARY

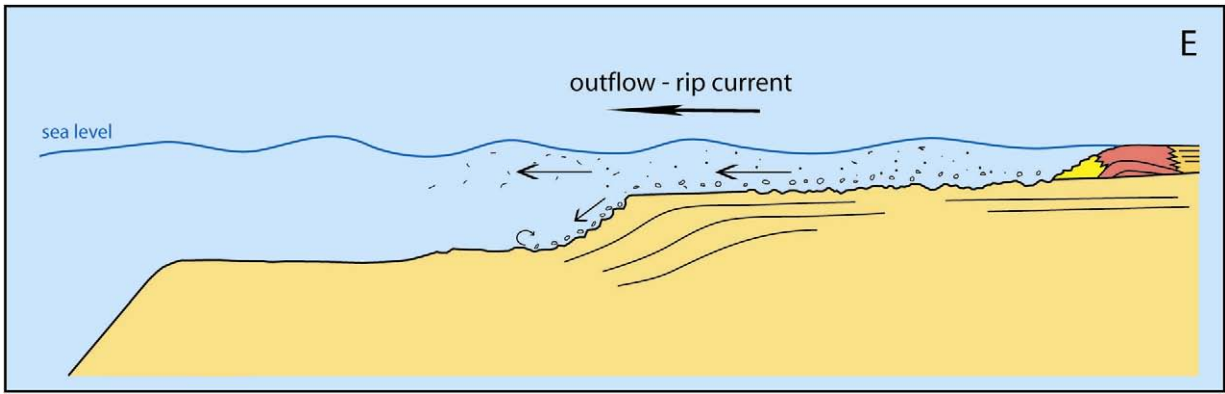
In shallow water platform the sediment has been reworked and entrained into suspension by the wave-actions. The occurrence of these coarse grained gravity flows is related to storm-events that were able to remove coarser sediment and to move it offshore towards the slope-break.

Those coarse grained flows occurred only along the axis of slide scars where they were channelized and accelerated down-slope. Pictures in the following sequence are not in scale, they just want to schematically resume the sequence of processes that drove to the sedimentation of backset bedded deposits.

- (A) The lower Tortonian distally steepened carbonate ramp; those figures are not in scale, but they are exaggerated to put in evidence the succession of processes that drove the deposition of backset bedded deposits.

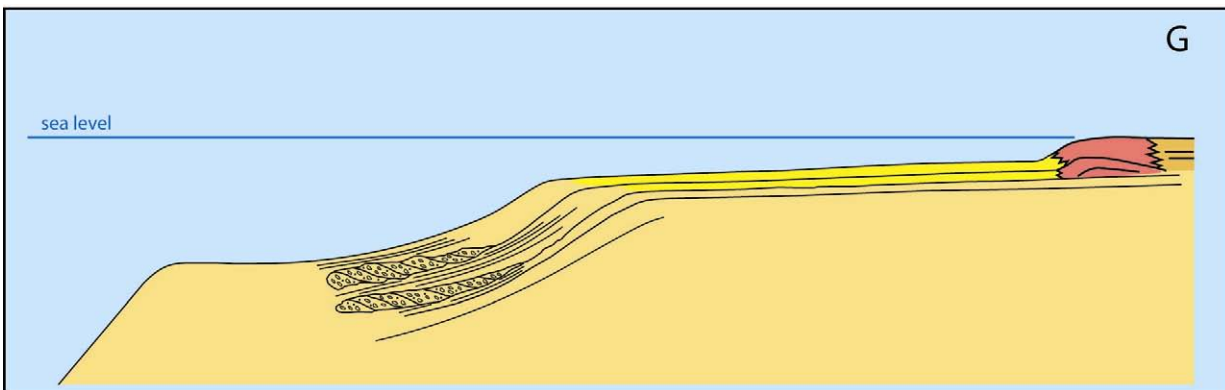
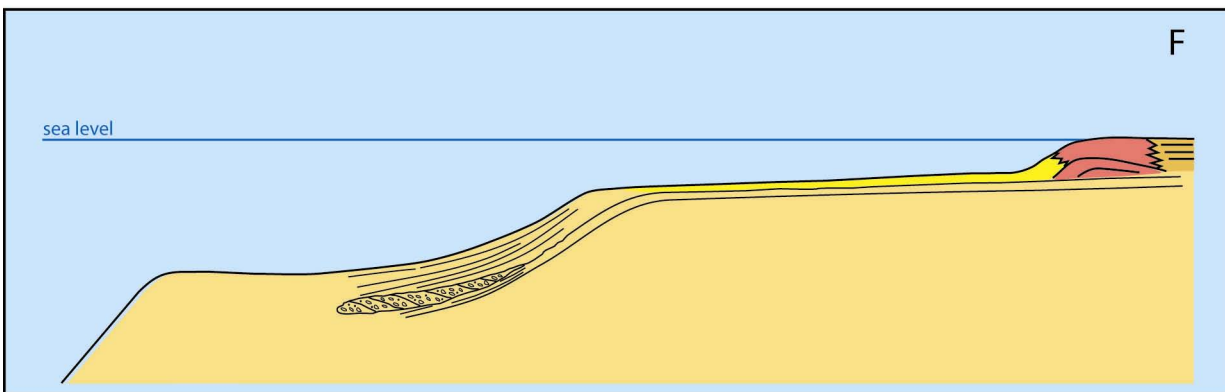
- (B) The lack of biostratigraphical constraints and the discontinuity of outcrops do not allow to know exactly during which interval of time these beds developed; for sure they are directly related to slope collapses. It is possible to suppose that some kind of reef already was developing since some *Porites* have been in some of the beds.
- (C) Collapses along the slope deeply scoured the outer ramp sediment and produced wide depression, altering the morphology of the topography.





(D) During storm events, wave action is able to suspend, rework and to remove sediment from shallow-water middle ramp and upper-slope. The presence of depression act like submarine canyon and cell circulation patterns may establish in the shallow water ramp.

(E) The establishment of cell circulation is accompanied by rip-current, unidirectional seaward high energy currents able to transport coarse sediment to the slope-break.



(F) The sediment is transported downslope by gravity flow through concentrated density flows, and deposited at the base of the slope due to the repetitive occurrence of hydraulic jumps in the lowermost part of the slope.

(G) The backset bedded deposits occur in several intervals, probably due to a repetitive occurrence of the above described conditions.

## 8. Numerical simulations

### 8.1 *Introduction to Computational fluid dynamics (CFD)*

The first bases for experimental fluid dynamics were laid in the 17th century in France and England (Tokaty, 1971). Throughout most of the last century, the study and practice of fluid dynamics laid on the use of pure theory and pure experiments.

The introduction of digital computer in the 1960s, and the development of accurate numerical algorithms solving physical problems with the use of computers, substantially changed this practice. The development of new technologies led to a new numerical approach in the study of fluid dynamics which was named computational fluid dynamics (CFD). This term has been used to refer to a wide topic regarding the numerical solution, by computational methods, of the governing equations that describe fluid flow:

- the Navier-Stokes equations, describing the conservation of momentum;
- the conservation of fluid mass
- any additional conservation equations that may be relevant (Wesseling, 2001).

It is important to remark that CFD can not replace any of the other methodologies in use because theory, observations from nature and laboratory experiments will always be fundamental, and they should therefore be taken as a whole.

The future advancement of fluid dynamics rests upon a proper balance of all three methodological approaches, with computational fluid dynamics helping to interpret and understand the results of theory and experiment, and vice versa. The acronym CFD is now universally accepted and will be used further below.

### 8.2 *Flow-3D™*

In the last years the CFD has been used in many branches of fluid dynamic, becoming an indispensable tool: it is widely used both in academic research as well as in the industrial one, because it is considered to be a standard numerical method in its design and development.

Of course, there are many CFD software programs available; the software used is Flow-3D™ which is a general purpose CFD software program that employs specially developed numerical techniques to solve the equations of motion for fluids to obtain transient, three-dimensional solutions to multi-scale, multi-physics flow problems. Fluid motion is described with non-linear, transient, second-order differential equations. The fluid equations of motion must be employed to solve these equations. A numerical solution of these equations involves approximating the various terms with algebraic expressions. The resulting equations are then solved to yield an

approximate solution to the original problem, and this process is called a *simulation*. In the use of the software, the first step is to define the surface over which the flow will be moving (Fig.8.2.1) and then to identify the flow domain defining a mesh, which is a grid of rectangular cell, also called brick elements (Fig.8.2.2). The physical space is therefore replaced by the mesh. It provides the means for defining the flow parameters at discrete locations, setting boundary conditions and for developing numerical approximations of the fluid motion equations.

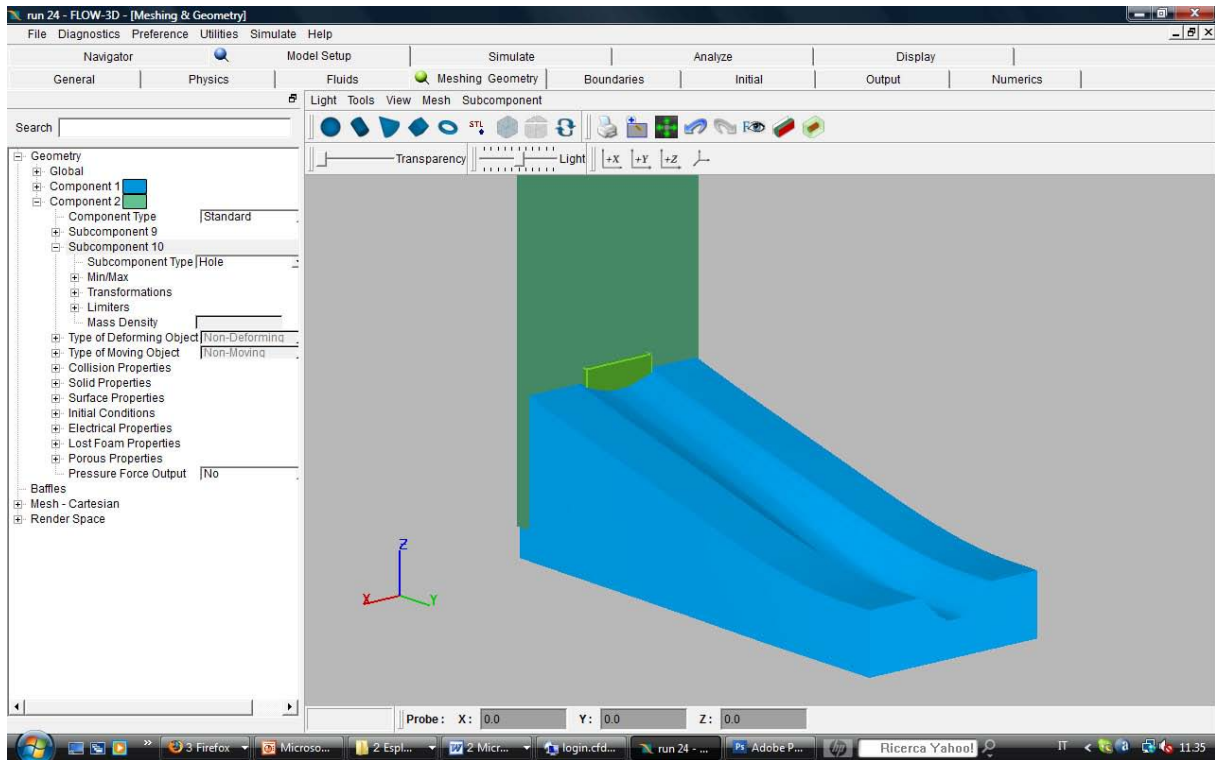


Fig.8.2.1 The software, Flow-3DTM itself only allows to create very simple geometries, therefore a more complex three dimensional surface was created with a graphic software Rhinoceros 4.0. The blue slope with a channel represent the surface over which the flow will run; the dark green wall represent the boundary from which the flow is meant to come and the light green window represent the flow inlet and defines the flow thickness.



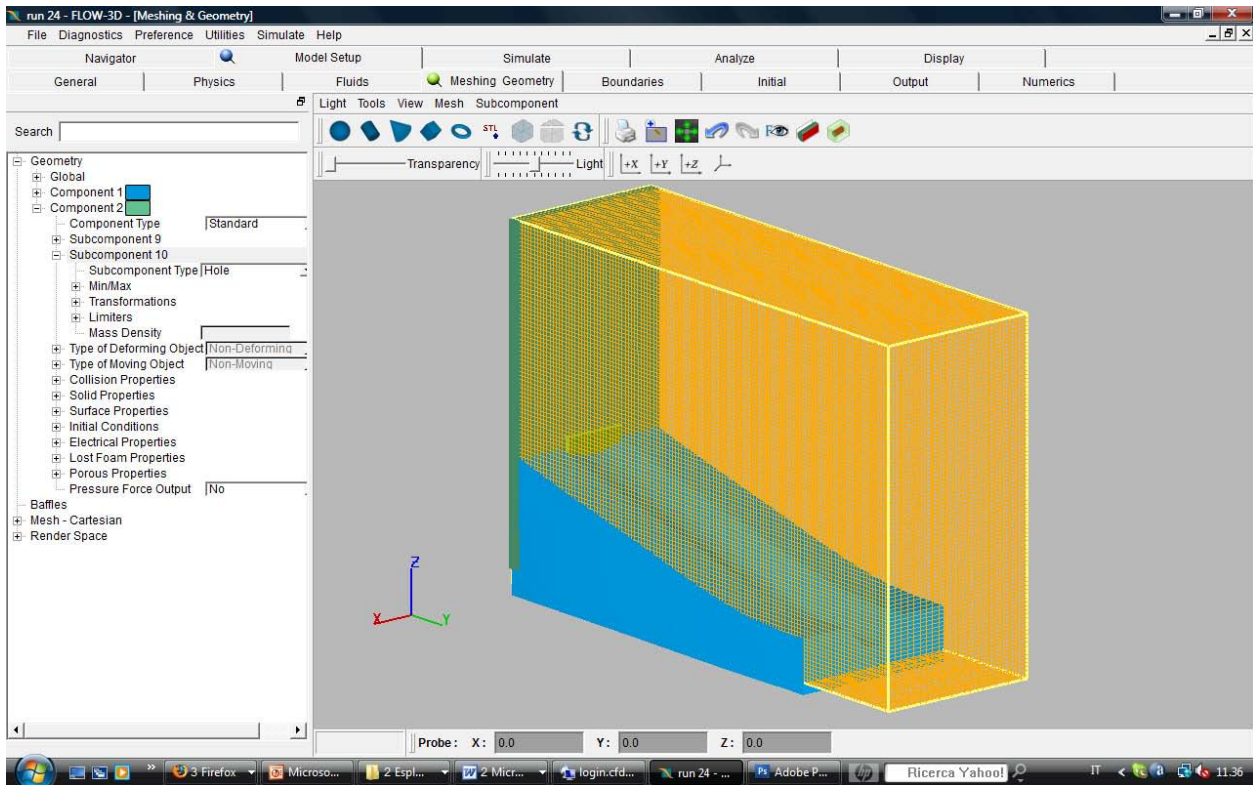


Fig.8.2.2 Creation of a computational mesh. The computational mesh is a grid of rectangular cells, whose size can be chosen by the simulator depending on the desired degree of precision of the simulation. The mesh represents the numerical space that replaces the original physical space.

Finite difference and finite volume methods form the core of the numerical approach used in Flow-3D™ and they are applied to obtain numerical solutions to differential equations on such meshes (Ames, 1992). The finite difference method is based on the properties of the Taylor expansion and on the straightforward application of the definition of derivatives. The finite volume method derives directly from the integral form of the conservation laws for fluid motion and, therefore, naturally maintains the conservation properties. Flow-3D™ has a range of physical models that increases its capabilities beyond those of many other CFD software programs. Flow-3D™ has been adopted, because it has the main physical models needed to simulate submarine density flows, in detail turbidity-current dynamics which have been tested on laboratory experiments therefore more reliable; those models are: the renormalization group (RNG) turbulence model, the drift-flux model, the particle model, and the sediment scour model.

**RNG turbulence model** — Flow-3D™ has implemented a more recent turbulence model based on renormalization-group methods (Yakhot and Orszag, 1986; Yakhot and Smith, 1992). This approach applies statistical methods for a derivation of the averaged equations for turbulence quantities, such as turbulent kinetic energy and its dissipation rate. The RNG based models rely less on empirical constants, while setting a framework for the derivation of a range of models at different scales. The RNG model uses equations similar to the equations for the k-

$\epsilon$  turbulence model (Harlow and Nakayama, 1967), but the equation constants that are found empirically in the standard  $k$ - $\epsilon$  model are derived explicitly in the RNG model. Therefore, the RNG model has wider applicability than the standard  $k$ - $\epsilon$  model. In particular, the RNG model is known to describe more accurately low-intensity turbulence flows and flows having strong shear regions.

**Drift-flux model** — In the fluids consisting of multiple components (e.g., fluid/solid particles, fluid/bubbles, fluid/fluid mixtures), where the components have different densities, it is observed that the components can assume different flow velocities. Velocity differences arise because the density differences result in non-uniform body forces. The differences in velocities can often be very pronounced (e.g., large raindrops falling through air or gravel clasts sinking in water). Under many conditions, however, the relative velocities are small enough to be described as a 'drift' of one fluid component through the other. Examples are dust in air and sediment in water. The 'drift' distinction depends on whether or not the inertia of a dispersed component moving in a continuous component is significant. If the inertia of relative motion can be ignored, and the relative velocity reduced to a balance between a driving force (e.g., gravity force or a pressure gradient) and an opposing drag force between the components, then it is a 'drift-flux' approximation. Drift velocities are primarily responsible for the transport of mass and energy. Some momentum may be transported as well, but this is usually quite small and has been neglected in the Flow-3D™ drift model. The idea behind the drift model is that the relative motion between the fluid components can be approximated as a continuum, rather than by discrete elements (e.g., sediment particles). This enhances computational efficiency, as there is no need for a computational tracking of the motion and interaction of discrete elements.

**Particle model** — The particle model implicitly couples the momentum of discrete-mass particles with a continuous fluid. Particles may have individual masses, which are computed to move under the action of forces that include body forces (gravity), viscous and form drag, and buoyancy forces computed from the local pressure gradient. Particles may bounce or stick to rigid surfaces according to a coefficient of restitution and are transmitted or reflected from granular surfaces with a probability proportional to the fraction of open area. In addition, particles can move in both void and liquid regions and particles may have a variable distribution of density or size. The particle motion is influenced by fluid flow through the drag forces. A fully coupled particle/fluid interaction model is included in the Flow-3D™ to account for interactions between the continuous and dispersed materials that arise due to the drag experienced by the dispersed particles as they move through the continuous fluid. The displacement of fluid volume by particle volume is not taken into account in the particle model, because the particle-fluid momentum exchange is considered to be a more important factor, as it can be significant even when the volume of particles is small. The momentum change in the

fluid resulting from the interaction with a particle is expressed as a drag coefficient multiplying the relative velocity between the fluid and the particle. An implicit numerical method is used in the Flow-3D™ to couple the momentum of the particles and fluid together.

**Sediment scour model** — The sediment scour model predicts the behaviour of packed and suspended sediment within the three-dimensional computational capabilities of Flow-3D™. This model is based on the drift-flux model and presumes that most of the sediment transport is by suspension (Van Rijn, 1987) and advection due to the influence of the local pressure gradient. Suspended sediment originates from inflow boundaries or from erosion of packed sediment. Packed sediment can only move if it becomes eroded into suspended sediment at the packed sediment – fluid interface. Suspended sediment can become packed sediment if the fluid conditions are such that the sediment drifts towards the packed bed more quickly than it is eroded away. At the surface of the packed bed of sediment, the fluid shear stress acts to remove sediment; the empirical Shields number (e.g., Guo, 2002) is used to correlate the minimum shear stress required to lift a sediment particle away from the packed bed interface for various particle diameters and densities. A drag model is used to mimic the solid-like behaviour of sediment particles in regions where the particle concentration exceeds a cohesive solid fraction. The angle of repose controls how steep a slope can be supported by the packed sediment in a quiescent flow region. Where the angle is zero (i.e., a horizontal surface with respect to gravity), the effective critical shear stress is equal to the critical shear stress. In the present study, these four models have been used in various combinations to simulate turbidity currents on both small (laboratory) and large (natural) scale.

### ***8.3 Research method***

The performed simulations do not intend to simulate the gravity processes transporting sediment downslope along the slope of the carbonate ramp of Menorca: finer grain sizes have been used (only sand-size grains and not coarser-grain sizes) and also the scale of the topography over which the flows move is smaller compared to the natural case. The impossibility to reproduce the nature-example is related to limitations of the software. Anyway, the availability of the described software, Flow-3D™, gave the opportunity to implement the knowledge on the hydrodynamic characteristics of flows and conditions that allow the development of backset bedded deposits in submarine environments. The simulations here reported regard concentrated turbidity currents carrying sand-grain-size sediment. The aim of the performed simulations was to give a quantitative analysis of the conditions for which a hydraulic jump form in a gravity flow and the related deposition. This study is in any case relevant, since this hydraulic process is still poorly understood.

The software used still unfortunately presents several limits especially related to the grain-sizes of sediment that can be simulated by the software, and/or it is not tested on laboratory experiments (for example for coarser-grain size like pebbles) so to ascertain the reliability of the results. Therefore it was not possible to reproduce the deposits studied in Menorca with a CFD simulation, both for a problem of outcrop-scale and for the coarse grain-sizes involved. In laboratory experiments, it is still impossible to reproduce gravity flows in submarine conditions at a natural scale, mainly because of the enormous laboratory that would be necessary and the cost of it.

Anyway the knowledge about the formation of these bedforms is still poorly understood and a quantitative analysis of the controlling factors is still missing. Therefore this work represents a preliminary work that lies some more information and data about these processes that can be important for farther studies.

Therefore for the simulations run, values of parameters compatible to the software have been used and for controlled conditions based on laboratory experiments, therefore high density turbidity currents have been simulated.

The first step in the procedure for the development of the simulations was first to create the environment where to simulate. In this case a three dimensional topography (Fig.8.2.1) has been created reproducing a base-of-slope with maximum inclination of about  $15^\circ$  and that passes into an horizontal plane as it occurs at the transition between lower slope and outer ramp. Introducing the obstacle, the morphology of the surface is changed and it becomes a slope with a break represented by the obstacle.

The mesh (Fig.8.2.2), represents the numerical space that replaces the original physical space, and its all six boundaries are defined: the boundary where the flow-inlet is placed is defined as the inflow boundary; the boundary on the opposite side is the outflow boundary and it is considered as well as the two boundaries at both lateral sides as a continuity boundary, therefore the space is considered as continuous and not as a wall. A wall is represented by the boundary at the base of the mesh which is never in contact with the flow; at the boundary at the top the hydrostatic pressure of a water column of about 70 m water-depth was set.

Towards the base of the slope an obstacle as been placed. The obstacle is meant to represent either a topographic irregularity or a frozen debris. The case in which the hydraulic jump develop due to flattening of the topography has not been investigated since it would have required an enormous number of simulations (= months in time) to find the right solution. The placing of an obstacle is therefore an artifice to induce the hydraulic jump.

The scale at which the environment has been built is at a meter-scale but it was not possible to study the flow from the slope-break down to the slope to avoid an excessive number of cells in the mesh which would produce and extremely large output file, which the quadcore processor available to run the simulations would either not be able to process or the time required to complete the simulation would be extremely long. To give a time-scale, at the scale used for these simulations and with the relative mesh, to run a flow running for 2 minutes, the

processor would take about 6 hours of calculations, with a related output file of about 5GB or more. These number are remarked here to underline the fact that, the larger the physical space, the higher the number of cells would be, enormously increasing the time and the size of the output file, therefore very powerful, multi-processors machine would be needed.

The second step was to establish the values for the parameters characterizing the flow. Since the aim is to see the occurrence of a hydraulic jump a supercritical flow was to be establish,

therefore  $Fr > 1$ , and knowing that  $Fr = \frac{\bar{U}}{\sqrt{RCgh}} > 1$  the important values to be defined are  $h$ ,

which is flow thickness, for which it has been chosen values comparable to the scale of the topography, the channel-depth and the obstacle;  $g$ , which is gravity acceleration is constant (9,81 m/s<sup>2</sup>);  $u$  is the mean flow velocity which is given by the simulator and  $R = \frac{\rho_s}{\rho} - 1$ ,

related to the density of the sediment. The values of this parameters have been chosen so that the flow before the obstacle was in a supercritical regime  $Fr > 1$ .

The values of  $C$ , represent the layer-averaged volume concentration of suspended sediment, for which a range of value from 5% to 35% have been simulated.

One of the great limit of the utilized software is represented by the grain-sizes that can be set as sediment put into suspension. In fact the model used is the *RNG turbulence model*, therefore the mechanisms contemplated by the software to keep sediment moving within the flow is the turbulence mechanisms. Therefore it is possible to use only a grain-size range that can be kept into suspension only thanks to turbulence, that means up to sand-size. Dispersive pressure resulting from clasts collisions would be the main supporting mechanism for coarser grain-sizes, but this model is not available in the software, thus the sediment would be rapidly deposited at the flow inlet occluding it. To keep coarser sediment, such as pebbles, only thanks to turbulence supporting mechanism, extremely high values of velocity are required which would not be realistic.

The flows simulated are thus supercritical turbiditic currents with variable concentration of sand-grain-size sediment. The initial values attributed to the various parameter are therefore realistic and it is know that they are reliable because for those grain-sizes the software has been tested with laboratory experiments.

The simulation therefore are not meant to re-create the deposits of Menorca, but to reproduce and observed the overall conditions within which an hydraulic jump may develop depositing sediment at the obstacle in an up-current direction.

The output file and the results can be observed on a 2D movies or the data can be plot into 2D diagrams.

## **8.4 Results of the present study**

The numerical simulations refer to turbidity currents. The variables parameters are:

- sediment concentration which has been varying from 5% to 35%;
- the densities used to define  $R$ , are 1027 kg/m<sup>3</sup> for sea water at 10°, and 1800 kg/m<sup>3</sup> for the limestone sand;
- Average Speed to be reach close to the obstacle: variable from 0,5 m/sec to 4 m/sec;
- Grain-size of sediment put into suspension: 0.5 – 1.0 mm;
- Height of obstacle: approximately 1.5 m;
- Thickness of flow has been defined at the inlet and it is comparable to the depth of the channel (channel maximum depth 2 m) and of the obstacle. This choice was made to avoid spill-over deposition, which would alter the controlled flow conditions.
- The values of parameters have been combined so to have  $Fr > 1$ .

The distribution of flow velocities in time has been simulated as a continuous-steady current, as surges and also as flow with varying velocity in time.

To find the right condition a large number of simulations have been run: almost a hundred of simulation with different combination of parameters for more than an overall 350 hours of simulation.

The deposition of sediment on the surface and at the obstacle occurred in the majority of the simulations run. The occurrence of a hydraulic jump at the obstacle, has been verified controlling the variations of parameters in three points: before the jump, above the jump and after the jump. Through the hydraulic jump, the flow velocity is halved and its thickness increase to more than double and there is a general transformation in the nature of the energy of the flow that passes from being kinetic energy to potential energy. Therefore, not only deposition at the obstacle has to occur but other parameters have to be controlled: velocity, thickness of flow, turbulence. The velocity should decrease, the turbulence increase and the flow becomes thicker.

The first set of simulation have been use to constrain the values to give to the parameters. In the following diagrams some results are compared to show that even if some conditions are respect, the hydraulic jump may not have been verified, therefore even if sedimentation occur this is not related to the occurrence of the jump and the related sediment will not displace a backset lamination.

The most significant simulations have been reported below to show the results progressively obtained and the description and interpretation of parameters and trend is presented for each simulation.

The IS scale has been used in diagrams and snapshots from 2D simulation.

## RUN 32

### Initial conditions:

Slope = 15°

Grain-size = 0.5 – 1.00 mm

Dynamic viscosity of sea water at 10° = 1027 kg/m<sup>3</sup>

Sediment density = 1500 kg/m<sup>3</sup> (underestimated from limestone density 1800kg/m<sup>3</sup>)

Initial sediment concentration = 10%

Initial flow velocity (m/sec) = 1.5 m/sec

Initial flow thickness = 4 m

Sediment entrainment coefficient (scour parameter) = 0.05

Fr = 1.12

Flow duration = 120 sec

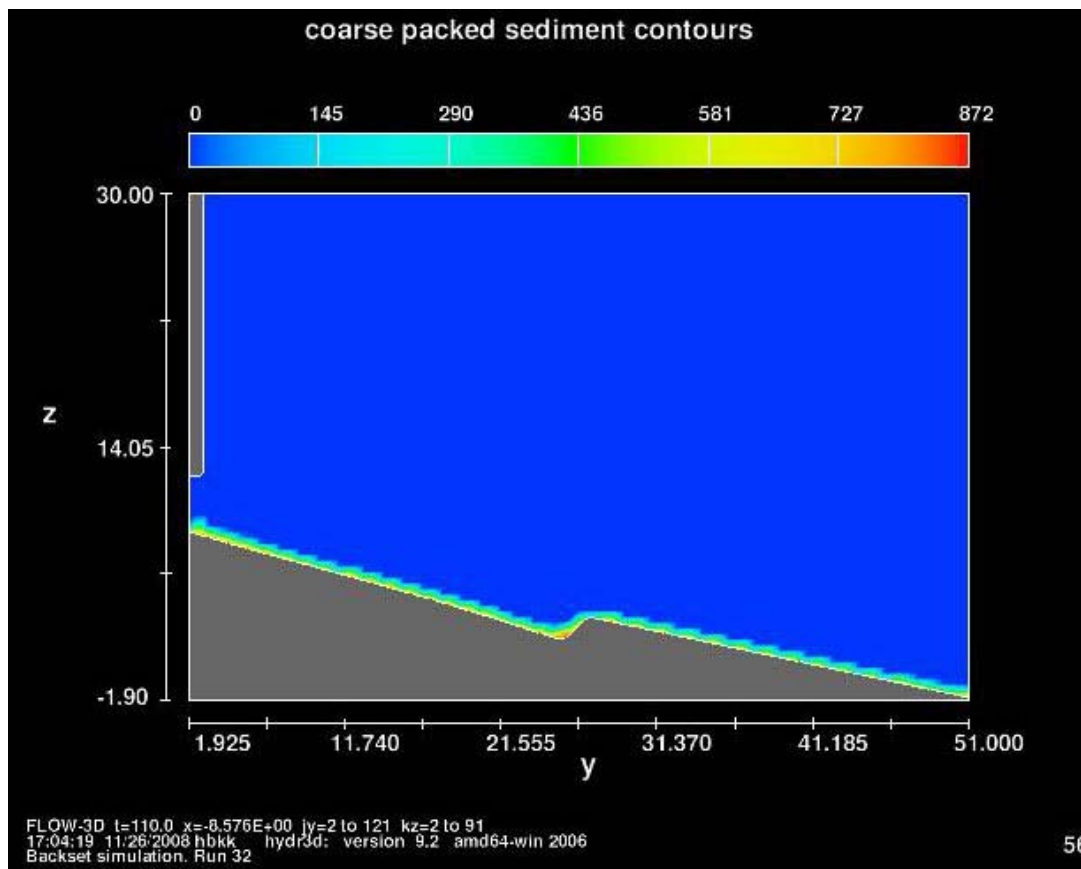


Fig.8.4.1 Run 32: the coarse pack sediment indicate the deposition of sediment. As shown in the snapshot at time=56sec , deposition occur along the whole surface draping the surface both before and after the obstacle. To be notice that the scale of the axis X and Y is in meters, therefore the thickness of the sediment deposited at the obstacle is quite relevant.

The diagrams lines below in Figure Fig.8.4.2 refer to three selected points one precedent to the obstacle, one above the obstacle and one after the obstacle.

run 32 density comparison

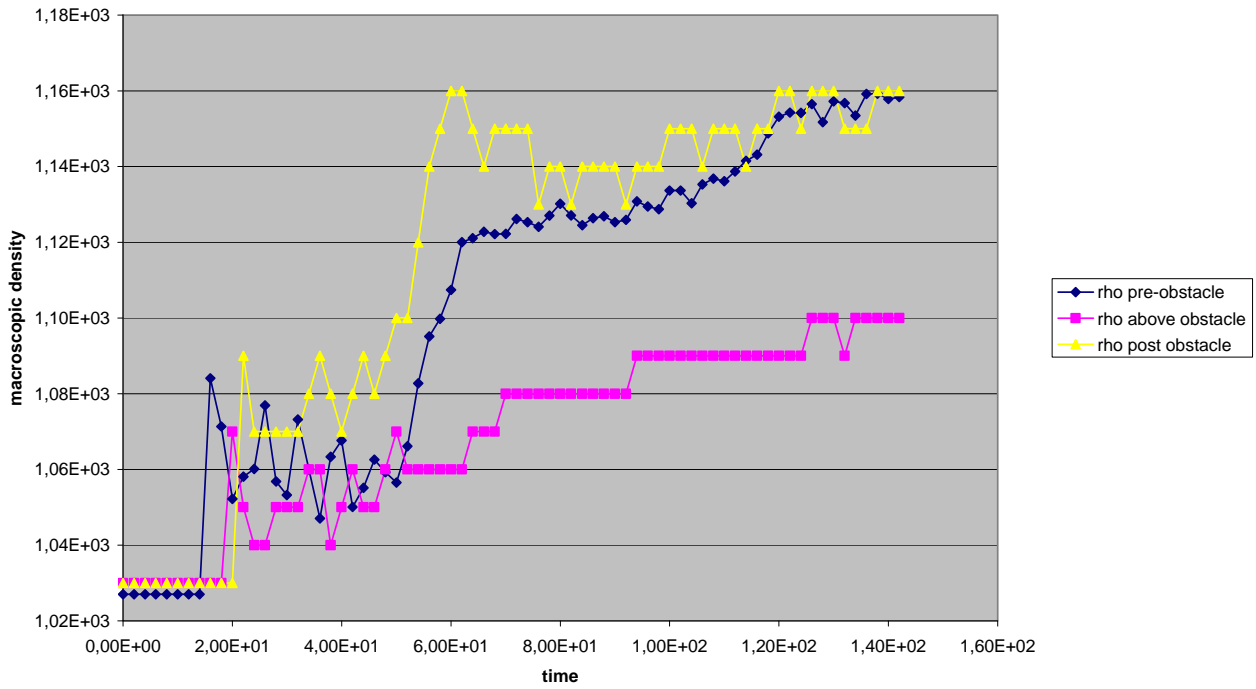


Fig.8.4.2 RUN 32: Macroscopic density values calculated in three point: the blue line correspond a point placed right before the obstacle; the pink line to the point above the obstacle and the yellow line to a point after the obstacle. The comparison between the three lines show that there is a quite linear trend with a progressive increase in macroscopic density. Time is measured in seconds

run 32 velocity magnitude comaprison

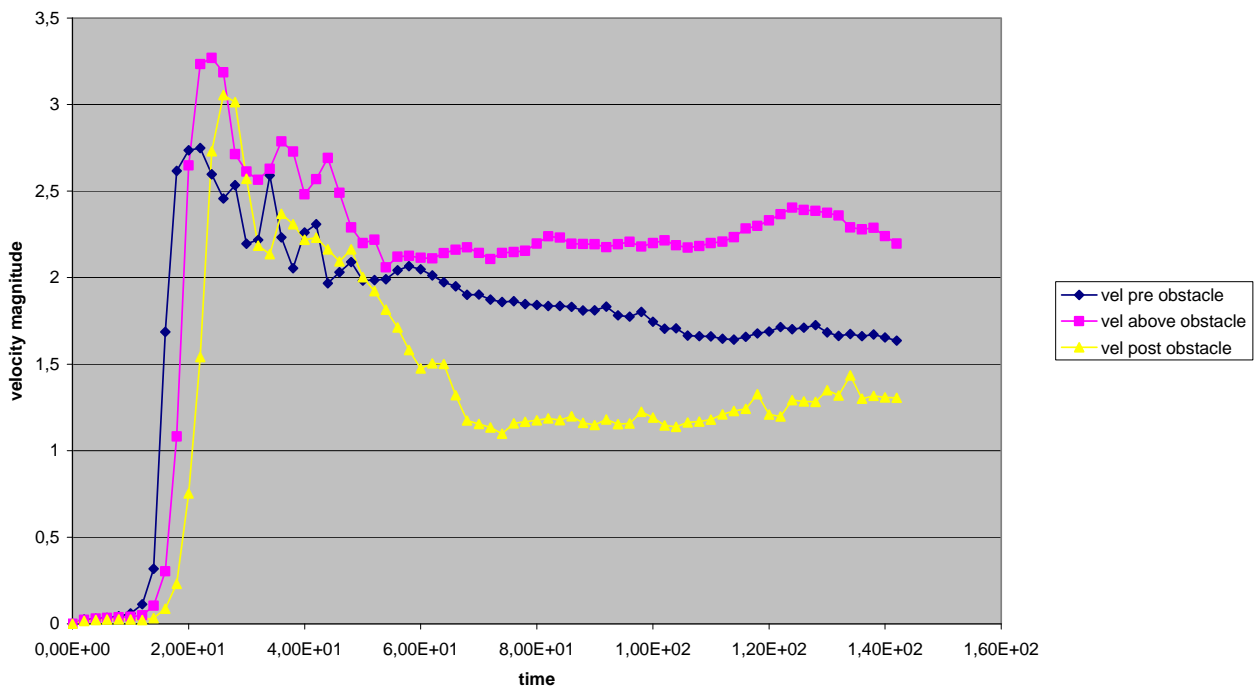


Fig.8.4.3 RUN 32: Velocity values calculated in three point as in the previous diagram, the colours corresponding always to the same points. Here we can notice that there is a relevant drop in velocity at the obstacle and decrease even more after the obstacle.



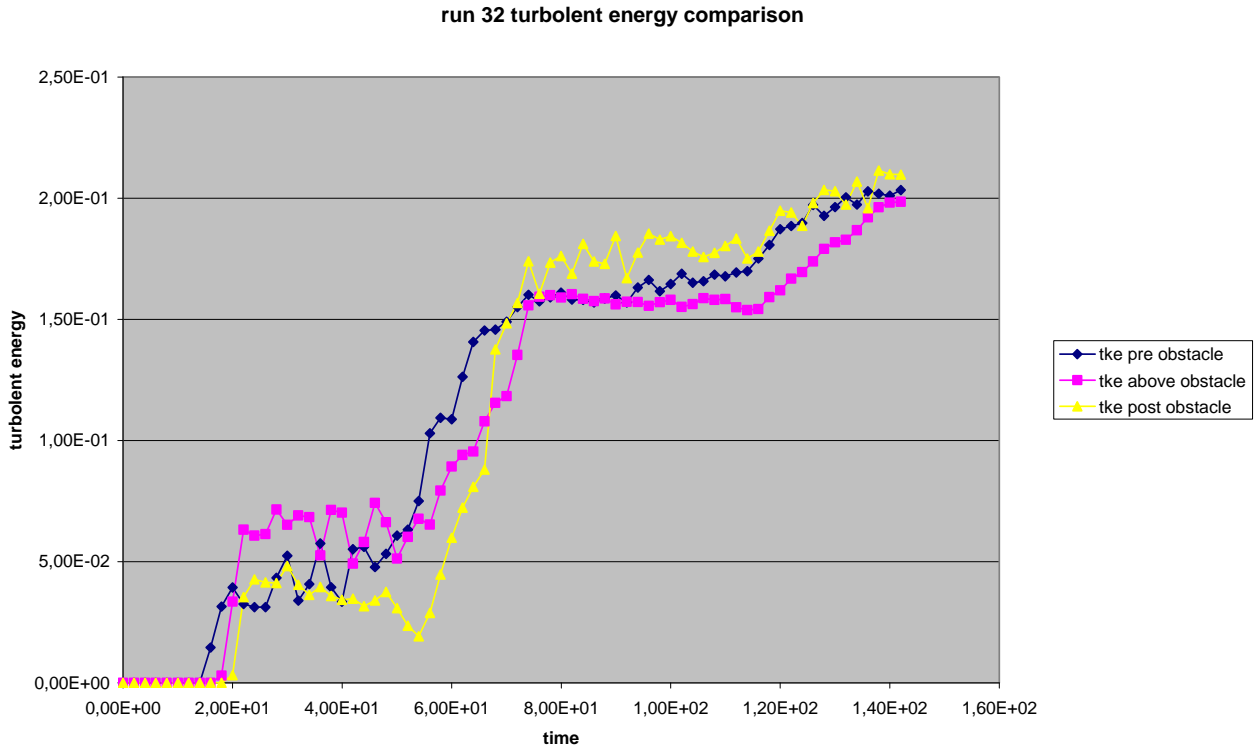


Fig.8.4.4 RUN 32: turbulent energy at the three points. The comparison between the three lines shows an overall increase of the turbulence firstly above the obstacle and then also in the point after the obstacle.

Simulation number 32 therefore shows a trend which compatible with the development of a hydraulic jump at the obstacle because all three conditions are verified: decrease in velocity, increase in turbulence and deposition at the obstacle. It has not been noted neither a substantial variation in flow thickness nor a migration of the jump up slope.

### RUN 43

- Slope = 15°
- Grain-size = 0.5 mm
- Dynamic viscosity of sea water at 10° = 1027 kg/m<sup>3</sup>
- Sediment density = 1800 kg/m<sup>3</sup> (underestimated from limestone density 1800kg/m<sup>3</sup>)
- Initial sediment concentration = 35%
- Initial flow velocity (m/sec) = 2.60 m/sec
- Initial flow thickness = 2 m
- Sediment entrainment coefficient (scour parameter) = 0.80
- Fr = 1.15
- Flow duration = 120 sec

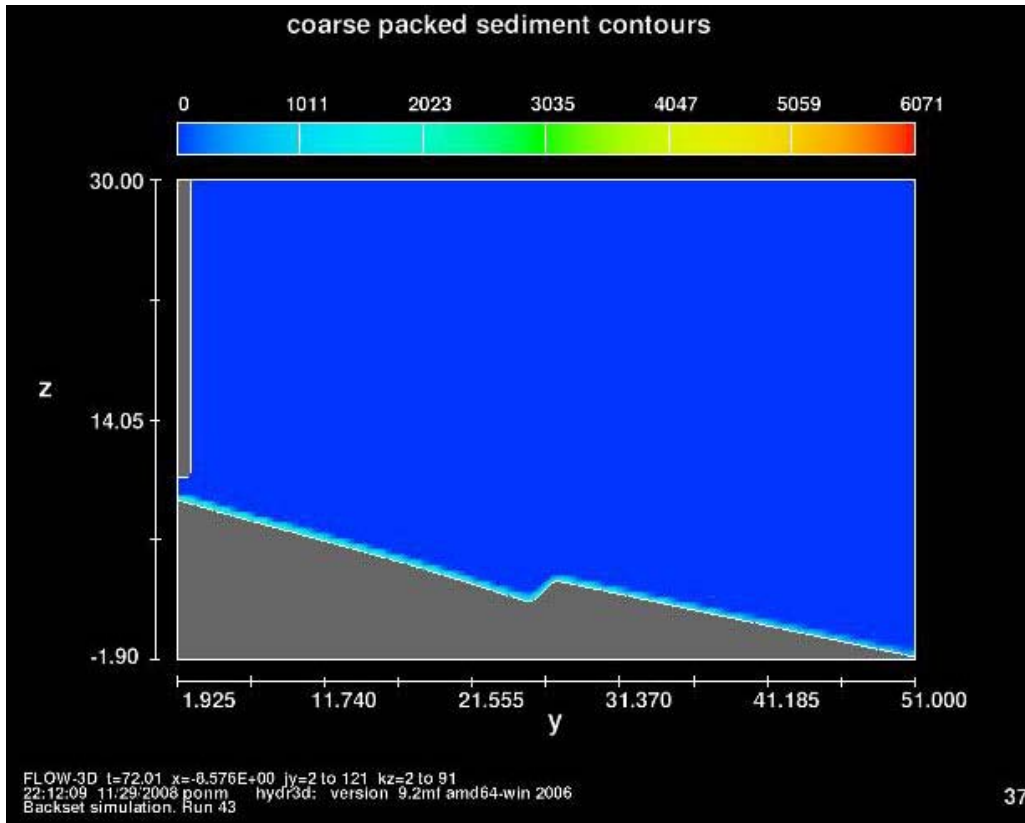


Fig.8.4.5 RUN 43: deposition of sediment shows an equal deposition along the whole surface, without a major deposition at the obstacle.

run 43 density comparison

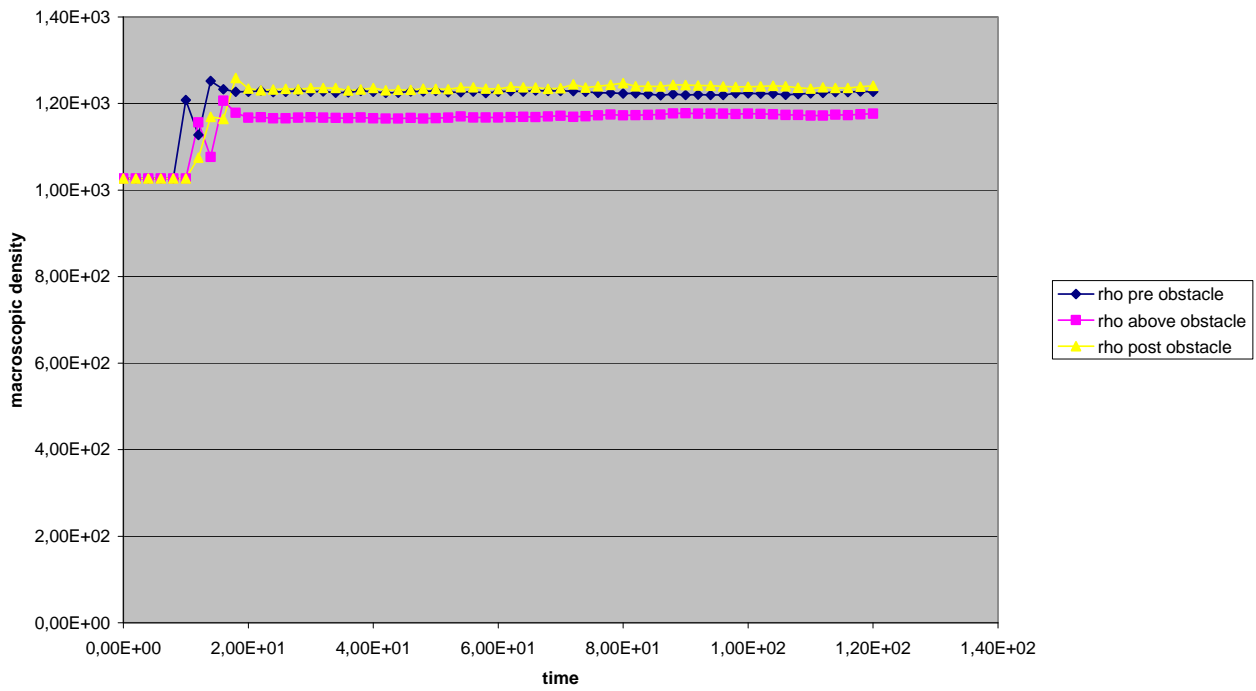


Fig.8.4.6 RUN 43: Comparison of macroscopic density in the three point shows that density tend to increase but the values before, above and after the obstacle only slightly change.

run 43 velocity magnitude comparison

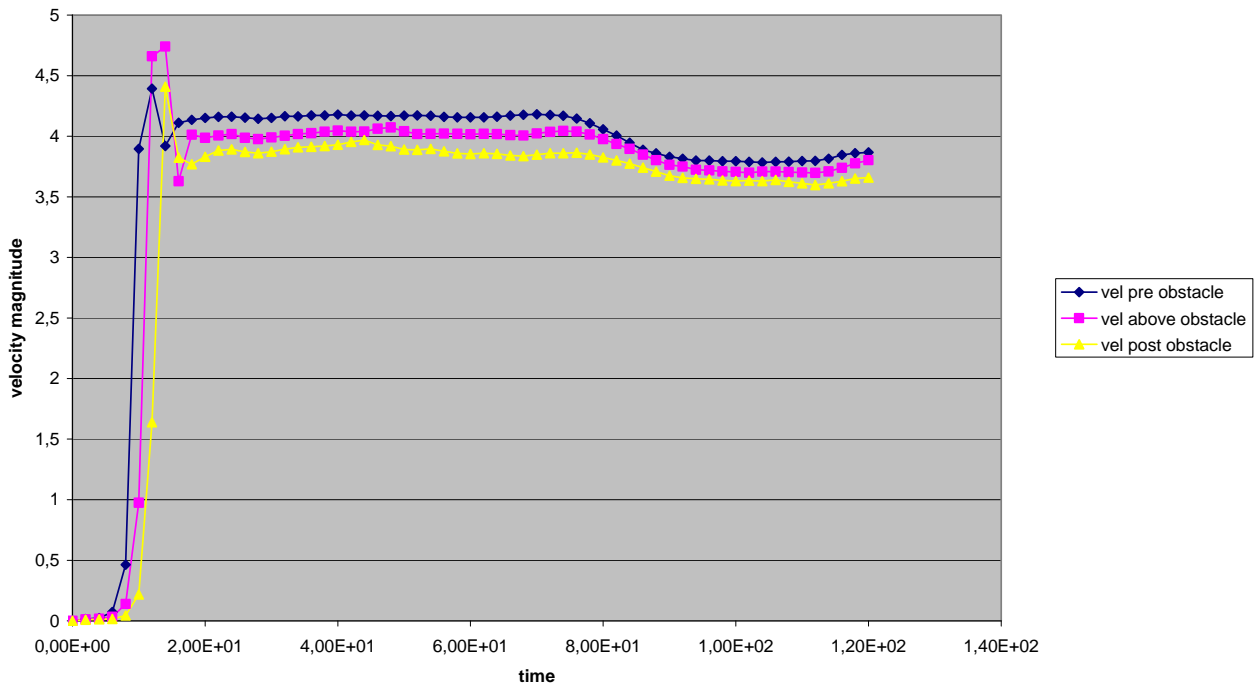


Fig.8.4.7 RUN 43 Comparison of velocities at the three points. The velocity shows a similar trend in all points with a small decrease of about 0.5 m/sec from before the obstacle and after the obstacle.

run 43 turbulent energy comparison

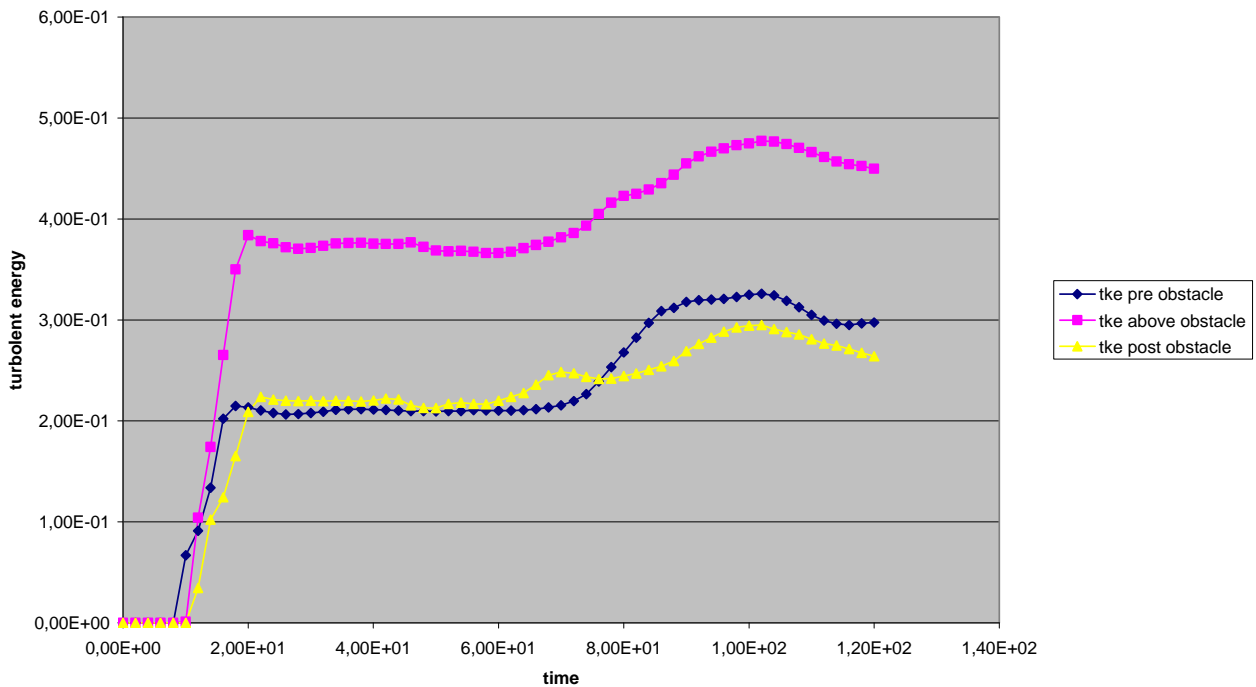


Fig.8.4.8 RUN 43 Comparison of turbulent energy in the three points. The diagram evidence a strong increase of turbulent energy above the obstacle which is increasing in time. Turbulent energy drops again after the obstacle to values similar to the ones before the obstacle.

Simulation number 43 shows a trend that is not completely compatible with the development of the hydraulic jump, which is also testified by the sedimentation rate that do not shows any particular higher deposition related to a drop in velocity at the obstacle. In this case also, the flow doesn't show any increase in thickness, and no up-slope migration is shown. It is possible to say that even if some of the conditions are validated others are not, therefore run 43 do not simulate deposition due to a hydraulic jump.

## RUN 45

Slope = 15°

Grain-size = 0.5 mm

Dynamic viscosity of sea water at 10° = 1027 kg/m<sup>3</sup>

Sediment density = 1800 kg/m<sup>3</sup> (underestimated from limestone density 1800kg/m<sup>3</sup>)

Initial sediment concentration = 35%

Initial flow velocity (m/sec) = 2.50 m/sec

Initial flow thickness = 2 m

Sediment entrainment coefficient (scour parameter) = 0.80

Fr = 1.10

Flow duration = 120 sec

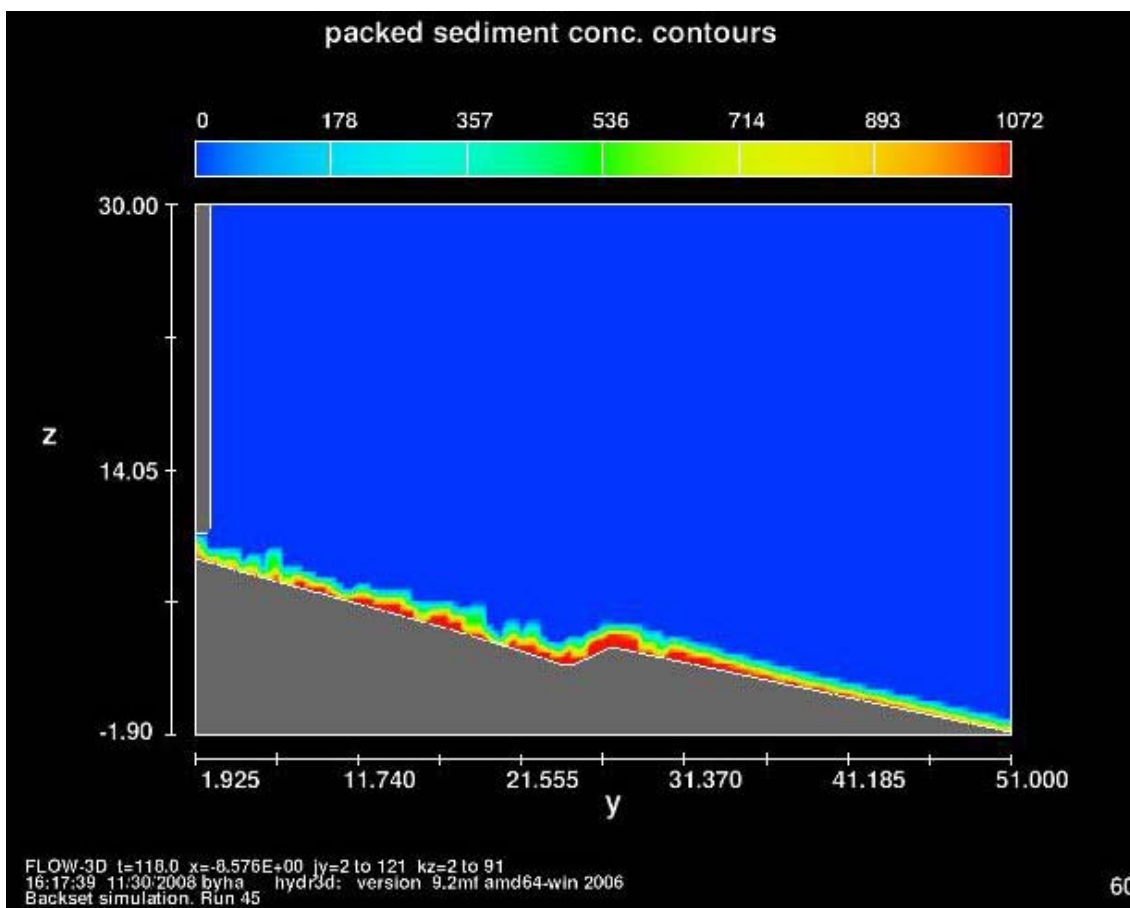


Fig.8.4.9 RUN 45: in this simulation a higher rate of sediment deposition is observed, in particular higher rates of deposition are observed before and especially at the obstacle. The irregularity of the shape of the depositing sediment is related to the size of mesh cells.

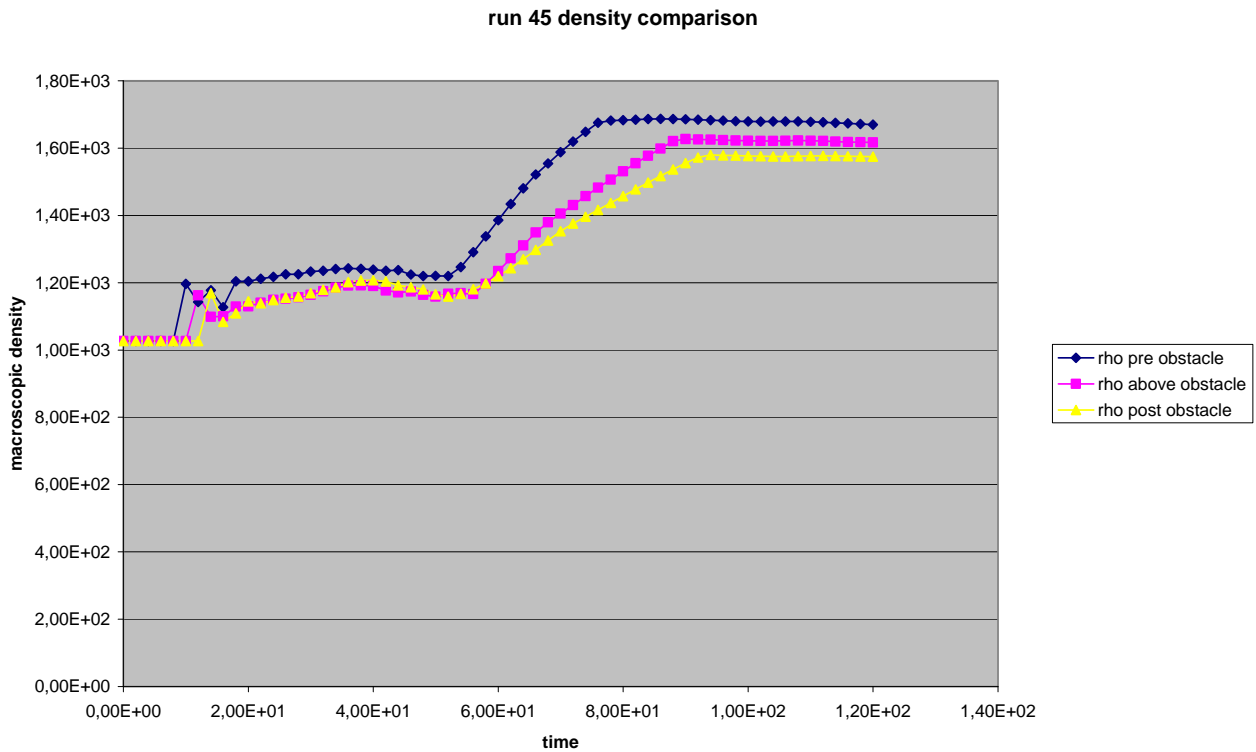


Fig.8.4.10 RUN 45: Comparison of macroscopic density values in the three points. The diagram shows a progressive decrease in macroscopic density therefore a higher rate of deposition before and at the obstacle comparing to the after obstacle point.

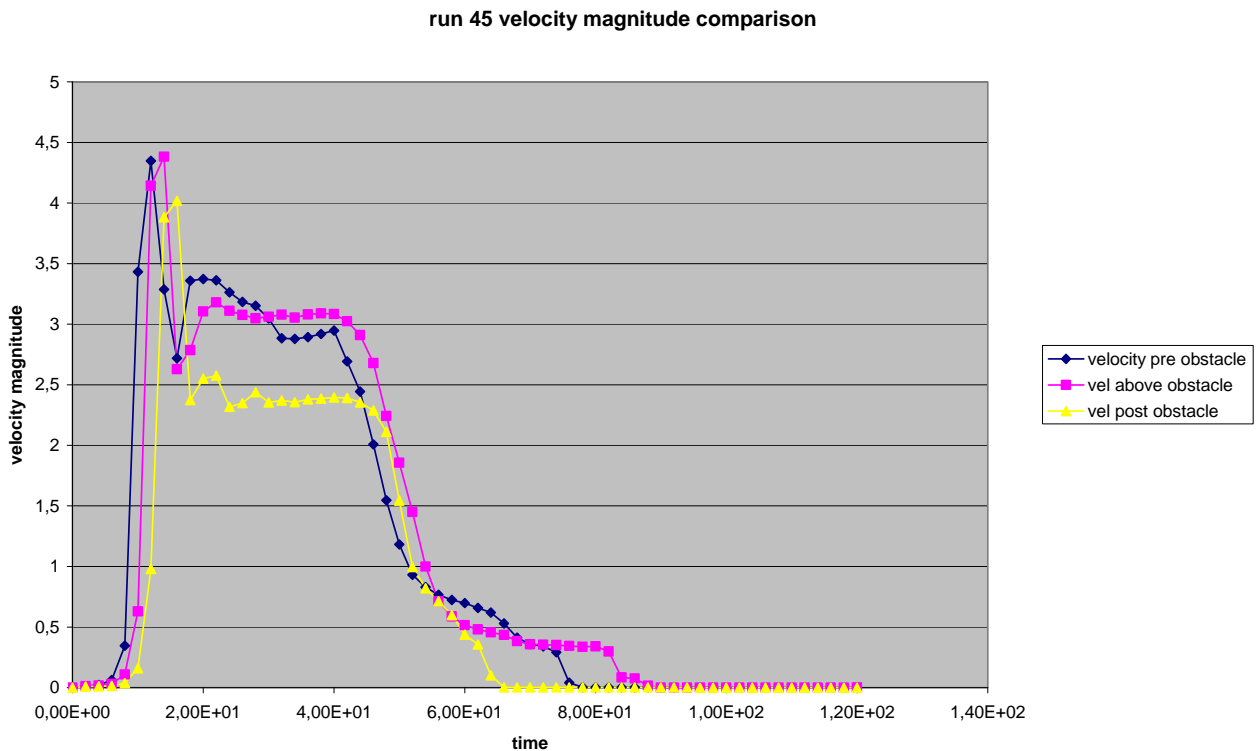


Fig.8.4.11 RUN 45: Comparison between velocities at the three points. In the first 60 seconds, the diagram shows a drop of velocity after the obstacle; the fall of velocities to zero is related to the high deposition rate that buried the

selected points. It is also possible to notice that the first point where sedimentation occur is after the obstacle, then the second is the one before the obstacle and at last above the obstacle.

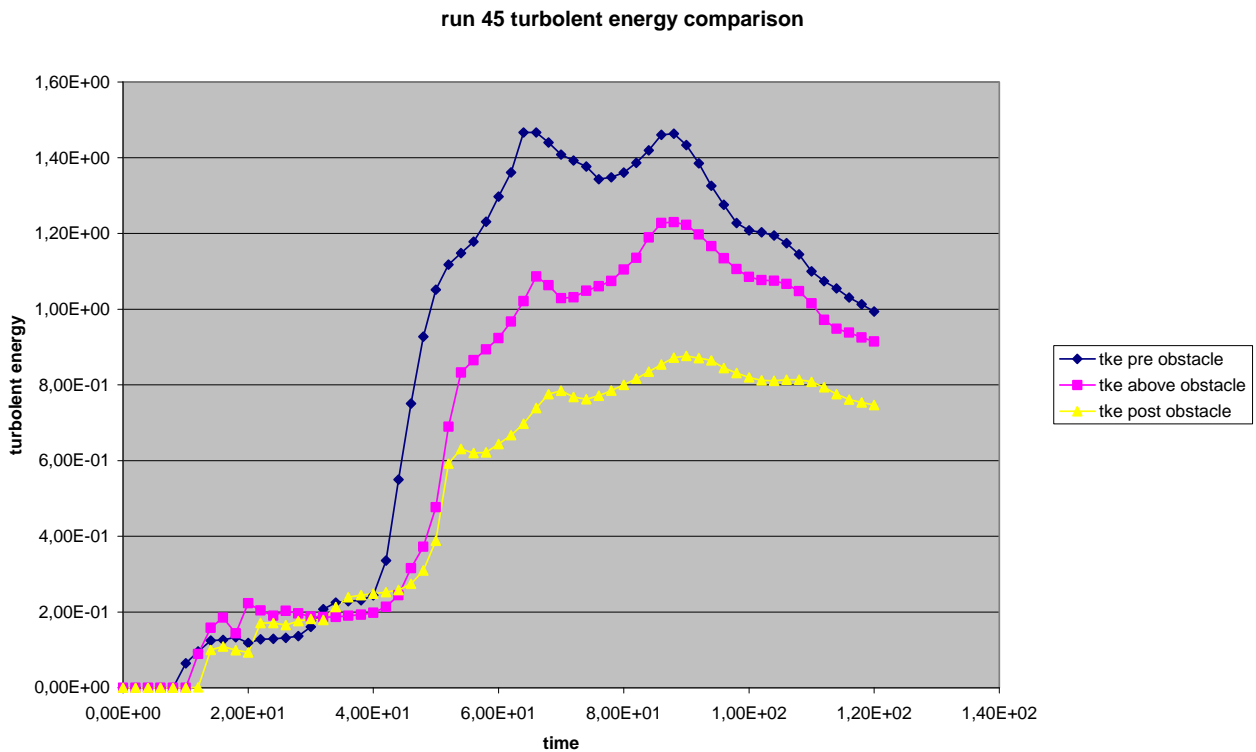


Fig.8.4.12 RUN 45: Comparison between turbulent energy at the three points. The turbulent energy after a first increase in the first 40 seconds, definitely decrease above and even more after the obstacle.

Simulation number 45 shows a trend that may be compatible to a hydraulic jump conditions only in the first 40 seconds of the simulation for both velocities and turbulent energy, while afterwards the values do not match to such conditions. In this case we can assume that the parameters favourable for the permanence of the hydraulic jump conditions create the right conditions only for a short time, which caused the majority of the sedimentation (snapshot of Fig.8.4.9 is taken after 60 seconds and afterwards no more sedimentation is registered). It is possible to assume that the conspicuous variation of the topography due to sedimentation during the first 40 seconds is enough to change the conditions favourable to a hydraulic jump related sedimentation.

## RUN 46

Slope = 15°

Grain-size = 0.5 mm

Dynamic viscosity of sea water at 10° = 1027 kg/m<sup>3</sup>

Sediment density = 1800 kg/m<sup>3</sup> (underestimated from limestone density 1800kg/m<sup>3</sup>)

Initial sediment concentration = 35%

Initial flow velocity (m/sec) = 2.50 m/sec

Initial flow thickness = 2 m

Sediment entrainment coefficient (scour parameter) = 0.50

Fr = 1.10

Flow duration = 120 sec

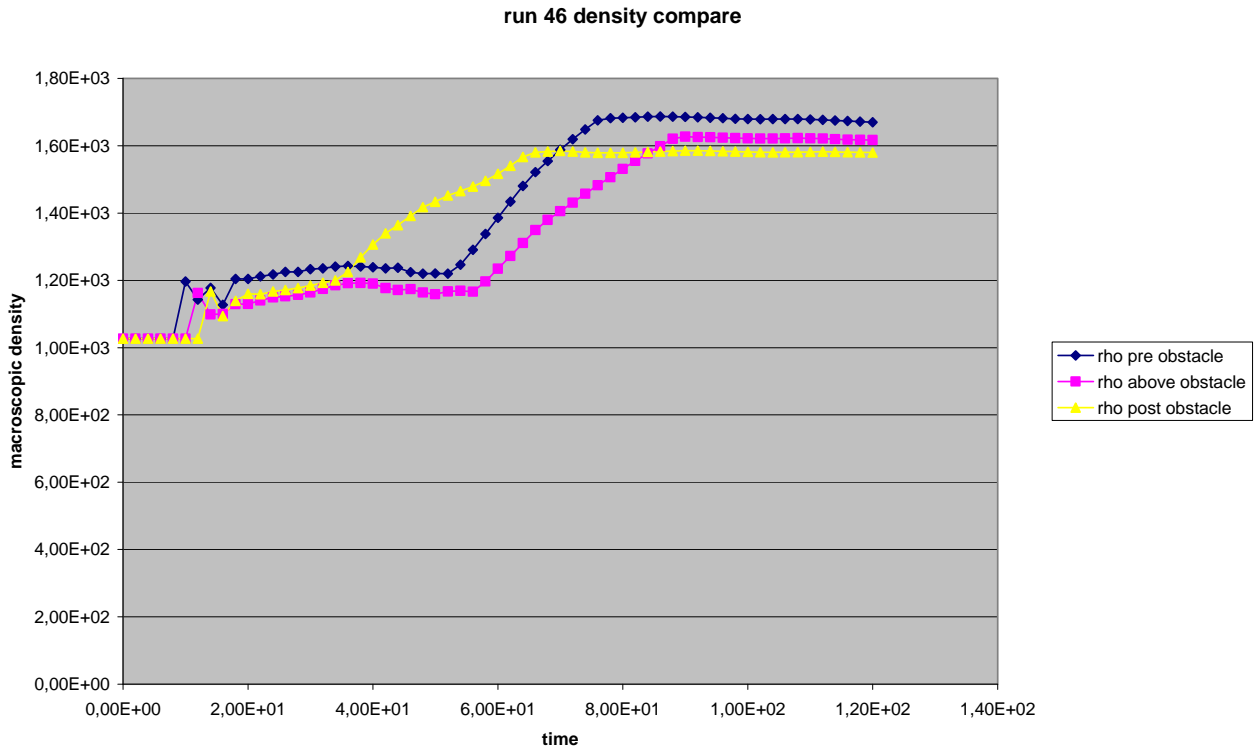


Fig.8.4.13 RUN 46: Macroscopic density trends shows a dominant highest sediment deposition at the point before the obstacle, which is higher after the obstacle only in the interval of time between 40 sec and 70 seconds. Above the obstacle is recorded the lower sedimentation rate which follows a trend similar to the one at the point before the obstacle.

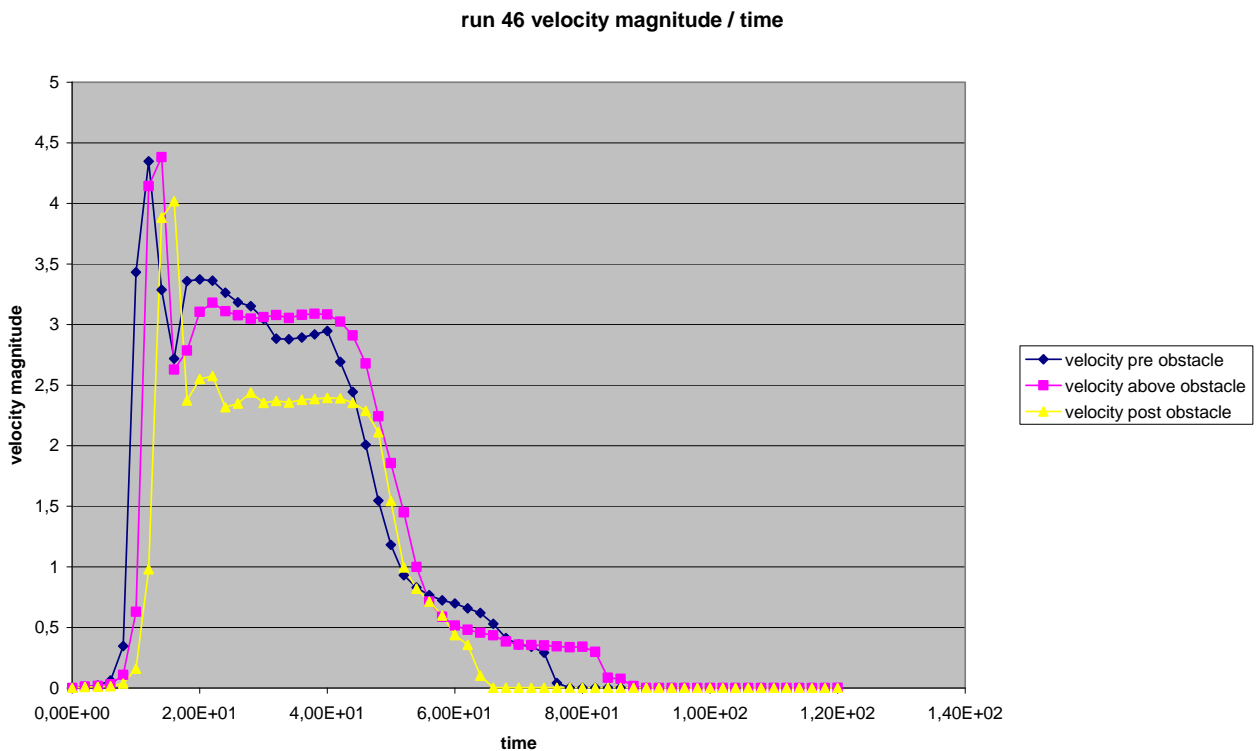


Fig.8.4.14 RUN 46: The diagram of velocities may be split in two parts: between time 20 to 50 seconds, velocity is lower after the obstacle compared to the point before the obstacle, therefore a drop in velocity occurs. After time 50 seconds on, the velocity at all three points fall due to sediment deposition which buried the control-points.

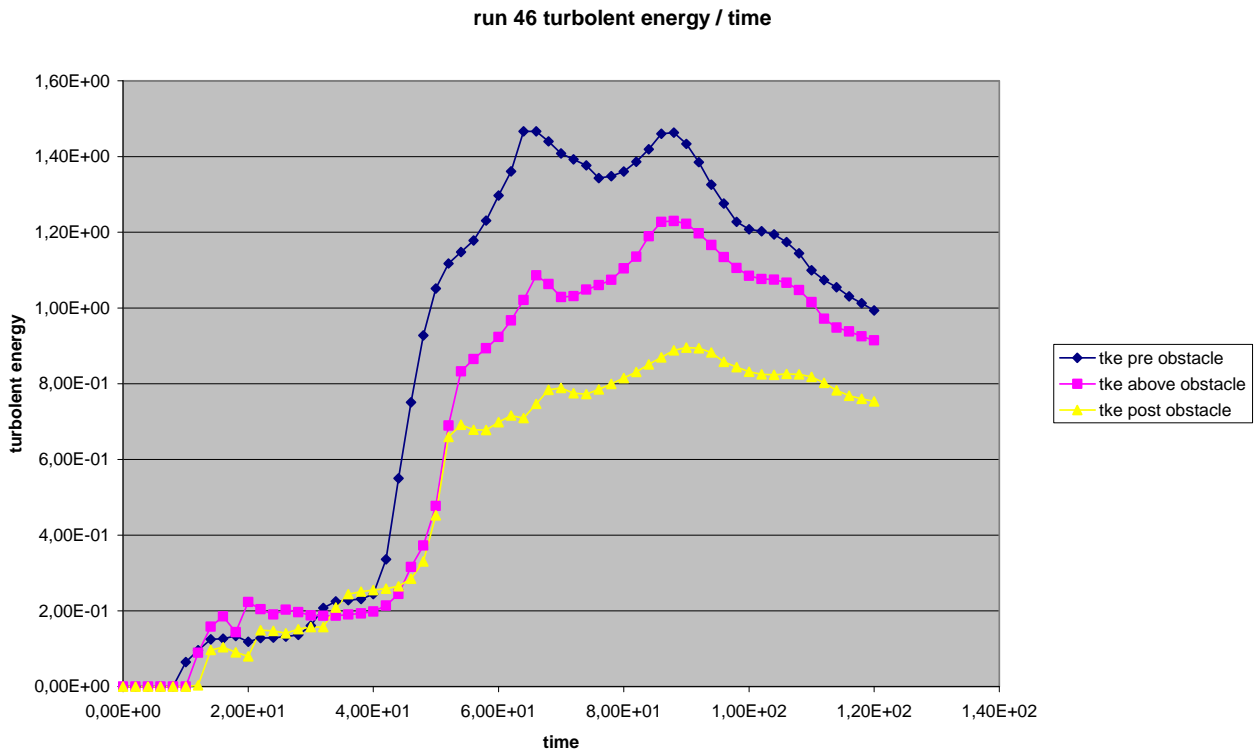


Fig.8.4.15 RUN 46: Diagram comparing turbulent energy at the three control-points. Turbulent energy, from time 15 to 40 seconds, the turbulence first slightly increase above the obstacle compare to the point before the obstacle, while at the point after the obstacle turbulent energy is always very close to values at the point before the obstacle. After time 40 seconds, the turbulent energy show a progressive decrease above and after the obstacle.

Simulation number 46 do not present at any time conditions favourable to the development of a hydraulic jump. Only the velocity shows an interesting trend but just for an interval of time, while the other parameters, flow thickness and turbulent energy do not comply with the required trends.

## RUN 69

Slope = 15°

Grain-size = 0.5 mm

Dynamic viscosity of sea water at 10° = 1027 kg/m<sup>3</sup>

Sediment density = 1800 kg/m<sup>3</sup> (underestimated from limestone density 1800kg/m<sup>3</sup>)

Angle of repose = 25°

Initial sediment concentration = 35%

Initial flow velocity (m/sec) = 1.0 m/sec

Initial flow thickness = 2 m

Sediment entrainment coefficient (scour parameter) = 0.20

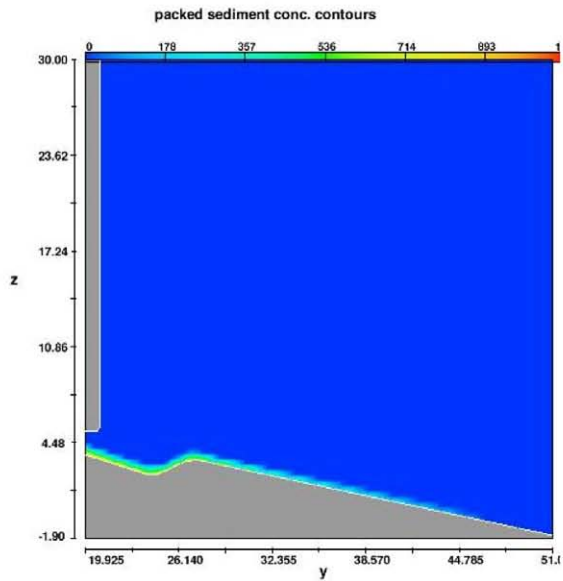


In run 69, flow velocity has been set not as a continuous steady currents but as pulsating surges, therefore the inflow of the flow is an alternation of flowing currents with times of not flow input. In this conditions one of the best result has been obtained. The interesting interval of time resulted to be towards the end of the flow input and it repeated itself for all the successive flows.

Fig.8.4.16 RUN 69 PACKED SEDIMENT CONCENTRATION CONTOURS: the numbers of frames represent the time measured as the number of seconds that passed from the beginning of the simulation. The packed sediment, represents the sediment that deposit on the surface. The 2D snapshots taken from the simulation show that there is sediment deposition both before the obstacle where there is aggradation and at the obstacle, while it is reduced after the obstacle. Notice that the X and Y are in meters, therefore the thickness of the sediment deposited by the flow has an approximate thickness of 1m. The deposition of the first sediment at the obstacle, will slightly move the obstacle up-slope.

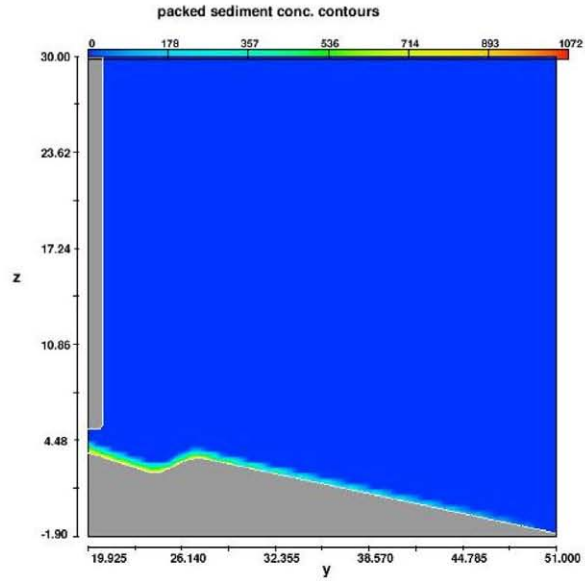
Fig.8.4.17 RUN 69 TURBULENT ENERGY CONTOURS: the same interval of time has been analyzed also to control turbulent energy trends. The snapshots allow to observe how turbulent energy is definitely higher after the obstacle and the thickness of flow also noticeably increase, becoming almost double the initial flow thickness at the inlet.

Fig.8.4.18 RUN 69 VELOCITY MAGNITUDE CONTOURS: first notice that the reference numbers in scale of colours that correspond to values of velocities are changing in time, that means that the same colour assumes different velocity value in different frames. Right after the obstacle a drop in velocity is evident. Moreover, a shadow of very low to zero velocity develops at the obstacle, allowing sediment deposition.



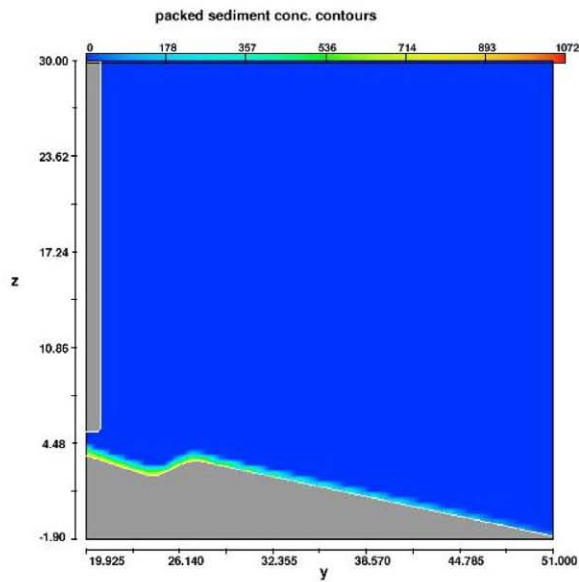
FLOW-3D t=22.01 s=-8.576E+00 [y=2 to 121 kz=2 to 91  
18:29:38 12:15:2006 cmj] hydr3d: version 9.2ml amd64-win 2006  
Basket simulation, run 69

23



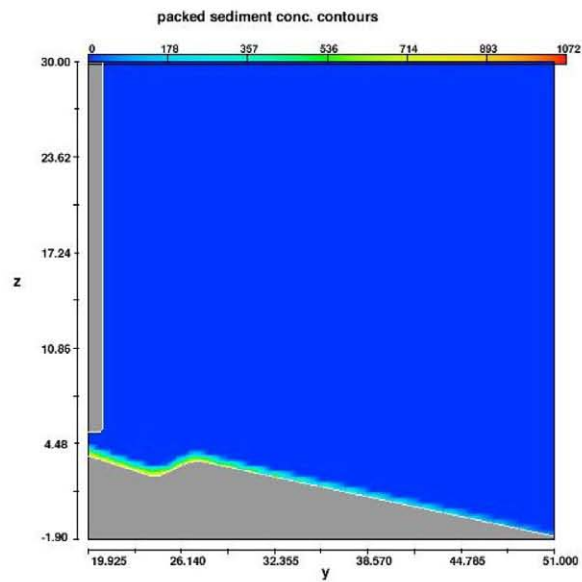
FLOW-3D t=26.00 s=-8.576E+00 [y=2 to 121 kz=2 to 91  
18:29:39 12:15:2006 cmj] hydr3d: version 9.2ml amd64-win 2006  
Basket simulation, run 69

27



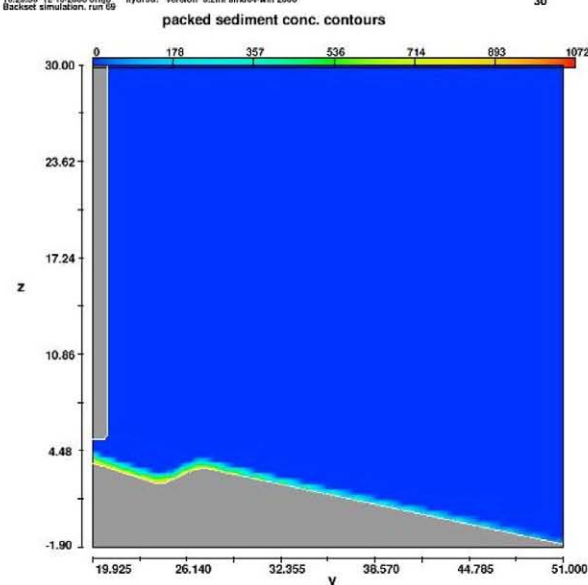
FLOW-3D t=28.99 s=-8.576E+00 [y=2 to 121 kz=2 to 91  
18:29:38 12:15:2006 cmj] hydr3d: version 9.2ml amd64-win 2006  
Basket simulation, run 69

30



FLOW-3D t=32.01 s=-8.576E+00 [y=2 to 121 kz=2 to 91  
18:29:38 12:15:2006 cmj] hydr3d: version 9.2ml amd64-win 2006  
Basket simulation, run 69

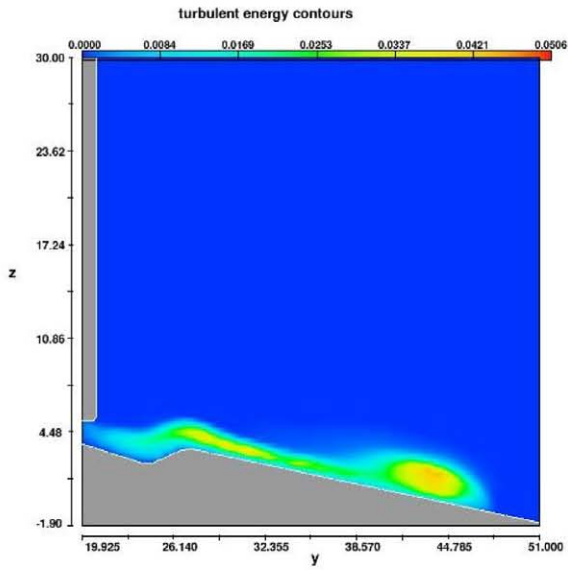
33



FLOW-3D t=34.01 s=-8.576E+00 [y=2 to 121 kz=2 to 91  
18:29:38 12:15:2006 cmj] hydr3d: version 9.2ml amd64-win 2006  
Basket simulation, run 69

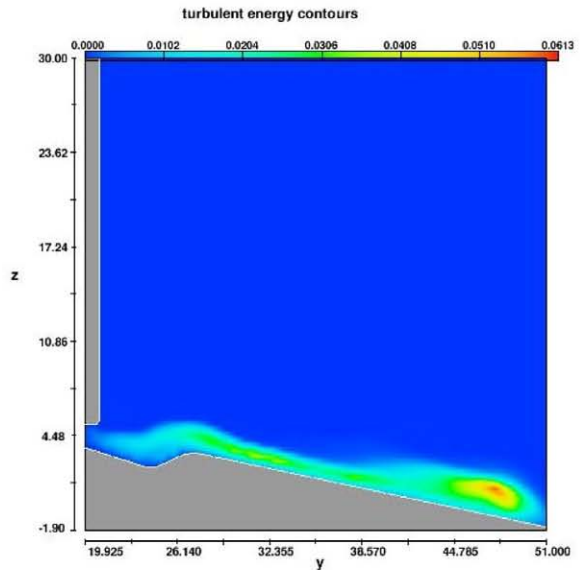
35

RUN 69 INTERVAL 1  
Packed sediment concentration contours  
Frames 23-27-30-33-35



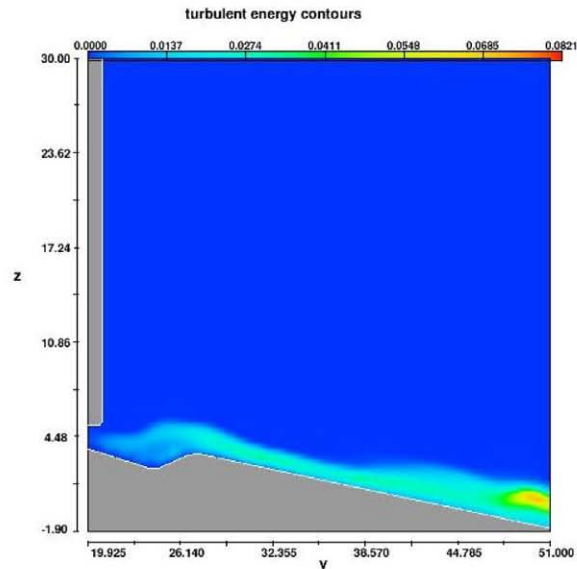
FLOW-3D t=22.01 x=-8.576E+00 (y=2 to 121 kz=2 to 91  
18:20:38 12:16:2008 omj) hydro3d: version 9.2ml smd64-win 2006  
Backset simulation, run 69

23



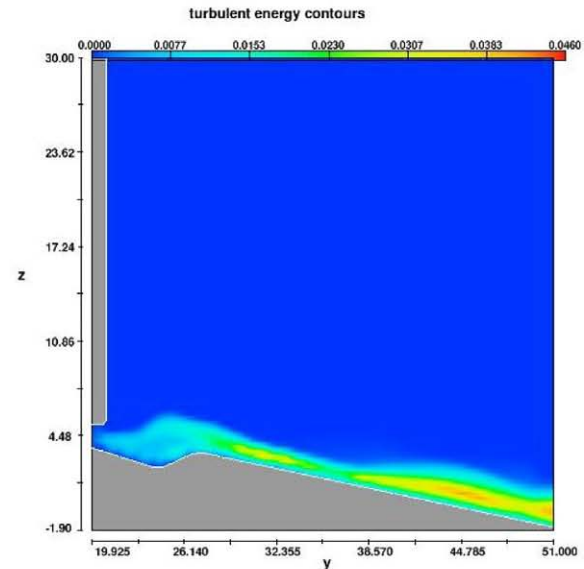
FLOW-3D t=26.00 x=-8.576E+00 (y=2 to 121 kz=2 to 91  
18:20:38 12:16:2008 omj) hydro3d: version 9.2ml smd64-win 2006  
Backset simulation, run 69

27



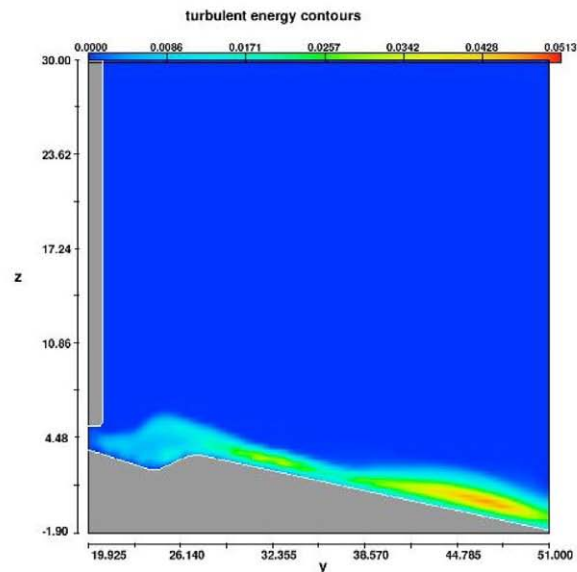
FLOW-3D t=28.99 x=-8.576E+00 (y=2 to 121 kz=2 to 91  
18:20:38 12:16:2008 omj) hydro3d: version 9.2ml smd64-win 2006  
Backset simulation, run 69

30



FLOW-3D t=32.01 x=-8.576E+00 (y=2 to 121 kz=2 to 91  
18:20:38 12:16:2008 omj) hydro3d: version 9.2ml smd64-win 2006  
Backset simulation, run 69

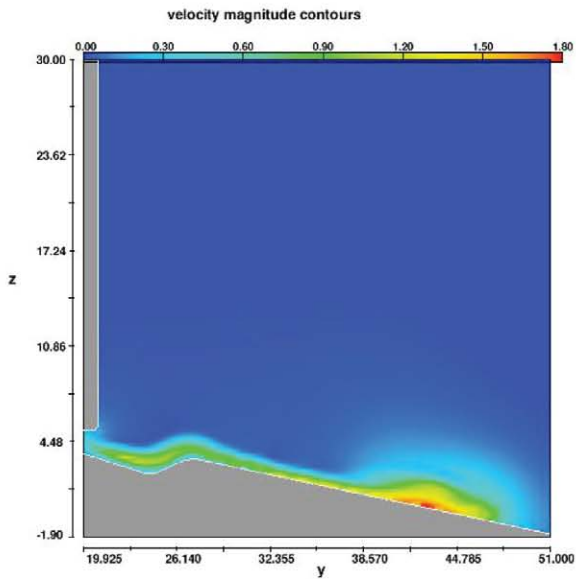
33



FLOW-3D t=34.01 x=-8.576E+00 (y=2 to 121 kz=2 to 91  
18:20:38 12:16:2008 omj) hydro3d: version 9.2ml smd64-win 2006  
Backset simulation, run 69

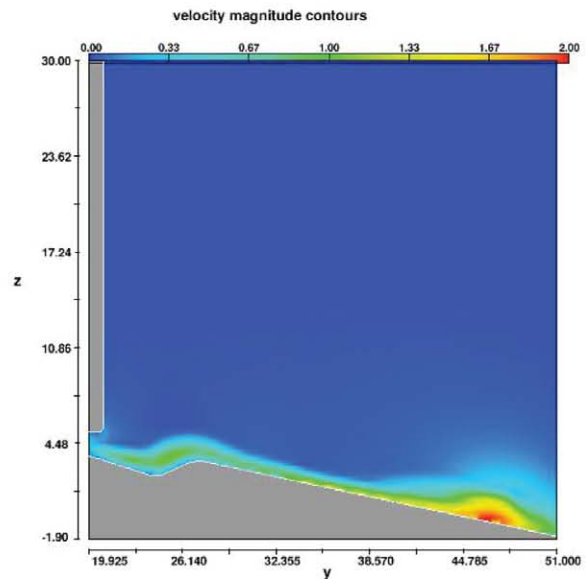
35

RUN 69 INTERVAL 1  
Turbulent energy contours  
Frames 23-27-30-33-35



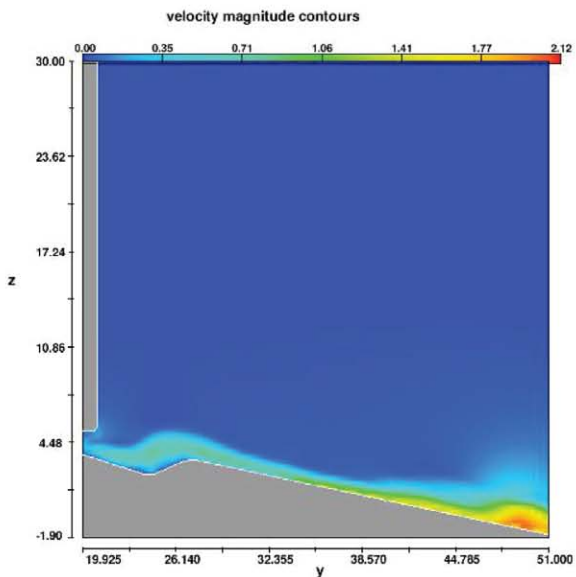
FLOW-JD 1:22.01 x=-8.576E+00 [t=2 to 121 k=2 to 91  
18:20:28 12-15-2008 omg] hyd56: version 9.2ml amd64-win 2006  
Backset simulation, run 69

23



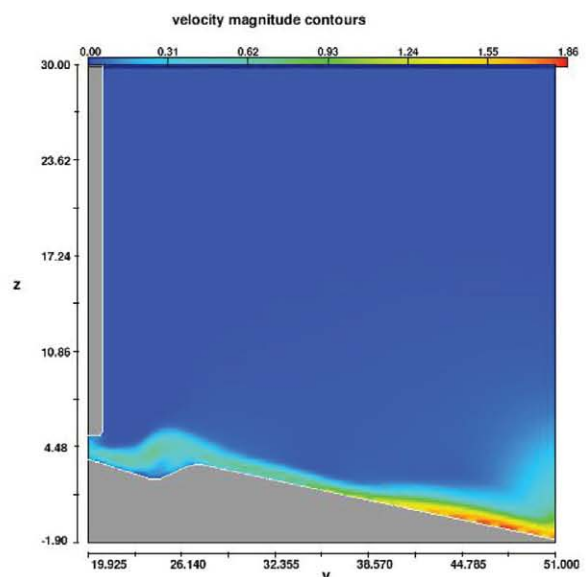
FLOW-JD 1:26.00 x=-8.576E+00 [t=2 to 121 k=2 to 91  
18:20:28 12-15-2008 omg] hyd56: version 9.2ml amd64-win 2006  
Backset simulation, run 69

27



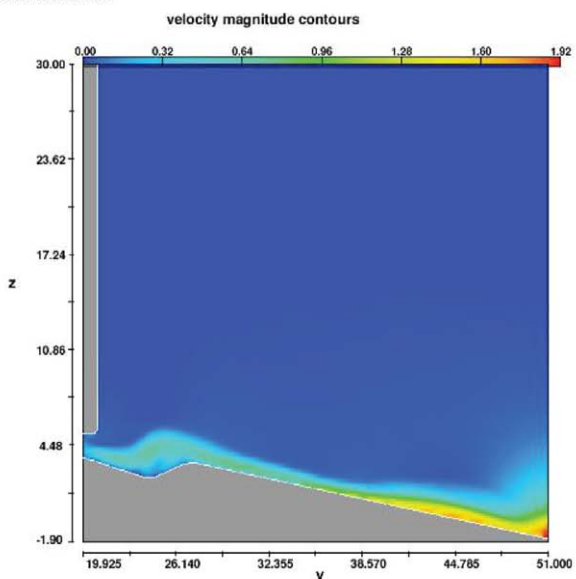
FLOW-JD 1:28.99 x=-8.576E+00 [t=2 to 121 k=2 to 91  
18:20:28 12-15-2008 omg] hyd56: version 9.2ml amd64-win 2006  
Backset simulation, run 69

30



FLOW-JD 1:34.01 x=-8.576E+00 [t=2 to 121 k=2 to 91  
18:20:28 12-15-2008 omg] hyd56: version 9.2ml amd64-win 2006  
Backset simulation, run 69

35



FLOW-JD 1:32.01 x=-8.576E+00 [t=2 to 121 k=2 to 91  
18:20:28 12-15-2008 omg] hyd56: version 9.2ml amd64-win 2006  
Backset simulation, run 69

33

RUN 69 INTERVAL 1  
Velocity magnitude contours  
Frames 23-27-30-33-35

The analysis of all the parameters of simulation 69 agree for the interpretation of the deposition of sediment at the obstacle as related to the occurrence of a hydraulic jump. The three major conditions are complied: velocity decrease, turbulent energy increase, increase of flow thickness and dumping of sediment at the obstacle. The successive flows behave in the same way. Unfortunately there is, again, a problem due to the software: the flow-inlet can not move upward with time, therefore the aggradation of sediment in the portion of the slope before the obstacle will progressively grow (aggrade) reducing the thickness of the flow-inlet and therefore of the flow and with passing time the inlet will be buried.

## **RUN 72**

Slope = 15°

Grain-size = 0.5 mm

Dynamic viscosity of sea water at 10° = 1027 kg/m<sup>3</sup>

Sediment density = 1800 kg/m<sup>3</sup> (underestimated from limestone density 1800kg/m<sup>3</sup>)

Angle of repose = 25°

Initial sediment concentration = 20%

Initial flow velocity (m/sec) = 0.5 m/sec

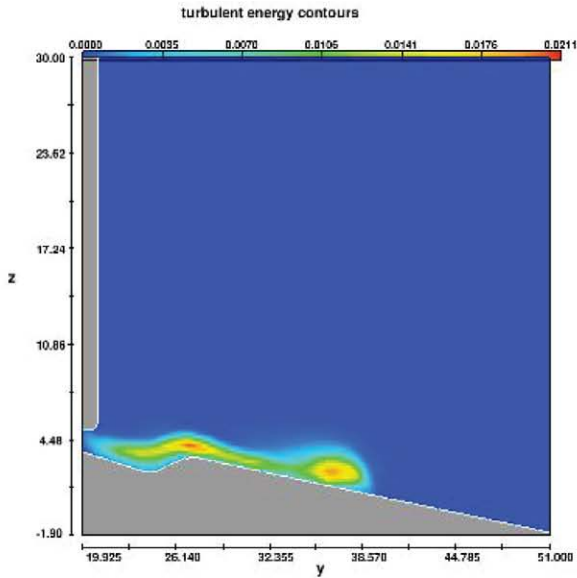
Initial flow thickness = 2 m

Sediment entrainment coefficient (scour parameter) = 0.80

Simulation number 72 behave in a similar way to run 69. Again the sediment flow at the inlet is not constantly shut from the inlet, but there are pauses between flows. This run differs from the previous one described above because of sediment concentration is reduce to 20% and flow speed has also been reduced. The scour parameter was tentatively increase to reduce aggradation due to sediment deposition before the obstacle.

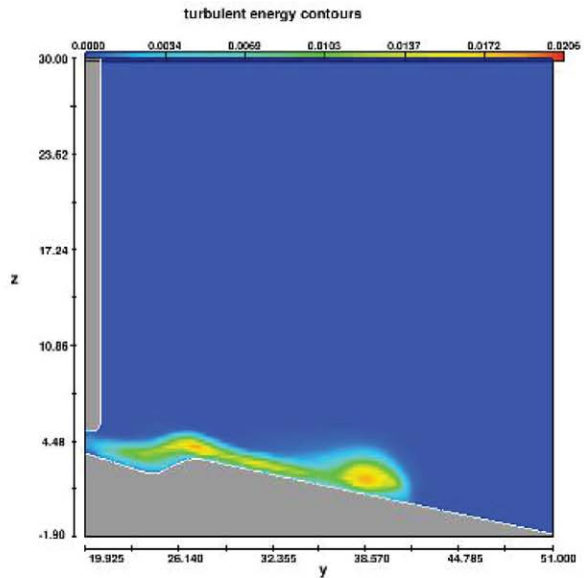
Fig.8.4.19 RUN 72 PACKED SEDIMENT CONCENTRATION CONTOURS: deposition results again to be higher before and at the obstacle but the thickness of the deposit is smaller than the one in run 69; this is due to the increasing of scour parameter which increase the rate of erosion not allowing the same rate of sediment deposition.

Fig. 8.4.20 RUN 72 TURBOLENT ENERGY CONTOURS: in this simulation the increase of turbulent energy is very evident, and it is also accompanied by a progressive increase of flow thickness.



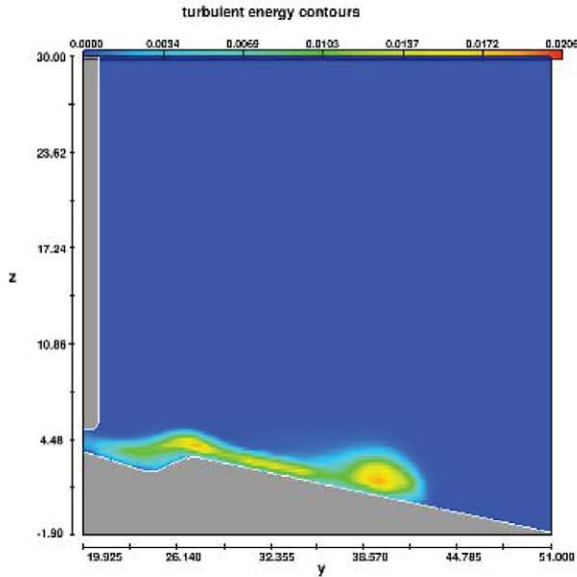
FLOW-3D 1:25:00 c:-6.971E+00 q:1 to 121 kuz2 to 91  
 17:52:24 12:30:2000 Inac. Hyd:50 variation 2.Zint unob4win 2018  
 Success simulation run 72

24



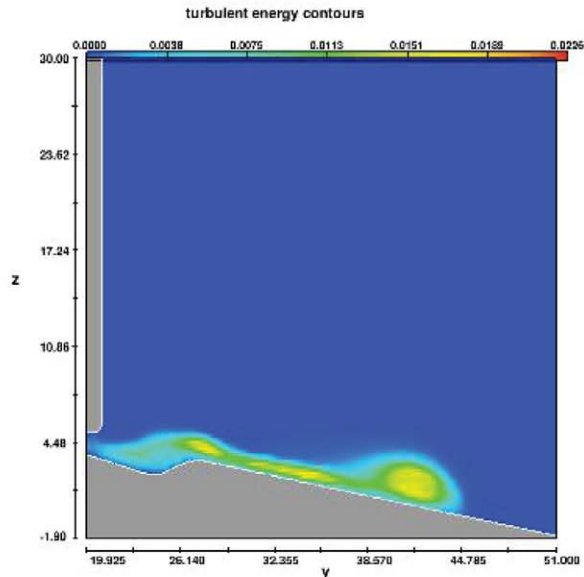
FLOW-3D 1:27:00 c:-6.971E+00 q:1 to 121 kuz2 to 91  
 17:52:24 12:30:2000 Inac. Hyd:50 variation 2.Zint unob4win 2018  
 Success simulation run 72

28



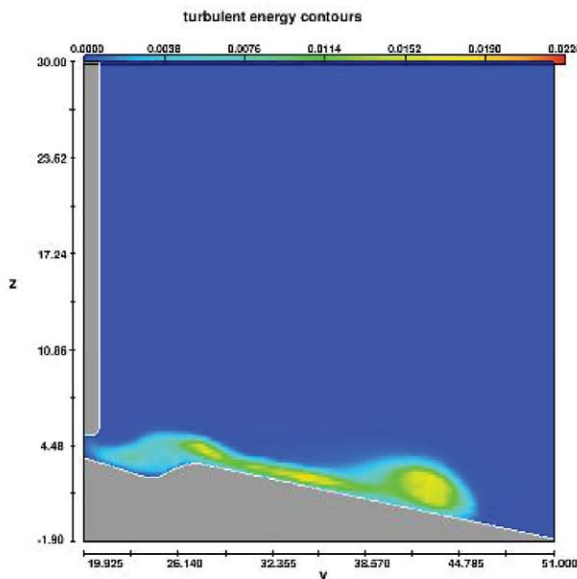
FLOW-3D 1:29:00 c:-6.971E+00 q:1 to 121 kuz2 to 91  
 17:52:24 12:30:2000 Inac. Hyd:50 variation 2.Zint unob4win 2018  
 Success simulation run 72

30



FLOW-3D 1:32:00 c:-6.971E+00 q:1 to 121 kuz2 to 91  
 17:52:24 12:30:2000 Inac. Hyd:50 variation 2.Zint unob4win 2018  
 Success simulation run 72

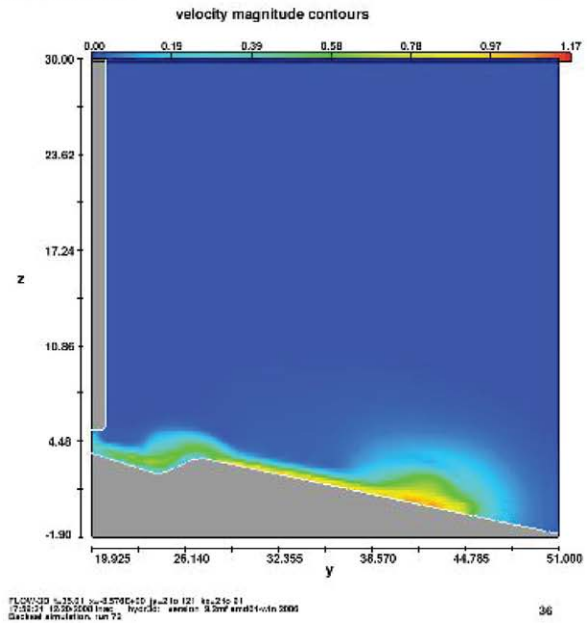
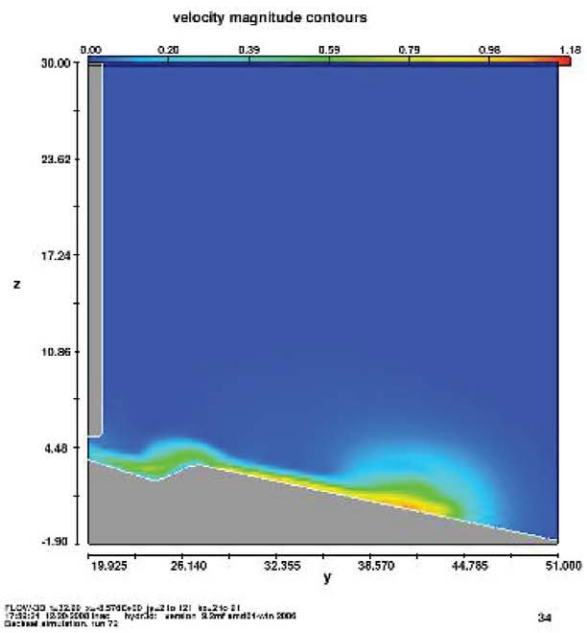
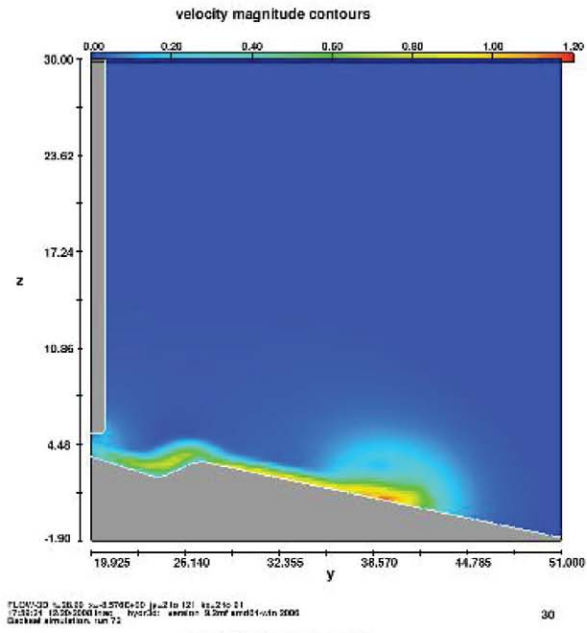
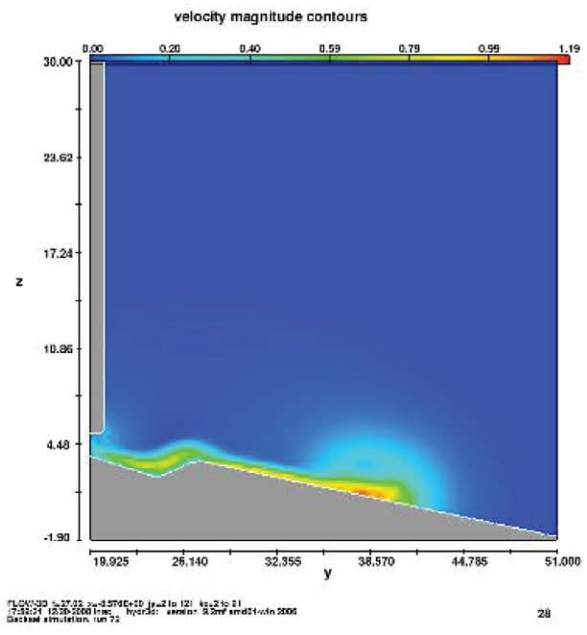
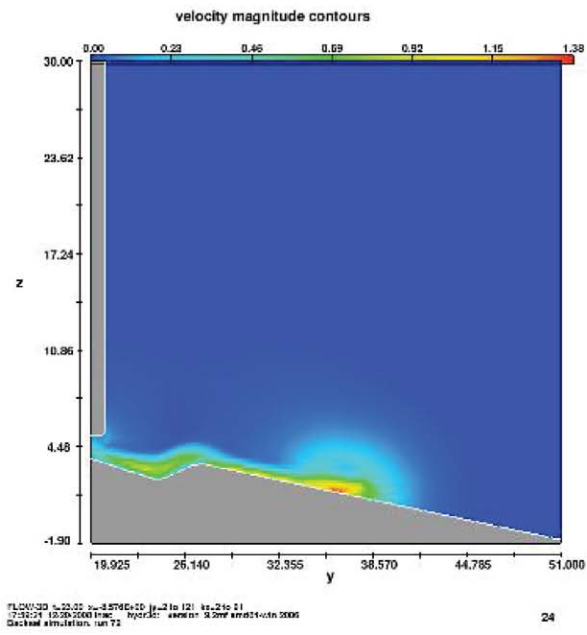
34



FLOW-3D 1:36:00 c:-6.971E+00 q:1 to 121 kuz2 to 91  
 17:52:24 12:30:2000 Inac. Hyd:50 variation 2.Zint unob4win 2018  
 Success simulation run 72

36

RUN 72  
 Turbulent energy contours  
 Frames 24-28-30-34-36



RUN 72  
Velocity magnitude contours  
Frames 24-28-30-34-36

Fig.8.4.21 RUN 72 VELOCITY MAGNITUDE CONTOURS: the snapshots taken from the 2D simulation again show a decrease of flow speed at the obstacle. The successive acceleration of the flow that is visible on the down-dip part is related to velocity increased velocity enhanced by gravity forces, that re-accelerate the flow.

## ***8.5 Conclusion***

The wide range of simulation that have been performed underlined the complexity of finding the right set of parameters to obtain the occurrence of a hydraulic jump. This is mainly be related to the large numbers of combinations of different parameters.

The results here presented do not refer to the example of Menorca, but they tentatively reproduce a hydraulic jump and the related backset deposition.

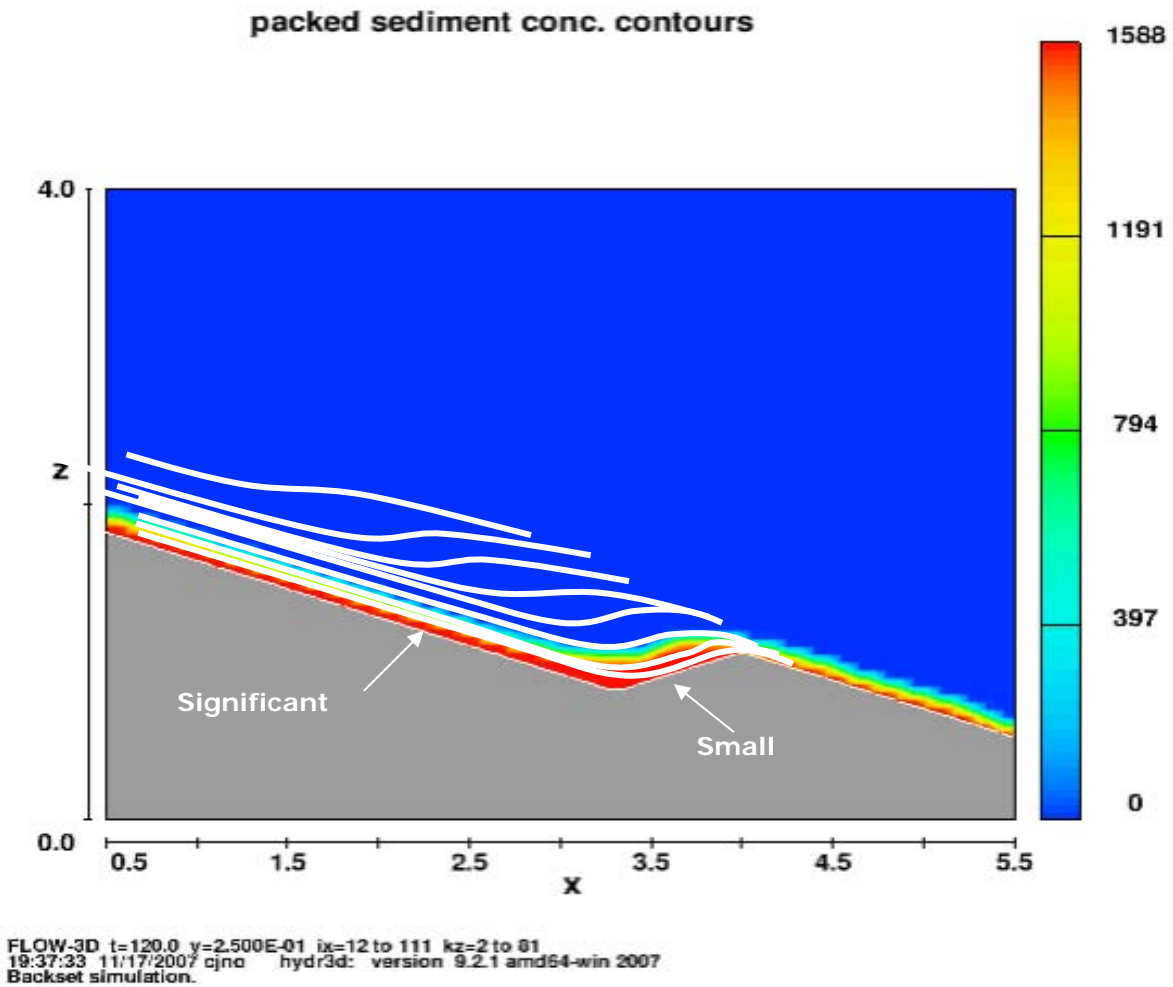
Even if the number of simulations performed are not enough to produce example of each possible combination (these would required either years of work or a very powerful processor able to process these simulation in few minutes instead of hours), the simulations produced already present some results over which some consideration can be done.

- When the incoming sediment flow is set with constant concentrations and speed, so that a steady flow forms, the occurrence of a hydraulic jump has never been observed, not even close to it; sediment deposition is usually the same all along the surface without evidencing portions of variable sedimentation rates.
- The best results have been obtained with a "pulsating" flow which can represent discontinuous feeding of the flow from above and would also explain the normal to inverse grading characterizing the backset beds.
- Sediment concentration itself doesn't seem also to determine the occurrence of a hydraulic jump, because it can be balanced in the equation of the Froude number by the flow speed.
- The thickness of the flow is also not so important: this has been proved by running two simulations characterized by the same set of parameters with the only difference that in one the flow is 2 m thick and in the other the flow is 4 m thick. In both cases the deposition at the obstacle was the same (about 1.5m), evidencing that in the case study of a hydraulic jump induced by a obstacle, the size of the obstacle controls the size of the backset bedded deposit.
- Flow speed resulted to be important, since when it is too high, for a given couple of flow-thickness and scale-comparable-obstacle, the flow doesn't feel the obstacle and the sediment flow runs straight above the obstacle.
- For the data-set simulated, the velocity at which the hydraulic jump occurred are quite low, ranging around 0.8 m/sec to 1.20 m/sec.
- The relative Froude number measured before the obstacle is very close to 1.



In the simulations where the hydraulic jump occurred, deposition occurred mainly at the obstacle and before it. In Figure 8.5.1 it is shown how the progressive deposition at the obstacle may create a backset bedding architecture.

To establish a more detail relationship between all single factors, a wider range of simulations will be needed. The work done, propose some starting points for further simulations to constrain more precisely the main parameters.



121

Fig.8.5.1 Simplified sketch of the development of backset beds.

## 9. CONCLUSIONS

- The presented thesis provide a new insight in the knowledge of backset lamination sedimentary structures. A detail sedimentological analysis and description of these bedforms in the carbonate depositional system of the distally steepened ramp of Menorca was carried out. The backset laminated deposits presented in this case study, are one of the few examples known from a carbonate slope. The sedimentological analysis give a detail description of lithological properties such as grain-sizes, sorting, textures; a wide and very detail description of the architectural geometries that characterize these bedforms has also been given. The subdivision in sedimentary facies has been used to mark the differences between different deposits and to evidence the relationships between the various features as for example the relationship between grains-size and backset foreset dipping angles.

The description of the components has been important to understand the position, along the carbonate ramp of the source of the sediment that composes the backset beds. The sediment in fact was produced in middle-ramp and upper-slope settings, and successively transported seaward. This has been fundamental for the comprehension and the interpretation of the sequence of processes that drove the development of the studied bedforms.

- The detail study of the sediments found at the transition between base-of-slope sediment and outer-ramp sediment provide an example that shows characteristics that differ from the facies models described by previous authors for this portion of the ramp. On the contrary of what is described by Read (1982) and Wright & Burchette, (1992), we can here add new data enlarging the spectrum of type of sediment that can be found at the base of the slope of a distally steepened ramp, including the possibility to find consistent large-scale (decametre-scale) channalized deposits of coarse grained sediment from sand-size up to boulder-size, proceeding from shallow water platform margin facies, in concomitance to slide-scars related to collapses along the slope.
- The study case of Menorca presents a further example of the ability of stormwave-generated seaward currents, to rework and remove coarse-grain sediment from shallow-water settings and to transport it off-shore to the slope break where gravity flows may generate and develop downslope. In particular, the peculiarity of the studied depositional setting is represented by the occurrence of collapses along the slope: the resulting variation in the morphology of the substrate, and the large depressions that originate, are therefore thought to play an important role in the behaviour of the shoaling waves when approaching the coast. In the studied case, these depressions are

interpreted to behave like submarine canyons, and the related waves to enhance cell-circulation patterns in shallow water settings with associated high energy rip-currents. Rip-currents have been interpreted to be the processes that transported the sediment to the slope-break.

- Through the sedimentological analysis of the backset laminated deposits, the study of the embedding sediment and their position in the ramp, an interpretation of the gravity flow that may have generated them has been proposed. Those beds have been interpreted to be the related to concentrated density currents that prematurely dumped the coarser-grained sediment because of the occurrence of hydraulic jump. This interpretation is based mainly on observations regarding the dominant grain-size populations that composed these deposits and the lack of finer-grained sediment (mud) and the channalized-shape of these units, with erosive surfaces at the base that deeply scour the underlying sediment.
  
- The comparison of the studied backset beds of the carbonate ramp of Menorca, with the known ones from Gilbert-type deltas, evidenced a large number of similarities that allow to give more constrains on the conditions that facilitate the development of these sedimentary structures. The similarities regard grain-size populations involved, values of backset foreset laminae dipping angles, trends of grain-size distribution and variation of lamination angles, chute- to channel-shape with erosive scouring surfaces at the base. The major factors that resulted to be important for the formation of these bedforms can be summarized in three main points: 1) the morphology of the depositional system, intending a shallow-water, slightly inclined ramp that presents a slope-break in a distal position, the slope having an angle of 15°-20° maximum, dominated either by fluvial regime or wave/storm-action; 2) the availability of loose sediment of variable grain-size that can be easily reworked and remove, partly in suspension and partly as bed-load from the shallow-water settings seaward; 3) the development of a unidirectional current directed seaward that can be related to a fluvial regime or it can be enhanced by wave-action in wave-dominated shallow-water platform, able to develop velocity high enough to carry coarse and very coarse clasts off-shore while finer-grained sediment is put into suspension and transported offshore by hypopycnal flows. The only difference regards the type of sediment even if, as previously discussed (chapter 6), sediment density are not easy to be compared due to high variability of bioclastic limestone density. Another difference is the hydraulic regime that origin the seaward unidirectional currents that reworked and transport the sediment across the shallow-water shelf/platform: in the Gilbert-type deltas this current is generated by the fluvial regime while in the carbonate ramp case the current is

enhanced by wave action. Anyhow, the resulting current is in both cases a high energy, unidirectional current directed seaward.

- The study of the depositional system of the carbonate ramp of Menorca assumes an important role in the comprehension of the ability of certain processes to remove sediment in shallow-water and to transported offshore towards the slope-break and then downslope. In relatively small platforms, proximal to the continental slope-break, these processes of sediment transport become considerably important in the study of deeper submarine systems, since they represent important sources of sediment that may feed the point-sources of deeper turbiditic systems.
- Computational fluid dynamic numerical simulations have been used to reproduce the development of backset lamination at the base of a slope. The simulation, even if due to the used software limits was not able to simulate the backset beds (for grain-size and for scale of outcrop) with the characteristics observed in the field in Menorca, it is an attempt of reproducing at a larger-scale the occurrence of a hydraulic jump within a concentrated turbidity current. The velocities at which the hydraulic jump occurs in the simulated examples is always relatively low, around 0.8m/sec, and the Froude number of the flow just before the jump is slightly above 1. The results of these simulation evidence the unsteadiness character of the flow depositing the sediment at the obstacle, the direct relationship between the possible obstacle and the thickness of the deposit, which on the contrary seems to be independent to flow thickness. The work done is meant to propose some stating points for further simulations to constrain more precisely the main parameters controlling and determining the occurrence of a hydraulic jump and the consequent deposition of sediment with backset bedding.

This thesis therefore presents an original study, since it deals with different topics which are still not fully comprehended. In detail, the study of carbonate ramps and backset beds represent two topics about which the available literature and known examples are unfortunately still very poor. This “study case” therefore offer a new insight into these subjects, adding new information about the facies that can be found at the base-of-slope to outer-ramp transition in distally steepened carbonate ramp.

The Menorca example offers an alternative model for up-slope migrating cross-bedded conglomerate occurrence other than shoreline related and shoals.

The observations on the environmental conditions within which these bedforms are usually found, holds an important role in the exploration and interpretation of the subsurface, since the relative small-size of these deposits can not be so clearly visible when only low resolution seismic.

## ACKNOWLEDGEMENTS

*The development of this thesis was supported by MIUR funds (PRIN 2004-2006), by supplementary funds from the IUSS-Ferrara 1391 for a 1 month scholarship, and thanks to international agreements, by the Italian Ministry of Foreign Affairs and the Norwegian Research Council for a 5 months scholarship.*

*This work significantly improved thanks to the comments and suggestions from my supervisors Dott. Michele Morsilli and Prof. Luis Pomar of the University of the Balearic Islands.*

*A special thanks goes to Prof. Antoni Obrador Tudurí for sharing with me his great knowledge of the island of Menorca, for his cosy hospitality and friendship.*

*I here heartily thank Prof. Wojtek Nemeč of the University of Bergen, for the many possibilities he offered me to grow as a researcher and as a person in an international research-environment, for his interesting and passionate lectures both in class and in the field and for his friendship; with him, I would also like to thank Ernst Hansen and Riccardo Basani of Complex Flow Design AS in Trondheim for let me use freely the Flow3D software and for giving me a free-personal tutorial. On the Norwegian side, I would also like to thank PhD-student Michael Janocko firstly for his friendship and also the for interesting discussions and criticism and for sharing with me his experience and knowledge about CFD and siliciclastic sedimentology.*

*I have no words to thank enough Prof. Piero Gianolla and Dott. Stefano Furin, whom in the last years have always helped me both as a PhD student and maybe more as a person. I also thank Dott. Sandro Furlanis for being there when unnecessary and always missing when needed and Dott. Alberto Riva for his unusual music and usual mess. To all of them I want to show a gigantic gratitude not only for interesting discussions, criticism and scientific suggestions, but more for their friendship, their jokes and enthusiasm in the fieldtrips, and for always finding sometime to listen to my stories.*

*My family comes at last, but not for importance. I thank them for always supporting my choices, for sharing with me joy and for holding me up when life was particularly tough.*

*I want to thank my parents also for financially support my studies, since in this country it would be impossible for a student to undertake a PhD without a personal-supplementary resource.*

## REFERENCES

- Acosta, J., Munoz, A., Herranz, P., Palomo, C., Ballesteros, M., Vaquero, M. and Uchupi, E.** (2001) Geodynamics of the Emile Baudot escarpment and the Balearic Promontory, Western Mediterranean. *Mar. Pet. Geol.*, **18(3)**, 349-369.
- Acosta J., Canals, M., Lopez-Martinez, J., Muñoz, A., Herranz, P., Urgeles, R., Palomo, C. and Casamor, J.L.** (2003) The Balearic Promontory geomorphology (western Mediterranean): morphostructure and active processes,. *Geomorphology*, **49**, 177-204.
- Alexander, J., Bridge, J.S., Cheel, R.J. and Laclair, S.F.** (2001) Bedforms and associated sedimentary structures formed under supercritical water flows over aggrading sand beds, *Sedimentology*, **48**, 133-152.
- Allen, J.R.L.** (1982) *Sedimentary Structures: Their Character and Physical Basis*, Vol. 1. Elsevier, Amsterdam.
- Alvaro, M., Barnolas, A., Del Olmo, P., Ramírez del Pozo, J. and Simó, A.** (1984) El Neógeno de Mallorca: caracterización sedimentologica y bioestratigráfica. *Boletín Geológico y Minero*, **95**, 3-25.
- Ahr, W.M.**, (1973) The carbonate ramp: an alternative to the shelf model. *Gulf Coast Association of Geological Societies Transactions*, **23**, 221-225.
- Aigner, T.** (1983) Facies and origin of nummulitic build-ups: an example from the Giza Pyramids Plateau (Middle Eocene, Egypt). *Neues Jahrbuch Geol. Palaont. Abh.*, **166**, 347-368.
- Alexander J., Bridge, J.S., Cheel, R.J. and Leclair, S.F.** (2001) Bedforms and associated sedimentary structures formed under supercritical water flows over aggrading sand beds. *Sedimentology*, **48**, 133-152.
- Allen, J.R.L.** (1982) *Sedimentary Structures: Their Character and Physical Basis*. **1**. Elsevier, Amsterdam.
- Allen, P.** (1997) Earth surface processes. Blackwell Science, Cambridge, 404 pp.
- Alvaro, M., Barnolas, A., Del Olmo, P., Ramírez del Pozo, J. and Simó, A.** (1984) El Neógeno de Mallorca: caracterización sedimentologica y bioestratigráfica. *Boletín Geológico y Minero*, **95**, 3-25.
- Ames, W.F.** (1992) *Numerical Methods for Partial Differential Equations*. 3<sup>rd</sup> Edition, Academic Press (USA), 433 pp.
- Andrieux, J., Fontobe´, J.M. and Mattauer, M.,** (1971). Sur un mode`le explicatif de l'arc de Gibraltar. *Earth Planet. Sci. Lett.*, **12**, 191– 198.
- Ashley, G.M.** (1990) Classification of large-scale subaqueous bedforms: a new look at an old problem. *J. Sed. Petrol.*, **60**, 160–172.
- Auzende, J.M., Bonnin, J. and Olivet, J.L.,** (1973a). The origin of the western Mediterranean Basin. *J. Geol. Soc. (London)*, **129**, 607– 620.
- Auzende, J.M., Olivet, J.L. and Pautot, G.,** (1973b). Balearic Islands: southern prolongation. In: Ryan, W.B.F., Hsu", K.J. et al., (Eds.), Initial Reports of the Deep Sea Drilling Project, vol. XIII. U.S. Government Printing Office, Washington DC, pp. 1441– 1447.
- Bagnold, R.A.** (1954) Experiments on a gravity-free dispersion of large, solid spheres in a Newtonian fluid model shear. *Proceedings of the Royal Society of London*, **A225**, 49-63.
- Bagnold, R.A.** (1962) Auto-suspension of transported sediment: turbidity currents. *Proc. R. Soc. Lond. Ser. A*, **265**, 315-319.

- Bagnold, R. A.** (1964) Auto-suspension of transported sediment: turbidity currents. *Royal Society of London Series A*, **265**, 315-319.
- Balanyá, J.C. and García-Dueñas, V.** (1987) Les directions structurales dans le Domaine d' Alborán de parte et d'autre du Détroit de Gibraltar. *C. R. Acad. Sci. Paris*, 304 (II), 929– 933.
- Balanyá, J.C. and García-Dueñas, V.** (1988) El cabalgamiento cortical de Gibraltar y la tectónica de Béticas y Rif. Simp. Cinturones Orogeológicos. *Actas II Congreso Geológico de España*, 35–44.
- Ball, M.M., Shinn, E.A. and Stockman, K.W.** (1967) The geologic effects of Hurricane Donna in south Florida. *Journal of Geology*, **75**, 583–597.
- Baria, I.R., Stoudt, D.I., Harris, P.M., and Crevello, P.D.** (1982) Upper Jurassic reef of the Smackover Formation, United States Gulf Coast, *American Association of Petroleum Geologists Bull.*, **66**, 1449-1482.
- Barón, A. and Pomar, L.** (1985) Area 2c Balearic Depression. In: *Stratigraphic Correlation Tables; Neogene of the Mediterranean, Tethys and Paratethys* (Eds F.F. Steininger, J. Senes, K. Kleemann and F. Rog), **1**, p. 17; **2**, p. 17. Institute of Palaeontology, University of Vienna, Vienna.
- Barón, A., Bayó, A. and Fayas, J.A.** (1983) Valor acuífero del modelo sedimentario de plataforma carbonatada del Mioceno de la isla de Menorca. *Com. del X Congr. Nac. Sedim.* Menorca, 645-648.
- Beer, R.M. and Gorsline, D.S.** (1971) Distribution, composition and transport of suspended sediment in Redondo submarine canyon and vicinity (California). *Mar. Geol.*, **10**, 153–175
- Bizon, G., Bizon, J.J., Bourrouilh, R. and Massa, D.** (1973) Présence aux Îles Baléares (Méditerranée Occidentale) de sédiments 'messiniens' déposés dans une mer ouverte á salinité normale. *CR Acad. Sci. Paris*, **277**, 985–988.
- Blow, W.A.** (1969) Late Middle Eocene to Recent planktonic foraminiferal biostratigraphy. *Proc. 1st Int. Conf. Planktonic Microfossils*, 199-422.
- Boggs, S.J.** (1995) *Principles of Sedimentology and Stratigraphy*. Prentice Hall, Upper Saddle River, N.J., 774 pp.
- Bondevik, S., Svendsen, J.I. and Mangerud, J.** (1997) Tsunami sedimentary facies deposited by the Storegga tsunami in shallow marine basins and coastal lakes, western Norway. *Sedimentology*, **44**, 1115–1131.
- Bonnecaze, R.T., Huppert, H.E and Lister, J.R.** (1993) Particle-driven gravity currents. *J. Fluid Mech.*, **250**, 339-369.
- Bowen, A. J.** (1969) Rip currents 1. Theoretical investigations. *J. Geophys. Res.* **74**, 5467–5478.
- Braga, J.C. and Martín, J.M.** (1996) Geometries of reef advance in response to relative sea-level changes in a Messinian (Uppermost Miocene) fringing reef (Cariatiz reef, Sorbas Basin, SE Spain). *Sediment. Geol.* **107**, 61-81.
- Brandano, M., Vannucci, G., Pomar, L. and Obrador, A.** (2005) Rhodolith assemblages from the lower Tortonian carbonate ramp of Menorca (Spain): Environmental and paleoclimatic implications. *Palaeogeography Palaeoclimatology Palaeoecology*. **226**, 307-323.
- Breda A, Mellere D. and Massari F.** (2007) Facies and processes in a Gilbert-delta-filled incised valley (Pliocene of Ventimiglia, NW Italy). *Sedimentary Geology*, **200**, 1-2, 31-55.
- Bridge, J.S. and Demicco, R.V.** (2008) *Earth Surface Processes, Landforms, and Sediment Deposits*, Cambridge University Press, Cambridge.
- Bryant, E.** (2001) *Tsunami. The Underrated Hazard*. Cambridge Univ. Press (2001) 320.

- Calvo, J.P., Daams, R., Morales, J., Lopez-Martinez, N., Agusti, J., Anadon, P., Armenteros, I., Cabrera, L., Civis, J., Corrochano, A., Diaz-Molina, M., Eliaga, E., Hoyos, M., Martin-Suarez, E., Martinez, J., Moissenet, E., Munoz, A., Perez-Garcia, A., Perez-Gonzalez, A., Portero, J.M., Robles, F., Santisteban, C., Torres, T., Van der Muelen, A.J., Vera, A. and Mein, P.** (1993) Up-to-date Spanish continental Neogene synthesis of the paleoclimatic interpretation. *Rev. Soc. Geol. Esp.*, **6**, 29-40.
- Cherns, L., Wheeley, J.R. and Wright, V.P.** (2008). Taphonomic windows and molluscan preservation. *Palaeogeography, Palaeoclimatology, Palaeoecology*, **270**, 220-229.
- Burchette T.P** (1981). European Devonian reefs: a review of current concepts and models. *Society of Economic Paleontology and Mineralogy Special Publication*, **30**, 85–142
- Burchette, T.P. and Britton, S. R** (1985). Carbonate facies analysis in the exploration for hydrocarbons: a case-study from the Cretaceous of the Middle East. In *Sedimentology—recent developments and applied aspects* (eds Brenchley, P. J. & Williams, B. P. J.), 311–338 (Geological Society, London, and Blackwell Scientific Publications, Oxford).
- Burchett, M.D., Clarke, C.J. Field C.D. and Pulkownik, A.** (1989) Growth and respiration in two mangrove species at a range of salinities. *Physiol. Plant.*, **75**, 299–303
- Burchette, T. P. and Wright, V. P.** (1992) Carbonate ramp depositional systems. *Sedimentary Geology* **79**, 3–57.
- Choquette, P.W and Pray, L.** (1970) Geologic nomenclature and classification of porosity in sedimentary carbonates. *A.A.P.G Bull.*, **54**, 207-250.
- Clague, J.J. and Bobrowsky, T.P.** (1994) Evidence for a Large Earthquake and Tsunami 100–400 Years ago on Western Vancouver Island, British Columbia. *Quaternary Res.*, **41**, 176–184.
- Colella, A.** (1988) Gilbert-type fan deltas in the Crati Basin (Pliocene-Holocene, southern Italy). In: *Int. Works. Fan Deltas (1988) – Excursion Guidebook* (Ed. By A. Colella), 19-77. Università della Calabria, Cosenza.
- Colella, A., De Boer, P.L. and Nio, S.D.** (1987) Sedimentology of a marine intermontane Pleistocene Gilbert-type fan-delta complex in the Crati Basin, Calabria, southern Italy. *Sedimentology*, **34**, 721-736.
- Collinson, J.D.** (1969) The sedimentology of the Grindslow Shales and the Kinderscout Grit: a deltaic complex in the Namurian of the northern England. *Journal of Sed. Petrol.*, **39**, 194-221.
- Collinson, J., Mountney, N. and Thompson, D.** (2006) Sedimentary structures. 3<sup>rd</sup> Ed., Terra Publishing, p.292.
- Davidson-Arnott, R.G.D. and Greenwood, B.** (1974) Bedforms and structures associated with bar topography in the shallow-water wave environment, Kouchibouguac Bay, New Brunswick, Canada; *Journal of Sedimentary Petrology*, **44**, 698 - 704.
- Davis, W.M** (1890) Structure and origin of glacial sand plains. *Bull. Geol. Soc. Am.*, **1**, 195-202.
- Davis, W.M. and Fox,** (1972) Coastal processes and nearshore sand bars. *Journal of Sedimentary Research.*, **42**, 2, 401-412.
- Dawson, A.G., Smith, D.E. and Long, D.** (1990) Evidence for a catastrophic tsunami at a Mesolithic site in Inverness, Scotland. *Journal of Archaeological Science*, **17**, 509–512.
- de Raaf, J.F.M., Reading, H.G. and Walker, R.G.** (1965) Cyclic Sedimentation in the Lower Westphalian of North Devon. *Sedimentology*, **4**, 1– 52.
- Dolan, R.** (1971) Coastal Landforms: Crescentic and Rhythmic', *Geological Society of America Bulletin* **82**, 177-180.



- Einsele, G., Chough, S.K. and Shiki, T.** (1996) Depositional events and their records—an introduction. *Sediment. Geol.*, **104**, 1–9.
- Ellison T.H. and Turner J.S.** (1959) Turbulent entrainment in stratified flows. *Journal of Fluid Mechanics*, **6**, 423–448.
- Hayes MO** (1967) Hurricanes as geological agents, south Texas coast. *Bull. Am. Ass. Petrol. Geol.*, **51**, 937-942.
- Eyles, C.H.** (1994) Intertidal boulder pavements in the northeastern Gulf of Alaska and their geological significance. *Sediment. Geol.* **88**, 161-173.
- Eyles, C.H., Eyles, N. and Gostin, V.A.** (1998) Facies and allostratigraphy of high-latitude, glacially influenced marine strata of the Early Permian southern Sydney Basin, Australia. *Sedimentology*, **45**, 121-161.
- Fildani, A., Normark, W.R., Kostic, S., and Parker, G.** (2006) Channel formation by flow stripping: large-scale scour features along the Monterey East Channel and their relation to sediment waves. *Sedimentology*, **53** -6, 1265-1287
- Flügel, E.** (2004) *Microfacies of carbonate rocks. Analysis, interpretation and application.* Springer, Berlin, Heidelberg, 976 pp.
- Frazier, D.E.** (1974) Depositional episodes: their relationship to the Quaternary stratigraphic framework in the northwestern portion of the Gulf basin: University of Texas at Austin, Bureau of Economic Geology Geological Circular, 74-1, 28p.
- Fujiwara, O., Masuda, F., Sakai, T., Fuse, K. and Saito, A.** (1997) Tsunami deposits in Holocene bay-floor muds and the uplift history of the Boso and Miura peninsulas. *Quat. Res. Jpn. Assoc. Quat. Res.*, **36**, 73–86.
- Fujiwara, O., Masuda, F., Sakai, T., Irizuki, T. and Fuse, K.** (1998) Tsunami deposits of the Holocene bay-floor muds along the Pacific coast of central Japan. 15th Int. Sediment. Congr. I.A.S., Alicante, Spain, 350–351.
- Fukushima, Y., Parker, G. and Pantin, H.M.** (1985) Prediction of ignitive turbidity currents in Scripps Submarine Canyon. *Mar. Geol.*, **67**, 55–81
- Galli, G.** (1990) Origins of event beds in the Jurassic Calcarei Grigi Formation, Venetian Alps, Italy. *Geol. En Mijnbouw*, **69**, 375-390.
- Galloway, W.E.** (1989) Genetic stratigraphic sequences in basin analysis I: architecture and genesis of flooding-surface bounded depositional units. *AAPG Bull.*, **73**, 125-142.
- Gary, M., McAfee, R. and Wolf, C.L.** (1972) Editors, Glossary of Geology, American Geological Institute, Washington, D.C., 805 pp.
- Gilbert, G.K.** (1914) The transportation of debris by running water. *Prof. Pap. U.S. geol. Surv.* **86**, 263pp.
- Goff, J., Chagué-Goff, C. and Nichol, S.** (2001) Palaeotsunami deposits: A New Zealand perspective. *Sedimentary Geology*, **143**, 1-6.
- Goldsmith, V., Bowman, D. & Kiley, K.** (1982) Sequential stage development of crescentic bars:Hahoterim beach, southeastern mediterranean. *J. Sediment. Petrol.*, **52**, 233-249.
- Gruszczynski, M., Rudowski, S., Semil, J., Slominski, J. and Zrobek, J.** (1993) Rip currents as a geological tool. *Sedimentology*, **40**,217–236.
- Gressly, A.** (1838). Observations géologiques sur le Jura Soleurois. *Ges. Ges. Naturw.*, **2**, 1-112.

- Grotzinger, J. P.** (1989) Facies and evolution of Precambrian carbonate depositional systems: emergence of the modern platform archetype, in, *P.D. Crevello et al. (eds.), Controls on Carbonate Platform and Basin Development, Society of Economic Paleontologists and Mineralogists Special Publication 44*, 79-106.
- Guo, J.** (2002) Hunter Rouse and Shields diagram. In: *Proceedings from the 13th IAHR-APD Congress*, Singapore, **2**, 1096-1098.
- Hallworth M.A. and Huppert H.E.** (1998) Abrupt transitions in high-concentration, particle-driven gravity currents. *Physics of Fluids*, **10**(5), 1083.
- Hand, B.M.** (1974) Supercritical flow in density currents. *J. Sed. Petrology*, **44**, 637-648.
- Hand, B.M., Wessel, J.M. and Hayes, M.O.** (1969) Antidunes in the Mount Toby Conglomerate (Triassic), Massachusetts, *Journal of Sedimentary Petrology*, **39**, 1310-1316.
- Hansen, K.S.** (1999) Development of a prograding carbonate wedge during sea level fall: Lower Pleistocene of Rhodes, Greece. *Sedimentology*, **46**, 559-576.
- Hardisty, J.** (1994) Beach and nearshore sediment transport. In Pye, K. (ed.), *Sediment Transport and Depositional Processes*. Blackwell Scientific Publications, Oxford, Chapter 7, pp. 219-256.
- Harlow, F.H. and Nakayama, P.I.** (1967) Turbulence transport equations. *Phys. Fluids*, **10**, 2323-2331.
- Herzer, R.H. and Lewis, D.W.** (1979) Growth and burial of a submarine canyon off Motunau, north Canterbury, New Zealand. *Sed. Geol.*, **24**, 69-83
- Hottinger, L.** (1997) Shallow benthic foraminiferal assemblages as signals for depth of their deposition and their limitations. *Bull. Soc. Géol. Fr.*, **168**, 491-505.
- Hsü, K.J., Ryan, W.B.F. and Cita M.B.** (1973) Late Miocene dessication of the Mediterranean. *Nature*, **242**, 240-244.
- Inman, D.L., Nordstrom, C.E. and Flick, R.E.** (1976) Currents in submarine canyons: an air-sea-land interaction. *Annu. Rev. Fluid Mech.*, **8**, 275-210
- James, N.P., Bone, Y. and Kyser, T.K.** (2005) Where Has All the Aragonite Gone? Mineralogy of Holocene Neritic Cool-Water Carbonates, Southern Australia. *J. Sed. Resear.*, **75**, 454-463.
- Johnson, J.W.** (1956) Dynamics of nearshore sediment movement. *AAPG Bull.*, **40**, 2211-32.
- Jopling, A.V. and Richardson, E.V.** (1966) Backset bedding developed in shooting flow in laboratory experiments. *J. Sed. Petrology*, **36**, 821-825.
- Jorry, S.J., Hasler, C.A. and Davaud, E.** (2006) Hydrodynamic behaviour of Nummulites: implications for depositional models. *Facies*, **52**, 221-235.
- Jurado, M.J.** (1985) Estudi sedimentològic del Neogen de l'àrea de Ciutadella. *Consell Insular de Menorca. Maó*, 145 pp.
- Kinsman, B.** (1965), Wind waves: their generation and propagation on the ocean surface. Prentice Hall.
- Kirlyš, V.** (1971) Some peculiarities of the coastal dynamics of the split of Kursiu Nerija, *Liet. TSR Mosklu Akad. Darb.*, Ser. B, **4**, 211-226 (in Russian, English summary).
- Komar, P.D.** (1971) Hydraulic jumps in turbidity currents. *Geological Society of America Bulletin*, **82**, 1477-1488.
- Komar, P.D.** (1971b) Nearshore cell circulation and the formation of giant cusps. *Bull. Geol. Soc. Am.*, **82**, 2643-2650.
- Komar, P.D.** (1976) Beach processes and sedimentation, 429 pp. Prentice-Hall, Englewood cliffs, NJ.
- Komar, P.D., Neudeck R.H. and Kulm, L.D.** (1972) Observation and significance of deep water oscillatory ripple marks on the Oregon continental shelf. In: D.J.P. Swift, D.B. Duane and O.H. Pilkey, Editors, *Shelf*

- Sediment Transport: Process and Pattern*, Dowden, Hutchinson and Ross, Stroudsburg, Penn, 601–619.
- Komar, P.D.** (1998). *Beach Processes and Sedimentation*. Englewood Cliffs, New Jersey: Prentice Hall.
- Krijgsman, W.** (2002) The Mediterranean: Mare nostrum of Earth sciences. *Earth and planetary science letters*, **205**, 1-12.
- Kuenen, Ph.H.** (1950) Turbidity currents of high density. In: *18th International Geological Congress (1948), London, Reports, pt. 8 The Geology of Sea and Ocean Floors (1950)*, 44–52.
- Kuenen, Ph.H., and Migliorini, C.I.** (1950) Turbidity currents as a cause of graded bedding. *Journal of Geology*, **58**, 91-127.
- Lavecchia, G.** (1988) The Tyrrhenian–Apennines system: structural setting and seismotectogenesis. *Tectonophysics*, **147**, 263–296.
- Lewis, K.B. and Pantin, H.M.** (2002) Channel-axis, overbank and drift sediment waves in the southern Hikurangi Trough, New Zealand. *Mar. Geol.*, **192**, 123–151.
- Lickorish, W.H. and Butler, R.W.H.** (1996) Fold amplification and parasequence stacking patterns in syn-tectonic shoreface carbonates. *Bull. Geol. Soc. America.*, **108**, 966-977.
- Longuet-Higgins, M.S.**, (1983) Wave set-up, percolation and undertow in the surf zone. *Proc. R. Soc. London Ser. A-Math. Phys. Eng. Sci.*, **390**, 283–291
- Lowe, D.R.** (1976) Grain flow and grain flow deposits, *Journal of Sedimentary Petrology*. **46**, 188–199.
- Lowe, D. R.**, (1982) Sediment gravity flows; II, Depositional models with special reference to the deposits of high-density turbidity currents. *Journal of Sedimentary Petrology*, **52-1**, 279-297.
- MacMahan, J.H., Thornton, E.B. and Reniers, A.J.H.M.** (2006) Rip current review. *Coastal Engineering*, **53**, 191-208.
- Maldonado, A. and Stanley, D.J.** (1979) Depositional patterns and late quaternary evolution of two Mediterranean submarine fans: a comparison. *Marine Geology*, **31**, 215-250.
- Mantovani, E., Babucci, D., Albarello, D. and Mucciarelli, G.** (1990) Deformation patterns in the central Mediterranean and behaviour of the African/Adriatic Promontory. *Tectonophysics* **179**, 63–79.
- Martín, J.M., Braga, J.C., Betzler, C. and Brachert, T.** (1996) Sedimentary model and high-frequency cyclicity in a Mediterranean, shallow-shelf, temperate-carbonate environment (Uppermost Miocene, Agua Amarga Basin, Southern Spain). *Sedimentology*, **43**, 263-277.
- Massari F.** (1984) Resedimented conglomerates of a Miocene fan-delta complex, Southern Alps, Italy. In: *Sedimentology of Gravels and Conglomerates* (Ed. By W. Nemeč and R.J. Steel), 318-340. Blackie and Son, London.
- Massari F.** (1996) Upper-flow-regime stratification types on steep-face, coarse-grained, Gilbert-type progradational wedges (Pleistocene, Southern Italy). *J. Sed. Res.*, **66**, 364-375.
- Massari F. and Chiocci, F.** (2006) Biocalcarenitite and mixed cool-water prograding bodies of the Mediterranean Pliocene and Pleistocene: architecture, depositional setting and forcing factors. In: Pedley, H.M. & Carannante, G. (eds) 2006. *Cool-Water Carbonates: Depositional Systems and Palaeoenvironmental Controls*. *Geol. Soc., London, Sp. Pub.*, **255**, 95-120.
- Massari F. and D'Alessandro A.** (2000) Tsunami-related scour-and-drape undulations in Middle Pliocene restricted-bay carbonate deposits (Salento, South Italy). *Sediment. Geol.*, **135**, 265-281.

- Massari F. and Parea, G.C.** (1990) Wave-dominated Gilbert-type gravel deltas in the hinterland of the Gulf of Taranto. In: Colella, A. and Prior, D.B., eds. *Coarse-Grained Deltas. International Association of Sedimentologists Special Publication*, **10**, 311-331.
- Mateu-Vicens, G., Hallock, P. and Brandano M.** (2008) A depositional model and paleoecological reconstruction of the lower Tortonian distally steepened ramp of Menorca (Balearic Islands, Spain). *Palaios*, **23**, 465-481.
- Mazzullo, S. J.** (1971) Storm roller. *Geological Society of America Bulletin*, **82**, 1973-1976.
- Middleton, G.V.** (1965), Antidune cross-bedding in a large flume. *Journal of Sedimentary Petrology*, **35**, 922-927.
- Middleton, G. V.** (1966). Experiments on density and turbidity currents. *Canadian Jour. Erth. Sci.*, **3**, 523-546.
- Middleton, G.V.** (1967) Experiments on density and turbidity currents. III. Deposition of sediments. *Can. J. Earth Sci.*, **4**, 475–505.
- Middleton, G.V.** (1978) Facies. In: Fairbridge R.W. & Bourgeois J. (eds.): *Encyclopedia of Sedimentology*. Dowden, Hutchison & Ross, Stoudsburg, PA, 323-325.
- Middleton, G. V. and Hampton, M. A.** (1973) Sediment gravity flows: Mechanics of flow and deposition. In" Middleton, G. V., and Bouma, A. H. (Eds.), *Turbidites and Deep Water Sedimentation*, Anaheim (SEPM Short Course), 1-38.
- Middleton, G. V. and Hampton, M. A.** (1976) Subaqueous sediment transport and deposition by sediment gravity flows. In: Marine sediment transport and environmental management (Ed. By D.J. Stanley and D.J.P. Swift), pp. 197-218, Wiley, New York.
- Middleton, G.V. and Southard, J.B.** (1984) Mechanics of sediment movement. *SEPM short course no. 3, 2<sup>nd</sup> edn. Soc. Econ. Paleont. Mineral.*, Tulsa, 401pp.
- Minoura, K. and Nakaya, S.** (1991) Traces of tsunamis preserved in Inter-tidal lacustrine and marsh deposits: some examples from Northeast Japan. *J. Geology*, **99**, 265–287.
- Moore, D.G.** (1969) Reflection Profiling Studies of the California Continental Borderland: Structure and Quaternary Turbidite Basins. *Geological Society of America, Special Paper*, **107**, 142 pp.
- Moore, G.W. and Moore, J.G.** (1988) Large-scale bedforms in boulder gravel produced by giant waves in Hawaii. *Geol. Soc. Am. (Spl. Pub.)*, **229**, 101-110.
- Mulder T. and Alexander J.** (2001) The physical character of sedimentary density currents and their deposits. *Sedimentology*, **48**, 269-299.
- Munk, W. H.** (1949) The Solitary Wave Theory and Its Applications to Surf Problems. *Annals of the New York Academy of Sciences*, **51**, 376-462.
- Nemec, W.** (1990) Aspects of sediment movement on steep delta slopes. In: *Coarse-grained Deltas* (Eds. A. Colella and D.B. Prior). *Int. Assoc. Sedimentol. Spec. Publ.*, **10**, 29-73.
- Nemec, W., Steel, R.J., Gjelberg, J., Collinson, J.D., Prestholm, E., Oxnevad, I.E. and Worsley, D.** (1988) Exhumed rotational slides and scar infill features in a Cretaceous delta front, eastern Spitsbergen. *Polar Research*, **6**, 105-112.
- Nemec, W., Postma, G. and Massari, F.** (2007) Evidence of hydraulic jumps associated with the subaqueous slopes of Gilbert-type deltas and distally-steepened carbonate ramps. BSRG Workshop on Hydraulic Jumps, Birmingham University.

- Normark, W.R., Piper, D.J.W. and Sliter, R.** (2006) Sea-level and tectonic control of middle to late Pleistocene turbidite systems in Santa Monica Basin, offshore California. *Sedimentology*, **53**, 867–897.
- Obrador, A.** (1970) Estudio Estratigráfico y sedimentológico de los materiales miocénicos de la Isla de Menorca. *Acta Geol. Hisp.*, **5**, 19-23.
- Obrador, A.** (1972–73) Estudio estratigráfico y sedimentológico de los materiales miocénicos de la Isla de Menorca. *Revista Menorca*, **64**, 37–197 and **65**, 35–97 and 125–189.
- Obrador, A. and Pomar, L.** (1983) El Neógeno del sector de Maò. In: L. Pomar, A. Obrador, J. Fornós and A. Rodríguez-Perea (Editors), *El Terciario de las Baleares (Mallorca-Menorca). Guía de las Excursiones del X Congr. Nac. Sedimentología. Inst. Estud. Baleàrics and Univ. de Palma de Mallorca*, 207-232.
- Obrador, A. and Pomar, L.** (2004) El Miocè del Migjorn. In: *Història Natural del Migjorn de Menorca* (Eds: J.J. Fornós, A. Obrador and M. Rosselló), pp. 73-92. Societat d'Història Natural de les Balears and Institut Menorquí d'Estudis – Fundació SA NOSTRA.
- Obrador, A., Pomar, L., Rodríguez, A. and Jurado, M.J.** (1983a) Unidades deposicionales del Neógeno menorquin. *Acta Geol. Hisp.*, **18**, 87–97.
- Obrador, A., Pomar, L., Jurado, M.J., Rodríguez-Perea, A. and Fornós, J.J.** (1983b) El Neógeno del Sector de Ciutadella. In: *El Terciario de las Baleares. Libro Guía de Las Excursiones del X Con. Nac. Sedimentología Maó* (Eds L. Pomar, A. Obrador, J. Fornós and A. Rodríguez-Perea), 233–255. Institut d'Estudis Balearics and Universitat de les Illes Balears, Palma de Mallorca.
- Obrador, A., Pomar, L. and Taberner, C.** (1992) Late Miocene breccia of Menorca (Balearic Islands): a basis for the interpretation of a Neogene ramp deposit. *Sed. Geol.*, **79**, 203–223.
- Oswald, E.J.** (1992) Dolomitization of a Miocene reef complex, Mallorca, Spain. Unpublished PhD thesis, State University of New York at Stony Brook, Stony Brook, 424 pp.
- Perkins R.D., and Enos, P.** (1968) Hurricane Betsy in the Florida-Bahamas area—geologic effects and comparison with Hurricane Donna. *Journal of Geology*, **76**, 710–717.
- Pickering, K.T.** (1995) Are enigmatic sandy wave-like bedforms in Jurassic Bridport Sands, Dorset, due to standing waves? *Journal of the Geological Society*, **152**, 481-485.
- Pickering, K.T., Soh, W. and Taira, A.** (1991) Scale of tsunami-generated sedimentary structures in deep water. *Journal of the Geological Society*, London, **148**, 211-214.
- Pomar, L.** (1991) Reef geometries, erosion surfaces and high-frequency sea-level changes, Upper Miocene Reef Complex, Mallorca, Spain. *Sedimentology*, **38**, 243-269.
- Pomar, L. (2001a)** Ecological control of sedimentary accommodation: evolution from a carbonate ramp to rimmed shelf, Upper Miocene, Balearic Islands. *Palaeogeography, Palaeoclimatology, Palaeoecology*, **175**, 249-272.
- Pomar, L. (2001b)** Types of carbonate platforms, a genetic approach. *Basin Research*, **13**, 313-334.
- Pomar, L., Marzo, M. and Barón, A.** (1983) El Terciario de Mallorca. In: L. Pomar, A. Obrador, J. Fornós and A. Rodríguez-Perea (Editors), *El Terciario de las Baleares (Mallorca-Menorca). Guía de las Excursiones del X Congr. Nac. Sedimentología. Inst. Estud. Baleàrics and Univ. de Palma de Mallorca*, 21-45.
- Pomar, L., Obrador A. and Westphal H.** (2002) Sub-wavebase cross-bedded grainstones on a distally steepened carbonate ramp, Upper Miocene, Menorca, Spain. *Sedimentology*, **49**, 139-169.

- Pomar, L. and Ward, W.C.** (1994) Response of a Miocene carbonate platform to high-frequency eustasy. *Geology*, **22**, 131–134.
- Pomar, L. and Ward, W.C.** (1995) Sea-level changes, carbonate production and platform architecture: the Lluçmajor Platform, Mallorca, Spain. In: *Sequence Stratigraphy and Depositional Response to Eustatic, Tectonic and Climatic Forcing* (Ed. B.U. Haq), pp. 87–112. Kluwer Academic Press, Dordrecht.
- Pomar, L., & Ward, W. C.** (1999) Reservoir-Scale Heterogeneity in Depositional Packages and Diagenetic Patterns on a Reef-Rimmed Platform, Upper Miocene, Mallorca, Spain. *AAPG Bulletin*, **83**, 1759-1773.
- Pomar, L., Ward, W.C. and Green, D.G.** (1996) Upper Miocene Reef Complex of the Lluçmajor area, Mallorca, Spain. In: *Models for Carbonate Stratigraphy from Miocene Reef Complexes of the Mediterranean Regions* (Eds E. Franseen, M. Esteban, W.C. Ward and J.M. Rouchy), pp. 191–225. *SEPM Concepts in Sedimentology and Paleontology Series*, **5**.
- Pomar, L.** (2005) Reservoir-scale heterogeneities in Upper Miocene carbonate platforms of the Balearic Islands, Spain. *Field Course Guidebook*.
- Popov, E. A.** (1956) *Ob ottoke nagonnykh vod v beregovoy zone* (in Russian). *Tr. Okeanogra. Kom. Akad. Nauk SSSR*, **1**, 98-104.
- Posamentier, H.W. and Vail, P.R.** (1988), Eustatic controls on clastic deposition II— sequence and systems tract models, in Wilgus, C.K., Hastings, B.S., Ross, C.A., Posamentier, H.W., Van Wagoner, J.C., and Kendall, C.G.S.C., eds., *Sea Level Changes, an Integrated Approach: SEPM, Special Publication*, **42**, p. 125–154.
- Posamentier, H.W., Jervey, M.T. and Vail, P.R.** (1988) Eustatic controls on clastic deposition I – conceptual framework. In: *Sea level changes – and integrated approach*, Ed. By C.K. Wilgus, B.S. Hastings, C.G. St C. Kendall, H. Posamentier, C:A: Ross and J. Van Wagoner, p. 109-124, Spec. Publ. Soc. Econ. Paleont. Miner., **42**, Tulsa.
- Postma, G.** (1979) Preliminary note on a significant sequence in conglomeratic flows of a mass transport-dominated fan-delta (Lower Pliocene, Almeria Basin, SE Spain). *Konin. Neder. Akad. Wetensch.*, **B 82**, 465-471.
- Postma, G.** (1984a) Slumps and their deposits in delta front and slopes. *Geology*, **12**, 27-30.
- Postma, G.** (1984b) Mass-flow conglomerates in a submarine canyon: Abrija Fan-delta, Pliocene, southeastern Spain, in Koster, E.H., and Steel, R.J., eds., *Sedimentology of gravels and Conglomerates*, Ca. Soc. *Petr. Geol., Mem.*, **10**, 237-258.
- Postma, G. and Roep, T.B.** (1985) Resedimented conglomerates in the bottomsets of Gylbert-type gravel deltas. *J. Sed. Petrol.*, **55**, 874-885.
- Postma, G., Roep, T.B. and Ruegg, G.J.H.** (1983) Sandy-gravelly mass-flow deposit in an ice-marginal lake (Saalian, Leuvenumsche Beek Valley, Veluwe, The Netherlands), with emphasis on plug-flow deposits. *Sed. Geol.*, **34**, 59-82.
- Power, W.R. Jr.**, (1961) Backset beds in the Coso Formation, Inyo County, California. *J. Sed. Petrol.*, **31**, 603-607.
- Puga-Bernabeu, A., Martín, J. M. and Braga, J. C.** (2007). Tsunami-related deposits in temperate carbonate ramps, Sorbas Basin, southern Spain. *Sedimentary Geology*, **199**, 107-127.

- Puga-Bernabeu, A., Martín, J. M. and Braga. J. C.** (2008). Sedimentary processes in a submarine canyon excavated into a temperate-carbonate ramp (Granada Basin, southern Spain). *Sedimentology*, **55**, 1449-1466.
- Puig, P., Ogston, A.S., Mullenbach, B.L., Nittrouer, C.A. and Sternberg, R.W.** (2003) Shelf-to-canyon sediment-transport processes on the Eel continental margin (northern California). *Mar. Geol.*, **193**, 129–149.
- Pykhov, N.V.** (1976) Gravitational Displacements of Sedimentary Masses on the Ocean Floor, *Litodinamika, litologiya i geomorfologiya shelfa* (Lithodynamics, Lithology, and Geomorphology of the Shelf), Moscow, 7–36.
- Read, J.F.** (1982) Carbonate platforms of passive (extensional) continental margins: types, characteristics and evolution. *Tectonophysics*, **81**, 195-212.
- Read, J. F.** (1985) Carbonate platform facies models. *Am. Assoc. Petrol. Geol. Bull.*, **69**, 1-21.
- Reimnitz, E.** (1971) Surf-beat origin for pulsating bottom currents in the Rio Balsas Submarine canyon, Mexico. *Bull. geol. Soc. Am.*, **83**, 81-90.
- Reading H.G and Levell, B K.** (1996) Controls on the sedimentary record. In: H.G. Reading, Editor, *Sedimentary environments: processes, facies and stratigraphy*, Blackwell, Oxford, 3–36.
- Reineck, H.E. and Singh, I.B.** (1980) *Depositional Sedimentary Environments*. Springer-Verlag, Berlin, 549.
- Rosell, J. and Llompарт, C.** (1983) Aportaciones al estudio del Mioceno del extremo oriental de Menorca. *Acta Geol. Hispànica*, **18**(2), 99-104.
- Rosell, J., Obrador, A. and Mercadal, B.** (1976) Las facies conglomeráticas del Mioceno de la Isla de Menorca. *Bol. Soc. Hist. Nat. Bal.*, **21**, 76-93.
- Rossetti, D.de F.** (1997) Internal architecture of mixed tide- and storm-influenced deposits: an example from the Alcântara Formation, northern Brazil. *Sediment. Geol.*, **114**, 163-188.
- Sarg, F.J** (1988) Carbonate sequence stratigraphy. In Wilgus, C.K., Hastings, B.S., Kendall, C.G.St.C., Posamentier, H., Ross, C.A., and Van Wagoner, J. (Eds.), *Sea-Level Changes: An Integrated Approach*. Spec. Publ.—Soc. Econ. Paleontol. Mineral., **42**, 155-181.
- Savage, S. B.** (1979) Gravity flow of cohesionless granular materials in chutes and channels. *J. Fluid Mech.* **92**, 53-96.
- Schmincke, H.U., Fisher, R.V., and Waters, A.C.** (1973) Antidune and chute and pool structures in the base surge deposits of the Laacher See area, Germany. *Sedimentology*, **20**, 553-574.
- Shadrin, I.E.** (1972) Tycheniya beregovoy zony bezprilivnogo moray, Izd. Nauka, Moska
- Shepard, F.P.** (1936) Undertow, rip tide, or “rip current”, *Science*, **84**.
- Shepard, F.P., Emery, K.O. and La Fond, E.C.** (1941) Rip currents: a process of geological importance, *J. Geol.*, **49**, 337–369.
- Shepard, F. P. and Inman, D. L.** (1950) Nearshore water circulation related to bottom topography and wave refraction. *Transactions of the American Geophysical Union*, **31- 2**, 196-212.
- Shepard, F.P. and Inman, D.L.** (1951) Wave refraction at La Jolla, California. *Proceedings of the 1st International Conference of Coastal Engineering*.
- Shepard, F.P. and Marshall, N.F.** (1973) Storm-generated current in La Jolla Submarine Canyon, California. *Mar. Geol.*, **15**, 19–24

- Shepard, F.P., Marshall, N.F. and McLoughlin, P.A.** (1974) Currents in submarine canyons. *Deep-Sea Res.*, **21**, 691–706.
- Shiki, T. and Yamazaki, T.** (1990) A conglomerate tsunamite. I.A.S. Intern. Congress, Nottingham 1990, Abstract Book, 497 pp.
- Simons, D.B. and Richardson, E.V.** (1963), Forms of bed roughness in alluvial channels: *Transactions of the American Society of Civil Engineers*, **128**, 284-302.
- Simons, D.B., Richardson, E.V. and Nordin, C.F.** (1965) Sedimentary structures generated by flow alluvial channels. In: G.V. Middleton (Editor), *Primary Sedimentary Structures and their Hydrodynamic Interpretation – Soc. Econ. Paleontologists Mineralogists, Spec. Publ.*, **12**, 34-52.
- Skipper, K.** (1971) Antidune cross-stratification in a turbidite sequence, Cloridorme Formation (Middle Ordovician) Gaspé, Quebec. *Sedimentology*, **17**, 51-68.
- Skipper, K. and Bhattacharjee, S.B.** (1978) Backset bedding in turbidites: a further example from the Cloridorme Formation (Middle Ordovician), Gaspé, Quebec. *J. Sed. Petrol.*, **48**, 193-202.
- Sloss, L. L.** (1950) Paleozoic sedimentation in Montana area. *Am. Assoc. Petroleum Geologists Bull.*, **34**, 423-451.
- Sloss, L. L.** (1963) Sequences in the cratonic interior of North America. *Geol Soc. America Bull.*, **74**, 93-114.
- Smit, J. and Roep, T.B.** (1998) Tsunami deposits at the KT boundary in the Gulf of Mexico. *15th Int. Sediment. Congr. I.A.S.*, Alicante, Spain, 728–729.
- Sonu, C.** (1972) Field observation of nearshore circulation and meandering currents. *J. Geophys. Res.*, **77** -18, 3232-3247.
- Soulsby, R. L.** (1997) *Dynamics of Marine Sands*. Thomas Telford, London.
- Sparks R. S. J., Bonnacaze R. T., Huppert H. E., Lister J. R., Hallworth M. A., Mader H., and Phillips J.** (1993) Sediment-laden gravity currents with reversing buoyancy. *Earth and planetary science letters*, **114**, 243-257.
- Stow, D.A.V. and Werzel, A.** (1990) Hemiturbidites: a new type of deep-water sediment. In: *Proc. ODP Sci. Results*, 116 (Ed. By J.R. Cochran, D.A.V. Stow et al.), 25-34.
- Takashimizu, Y. and Masuda, F.** (1998) Sedimentary structures of earthquake-induced tsunami layers in the Upper Pleistocene incised valley system. Shizuoka, Japan. 15th Int. Sediment. Congr. I.A.S., Alicante, Spain, 753–754.
- Tappin, D.R.** (2004) Submarine slump-generated tsunamis. *Marine Geology*, **203**, 199-200.
- Tokaty, G.A.**, (1971) *A History and Philosophy of Fluid Mechanics*, G.T. Foulis & Co. Ltd., Henley-on-Thames (HK), 272 pp.
- Uličný, D.** (2001) Depositional systems and sequence stratigraphy of coarse-grained deltas in a shallow-marine, strike-slip setting: the Bohemian Cretaceous Basin, Czech Republic. *Sedimentology*, **48**, 599-628.
- Vail, P.R., Mitchum, R.M., Jr., and Thompson, S.**, (1977), Seismic stratigraphy and global changes of sea level, Part 3: Relative changes of sea level from coastal onlap, in Payton, C.E., ed., *Seismic Stratigraphy Applications to Hydrocarbon Exploration: AAPG, Memoir*, **26**, p. 63–81.
- Van Rijn, L. C.** (1987) *Mathematical Modeling of Morphological Processes in the Case of Suspended Sediment Transport*. Unpubl. Ph.D. Thesis, The Delft University of Technology, 208 pp.
- Van Wagoner, J.C, Posamentier, H.W., Mitchum, R.M., Vail P.R., Sarg, J.F., Loutit, T.S. and Hardenbol, J.** (1988) An overview of sequence stratigraphy and key definitions. In: *Sea level changes – and integrated*



- approach, Ed. By C.K. Wilgus, B.S. Hastings, C.G. St C. Kendall, H. Posamentier, C.A: Ross and J. Van Wagoner, p. 39-45, Spec. Publ. Soc. Econ. Paleont. Miner., **42**, Tulsa.
- Vegas, R.** (1992) The Valencia Trough and the origin of the western Mediterranean basins. *Tectonophysics*, **203**, 249– 261.
- Vvdenskaya, A. I.** (1977) A layer of storm reworking of sediments in the Rudnya Bay (The Sea of Japan) *Okeanologiya*, **17**, 506-510 (in Russian, English summary).
- Wallis, G.** (1969) One-Dimensional Two-Phase Flow. McGraw-Hill.
- Walker, R.G.** (1967) Upper-flow-regime bed forms in turbidites of the Hatch Formation, Devonian of New York State. *Journal of Sedimentary Petrology*, **37**, 1052-1058.
- Walker, R.G.** (1992) *Facies Models: Response to Sea Level Change* (Ed. by R.G. Walker and N.P. James), Geological Association of Canada, St. John's.
- Wesseling, R.** (2001) *Principles of Computational Fluid Dynamics* Springer Ed., Berlin, 644. pp.
- Wilson, J.L.** (1975) Carbonate Facies in Geologic History. Springer-Verlag, New York, N.Y., 471 pp.
- Wood, IR** (1967) Horizontal two-dimensional density current. *Amer. Soc. Civil Engr., J. Hydraulics Div., Proc.*, **93**, No.Hy2, 35-4.
- Wright V.P. and Burchette T.P** (1998) Carbonate Ramps, *The Geological Society Special Publication*. **149** London, 465 pp.
- Wunderlich, F.** (1972) Georgia Coastal Region, Sapelo Island, U.S.A., Sedimentology and Biology. III Beach Dynamics and Beach Development. *Senckenbergiana marit.*, **4**, 47-79.
- Wunderlich, F.** (1973) "Backset Bedding" durch Rhomboederrippeln. *Senckenbergiana marit.*, **5**, 161-164.
- Yakhot, V. and Orszag, S.A.** (1986) Renormalization group theory of turbulence, I. Basic theory. *J. Sci. Comput.*, **1**, 1–51.
- Yakhot, V. and Smith, L.M.** (1992) The renormalization group, the " expansion and derivation of turbulence models. *J. Sci. Comput.*, **7**, 35–61.
- Yih, C.S. and Guda, C.R.** (1955) Hydraulic jump in a fluid system of two layers, *Tellus*, **7**, 3, 358-365.